NASA CONTRACTOR REPORT

NASA CR-1896

HEAT AND MOMENTUM TRANSFER MODEL STUDIES APPLICABLE TO ONCE-THROUGH, FORCED CONVECTION POTASSIUM BOILING

by C. M. Sabin and H. F. Poppendiek

Prepared by
GEOSCIENCE LTD.
Solana Beach, Calif. 92075
for Lewis Research Center

NATIONAL AERONAUTICS AND SPACE ADMINISTRATION • WASHINGTON, D. C. • SEPTEMBER 1971

1. Report No.	2. Government Accession No.	3. Recipient's Catalog No.
NASA CR-1896		

4. Title and Subtitle	5. Report Date
HEAT AND MOMENTUM TRANSFER MODEL STUDIES APPLICABLE TO ONCE-THROUGH, FORCED CONVECTION POTASSIUM BOILING	September 1971
	6. Performing Organization Code

7. Author(s)	8. Performing Organization Report No.
C. M. Sabin and H. F. Poppendiek	GLR-71
	10. Work Unit No.

9. Performing Organization Name and Address	11. Contract or Grant No.
Geoscience Ltd. 410 South Cedros Avenue Solana Beach, California 92075	NAS 3-9426
	13. Type of Report and Period Covered
12. Sponsoring Agency Name and Address	Contractor Report
National Aeronautics and Space Administration Washington, D. C. 20546	14. Sponsoring Agency Code

15. Supplementary Notes

16. Abstract

A number of heat transfer and fluid flow mechanisms that control once-through, forced convection potassium boiling are studied analytically. The topics (1) flow through tubes containing helical wire inserts, (2) motion of droplets entrained in vapor flow, (3) liquid phase distribution in boilers, (4) temperature distributions in boiler tube walls, (5) mechanisms of heat transfer regime change, and (6) heat transfer in boiler tubes comprise the scope of the study. Whenever possible, comparisons of predicted and actual performances are made. The model work presented aids in the prediction of operating characteristics of actual boilers.

17. Key Words (Suggested by Author(s))		18. Distribution Statement
Potassium boiling	Once-through boiling	Unclassified - unlimited
Swirl flow	Rivulet heat transfer	
Heat transfer	Droplet heat transfer	
Pressure loss		

19. Security Classif. (of this report)	20. Security Classif. (of this page)	21. No. of Pages	22. Price*
Unclassified	Unclassified	268	$3.00

*For sale by the National Technical Information Service, Springfield, Virginia 22151

FOREWORD

The research described in this report was conducted by Geoscience Ltd. under subcontract from General Electric (NASA contract NAS 3-9426). Mr. Martin U. Gutstein of the Lewis Research Center Space Power Systems Division was the NASA Project Manager. The report was originally issued as Geoscience Ltd. report GLR-71.

TABLE OF CONTENTS

I. INTRODUCTION

This report contains the results of a two and one-half year analytical study* of forced convection boiling of potassium. The study was undertaken in an effort to provide mathematical descriptions of the controlling processes in a forced-convection boiler tube, where such analyses were not already available. The analytical descriptions, when verified by comparison with experimental data, would then contribute to the rational engineering design of forced convection potassium boilers for space applications.

All of the boilers presently under development or being proposed for use in Rankine-cycle engines for space auxiliary power are of the forced-convection once-through design. Such boilers receive subcooled or saturated liquid at the inlet of a continuous tube, and discharge dry, possibly superheated vapor from the outlet. In steady state operation, the flow past each point in the boiler is described by a fixed vapor quality. Typical flow regimes in such a boiler may be (in order, from inlet to outlet):

1. All liquid.
2. A bubbly, quasi-homogeneous mixture of liquid and vapor.
3. Separated annular flow with liquid on the wall and vapor in the core. Liquid droplets may be entrained in the vapor. A wave structure may exist on the liquid film, and liquid fragments may be stripped from the waves by the vapor stream, ejected from the film by nucleate boiling, or deposited in the liquid layer from the vapor.
4. Wetted liquid rivulets or droplets on the wall, wet or dry vapor in the core.
5. Film boiling droplets.
   Under some conditions, film boiling droplets slide along the wall (on a film of their own vapor) while the vapor in which they are carried

*Equivalent to a three man-year effort.

superheats above the saturation temperature. Departures of the mixtures from thermodynamic equilibrium may be quite large.

6. Fog flow.

   Under some conditions, fog flow, with a dispersion of fine droplets evaporating in superheated vapor, may occur.

7. Vapor superheating.

   After all of the liquid is vaporized, dry vapor superheating, a process identical to the forced convection heating of any gas, occurs.

This sequence of processes does not appear in every boiler. In some cases, flow regimes listed do not occur, or are replaced by others. A number of transition processes can occur which fall in between the flow regimes listed above. Some of these are:

1. Surface boiling with the mixed mean of the liquid subcooled.

   This condition is readily obtained with low turbulence flows of poor thermal conductors such as organic liquids. It is probably not usually encountered in flows of liquid metals.

2. Superheating of liquid above the saturation temperature without vapor generation.

3. Transition boiling.

   At the end of the annular liquid film (or rivulet flow), there is usually a sudden and very large drop in heat transfer conductance. However, some experiments have shown a relatively gradual decrease in conductance, indicating that liquid still partially covers the wall, possibly because spray is deposited from the vapor core, or wetted patches are swept downstream from the ruptured liquid layer.

The literature of forced convection boiling includes many experimental investigations of "burnout" or "critical heat flux."

"Burnout" in such experiments does not occur uniformly over the length of the tube, but at a distinct axial location, usually at vapor qualities significantly below one hundred percent. It is clear that the term "burnout" has no

meaning in boilers of the type being discussed in this report since these boilers are required to produce dry vapor (one hundred percent quality) at the outlet without failure. The usual interpretation of the "burnout" phenomenon is that the annular film of liquid on the inner tube wall terminates at the vapor quality and axial location where the tube failure occurs. In the "once-through" forced convection boilers with which this report is concerned, this downstream termination of annular flow is an important location, and the parameters which determine it are very much of interest, but the boiler must operate around this phenomenon, and not be limited by it.

In order to prevent entrainment of liquid into the vapor or to force the deposition of entrained liquid on the wall, boiler tube inserts are usually used. These may be of many configurations, but almost all rotate the fluid about the tube axis to promote phase separation by centrifugal force. The most commonly used inserts are:

1. A plug with helical passages on the periphery.
   This has been used in the low quality region where the decreased flow area may be necessary to bring the vapor velocities up, thereby strengthening the separation forces.
2. One or more helical vanes wrapped about a cylindrical centerbody.
   The centerbody lies along the tube axis, and may carry temperature and pressure instrumentation in experimental boilers, but its primary purpose is as a support for the vane.
3. A twisted tape helical divider.
   This divides the boiler tube into two passages. It requires no centerbody for support.
4. A helical wire insert.
   This is simply a wire coil spring whose wire diameter and coil pitch can be chosen over wide limits. Sometimes a centerbody is used with wire coils to locate the coil axially (through struts). If the centerbody is as large as the inside diameter of the coil, the action of the insert is in most respects identical to that of a single

vane helix.

5. Single vane helix without centerbody.

   Such an insert has been used but its fabrication and support in the boiler both present difficulties.

It is clear that these inserts must have a significant effect upon the processes occurring in the boiler, and not all of the inserts affect a process in the same way. The nature of the insert, if any, must be considered in the analysis of forced convection boiling processes.

Not all of the processes to be expected in a forced convection boiler are of equal importance to the designer. From a practical point of view, it probably makes little difference in the process of boiler design whether the flow early in the boiler is characterized by a homogeneous mixture of vapor and liquid, or by annular separated flow. In either case, the heat transfer conductances to be expected are higher than the already large liquid metal conductances of the inlet flow. (Which of these two regimes exists at a location may have a large effect on the amount of liquid entrained in the vapor at downstream locations, however.) On the other hand, it is of extreme importance to the designer to know what are the conditions controlling processes in the region of, and past the end of, the annular film, since the overall length of the boiler is strongly affected by the location of this region.

In the study reported here, primary emphasis has been placed upon the analysis of processes which would be of maximum interest to a designer of practical equipment (although not all such processes have been considered).

As may be inferred from the foregoing discussion, most forced convection processes are, in detail, extremely complex, and a comprehensive analysis of a particular process might be expected to yield quite complex and unwieldy results and, in addition, be filled with assumed functional relationships of unknown merit. Such analyses have been avoided in the present work. The analyses presented here

are based on simple models of the flow, and the idealizations upon which the models are based are described in detail. The analytical results are simple enough in most cases so that the interrelationship between controlling parameters may be understood readily. Such simplicity, of course, limits the applicability of the analytical result to ranges in which the real flow is suitably approximated by the idealized model. In many cases, it is possible to establish the applicability range analytically, and this has been done. In other cases the reader must use his judgment as to the applicability of a given analysis for a particular set of parameter values.

II. ANALYTICAL STUDIES

A. Flow Through Tubes Containing Helical Wire Inserts

1) Helical Wires With Very Short Pitch-Tube Diameter Ratios

The investigation of single phase pressure drop in tubes containing helical wire coils has shown that for very short pitch coils a good approximation of the pressure drop may be obtained by considering flow in a tube containing annular rings.

A wire ring whose diameter is small compared to the diameter of the tube lies in the boundary layer of the flow in the tube. The boundary layer flow, which is separated from the tube wall downstream of the wire may or may not reattach to the wall before the next wire is encountered, depending upon the helix pitch. For the longer pitches used in General Electric experiments described in References 1, 2, 3, and 4, the boundary layer reattaches to the wall before the next wire is encountered, but reattachment does not occur for the shorter pitches.

In the case of the model of axial flow in a tube with annular rings, one would expect that a maximum would occur in the pressure drop versus ring spacing curve at the shortest pitch for which the flow still reattaches to the wall between rings, and that the pressure drop function would decrease somewhat with closer spacing. The pitch at which this maximum occurred would be dependent upon the relative diameter of the rings, since this height controls the reattachment length.

In order to relate the pressure drop in such a tube to other configurations which have been studied, a brief discussion will be made of the flow through a tube containing annular rings.

Where the ridge spacing is wide compared to the height of the ridge, a relatively small stalled area in the tube wall boundary layer will exist upstream of the ridge, and a relatively large recirculating stall will lie downstream of the ridge. If the ridge spacing is wide enough, the main stream will expand behind the ridge and reattach to the wall before the next ridge is encountered. An extensive study of two-dimensional plane stalled regions is given by Abbott in Reference 5. Although the present case is axially symmetric, the flow patterns are similar.

Downstream of the reattachment point a laminar boundary layer grows and changes to turbulent, just as in the entrance region of a tube, although the turbulence level is very high due to the eddies in the free shear layer coupling the main stream and the recirculation. It will be recognized that in the axially symmetric case the flow described is similar to that in the familiar orifice meter, and it will be remembered that the pressure fluctuations in the orifice meter are due to very high turbulence levels downstream of the orifice plate.

Where the spacing of the ridges is short compared to their height, the flow will not reattach to the wall. Instead it will expand very little between ridges and the apparent tube diameter will be essentially the minimum diameter of the ridges. In the cavities between, a recirculating flow will be coupled to the main stream by a free shear layer, again of very high turbulence level. The pressure loss between ridges in this latter case will be less than in the case of reattachment, because there is no acceleration between the ridges.

Between the reattached flow case (wide spacing) and completely separated case (short spacing), a region will be encountered in which the flow oscillates between these two cases with time, or in which some cavities are completely separated and others reattached, leading to pressure drop characteristics between the two extremes.

Corrugated tubing and piping, which has been in use for many years and which has been investigated fairly extensively, has flow patterns quite similar to those just described, although it has only been fairly recently observed that the friction factors depend as strongly as they do upon corrugation pitch and height (reference 6). The ranges of some of the early friction factor correlations for these tubes are very narrow.

In the case of tubes containing short pitch helical wire inserts, the flow pattern is virtually the same, although now, since the recirculating regions are connected a pressure gradient will exist parallel to the wire, and the fluid in the stalled regions will drift helically downstream. Thus, in a flow visualization experiment using dyes, the concentration of dye in the stall downstream of the wire has a helical motion. Such a photograph, taken from Reference 3, is shown in Figure 1. The main flow need not have any significant rotation at all for this helical motion to be observed, since it is the local pressure gradient in the stall which is causing the motion.

A comparison of a non-wetting two phase flow such as mercury-air in glass in a short pitch helical wire system and in a helical vane system of the same pitch and quality shows that the liquid component on the wall lies <u>downstream</u> of the helical wire, and <u>upstream</u> of the

Tube I.D. = 0.875 in. X = 0.84 p/D = 0.83

Wire Dia. = 0.125 in. ΔP = 0.348 psi/ft d_w/D = 0.143

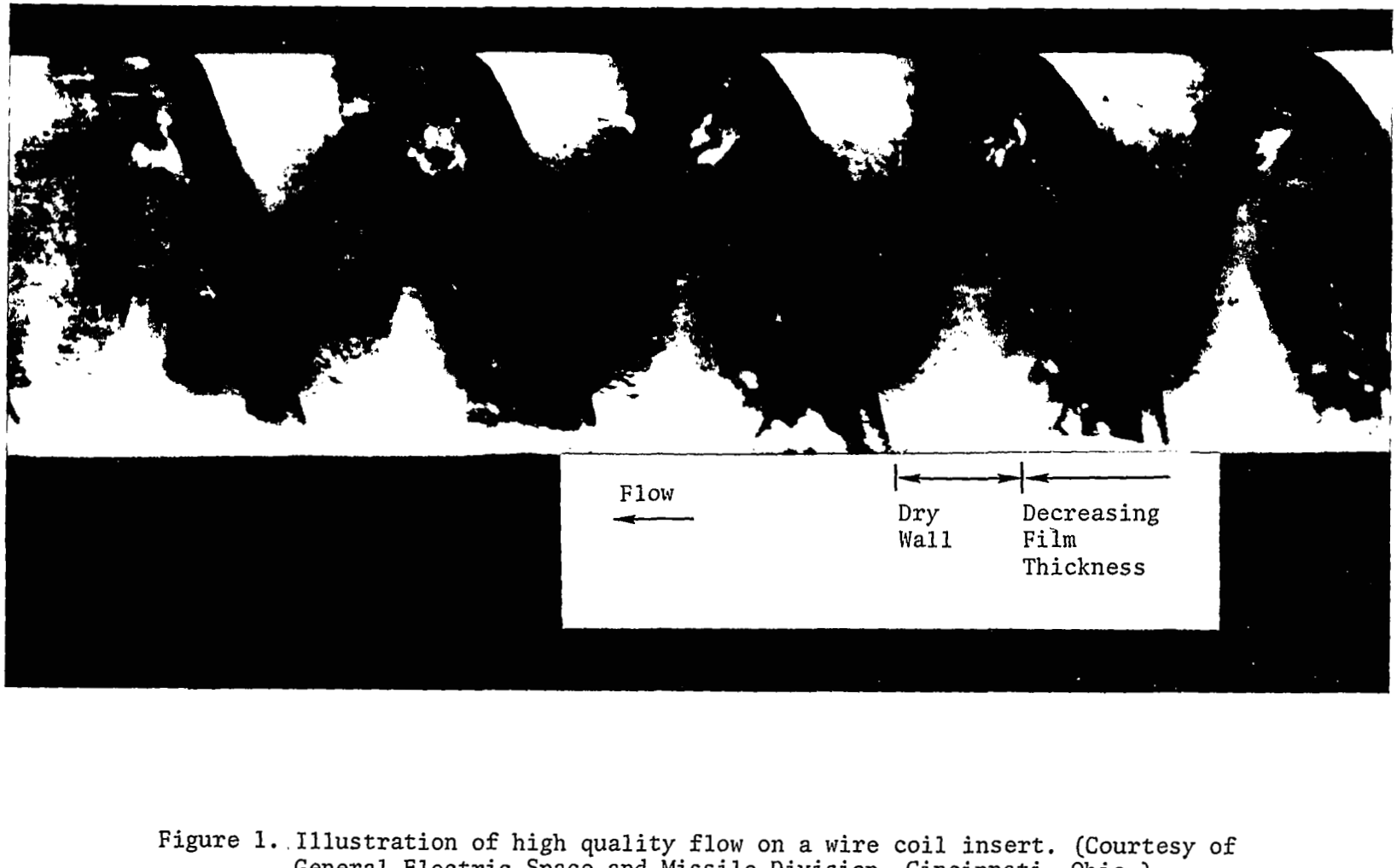

Figure 1. Illustration of high quality flow on a wire coil insert. (Courtesy of General Electric Space and Missile Division. Cincinnati, Ohio.)

helical vane. Secondary flows and the leakage between the vane and tube wall cause the liquid to pile up against the vane. This comparison also shows much less fluid against the wall in the helical wire system since the helical wire does not remove the liquid from the main stream as effectively.

Abbott has given a relationship for the approximate length of the stall behind a single backward facing step, which may be used to compute the minimum pitch for which a reattached flow may be expected. Since Abbott's relationship is for plane rather than axially symmetric flow, and does not consider either the effect of the next downstream ridge or the contraction upstream of the ridge, the minimum pitch obtained from his work would be expected to be less than that actually encountered. The criterion for reattached flow based on Abbott's work may be reduced to

$$\frac{p}{D} > 2.89 \quad \frac{d_w}{D} \qquad (1)$$

The line of points coinciding with this relationship is shown on the friction data due to Sams[7] and Converse[8] in Figure 2. The data point represented by Figure 1, which clearly shows reattached flow, appears at p/D = .83. Also shown on this graph are several friction factor measurements taken from corrugated tube pressure drop experiments.[9,10]

The minimum pitch for a helical wire coil system is that in which the adjacent coils touch each other, i.e., $p/D = d_w/D$. Two of the points due to Sams are for this case. It is clear that a large portion of the increase in friction factor for close-wrapped coils is due to the decreased flow area, since the effective diameter of the tube is smaller by twice

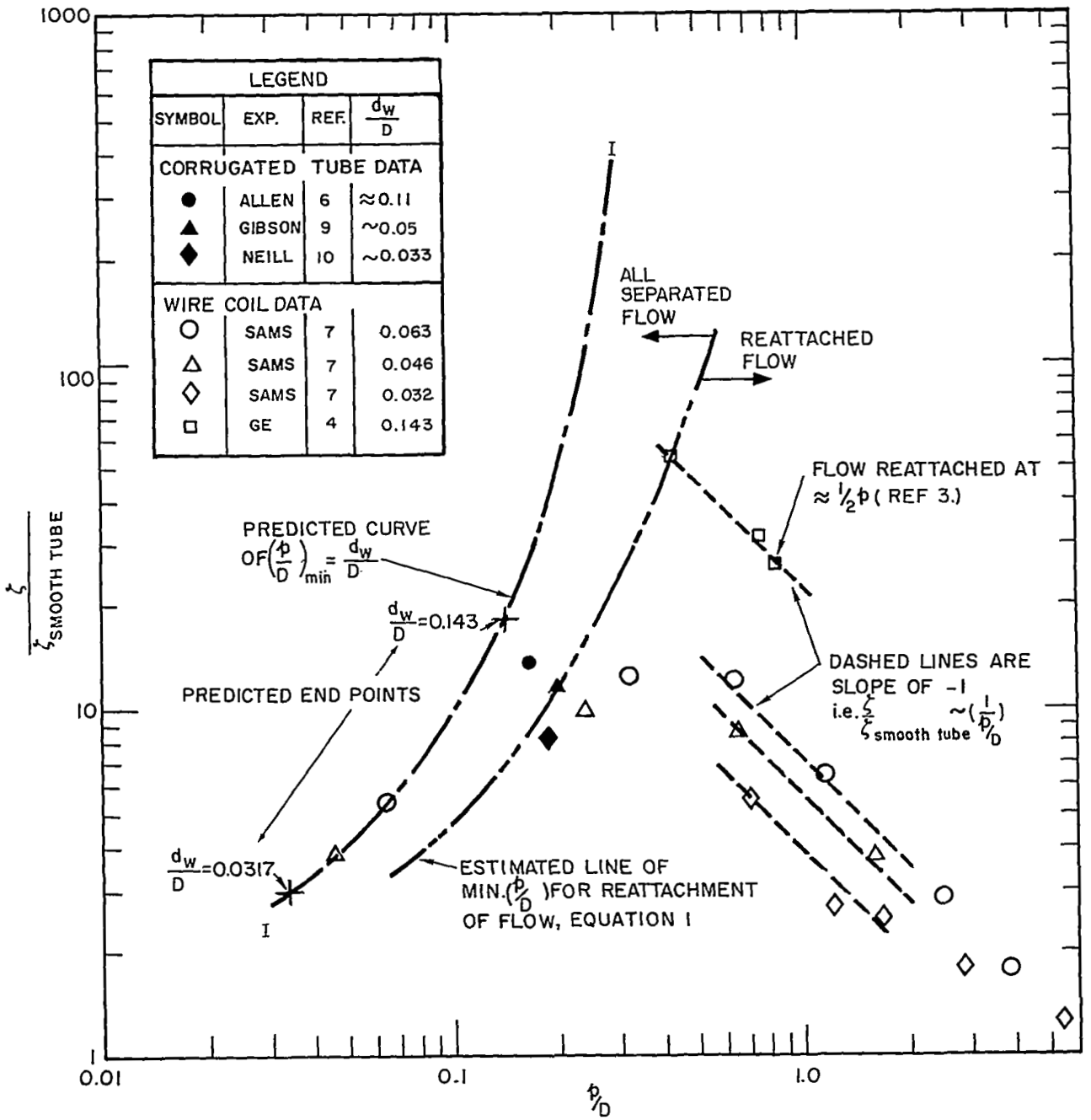

Figure 2. Helical wire coil friction factors as functions of flow regimes.

the thickness of the wires. It may be shown that the ratio of the friction factor based upon the tube diameter to that based upon the wire coil inside diameter is

$$\frac{\zeta_D}{\zeta_{D_m}} = \left(\frac{1}{1 - 2 \frac{d_w}{D}} \right)^5 \qquad (2)$$

where

ζ , friction factor

D , tube diameter

D_m, coil inside diameter

d_w , wire diameter

The quantity ζ_{D_m} , is a function also of d_w/D where d_w/D is essentially a measure of tube "roughness." This quantity has been taken from Sams' data and corrugated tube data from References 6, 8, 9, and 10. The predicted curve of minimum pitch friction factor, based on these sources is also shown on Figure 2 as line I-I. Predicted asymptotes for some of the helical coil cases are indicated on this line.

In the cases where the flow reattaches to the wall the pressure drop due to the annular rings is much greater than that due to wall friction and it may be expected that the pressure drop would be directly proportional to the number of rings in the tube, which is inversely proportional to the pitch. In this case, the slope of the friction factor versus pitch should be -1. That this appears to be the case is also shown in Figure 2.

As the spacing becomes very large compared to the reattachment length, two other effects will begin to control the pressure drop. The first of these is that the wall friction becomes a significant portion of the pressure drop. The other is that rotation of the core flow becomes significant. The friction factor may, therefore, be expected to asymptotically approach the value for a smooth tube at large pitch. It should be observed, however, that the wall boundary layer downstream of an annular ring is an inlet boundary layer with friction factor higher than that for a fully established flow. The "entrance" effects would not be expected to be negligible for 25 or more diameters downstream.

2) Fully Established Flow Through Tubes Containing Helical Wires With p/D Greater than about 0.8

In a long tube containing only a helical wire insert, some rotation of the core flow may be expected to occur, since a component of the drag force exerted upon the fluid by the wire is in the direction to cause rotation. A simple model of this flow has been developed. The model studied consists of a fluid flowing in a tube containing a helical wire insert. The helical wire insert causes a torque on the fluid which rotates it in the direction of the coil, and skin friction opposes the rotation. Making the idealization that the fluid bulk rotates as a solid body, but slips with respect to the wire insert, an equation may be written for the balance of forces in the direction of rotation normal to the tube axis. The wire geometry and force system directions are shown in Figures 3a and 3b.

The force exerted on the fluid by the wire, measured in the direction normal to the wire, is

$$F_n = C_D \, d_w \, \ell_w \, \frac{1}{2} \rho \, v_n^2 \qquad (3)$$

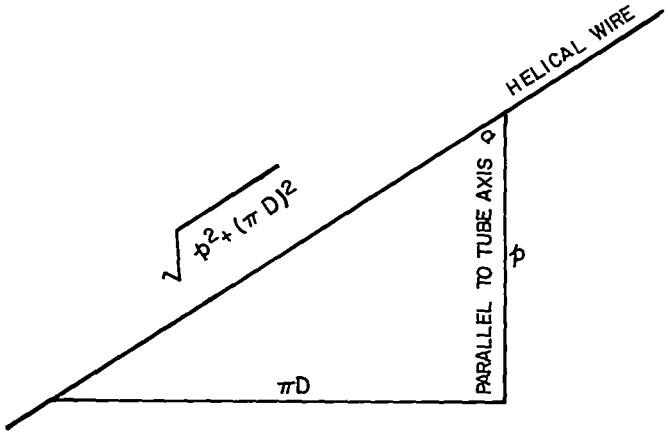

Figure 3a. One pitch length of helical wire, unrolled.

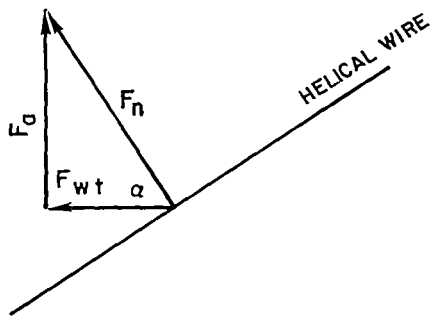

Figure 3b. Force system exerted on fluid by wire.

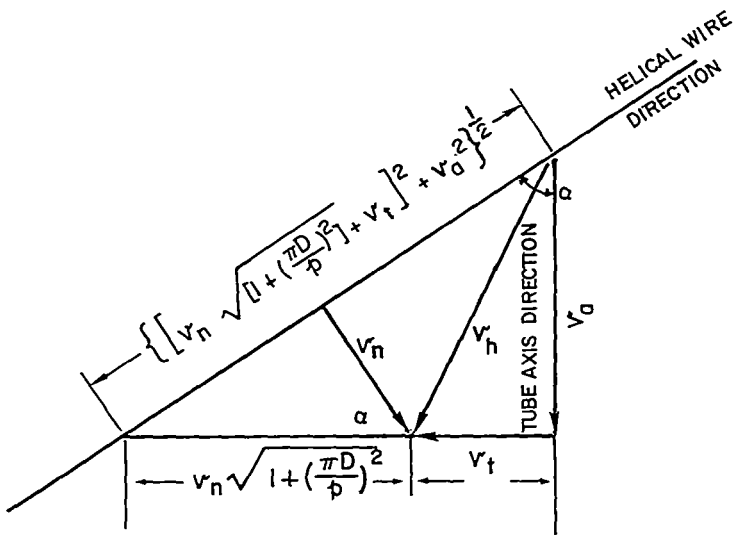

Figure 3c. Velocity components.

where d_w, wire diameter

ℓ_w, wire length

C_{D_w}, drag coefficient

ρ, fluid density

v_n, velocity component normal to wire.

ℓ_w, the actual wire length, is given by

$$\ell_w = \ell_a \sqrt{1 + \left(\frac{\pi D}{p}\right)^2} \tag{4}$$

where ℓ_a, axial tube length

p, wire helix pitch

D, tube inside diameter

The component of F_n in the direction normal to the tube axis is

$$F_{wt} = \frac{F_n}{\sqrt{1 + \left(\frac{\pi D}{p}\right)^2}} \tag{5}$$

The frictional force in the direction normal to the tube axis is

$$F_{ft} = \frac{\zeta}{8} \rho v_t^2 \pi D \ell_a \tag{6}$$

where ζ, friction factor (0.02 used in the calculations)

v_t, velocity component normal to tube axis, at inside tube wall, neglecting boundary layer effects

Where the flow is fully established, so that v_t is not changing, the following force balance must hold:

$$F_{ft} = F_{wt} \tag{7}$$

therefore

$$C_{D_w} d_w v_n^2 = \frac{\zeta}{4} \pi D v_t^2 \tag{8}$$

or by rearrangement,

$$\frac{v_n}{v_t} = \left(\frac{\zeta \pi D}{4 C_D d_w} \right)^{1/2} \tag{9}$$

From Figure 3c, it may be determined that

$$v_n = \frac{\left(\frac{\pi D}{p} v_a - v_t \right)}{\sqrt{1 + \left(\frac{\pi D}{p} \right)^2}} \tag{10}$$

This relationship may be used to eliminate v_n from Equation (9) to yield

$$\frac{v_t}{v_a} = \frac{\frac{\pi D}{p}}{\left\{ \kappa \left[1 + \left(\frac{\pi D}{p} \right)^2 \right] \right\}^{1/2} + 1} \tag{11}$$

where v_a is mean axial velocity

$$\kappa = \frac{\pi \zeta D}{4 C_{D_m} d_w}$$

C_{D_m}, a modified wire frontal drag coefficient, is defined by

$$C_{D_m} = 1.41 \left(\frac{d_w}{D} \right)^{2/7} C_{D_w} \tag{12}$$

This modified drag coefficient includes the decrease in velocity of the flow impinging on the wire due to the tube boundary layer. The form is based on a 1/7 power velocity profile. C_{D_w} has been taken equal to unity.

If the flow did not slip with respect to the wire, the velocity ratio would be

$$\left(\frac{v_t}{v_a}\right)_{\text{no slip}} = \frac{\pi D}{p} \tag{13}$$

The ratio of rotational velocity with slip to that without slip is there-

$$\frac{v_{t\,\text{slip}}}{v_{t\,\text{no slip}}} = \frac{1}{\left\{\kappa\left[1 + \left(\frac{\pi D}{p}\right)^2\right]\right\}^{1/2} + 1} \tag{14}$$

A graph of this relationship as a function of coil pitch and coil wire diameter ratio is shown in Figure 4 .

The axial pressure drop consists of two terms. One of these is the skin friction increase due to the angular motion. Neglecting both the change in equivalent diameter caused by the presence of the wire and change in friction factor due to higher helical flow Reynolds number, the friction term is

$$\frac{\Delta p_f}{\zeta \frac{\ell_a}{D} \frac{1}{2} \rho v_a^2} = \frac{\ell_h}{\ell_a}\left(\frac{v_h}{v_a}\right)^2 \tag{15}$$

where ℓ_h, helical flow path length along surface

v_h, surface helical velocity with slip (neglecting boundary layer effects)
$= \sqrt{v_t^2 + v_a^2}$

The quantity $\zeta \frac{\ell_a}{D} \frac{1}{2} \rho v_a^2$ is of course the pressure drop for an axial flow through a smooth tube.

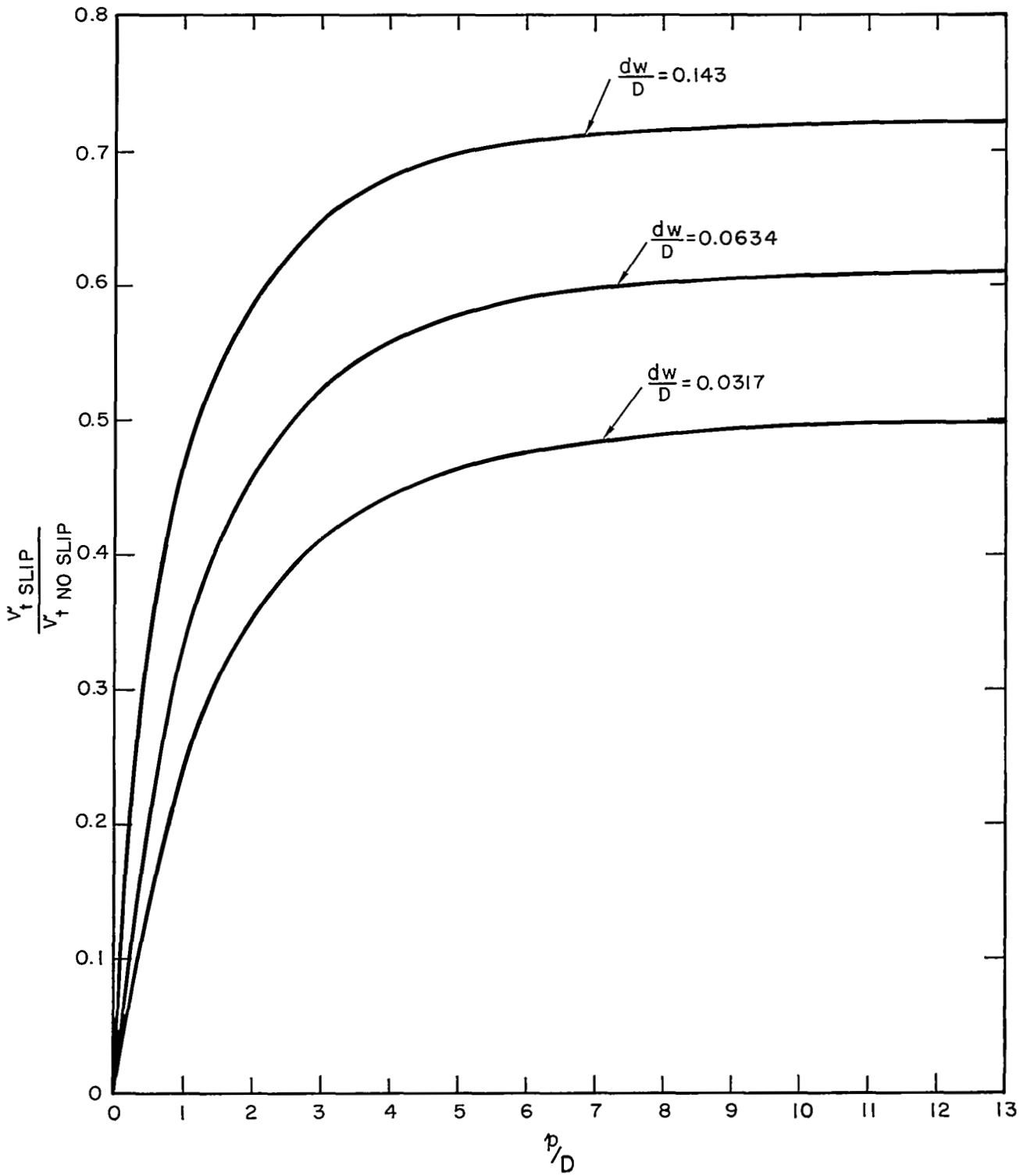

Figure 4 Rotating component of velocity as a function of pitch and wire diameter.

The second term in the axial pressure drop is due to the axial component of drag on the helical wire. Normalized on the same basis as the friction term, this component is

$$\frac{\Delta p_{drag}}{\Delta p_{smooth}} = \frac{\left(\frac{\pi D}{p}\right)^3}{\left[\left\{\kappa\left[1 + \left(\frac{\pi D}{p}\right)^2\right]^{1/2}\right\} + 1\right]^2} \qquad (16)$$

From geometry,

$$\frac{\ell_h}{\ell_a} = \frac{v_h}{v_a}$$

$$= \left[1 + \left(\frac{v_t}{v_a}\right)^2\right]^{1/2} \qquad (17)$$

The pressure drop in a tube containing a long pitch helical wire may be written

$$\frac{\Delta p_{hw}}{\Delta p_{smooth}} = \left\{1 + \frac{\left(\frac{\pi D}{p}\right)^2}{\left[\kappa\left(1 + \left(\frac{\pi D}{p}\right)^2\right)\right]^{1/2} + 1}\right\}^{3/2} + \frac{\left(\frac{\pi D}{p}\right)^3}{\left\{\left[\kappa\left(1 + \left(\frac{\pi D}{p}\right)^2\right)\right]^{1/2} - 1\right\}^2} \qquad (18)$$

A graph of this function, using values of κ appropriate to helical wires for which friction factor data are available is shown in Figure 5.

It may be seen that the analytical curves have the same shape as the experimental data, and that the proper relationship between wire diameter ratio and friction pressure drop is predicted by the analysis. For the larger diameter wires the agreement between analysis and experiment is very good. The pressure drop for small diameter wires is overestimated by the analysis.

As can be observed in Figure 4, the slip becomes quite large for small diameter wires and short pitches, and it might be expected that departure from solid body rotation, disturbance to the velocity profile, (which probably bears little similarity to a 1/7 power velocity distribution at short pitches) and in-

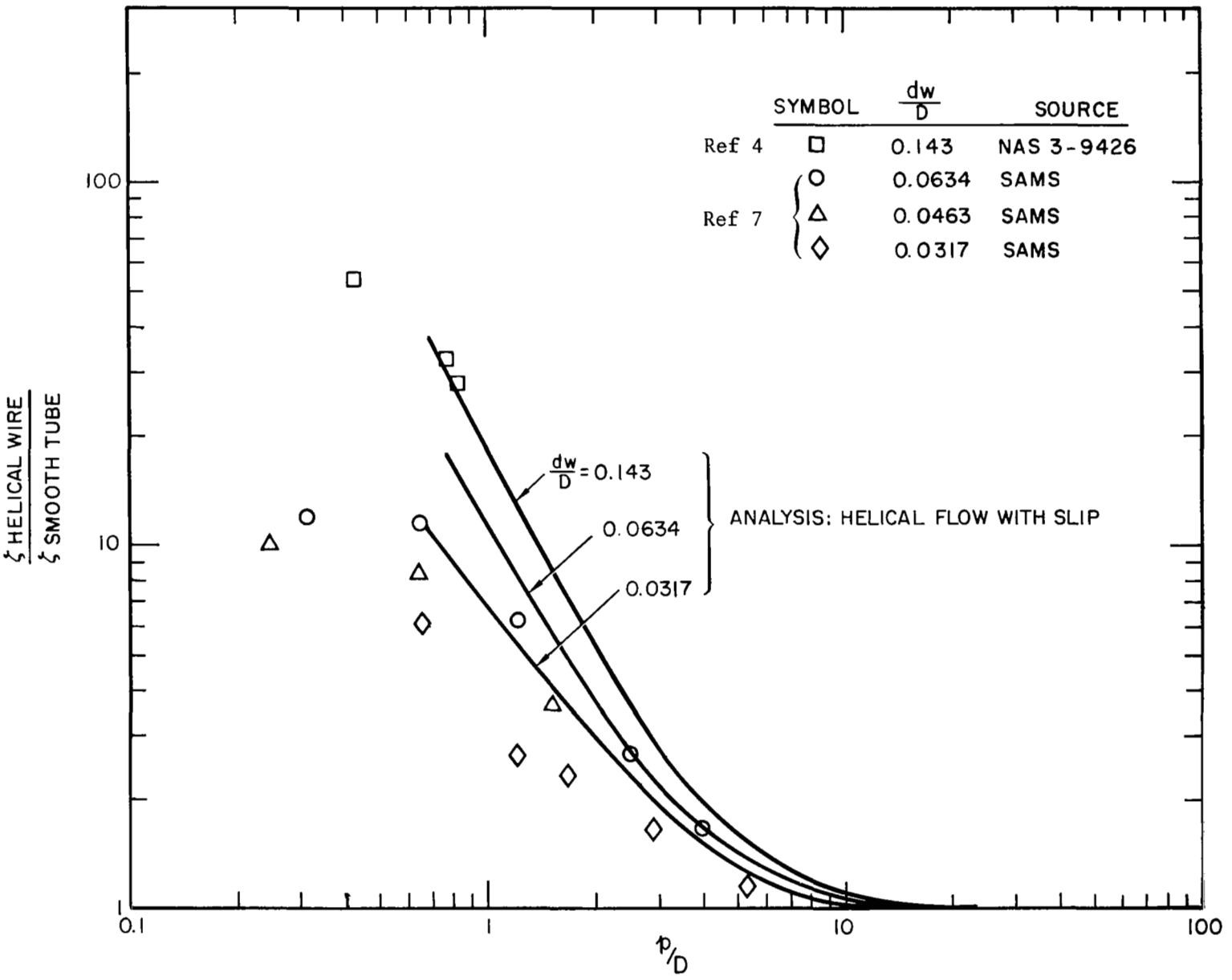

Figure 5. Comparison of helical wire pressure drop data with analysis.

creased amount of the surface area involved in the recirculating stalled areas downstream of the wires, all contribute to cause departure of the actual flow from that modeled. One would expect also that flows through thick wire coils which allow less slip at a given pitch than thin wires would more closely approximate the model flow, and this does appear to be the case.

The analysis should be adequate for making pressure drop calculations for wires of $d_w/D > 0.06$ at $p/D > .8$. Additional discussion of the comparison of Sams' data and the analysis may be found in the next section.

3) Transition From A Wire-Wrapped Plug to a Helical Wire Insert

Consider the single phase fluid which flows through a tube with an abrupt change in insert geometry. The insert geometry changes from a helical vane to a helical wire coil at the station $\ell_a = 0$. The pitches of the two inserts need not be the same. The asymptotic case to which this transition flow tends far downstream is given by the preceeding section of this report. The initial rotation is known since the fluid is constrained to follow the helical vane, and resembles solid body rotation. Thus, the transition flow may be modeled as a flow with solid body rotation which decays from one known value to another known value. The damping forces causing the rotation to decay may be extracted from the asymptotic solution represented by the helical coil analysis of the preceeding section.

Consider the rotational accelerations on a mass of fluid rotating as a solid body. The equation of motion is

$$M = I \frac{dw}{dt} \qquad (19)$$

where M, applied torque

I, rotational moment of inertia

w, angular velocity

t, time

Since the axial velocity is a constant through the transition process, axial distance and time are linearly related, so that

$$dt = \frac{d\ell_a}{v_a} \tag{20}$$

where ℓ_a, axial length

v_a, axial mean velocity

The angular velocity may be related to the velocity component parallel to the surface and normal to the tube axis so that

$$w = \frac{2\, v_\theta}{D} \tag{21}$$

where v_θ, velocity component normal to the tube axis

D, tube diameter

The moment of inertia of a fluid mass one pitch length long is

$$I = \frac{\rho\, p\, \pi\, D^4}{32} \tag{22}$$

where ρ, fluid density

p, helical wire pitch length

The torque applied to the fluid mass is equal to the difference between the wire drag force component exerted in the direction of rotation, and the wall shear

force component exerted opposite to the direction of rotation, both multiplied by the inside radius of the tube. From Equations (3), (4), (5), and (6) (preceeding Section) this net torque in the direction normal to the tube axis is equal to

$$M = \left(C_D d_w p \frac{1}{2} \rho v_n^2 - \frac{\zeta}{8} \rho \pi D p v_t^2 \right) \frac{D}{2} \qquad (23)$$

From Equation (10)

$$v_n = \frac{\left(\frac{\pi D}{p} v_a - v_t \right)}{\sqrt{1 + \left(\frac{\pi D}{p} \right)^2}} \qquad (24)$$

Equations (19), (20), (21), (22), (23), and (24) may be combined to yield a differential equation relating v_t and ℓ_a.

This equation is

$$\left[C_D d_w p \frac{1}{2} \rho \frac{\left(\frac{\pi D}{p} v_a - v_t \right)^2}{1 + \left(\frac{\pi D}{p} \right)^2} - \frac{\zeta}{8} \rho \pi D p v_t^2 \right] = \frac{\rho p \pi D^2 v_a}{8} \frac{dv_t}{d\ell_a} \qquad (25)$$

Define the following normalized variables:

$$\bar{\ell} = \frac{\ell_a}{p}$$

$$\bar{v}_t = \frac{v_t}{v_{t_f}}$$

where v_{t_f}, asymptotic value, given by Equation (11).

By use of Equation (11),

$$\bar{v}_t = \frac{v_t}{v_a \frac{\pi D}{p}} \left[\left\{ \kappa \left[1 + \left(\frac{\pi D}{p} \right)^2 \right] \right\}^{1/2} + 1 \right] \qquad (26)$$

where κ, defined as before $\kappa = \frac{\pi \zeta D}{4 C_{D_m} d_w}$

Introduction of the dimensionless variables and rearrangement yields

$$\bar{v}_t^2 \left\{ \frac{1 - \sqrt{\kappa \left[1 + \left(\frac{\pi D}{p}\right)^2\right]}}{\left[1 + \left(\frac{\pi D}{p}\right)^2\right]} \right\} \frac{4 C_D d_w}{D} + \frac{8 C_D d_w}{D \left[1 + \left(\frac{\pi D}{p}\right)^2\right]} \bar{v}_t$$

$$- \left\{ \frac{1 + \sqrt{\kappa \left[1 + \left(\frac{\pi D}{p}\right)^2\right]}}{\left[1 + \left(\frac{\pi D}{p}\right)^2\right]} \right\} \frac{4 C_D d_w}{D} = - \frac{d\bar{v}_t}{d\bar{\ell}} \qquad (27)$$

This differential equation is of the form

$$a \bar{v}_t^2 + b \bar{v}_t + c = - \frac{d\bar{v}_t}{d\bar{\ell}} \qquad (28)$$

The equation is separable and easily integrated. If $\bar{\ell}$ is measured so that the insert type changes at $\bar{\ell} = 0$, then the initial condition is

$$\bar{\ell} = 0, \quad \bar{v}_t = \bar{v}_{t_1} \qquad (29)$$

After integration and considerable algebra, the result may be written in the form

$$\bar{v}_t = \left(\frac{1}{1 - \mu}\right) - \left(\frac{\mu}{1 - \mu}\right) \frac{1 + k_2 e^{-k_1 \bar{\ell}}}{1 - k_2 e^{-k_1 \bar{\ell}}} \qquad (30)$$

where $\mu = \sqrt{\kappa \left[1 + \left(\frac{\pi D}{p}\right)^2\right]}$

$$k_1 = \sqrt{b^2 - 4ac}$$

$$= 4 \sqrt{\frac{\pi \zeta C_D d_w}{D \left[1 + \left(\frac{\pi D}{p}\right)^2\right]}}$$

and

$$k_2 = \left[\frac{\bar{v}_{t_i} - 1}{\bar{v}_{t_i} + 1 - \frac{2}{1 - \mu}}\right]$$

For the special cases in which the helical vane and the helical wire inserts have the same pitch.

$$\bar{v}_{t_i} = \sqrt{\kappa \left[1 + \left(\frac{\pi D}{p}\right)^2\right]} + 1 \tag{31}$$

$$= \mu + 1 \tag{32}$$

This result is taken directly from Equation 14. The solution then reduces to

$$\bar{v}_t = \frac{1}{1 - \mu} \left\{ 1 - \mu \frac{(1 + \mu) - (1 - \mu)\, e^{-k_1 \bar{\ell}}}{(1 + \mu) + (1 - \mu)\, e^{-k_1 \bar{\ell}}} \right\} \tag{33}$$

A graph of this function is shown in Figure 6.

The characteristic length for this transition is

$$\mathcal{L} = \frac{p}{k_1} \tag{34}$$

Two graphs of this function are given here. In Figure 7, $\mathcal{L}/p$ is shown as a function of wire diameter and helix pitch. In Figure 8, $\mathcal{L}/D$ is shown. For the longer pitch helices, fewer turns are necessary for the flow to accommodate to the new conditions, but a greater tube length is required because of the lengthened pitch.

It is interesting that many diameters of tube are necessary for flow accommodation. It appears that for long pitches and small wire diameters, fully established flow would be rather difficult to attain.

The tube which Sams (Reference 7) used to obtain his data for helical wire systems was 0.41 inch ID and 24 inches long for a ℓ/D ratio of 59. This

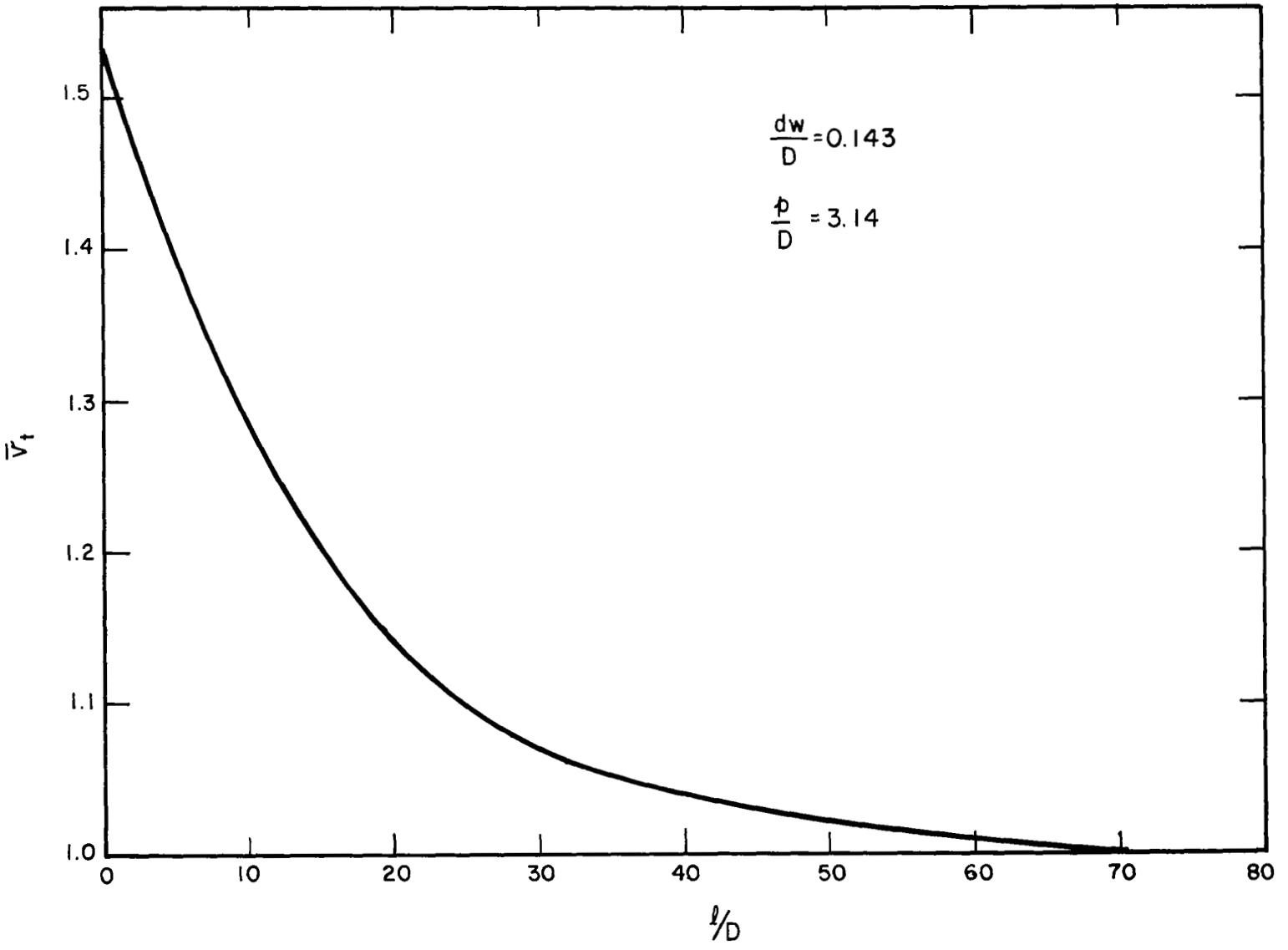

Figure 6. Change in rotational velocity of a flow passing from a helical vane insert to a helical wire insert, both of the same pitch.

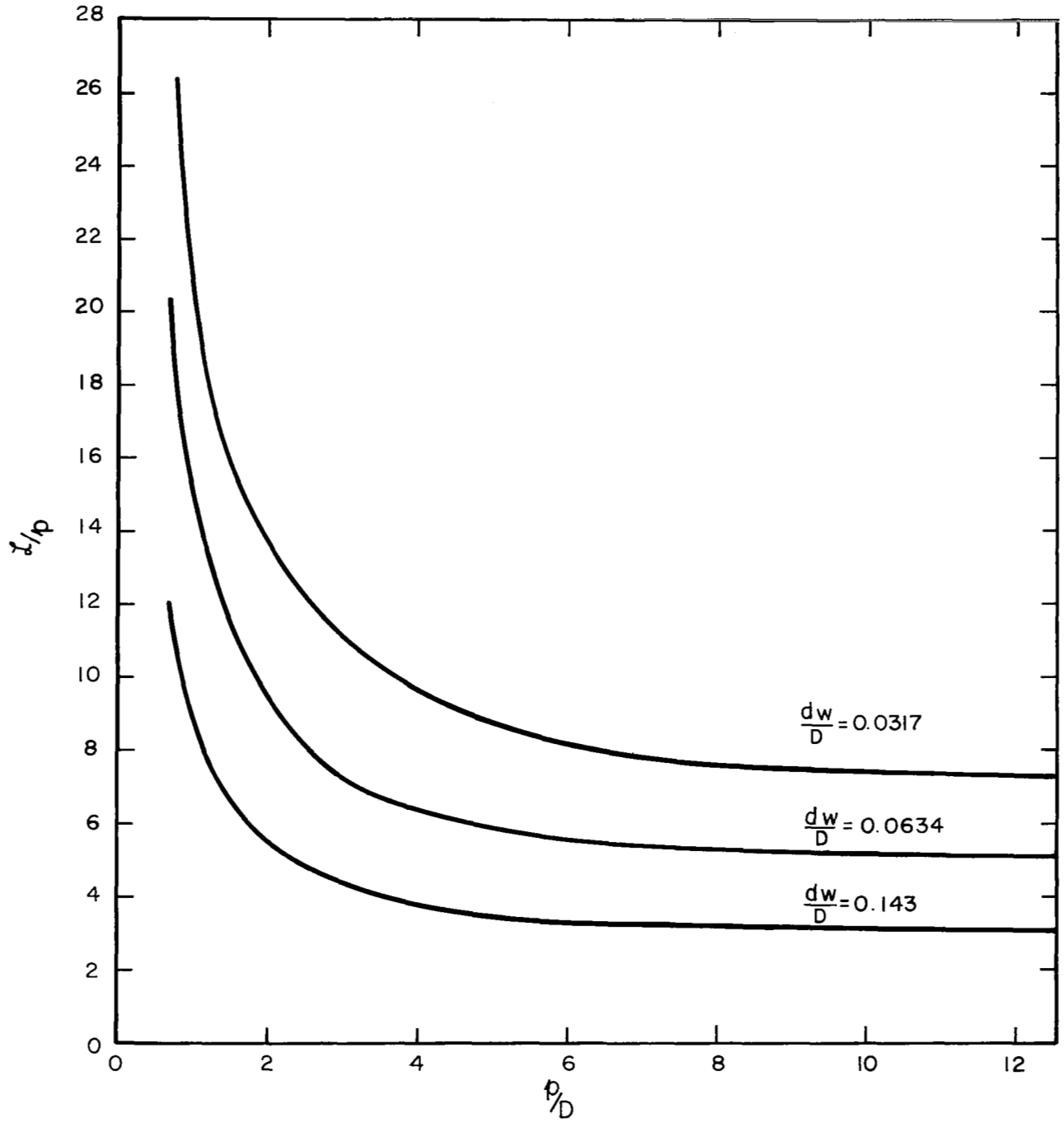

Figure 7. Characteristic length as a function of wire diameter and pitch, normalized using pitch length.

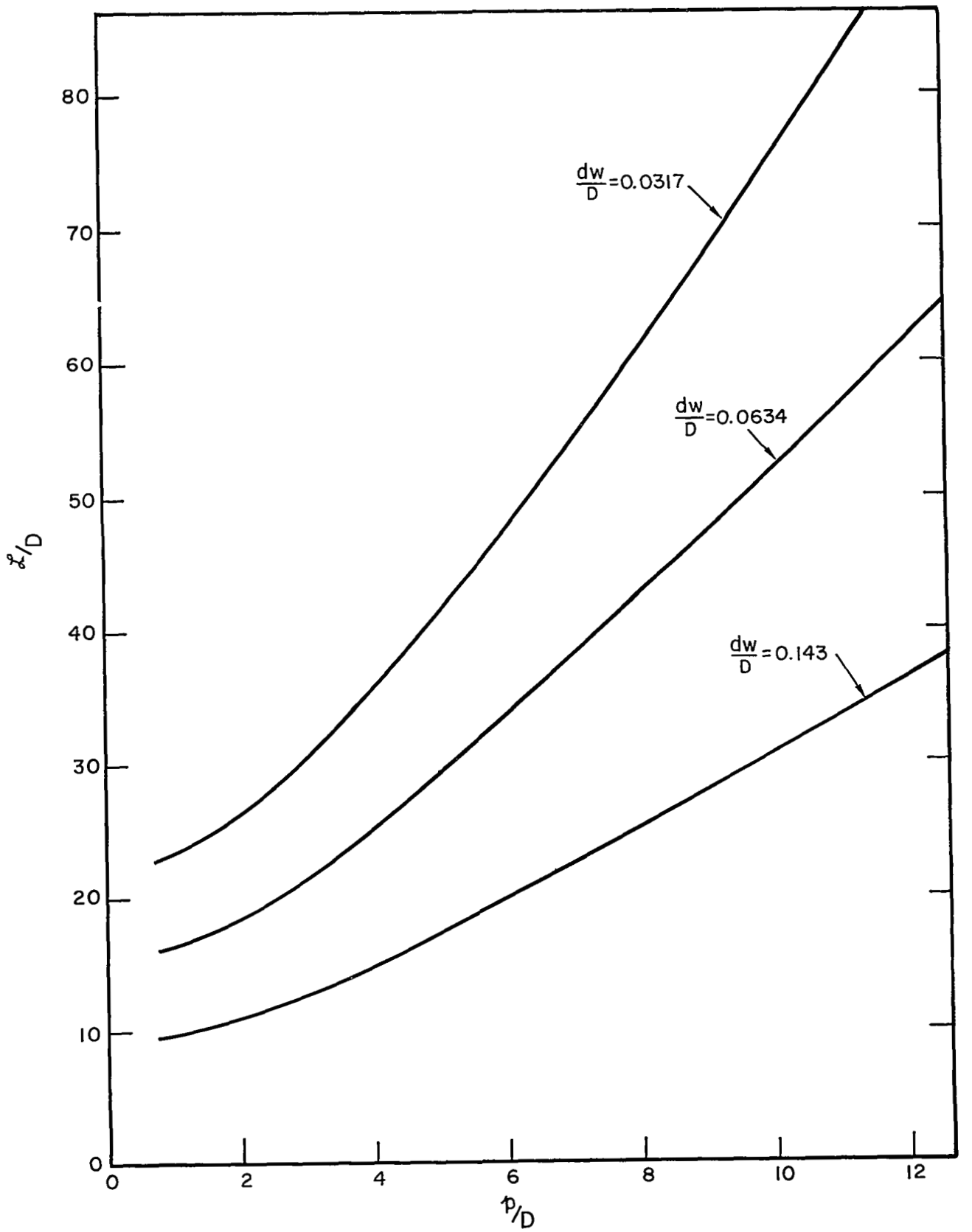

Figure 8. Normalized characteristic length.

length is barely adequate to obtain fully established turbulent flow in a smooth tube (Reference 11) and for the longer pitches he tested was probably inadequate in length for fully established rotational flow. Thus, one might expect his data to correspond to cases in which the flow is changing along the length. Unfortunately, he does not publish axial temperature profiles in which a variation, if it occurred, might be seen. It is certainly true that checks he made with no insert agree with published data for fully established flows. The inlet to the test section in his apparatus appears to have been a sharp-edged reduction, which because of the very high turbulence level generated, would tend to reduce the entrance length effects and make the smooth tube results agree more closely with published data, but this high inlet turbulence level would probably not enhance the rotational component accommodation significantly.

In the discussion of Section A2, the discrepancy found between predicted helical wire friction factors and Sams' experimental data for small wires was attributed to departure of the actual flow from that of the model. It is likely, however, that a portion of this discrepancy is actually due to the fact that flow was not fully established in the experimental apparatus.

4) Pressure Drop in the Transition to a Helical Wire Insert

The helical vane to helical wire transition results obtained in the preceeding section may be used to compute the integral average friction factor for a single phase flow through the transition. This is accomplished as follows.

First the equations for helical wire friction pressure drop are rewritten in terms of the rotational velocity component v_t. After transformation, these equations are as follows. Increase in friction due to longer helical path:

$$\frac{\Delta p_f}{\zeta \frac{\ell a}{D} \frac{1}{2} \rho v_a^2} = \left[1 + \left(\frac{v_t}{v_a}\right)^2\right]^{3/2} \qquad (35)$$

Pressure drop due to drag on helical wire

$$\frac{\Delta p_d}{\zeta \frac{\ell a}{D} \frac{1}{2} \rho v_a^2} = \frac{\pi D}{p} \left(\frac{v_t}{v_a} \right)^2 \tag{36}$$

The sum of these two terms, which is the normalized axial pressure drop, may be used to define a friction factor for helical wire flow, so that

$$\frac{\Delta p_{hw}}{\Delta p_{axial}} = \frac{\zeta_{hw}}{\zeta_a} \tag{37}$$

$$= \bar{\zeta}$$

In the transition flow v_t is a function of axial length from the transition. If it is assumed that the local friction in a changing flow is no different from that at the same local conditions in a fully established flow (a common assumption for varying flows) then a mean value for the helical wire friction factor may be defined.

$$\bar{\zeta}_{av} = \frac{1}{\bar{\ell}} \int_0^{\bar{\ell}} \bar{\zeta}(\bar{\ell})\, d\bar{\ell} \tag{38}$$

$$= \frac{1}{\bar{\ell}} \int_0^{\bar{\ell}} \left[1 + \left(\frac{v_t}{v_a} \right)^2 \right]^{3/2} d\bar{\ell} + \frac{1}{\ell} \frac{\pi D}{p} \int_0^{\bar{\ell}} \left(\frac{v_t}{v_a} \right)^2 d\bar{\ell} \tag{39}$$

The velocity component v_t in the transition from a helical vane to a helical wire of the same pitch is given by Equation (33). By definition

$$\bar{v}_t = \frac{v_t}{v_{t_{final}}} \tag{40}$$

$$= \frac{v_t}{v_a} \frac{v_a}{v_{t_f}} \tag{41}$$

The second ratio is a constant for a given wire system and is given by

$$\frac{v_{t_f}}{v_a} = \frac{\frac{\pi D}{p}}{1 + \mu} \tag{42}$$

With the relationships computed above, the average friction factor, which is a function only of the geometry and tube length, may be computed for a given case. Evaluation of the integrals must be done numerically, but may be accomplished with a computer. Once the average friction factor for a given geometry is computed, the helical wire transition section may be treated as a section of smooth tube.

5) Heat Transfer in the Transition to a Helical Wire Insert

The single phase heat transfer conductance for helical flow is given by Equations (216), (217), and (218) in Section E3. These relationships are based on the idealization that the forced convection effects and the free convection due to radial acceleration may be added linearly. For a helical wire system all of the equivalent diameters may be taken as equal, as a reasonable approximation. β, the volumetric thermal expansion coefficient is equal to 1/T for a perfect gas, where T is the absolute temperature. Re_ℓ is the linear flow Reynolds modulus, given by

$$Re_\ell = \frac{v_a D_e \rho_v}{\mu_v} \tag{43}$$

$$Nu_{\text{linear turbulent vapor}} = \frac{h D_e}{k_v}$$

$$= 0.023 (Re_\ell)^{0.8} (Pr)^{0.4} \tag{44}$$

From these relationships, and the concepts employed in the computation of the average friction factor in a varying flow, it may be shown that the average Nusselt modulus is given approximately by

$$\left(\frac{Nu_{\text{helical wire}}}{Nu_{\text{linear turbulent flow}}}\right)_{\text{average}} = \frac{1}{\bar{\ell}} \int_0^{\bar{\ell}} \left[1 + \left(\frac{v_t}{v_a}\right)^2\right]^{0.4} d\bar{\ell} + \frac{B}{\bar{\ell}} \int_0^{\bar{\ell}} \left(\frac{v_t}{v_a}\right)^{2/3} d\bar{\ell} \tag{45}$$

where $B = \dfrac{7.1\,(\beta\,\Delta T)^{1/3}}{Re_{\ell}^{0.13}\,Pr^{0.07}}$

Again, the integrations must be performed numerically, but they depend only on the geometry of the insert and its length, and are independent of the flow properties as long as the flow is single phase and turbulent.

B. The Motion of Droplets Entrained in a Vapor Flow

In the general case of forced convection boiling with entrained liquid, droplets of time- and space-varying size accelerate in a vapor stream which is non-uniform in three directions. A gravitational field, rotation about the tube axis, possible collisions between droplets or between droplet and wall, and droplet number density change by ejection from a liquid layer, may all add to the complexity of the motion in a general analysis.

It is clear that a single comprehensive treatment of droplet motion, even if suitable functional relationships were known, would be very difficult to interpret, and would be far too inclusive for many practical problems. In order to maintain the maximum utility in these analyses of this section, many restricted models of various aspects of entrained droplet motion have been analysed. Several models are also presented which are developed by synthesis of the simple models to study a complex motion.

1) Droplet Number Densities in a Boiler Tube Containing a Fog Flow

In a boiler tube with a dry wall at qualities less than unity, the number density of the droplets entrained in the vapor depends upon vapor quality X, vapor density ρ_v, liquid density ρ_ℓ, vapor velocity v_v, droplet velocity v_p, droplet diameter D_p, and tube diameter D. If the droplets are idealized as spherical, the relationship between the variables may be shown to be

$$N = 1.5 \left(\frac{1 - X}{X} \right) \frac{\rho_v}{\rho_\ell} \frac{1}{(v_p/v_v)\ (D_p/D)^3} \qquad (46)$$

where N is the number of droplets in an axial length equal to the tube diameter. This expression has been evaluated and is presented in Figure 9.

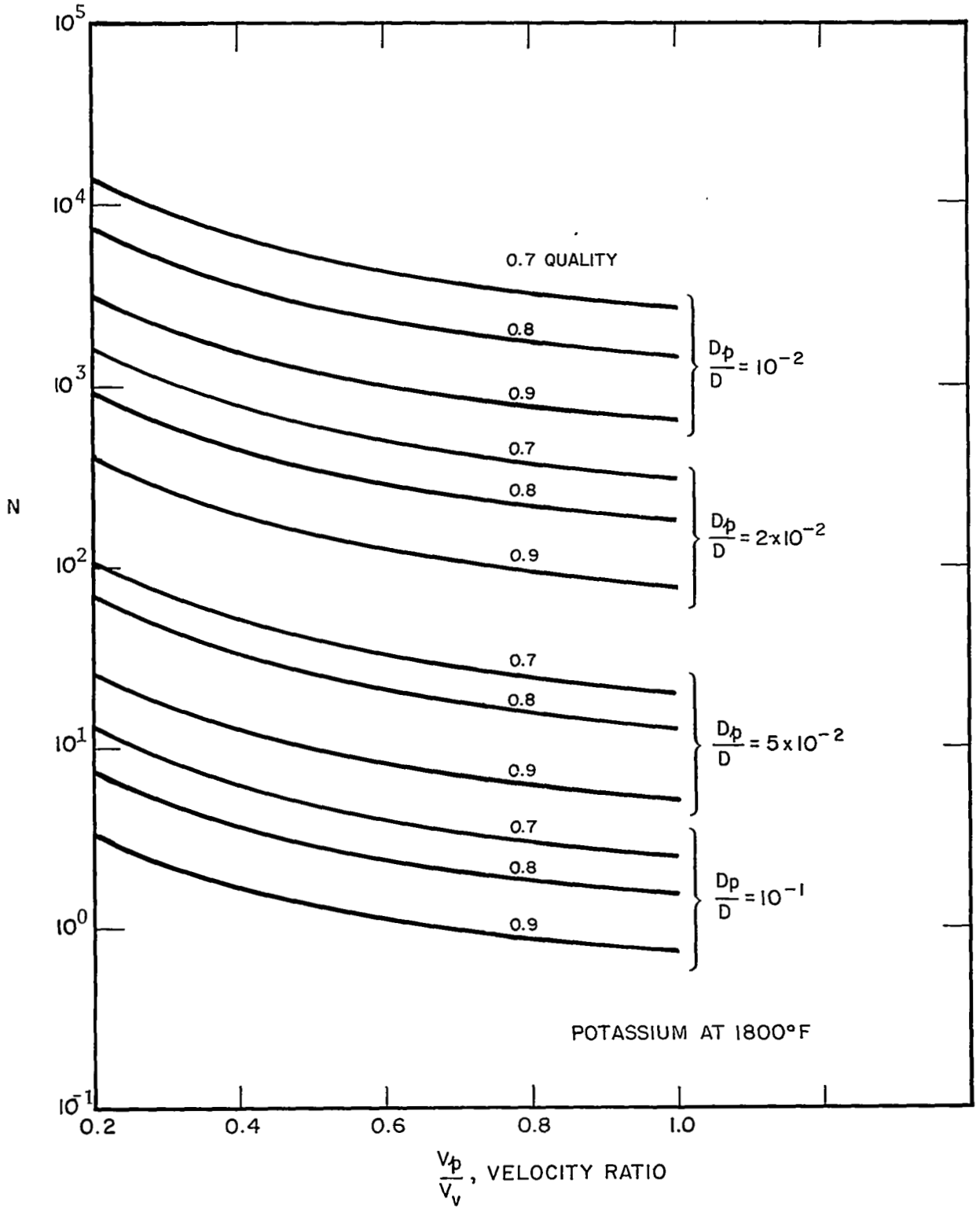

Figure 9. Number of droplets in an axial length equal to one diameter.

2) Axial Velocity Component of Constant Mass Droplets in a Uniform Velocity Stream

This analysis pertains to the motion of entrained droplets in an upward flowing vapor stream. In order to eliminate heat flux as a parameter in the analysis, the idealization is made that the change in vapor mass flow rate is small over the boiler length of interest.

Other idealizations are:

1) droplets are of constant mass
2) droplets are spherical
3) the flow is vertically upward so the gravitational field opposes the motion
4) the droplet drag coefficient is constant*
5) the liquid phase occupies negligible volume in the boiler
6) the pressure gradient is negligible

*For commentary on this simplification, refer to pages 52 and 55.

2) Axial Velocity Component of Constant Mass Droplets in a Uniform Velocity Stream

This analysis pertains to the motion of entrained droplets in an upward flowing vapor stream. In order to eliminate heat flux as a parameter in the analysis, the idealization is made that the change in vapor mass flow rate is small over the boiler length of interest.

Other idealizations are:

1) droplets are of constant mass
2) droplets are spherical
3) the flow is vertically upward so the gravitational field opposes the motion
4) the droplet drag coefficient is constant*
5) the liquid phase occupies negligible volume in the boiler
6) the pressure gradient is negligible

---

*For commentary on this simplification, refer to pages 52 and 55.

7) the axial component of vapor velocity is uniform across the boiler.

The normalized equation of motion is

$$\frac{d\bar{v}_p}{d\bar{t}_a} = (1 - \bar{v}_p)^2 - \bar{g}_e \qquad (47)$$

where

$$\bar{v}_p = \frac{v_p}{v_a}$$

$$\bar{t}_a = \frac{t}{\tau_a}$$

$$\bar{g}_e = \frac{g_e \tau_a}{v_a}$$

v_p = droplet velocity

v_a = vapor axial velocity

t = time, measured from initiation of droplet motion

g_e = earth's gravitational field

$$\tau_a = \left(\frac{3}{4} \frac{C_D}{D_p} \frac{\rho_v}{\rho_\ell} v_a \right)^{-1}, \text{ a time scale}$$

C_D = droplet drag coefficient, numerically equal to 0.4

D_p = droplet diameter

ρ_v = vapor density

ρ_ℓ = liquid density

This equation may be integrated readily and rearranged to yield the relationship between velocity and time

$$\bar{v}_p = (1 - \bar{g}_e)\frac{1 - e^{2\sqrt{\bar{g}_e}\,\bar{t}_a}}{\left(1 - \sqrt{\bar{g}_e}\right) - \left(1 + \sqrt{\bar{g}_e}\right) e^{2\sqrt{\bar{g}_e}\,\bar{t}_a}} \tag{48}$$

The relationship between axial location and time is obtained from a second integration.

$$\bar{v}_p = \frac{d\bar{z}}{d\bar{t}_a}$$

where

$$\bar{z} = \frac{z}{v_a \tau_a}$$

z is the axial length from initiation of droplet motion.

By integration of Equation (48) and rearrangement one obtains

$$\bar{z} = \left(1 + \sqrt{\bar{g}_e}\right)\bar{t}_a - \log \frac{\left(1 + \sqrt{\bar{g}_e}\right) e^{2\sqrt{\bar{g}_e}\,t_a} - 1 + \sqrt{\bar{g}_e}}{2\sqrt{\bar{g}_e}} \tag{49}$$

Under many circumstances, where the axial drag force is large and small axial distances are of interest (so that droplet slip velocities are much larger than the asymptotic slip due to gravity) the gravitational force term is negligible. The resulting simpler form of Equation (47), namely

$$\frac{d\bar{v}_p}{d\bar{t}_a} = (1 - \bar{v}_a)^2 \tag{50}$$

may be integrated twice to yield

$$\bar{v}_p = 1 - \frac{1}{1 + \bar{t}_a} \tag{51}$$

and

$$\bar{z} = \bar{t}_a - \log (1 + \bar{t}_a) \tag{52}$$

The results of Equations (48), (49), (51), and (52) are shown in Figures 10 and 11.

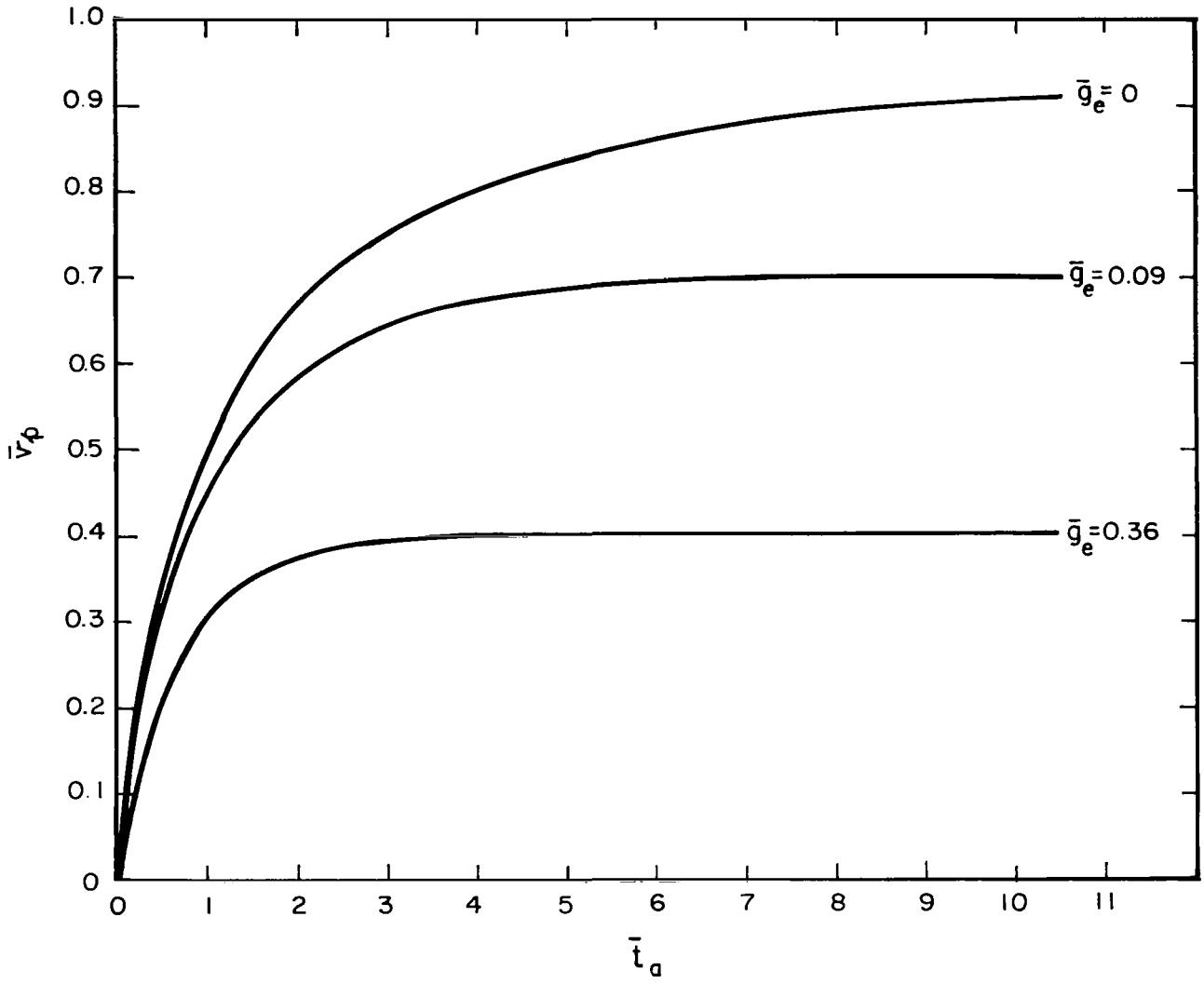

Figure 10. Droplet accelerating in a uniform stream: Axial velocity versus time.

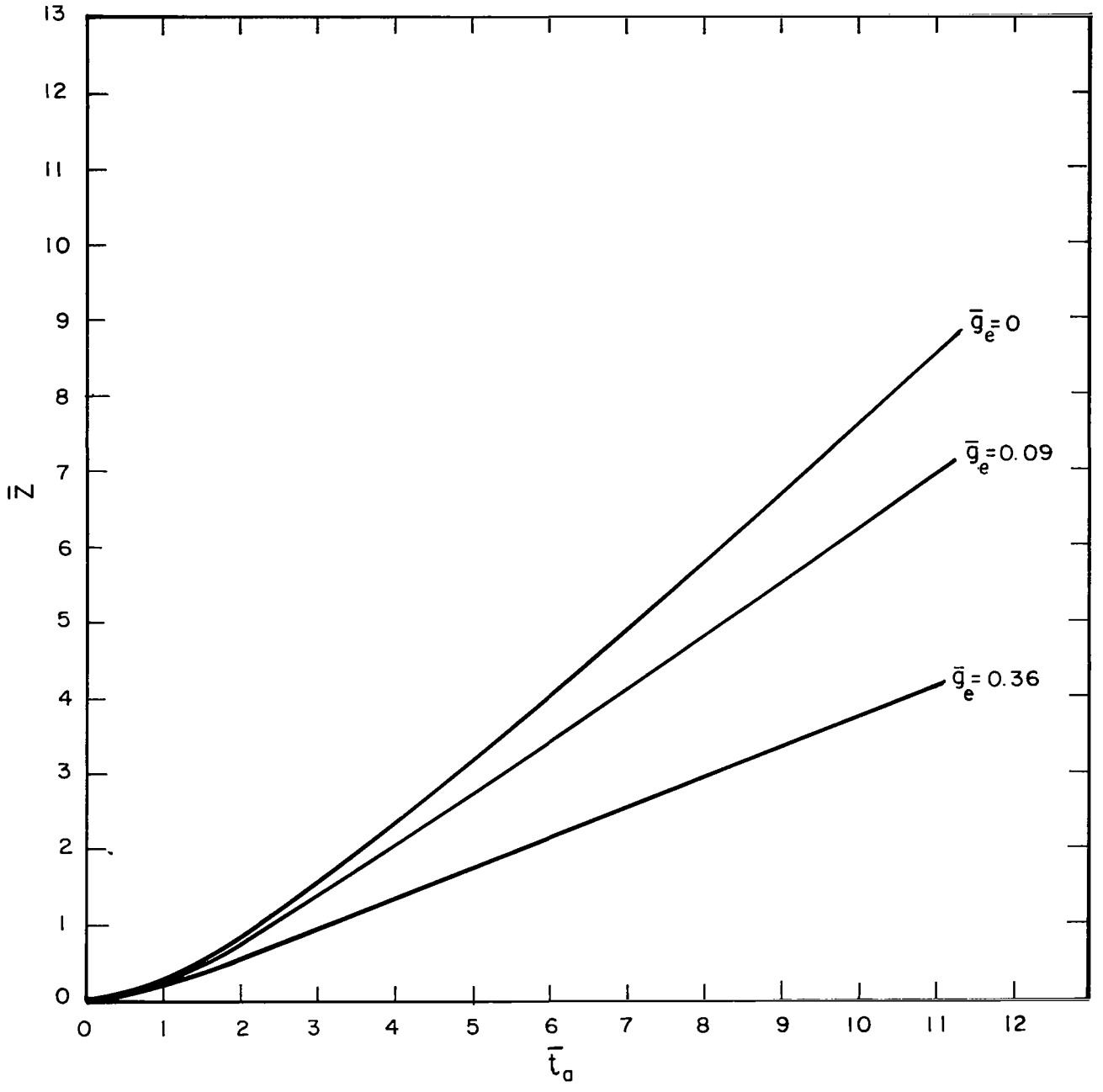

Figure 11. Droplet accelerating in a uniform stream: Axial travel versus time.

3) Axial Velocity Component of Constant Mass Droplets in a Boiler Tube Subjected to a Uniform Heat Flux

This analysis is of a model of droplet motion in a vertical upward flow in which the vapor flow increase due to vaporization is significant within the boiler length of interest.

The idealizations on which the model is based are:

1) droplets are of constant mass
2) droplets are spherical
3) the boiler is subjected to a uniform heat flux
4) the flow is vertically upward, so that the gravitational field opposes the motion
5) the droplet drag coefficient is constant
6) the liquid phase occupies negligible volume in the boiler
7) the droplets are injected with zero axial velocity at an arbitrary location in the boiler
8) the vapor velocity is uniform across the tube diameter.

These idealizations lead to the following normalized differential equation

$$(\bar{\ell} - \bar{v}_p)^2 - \gamma = \bar{v}_p \frac{d\bar{v}_p}{d\bar{\ell}} \tag{53}$$

where

$$\bar{v}_p = \frac{v_p}{v_r}$$

$$\bar{\ell} = \frac{\ell}{\ell_r}$$

$$\gamma = \frac{g_e}{\lambda^2 \ell_r}$$

$$\ell_r = \left(\frac{3}{4} \frac{C_D}{D_p} \frac{\rho_v}{\rho_\ell}\right)^{-1}, \text{ a characteristic length}$$

$$v_r = \lambda \ell_r, \text{ a characteristic velocity}$$

where

$\lambda = \dfrac{4\left(\frac{q}{A}\right)}{\rho_v D L}$, reciprocal of a characteristic time

C_D = drag coefficient of droplet, taken equal to 0.4

D = tube diameter

D_p = droplet diameter

g_e = acceleration of gravity of earth

ℓ = axial length

ℓ_o = point of injection of droplet

L = latent heat of vaporization

$\frac{q}{A}$ = heat flux

v_v = vapor velocity

v_p = droplet velocity

γ = normalized gravitational force

In this coordinate system the vapor velocity at any point is given by

$$\overline{v}_v = \frac{v_v}{v_r} = \frac{\lambda \ell}{\lambda \ell_r} = \overline{\ell}$$

Equation (1) has been numerically integrated for several droplet injection points $\overline{\ell}_o$, and for several values of the gravitational parameter γ. The results are shown in Figures 12 and 13.

The normalized velocity difference (between the vapor velocity and the particle) for a particle with suitably long path length in the boiler, defined by

$$V_s = \frac{v_v - v_p}{v_v} \qquad (54)$$

$$= \frac{\overline{\ell} - \overline{v}_p}{\overline{\ell}}$$

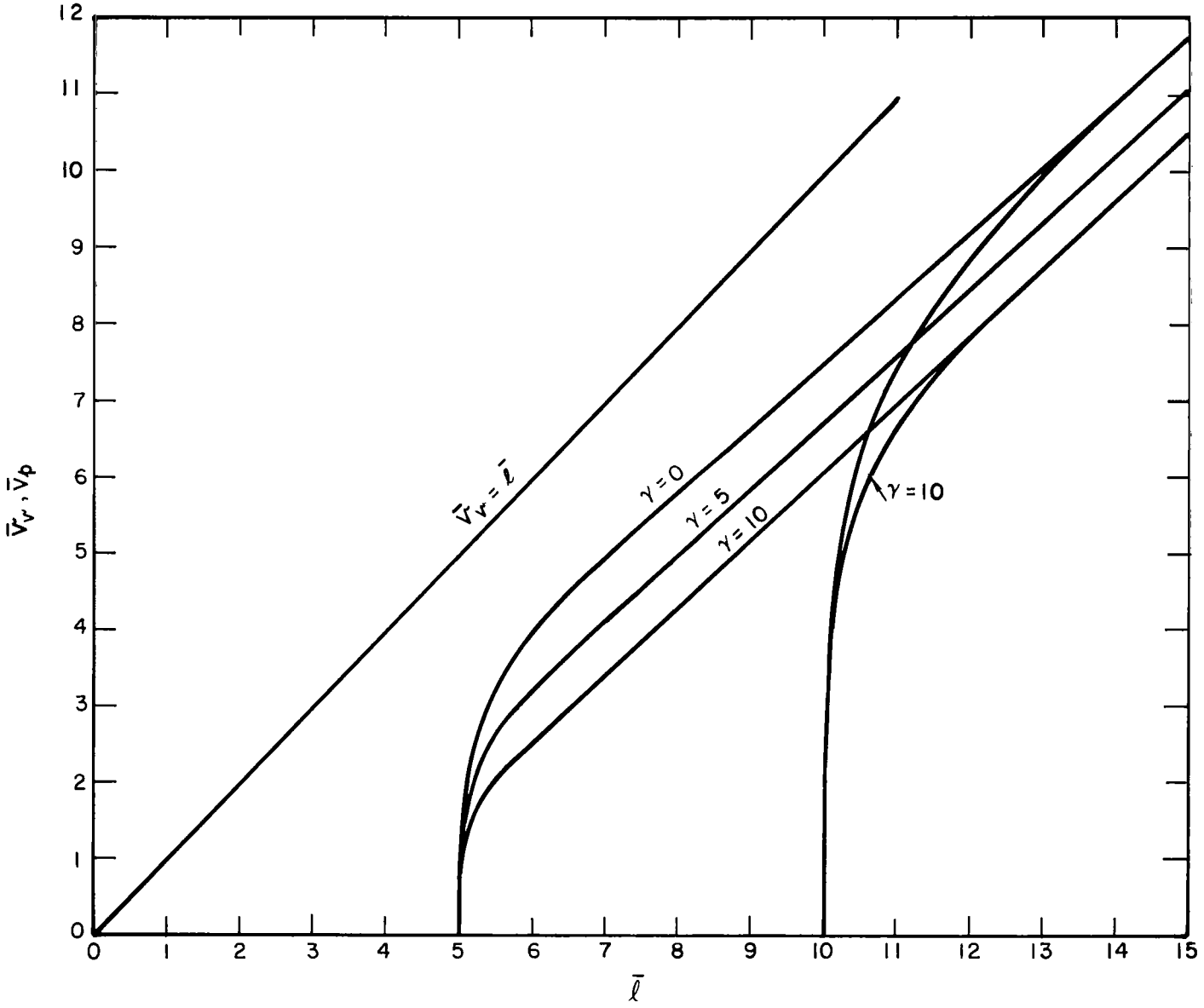

Figure 12. Constant mass droplets accelerating in a uniform heat flux boiler: Velocity versus location.

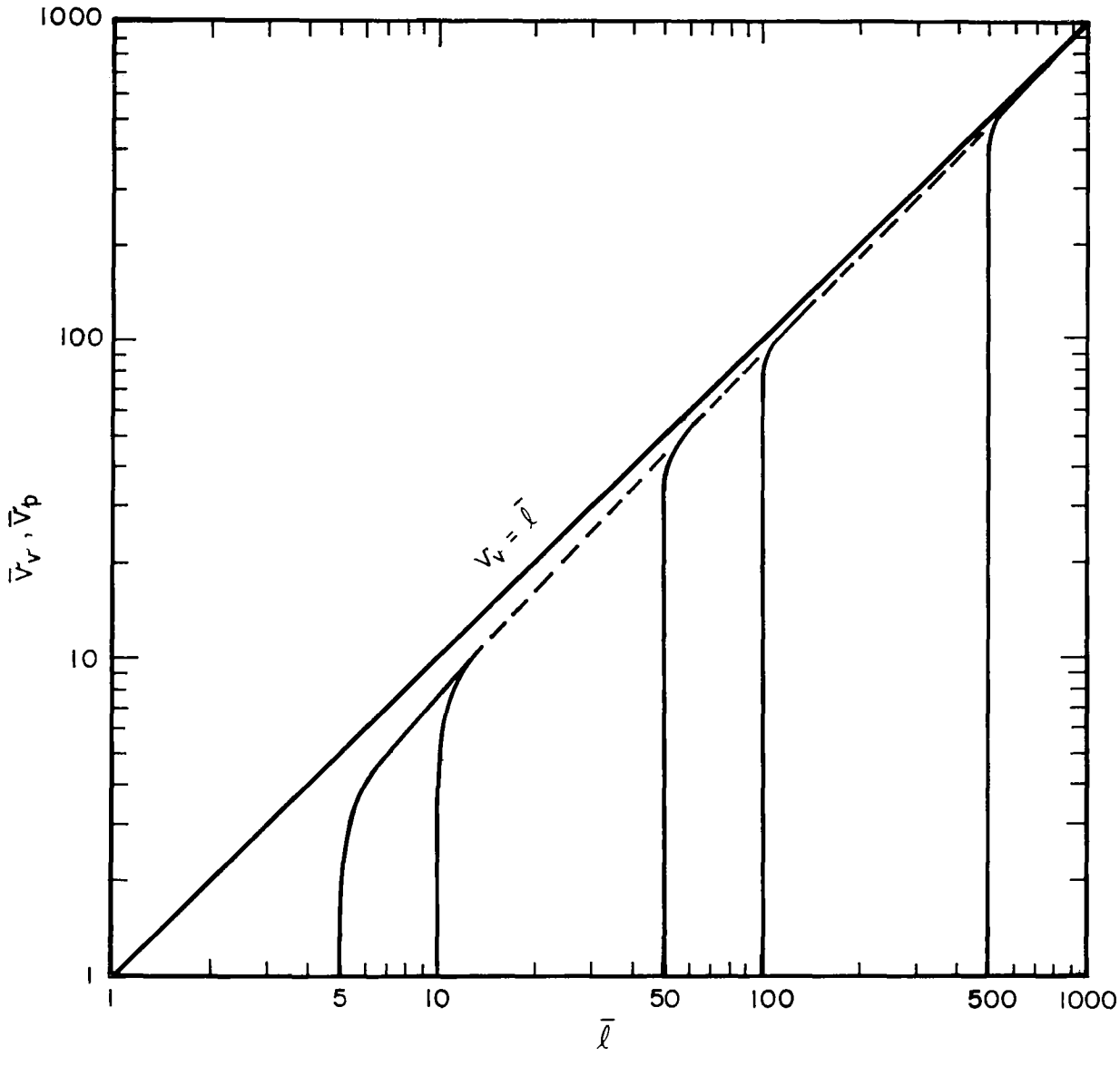

Figure 13. Constant mass droplets accelerating in a uniform heat flux boiler: Velocity versus location for gravity term negligible.

continually decreases. The variation of this quantity is shown in Figures 14 and 15.

The variation in spatial location and particle velocity with time must be extracted from the above results numerically, by the relation

$$\Delta \bar{t}_a = \frac{\Delta \bar{\ell}}{\bar{v}_p} \tag{55}$$

where

$\bar{t}_a = \lambda t$

t = time from instant of droplet injection

and Δ = denotes a small increment.

The initial variation of ℓ with time is shown in Figure 16.

Because of the gravitational field, there is a minimum vapor velocity below which upward motion of droplets will not occur. This minimum is given by the relationship

$$\bar{\ell}_o^{\,2} = \gamma \tag{56}$$

By use of the definitions of the normalized variables, Equation (56) may be reduced to

$$\frac{\ell_o}{D} = \frac{1}{2\sqrt{3}} \frac{L}{\left(\frac{q}{A}\right)} \left(\frac{\rho_\ell \rho_v g D_p}{C_D} \right)^{\frac{1}{2}} \tag{57}$$

Droplet Velocities in a Specific Boiler

The boiler chosen for this example is described by the following parameters.

Fluid: Potassium at 1800°F

Tube Diameter: 0.42 inch

Heat Flux (Uniform): 28 Btu/ft^2 sec

Mass Velocity G: 30 lb/ft^2 sec

These conditions correspond to some experimental conditions reported in Reference 2.

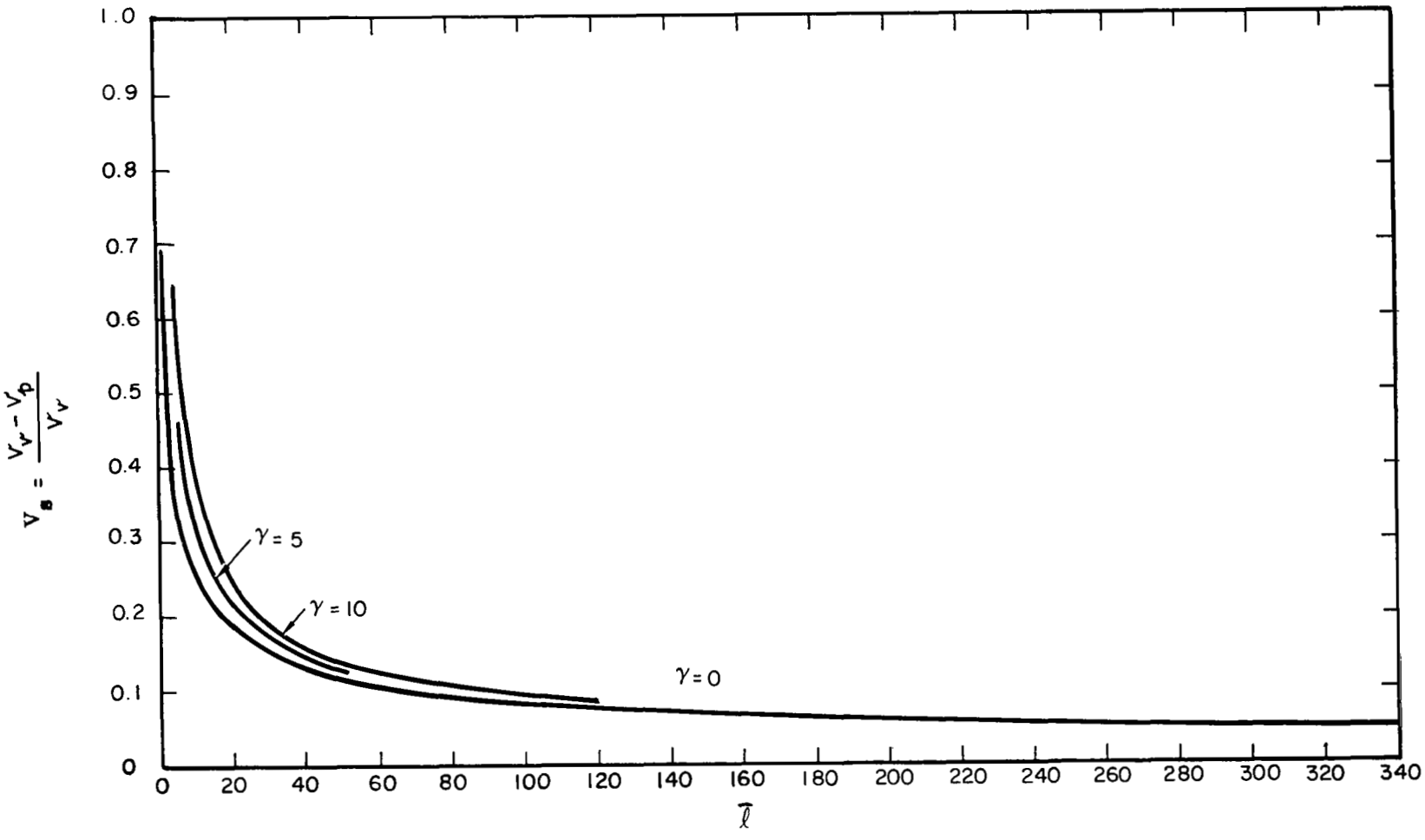

Figure 14. Constant mass droplets accelerating in a uniform heat flux boiler: Minimum (asymptotic) slip versus location in boiler.

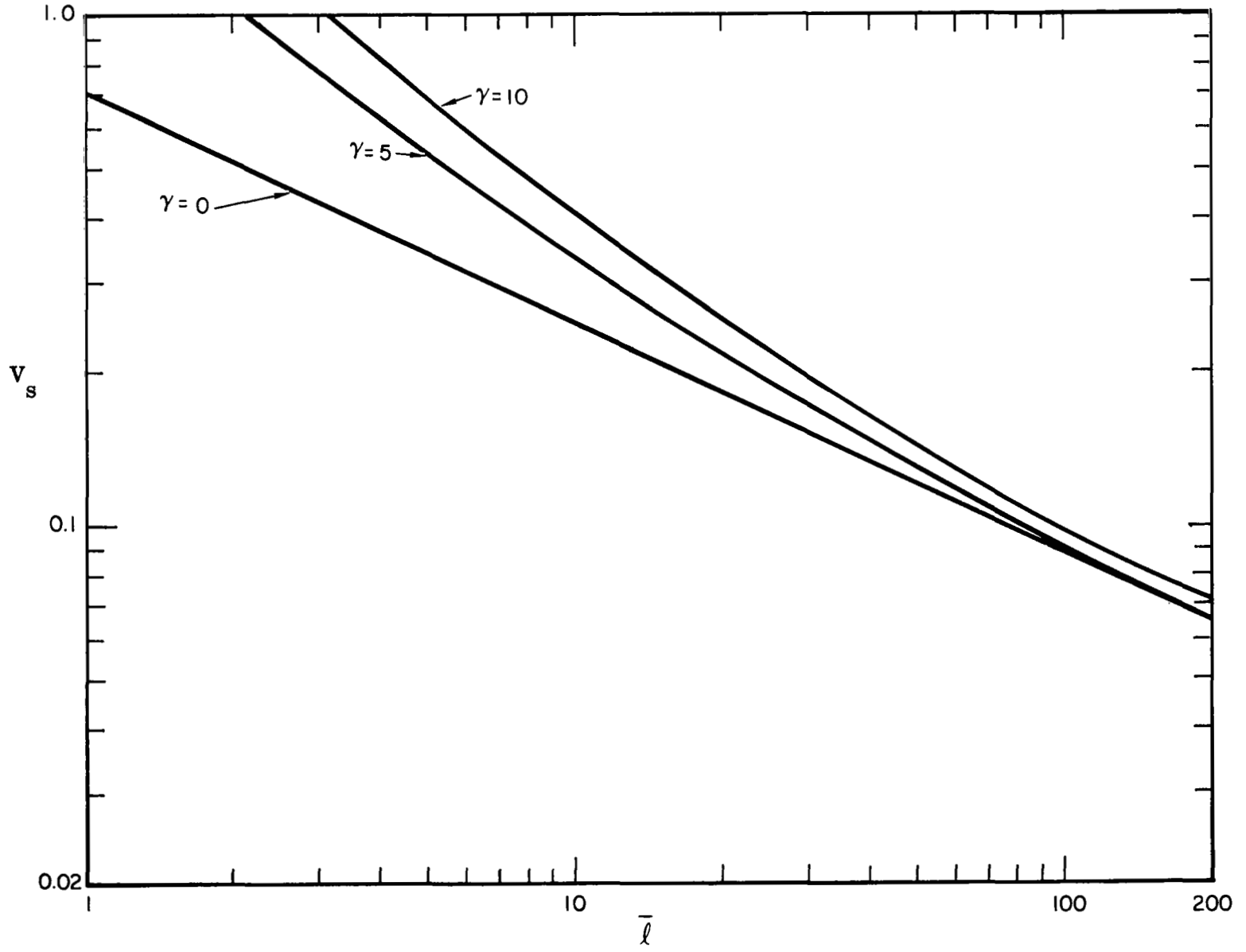

Figure 15. Constant mass droplets accelerating in a uniform heat flux boiler: Asymptotic slip.

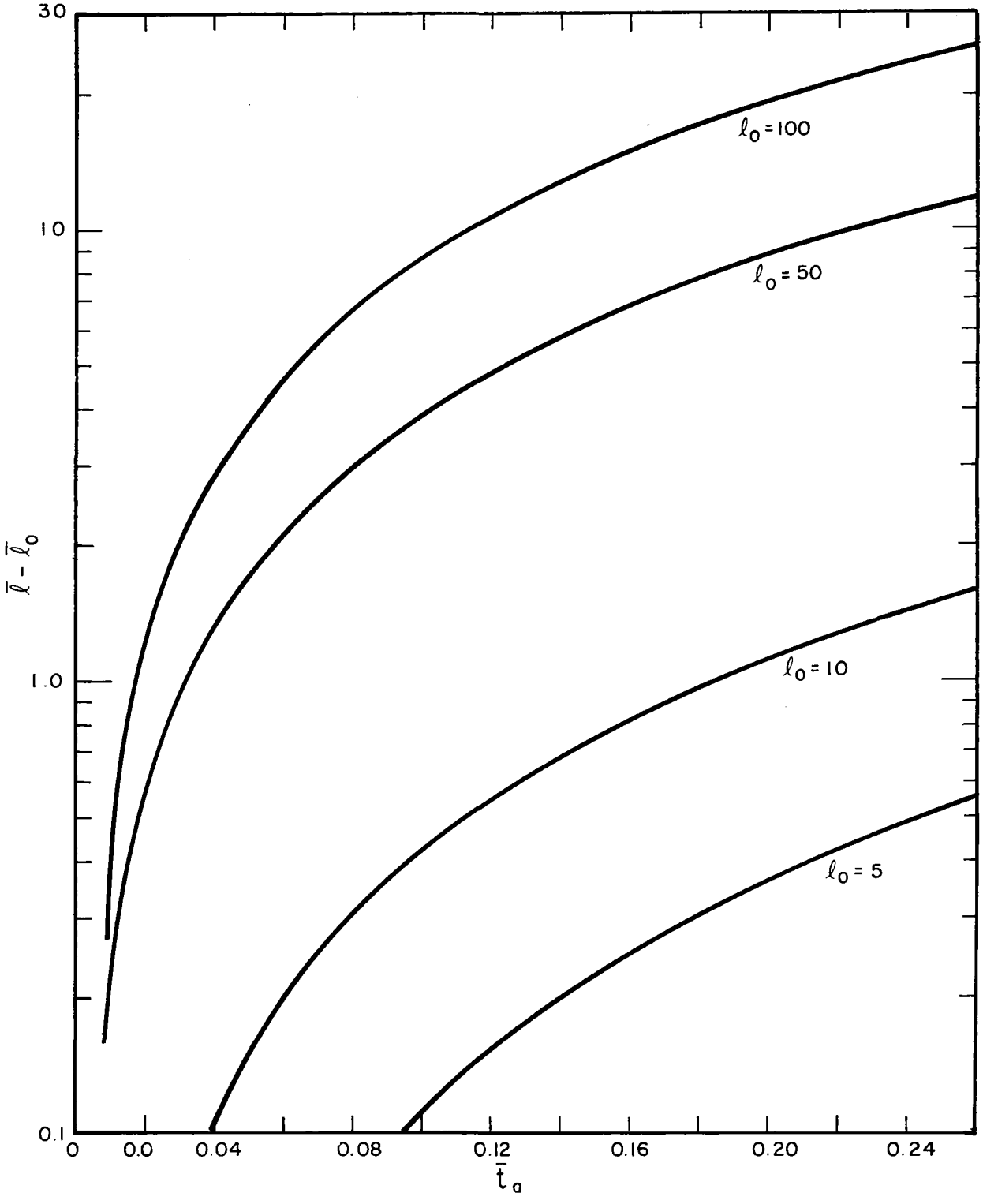

Figure 16. Constant mass droplets accelerating in a uniform heat flux boiler: Displacement versus time for gravity term negligible.

The particular point in this boiler to be considered is

Quality X: 0.8

Length from Onset of Boiling: 5.73 ft.

Computed parameters of interest are

$$\lambda = \frac{4\left(\frac{q}{A}\right)}{\rho_v D \ L}$$

$$= \frac{27.7}{\text{sec}}$$

$$\frac{\ell}{D} = 164$$

$$\gamma = \frac{1.2}{\left(\frac{\ell_r}{D}\right)}$$

$$\frac{\ell_r}{D} = \frac{4}{3}\frac{1}{C_D}\frac{\rho_\ell}{\rho_v}\frac{D_p}{D}$$

$$= \frac{4}{3}\left(\frac{1}{0.4}\right)\left(250\right)\frac{D_p}{D}$$

$$= 831 \ \frac{D_p}{D}$$

D_p (inches)	$\frac{D_p}{D}$	$\frac{\ell_r}{D}$	γ	$\left(\frac{\ell}{\ell_r}\right)_{X=.8}$	V_s
1×10^{-3}	2.4×10^{-3}	2	.6	82	.10
2×10^{-3}	4.8×10^{-3}	4	.3	41	.13
5×10^{-3}	12×10^{-3}	10	.12	16.4	.20
1×10^{-2}	24×10^{-3}	20	.06	8.2	.28
2×10^{-2}	48×10^{-3}	40	.03	4.1	.37

Because actually observed droplets may not have been in the stream long enough to attain minimum slip, one would expect droplets of these sizes to have greater slip than that tabulated, but not less.

It may be seen from Figure 15 of this report that the effect of the gravity term is small for all of these cases. For this specific boiler, entrainment of even the largest droplets considered would be expected for locations in the boiler above

$$\frac{\ell_o}{D} = 6.9$$

This is approximately three inches after the onset of boiling.

4) Axial Velocity Component of Fragmenting Droplets in an Accelerating Stream

It has been shown in a number of investigations (see for example, Reference 12) that a liquid droplet is unstable when its Weber number becomes greater than a fixed value, usually taken to be about 16*. The unstable droplet fragments very rapidly, so that the maximum droplet size under a given set of conditions may be near that given by the critical Weber number. Consider a droplet of varying size accelerating in the vapor stream of a uniform

*It is recognized that there are no doubt other mechanisms that can play a role in controlling droplet size, such as spallation or fission when droplets contact the boiler tube surface. In the present analysis an attempt is being made to investigate drop slip velocities in the bulk region on the premise that the Weber criterion is in operation.

heat flux boiler. At the instant before fragmentation, the droplet is accelerating under the influence of the drag force exerted by the accelerating vapor stream. After the (instantaneous) fragmentation process, each of the fragments continues acceleration under influence of the vapor drag force, but now there is a new frontal area and mass for each fragment. On the average the fragmentation process does not contribute to the axial momentum of any of the fragments. This process may be idealized as continuous. The equation of motion is

$$F = \frac{d}{dt}(mv)_p + (v_p + \Delta v)_p \frac{dm}{dt} \tag{58}$$

when

F is the force applied to the system

m is the droplet mass

v_p is absolute axial velocity of the droplet

t is time,

$\frac{dm}{dt}$ is the mass change due to fragmentation

The term $(v_p + \Delta v)_p \frac{dm}{dt}$ is the momentum carried away by the fragments. Since there is no net axial velocity change due to the fragmentation process, $\Delta v_p = 0$. When this equation is expanded, the two terms containing $\frac{dm}{dt}$, which have opposite signs, cancel. The equation is therefore

$$F = m\frac{dv_p}{dt} \tag{59}$$

For the present purpose, distance is a more suitable coordinate than is time.

$$\frac{dv_p}{dt} = \frac{dv_p}{d\ell}\frac{d\ell}{dt}$$

$$= v_p \frac{dv_p}{d\ell}$$

The equation of motion may be written

$$F = mv_p\frac{dv_p}{d\ell} \tag{60}$$

where ℓ is the axial distance measured from onset of boiling. The drag force is given by

$$F_D = C_D \frac{\pi}{4} D_p^2 \frac{1}{2}\rho_v v_s^2 \tag{61}$$

where

C_D is the drag coefficient

D_p is the particle diameter (the particles are idealized as spherical)

ρ_v is the vapor density

v_s is the slip velocity.

v_s is defined by

$$v_s = v_v - v_p \tag{62}$$

where v_p is the absolute particle velocity, v_v is the vapor velocity. The force on the droplet due to gravity will be neglected in this analysis.

In general, the drag coefficient is a function of the droplet Reynolds number, but as will be shown later, the Reynolds numbers for droplets of interest in this investigation are in the range of $.5 \times 10^3$ to 2×10^5, where the drag coefficient is almost constant at $C_D = 0.4$. For the present purposes it will be assumed that the drag coefficient is invariant. Neglecting the liquid volume, and considering the case in which the boiler is subjected to a uniform

heat flux, the mean vapor velocity at a cross section is linearly dependent upon length ℓ.

$$v_v = \frac{4\left(\frac{q}{A}\right)}{\rho_v D L}\ \ell \tag{63}$$

where

$\frac{q}{A}$ is the heat flux

ρ_v is vapor density

D is tube inside diameter

and

L is latent heat of vaporization.

On an average basis one may calculate the droplet diameter from the Weber number, so that

$$D_p = \frac{16\sigma g_c}{\rho_v v_s^2} \tag{64}$$

where

σ is surface tension of the liquid

D_p is droplet diameter

The droplet mass may be calculated from

$$m = \frac{\pi}{6}\rho_\ell\ D_p^3 \tag{65}$$

where

ρ_ℓ is the liquid density.

By combining Equations 60 through 65 and rearranging, one obtains

$$\frac{3}{64}\frac{C_D}{\sigma g_c}\frac{\rho_v^2}{\rho_\ell} = \frac{v_p}{v_s^4}\frac{dv_p}{d\ell} \tag{66}$$

The slip velocity may be replaced by

$$v_s = v_v - v_p \tag{67}$$

$$= \frac{4\left(\frac{q}{A}\right)}{\rho_v D \quad L} \ell - v_p \tag{68}$$

Define the reference length and velocity

$$\ell_r = \left\{ \frac{4}{3} \frac{\sigma g_c \rho_\ell D^2}{C_D} \left(\frac{L}{\frac{q}{A}} \right)^2 \right\}^{\frac{1}{3}} \tag{69}$$

$$v_r = \frac{4\left(\frac{q}{A}\right)}{\rho_v D \quad L} \ell_r \tag{70}$$

Also define the dimensionless variables:

particle velocity

$$V_p = \frac{v_p}{v_r}$$

axial length

$$s = \frac{\ell}{\ell_r}$$

(71)

In this coordinate system, the normalized vapor velocity, defined by

$$V_v = \frac{v_v}{v_r}$$

has a slope of one. Equation (66) becomes

$$1 = \frac{V_p}{(s - V_p)^4} \frac{dV_p}{ds} \tag{72}$$

or

$$\frac{dV_p}{ds} = \frac{\left(s - V_p\right)^4}{V_p} \tag{73}$$

This equation is nonlinear and apparently cannot be solved in closed form.

An approximate solution has been obtained by the method of isoclines for several values of starting position for the droplet. These results are shown in Figures 17 and 18. It may be seen that the droplets accelerate very rapidly and approach a limiting slip. Define a normalized local slip velocity as before (Eq. 54)

$$\frac{v_s}{v_v} = \frac{v_v - v_p}{v_v} \tag{74}$$

$$= V_s$$

The local slip velocity for a particle which has been in the stream long enough to come to equilibrium acceleration varies as shown in Figure 19. According to this analysis, the droplets fragment and accelerate so rapidly that one would expect most droplets entrained in a vapor flow at a particular axial station to be traveling at nearly the same velocity regardless of whether they had been entrained early in the boiler or only a short distance upstream from the point of observation.

5) Size of Fragmenting Droplets in an Accelerating Stream

In the calculation of slip velocity with acceleration, it has been assumed that the droplet size is defined by the maximum Weber number for which liquid droplets are stable, namely Equation (64). Equation (64) may be transformed by use of Equations (63) and (74) to yield

$$\frac{D_p}{D} = \sigma \rho_v D \left(\frac{L}{\frac{q}{A}}\right)^2 \frac{1}{\ell^2 V_s^2} \tag{75}$$

Introducing the characteristic length ℓ_r, defined by Equation (69) one obtains

$$\frac{D_p}{D} = \rho_v \left\{ \frac{\sigma g_c}{D} \left[\frac{3C_D}{4\rho_\ell} \left(\frac{L}{\frac{q}{A}}\right)^2 \right] \right\}^{\frac{1}{3}} \frac{1}{s^2 V_s^2} \tag{76}$$

This relationship is shown graphed in Figure 20. It may be seen that the decrease in droplet size is very rapid during the initial portion of the boiler. Because of the nature of this analysis, the predicted droplet size is near the maximum one would expect to observe. An unstable droplet probably fragments into several particles all of which would be below the critical Weber number. However, if a droplet fragments into for example two particles of equal mass, the diameters of these two particles are 80% of the diameter of the original drop, or almost the same size. Therefore, unless fragmentation is into a very large number of droplets, the observed diameter range would not be expected to be very great due to this effect.

The velocity of the vapor is not uniform across the tube, and not all droplets are subjected to the same accelerations. Although accelerating flows have more uniform velocity profiles than fully established flows, the liquid vaporization on the wall injects vapor into the core flow with no axial velocity component, and this would be expected to cause a velocity profile distortion near the wall. Therefore a scattering of droplet size due to the nonuniform velocity profile would be expected.

The idealization was made that the sphere drag coefficient is constant for the range of droplet Reynolds numbers of interest here. The Reynolds number, based on the slip velocity, is

$$Re = \frac{v_s D_d \rho_v}{\mu_v} \tag{77}$$

This relationship may be transformed to

$$Re = \left[\frac{4\left(\frac{q}{A}\right)}{\mu_v L} \ell_r \right] \left(\frac{D_d}{D} \right) \left(V_s \right) \left(s \right) \tag{78}$$

For Freon 12, typical conditions are (see Reference 12)

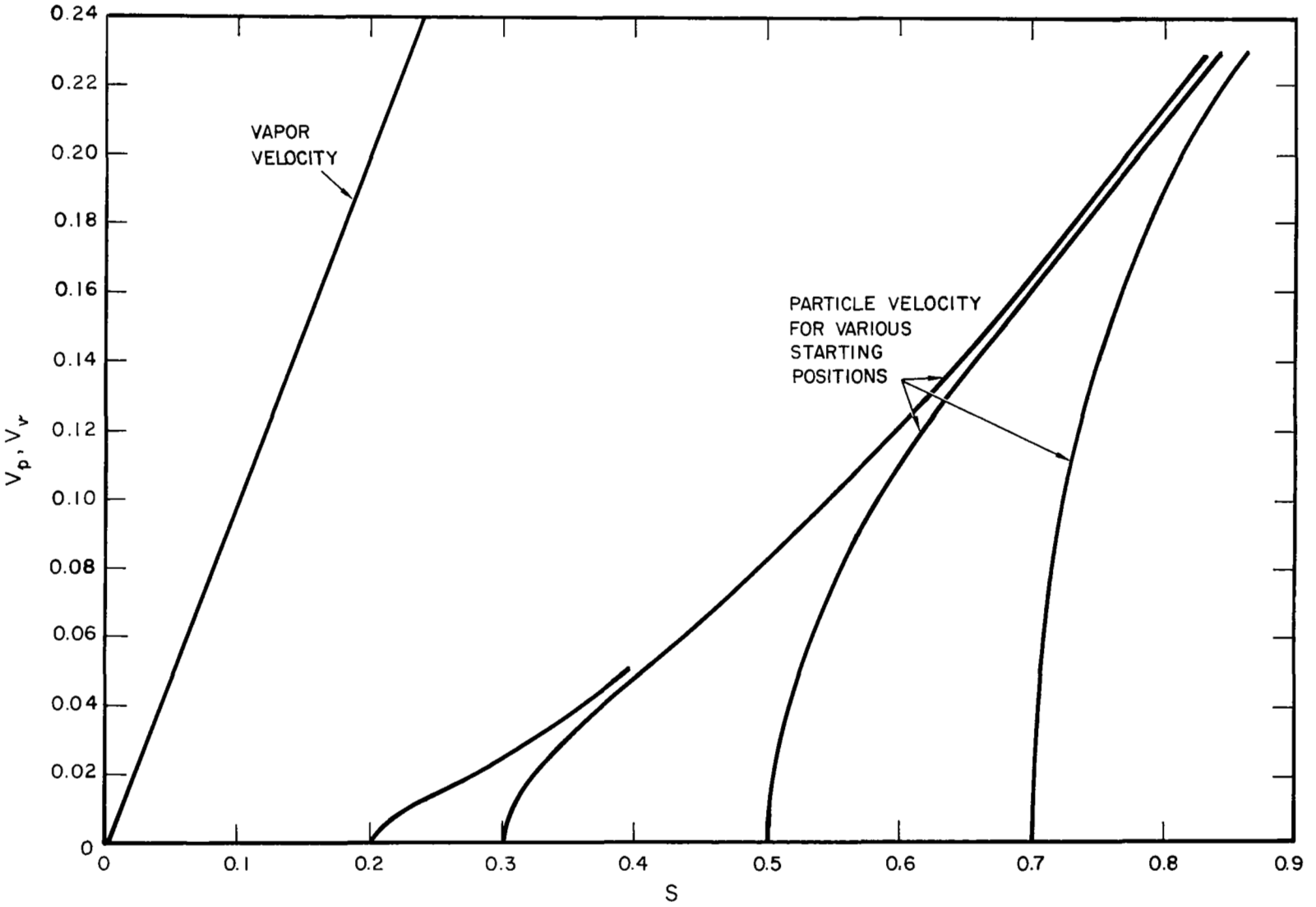

Figure 17. Normalized velocity of accelerating fragmenting droplets, small normalized lengths.

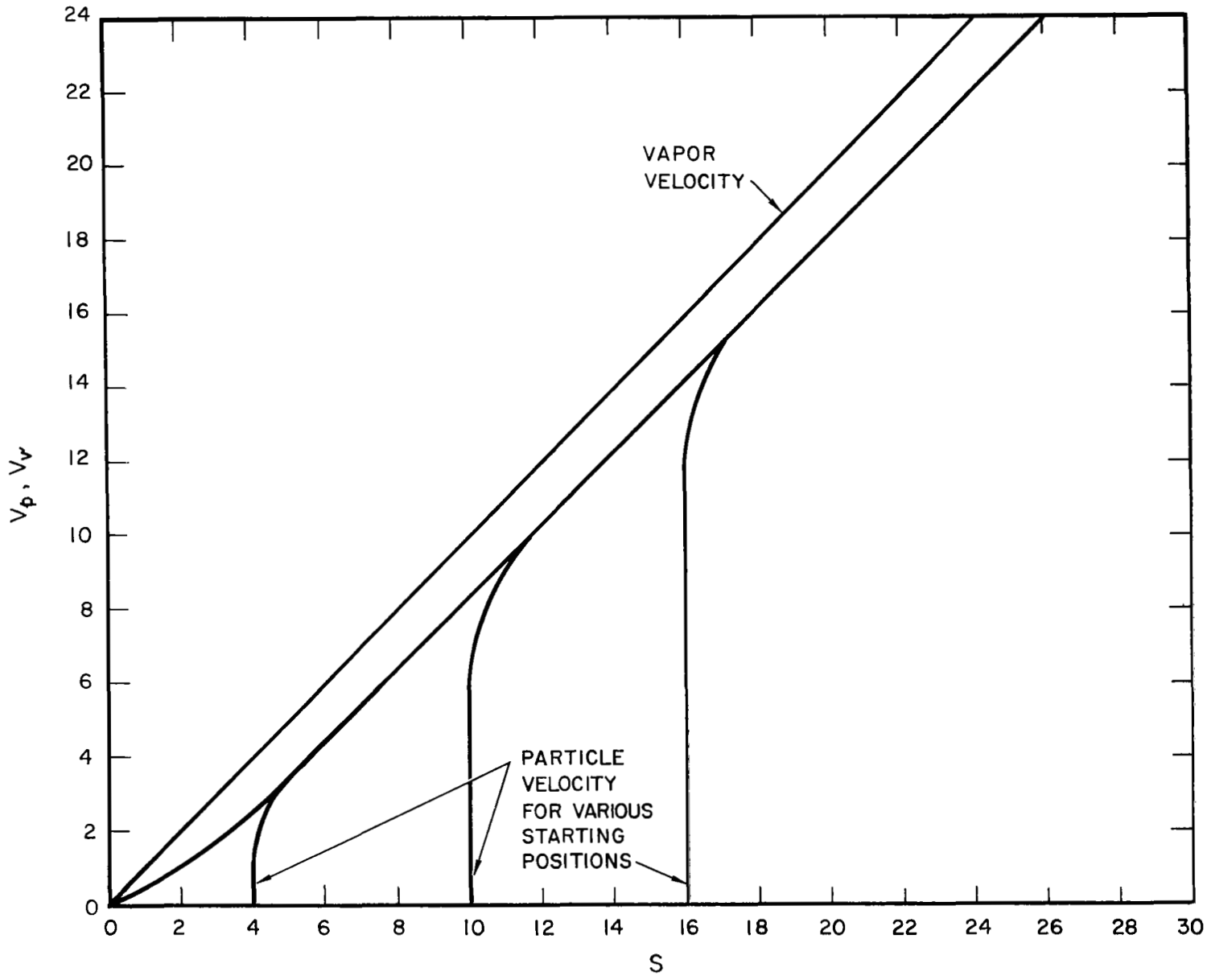

Figure 18. Normalized velocity of accelerating fragmenting droplets, s greater than unity.

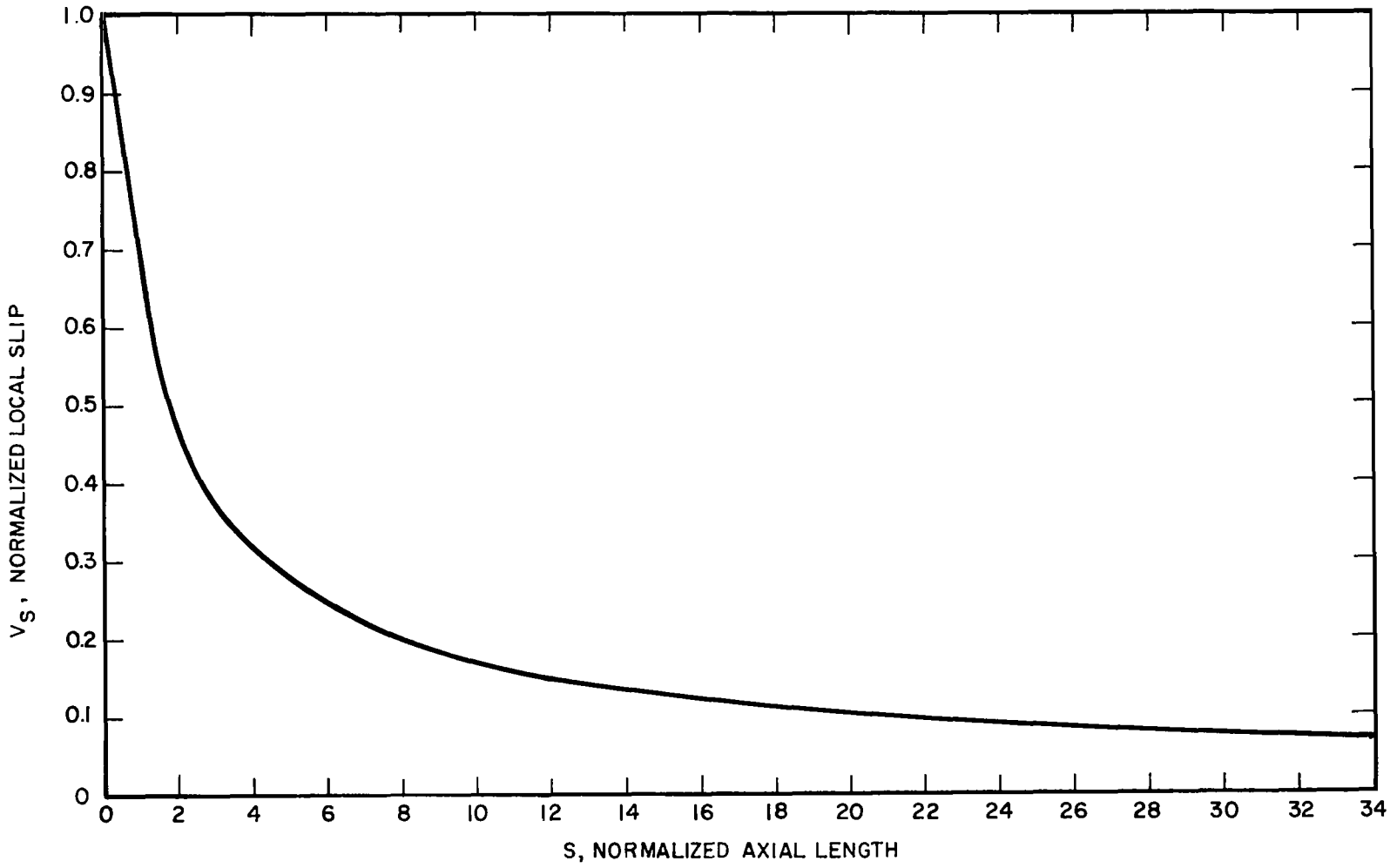

Figure 19. Asymptotic slip velocity for accelerating fragmenting droplets.

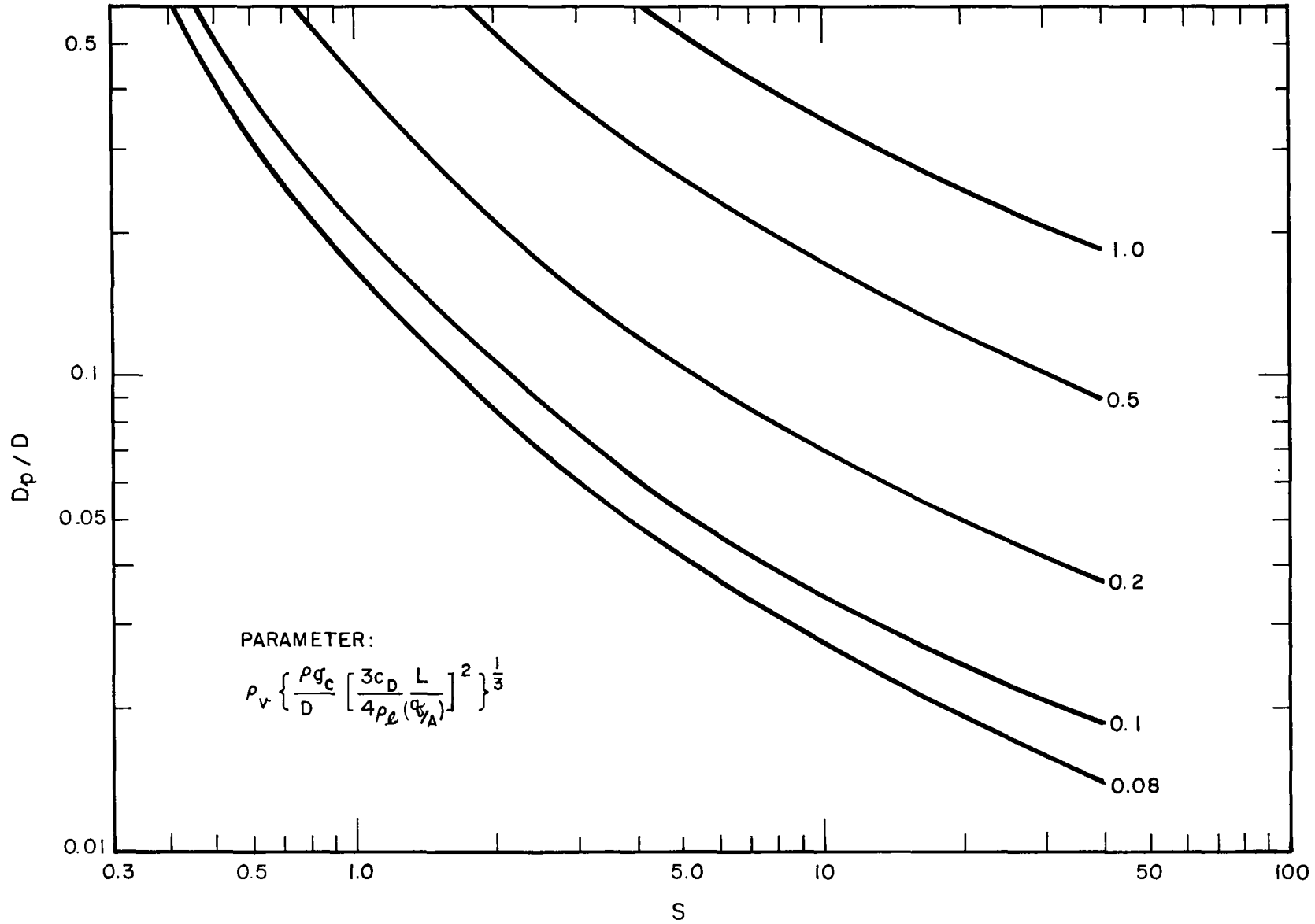

Figure 20. Sizes of accelerating fragmenting droplets.

$$\frac{q}{A} = 10 \ \frac{\text{Btu}}{\text{ft}^2 \text{sec}}$$

$$D = 0.452 \text{ inch}$$

$$P_s = 155 \text{ psia}$$

The characteristic length is $\ell_r = 0.55$ ft and the parameter in the Reynolds number has the value 6.9×10^3. The Reynolds number range is

s	Re
1	2.4×10^3
10	$.93 \times 10^3$
30	$.65 \times 10^3$

These Reynolds numbers are within the range for which C_D is nearly constant.

The results of this analysis predict very much different behavior for a low surface tension fluid such as Freon, and a high surface tension fluid such as mercury. Typical data taken from actual experiments are

	Mercury (700°F)	Freon (110°F)	Potassium (1800°F)
Heat Flux $\frac{\text{Btu}}{\text{ft}^2 \text{ sec}}$	2	10	28
Tube Diameter, inches	0.18	0.452	.42

These values lead to the following computed conditions at a position 8 feet from the initiation of boiling:

Droplet Size Parameter (in Equation (76))	0.095	.208	.16
Reference Length ℓ_r, ft	12.6	.548	4.6
V_s at 8 ft	0.77	.13	.5
Vapor Velocity, ft/sec	114	41.9	216
Droplet Velocity, ft/sec	26	36.5	108
Droplet Diameter, inches	0.057	.027	.08

6) Deposition of Entrained Droplets in Linear Flow

The vapor flow in a linear flow boiler tube almost always has some liquid droplets entrained in it when the quality is less than unity. If the wall temperature is not so high that film boiling occurs, and if the liquid wets the boiler tube wall, then presumably liquid droplets which strike the wall spread out and vaporize. If there is a continuous liquid film on the wall, the impinging droplet would be expected to become a part of the film and not to be returned to the vapor flow. It is possible of course, that entrainment of liquid from the film may also be occurring, but the idealization will be made that these processes are independent and may be treated separately.

The rate of deposition may be expected to be related to the concentration of droplets entrained in the vapor, and if the droplets are suitably small it may be valid to treat the deposition process as a process of diffusion of very small particles from the bulk to the wall. The controlling equation is then of the form

$$\frac{w_d}{A} = h_d \, (c_s - c_w) \tag{79}$$

where $\frac{w_d}{A}$ is the mass flux impinging upon the tube wall

h_d is a diffusion conductance

c_s is the vapor stream droplet concentration

and c_w is the concentration of droplets at the wall.

According to the present flow model, the wall acts as a "sink" for the droplets, so that $c_w = 0$. According to Reynolds' analogy between the turbulent transfer of mass and heat, (see for example Reference 13)

$$h_d = \frac{h}{c_p}$$

where h is the heat transfer conductance and c_p is the vapor specific heat. Continuing the analogy, the Dittus - Boelter equation for the Nusselt modulus describing turbulent heat transfer in tubes is transformed to

$$\frac{h_d D}{\mathscr{D}} = 0.023 \ Re^{0.8} \left(Sc \right)^{0.4} \tag{80}$$

where D is tube inside diameter

$\mathscr{D}$ is the molecular diffusion coefficient

Re is the Reynolds modulus, defined by

$$Re = \frac{v_v D \ \rho_v}{\mu_v}$$

v_v is mean vapor velocity

ρ_v is vapor density

μ_v is vapor viscosity

Sc is the Schmidt modulus, defined by

$$Sc = \frac{\mu_v}{\rho_v \mathscr{D}}$$

In the present analysis the Schmidt modulus is taken equal to unity. The mean liquid concentration in the vapor core is

$$c_s = \frac{w_e}{v_p A_T} \tag{81}$$

where w_e is the entrained liquid mass flow rate

v_p is the droplet mean velocity

A_T is the tube cross section area.

The decrease in effective diameter of the tube due to a possible liquid film on the wall has been neglected. The mass flux to the wall, w_d, may be related by continuity to the loss in entrained flow.

$$-\frac{dw_e}{d\ell} = \frac{w_d}{A}\pi D \tag{82}$$

where ℓ is the axial length, measured from a datum location as yet unspecified.

Combining Equations (79), (81), and (82), one obtains

$$-\frac{dw_e}{d\ell} = \frac{4h_d w_e}{v_p D} \tag{83}$$

In the analysis of Section B.4, a relationship between the droplet velocity v_p and the axial coordinate ℓ was derived for fragmenting droplets in a boiler with uniform heat flux. This relationship is of the form

$$v_p = v_r \phi(s) \tag{84}$$

where

$$s = \frac{\ell}{\ell_r}$$

$$v_r = \lambda \ell_r$$

$$\ell_r = \left\{ \frac{4}{3} \frac{\sigma g_c \rho_\ell D^2}{C_D} \left(\frac{L}{\frac{q}{A}} \right)^2 \right\}^{\frac{1}{3}} \tag{85}$$

$$\lambda = \frac{4\left(\frac{q}{A}\right)}{\rho_v D L}$$

σ is liquid surface tension

C_D is droplet drag coefficient, equal to 0.4 for the range of droplet slip Reynolds moduli of interest

ρ_ℓ is liquid density

L is latent heat of vaporization

$\frac{q}{A}$ is the uniform heat flux

v_v is the vapor velocity, a function of length.

For the uniform heat flux case, and neglecting liquid volume in order to be consistent with preceding approximations,

$$v_v = \frac{4\,\frac{q}{A}}{L\rho_v D}\,\ell$$

$$= \lambda\ell \tag{86}$$

then

$$-\frac{dw_e}{ds} = \frac{4\,w_e \ell_r}{D}\left(\frac{h_d(s)}{v_r \phi(s)}\right) \tag{87}$$

the diffusion conductance is given by (80), (85), and (86) and is

$$\left.\begin{aligned} h_d(s) &= 0.023\,\frac{\mathscr{D}}{D}\left(\frac{D\,\rho_v}{\mu_v}\right)^{.8} \lambda^{.8}\,\ell_r^{\,.8}\,s^{.8} \\ &= \alpha\, s^{.8} \\ \text{where}\quad \alpha &= .023\,\frac{\mathscr{D}}{D}\left(\frac{D\,\rho_v}{\mu_v}\right)^{.8} \lambda^{.8}\,\ell_r^{\,.8} \end{aligned}\right\} \tag{88}$$

Combining Equations (83) through (88), one obtains an equation for the entrained flow

$$-\frac{dw_e}{ds} = k_1\,\frac{s^{.8} w_e}{\phi(s)} \tag{89}$$

where $k_1 = \dfrac{4\alpha}{D\,\lambda}$

For cases in which entrainment of liquid into the vapor stream from the wall film is negligible, then no liquid is added to the vapor flow along the boiler. For these cases the entrained flow has some point at which the liquid droplet flow is a maximum. This will be taken as the initial condition for the entrained flow. The initial condition is therefore

$$s_1,\ w_e = w_{e_0} \tag{89a}$$

Integration of Equation (89) subject to (89a), yields

$$\frac{w_e}{w_{e_0}} = e^{-\left[k_1 \int_{s_1}^{s} s^{.8} \frac{ds}{\phi(s)}\right]} = e^{-k_1 I} \tag{90}$$

The dimensionless constant k_1 in the exponent is

$$k_1 = .0758 \frac{L\rho_v}{\frac{q}{A} D} \left[\frac{1}{\mu_v}\left(\frac{\frac{q}{A}}{L} \frac{\sigma g_c \rho_\ell D^2}{C_D}\right)^{\frac{1}{3}}\right]^{0.8} \tag{91}$$

It remains to evaluate the integral I.

The functional relationship between the particle velocity v_p and s, denoted symbolically by ϕ, cannot be obtained in explicit form. The slip velocity, defined by $v_s = v_v - v_p$, is fit approximately, for $s > 1$, by the relationship

$$v_s = v_r \left[\frac{0.87}{s^{0.7}}\right] \tag{92}$$

In Figure 21, Equation (92) is compared to the particle velocity given in Section B.4. It may be seen that for present purposes the fit is acceptable.

$$\frac{v_p}{v_r} = \frac{v_v}{v_r} - \frac{v_s}{v_r}$$

$$= s - \left[\frac{0.87}{s^{0.7}}\right]$$

$$= \phi(s)$$

The integral exponent in Equation (90) becomes

$$I = \int_{s_1}^{s} \frac{s^{1.5} ds}{s^{1.7} - 0.87} \tag{93}$$

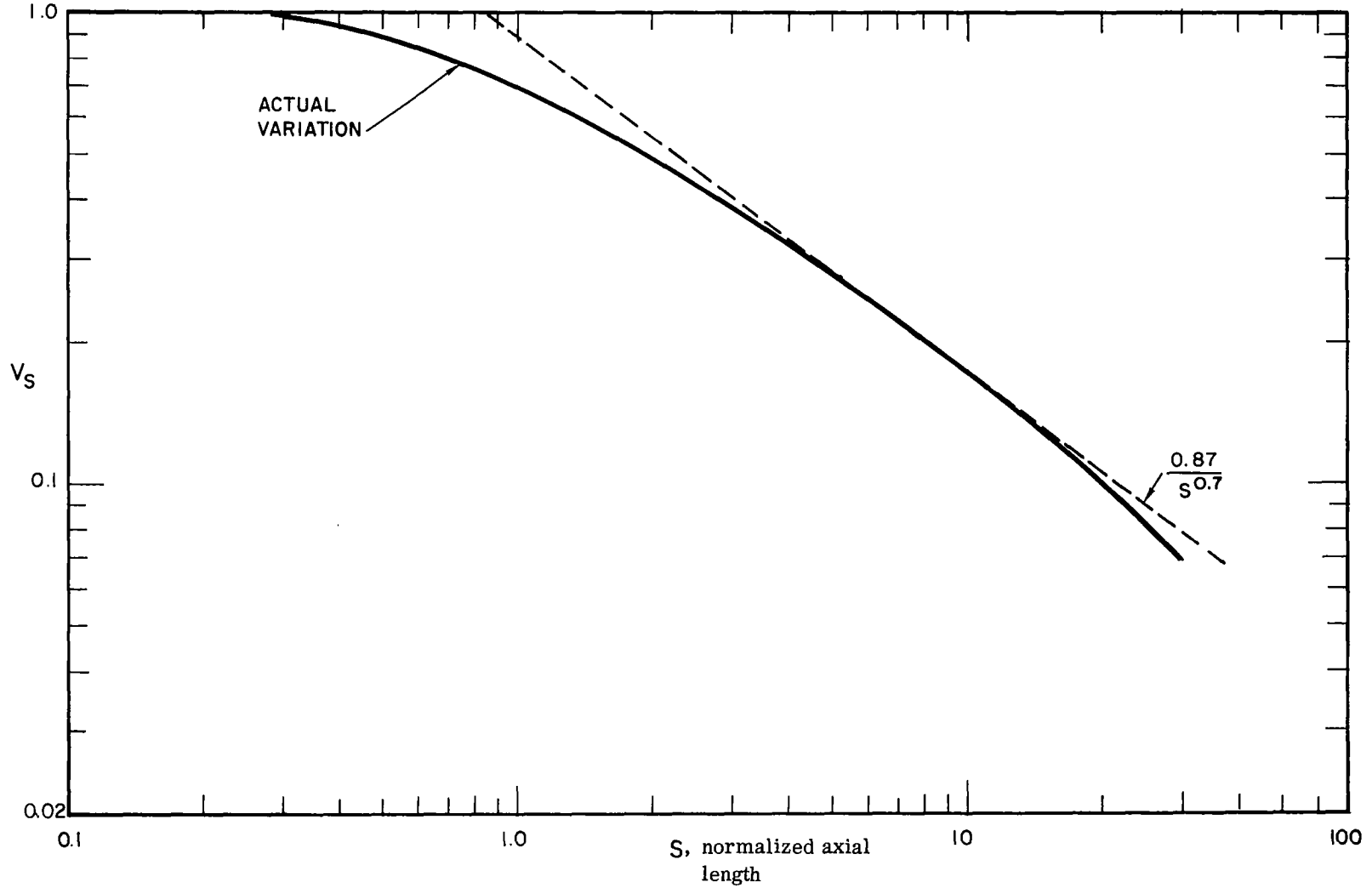

Figure 21. Comparison of approximate expression to slip velocity predicted in Section B.4.

For values of $s > 1$, the integrand is fit acceptably by the expression

$$\frac{1}{s^{0.2}} + \frac{1}{s^2} + \frac{5.7}{s^7} \tag{94}$$

A comparison of the integrand in Equation (93) and the approximate relation of Equation (94) is shown in Figure 22. From the integral with the approximate integrand of Equation (94), the result is

$$I = (1.25)\,(s^{0.8} - s_1^{0.8}) - \left(\frac{1}{s} - \frac{1}{s_1}\right) - .95\left(\frac{1}{s^6} - \frac{1}{s_1^6}\right) \tag{95}$$

Examples of the predicted droplet deposition rates based on this analysis have been prepared for two representative cases, one Freon 12, and the other potassium. The conditions are

	Freon 12	Potassium
Specified Conditions		
	$T_s = 110°F$	$T_s = 1800°F$
	$D = .452"$	$D = .42"$
	$\frac{q}{A} = 10 \frac{Btu}{ft^2 - sec}$	$\frac{q}{A} = 28 \frac{Btu}{ft^2 - sec}$
	X at $s_1 = .516$	X at $s_1 = .488$
Computed Constants		
	$s_1 = 5$	$s_1 = 1$
	$\ell_r = .548$	

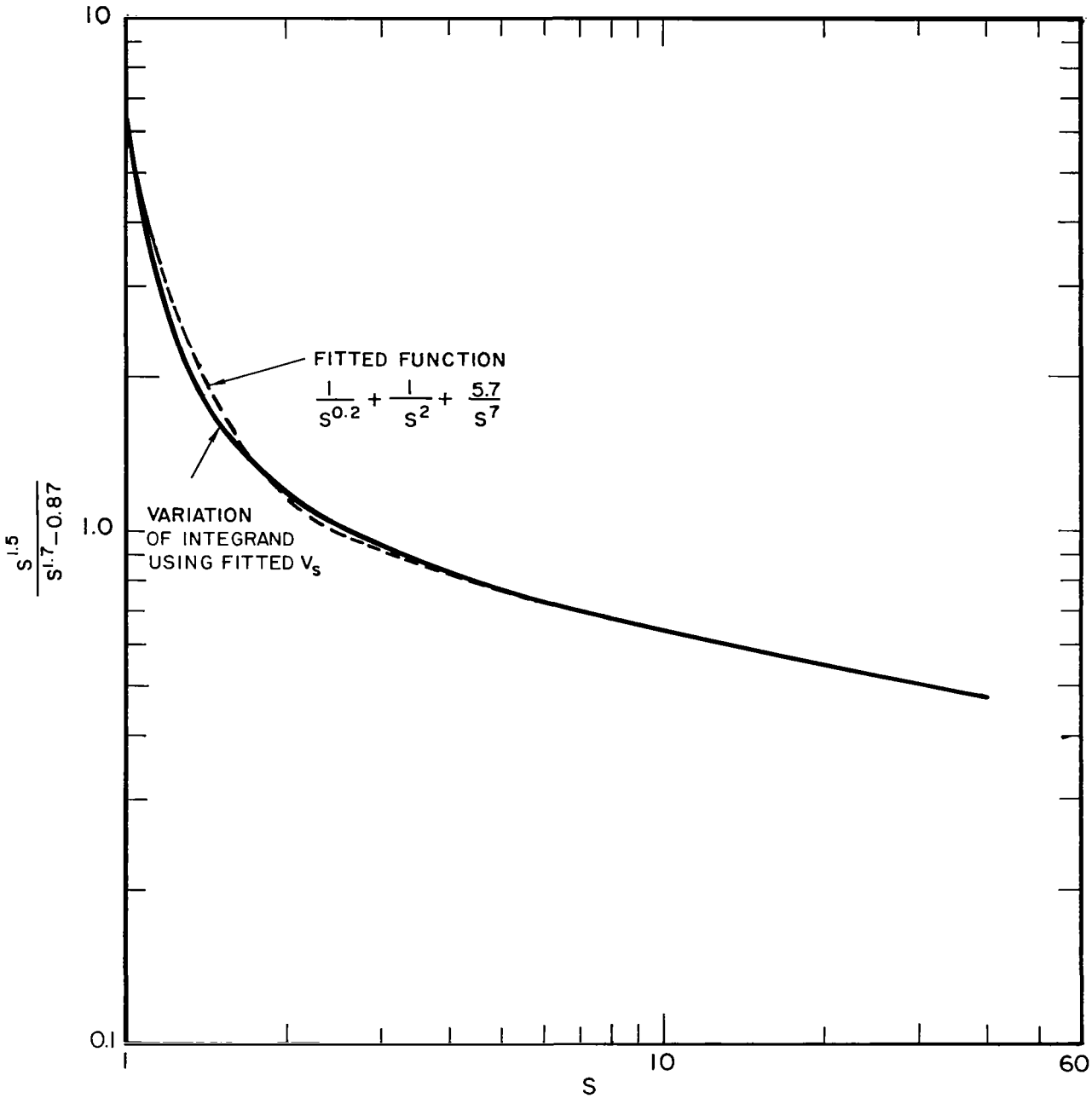

Figure 22. Comparison of integrand in Equation (94) with approximate function.

The resulting deposition rate graphs are shown in Figures 23 and 24. Although these curves are not exponentials in the coordinate s, an approximate effective characteristic length can be obtained from the variation of

$$\frac{w_e}{w_{e_0}}$$

as a function of s. For potassium, at

$$\frac{w_e}{w_{e_0}} = \frac{1}{e}, \quad (s - s_1) = .8$$

this corresponds to an axial tube length of 3.68 feet. For Freon 12, at

$$\frac{w_e}{w_{e_0}} = \frac{1}{e}, \quad (s - s_1) = .8$$

This corresponds to an axial tube length of .438 feet. The rate of decrease of entrained flow is almost an order of magnitude higher for Freon 12 than for potassium at the specified conditions.

7) Axial Path Lengths for Droplets with Transverse Velocity Components

Several of the preceeding analyses have described the axial motion of droplets in a boiler tube. There are a number of mechanisms by which droplets might obtain significant transverse velocities as well. One such possible mechanism, which is described and analyzed in Section C.5 of this report, is due to bursting of vapor bubbles in a nucleate boiling liquid film.

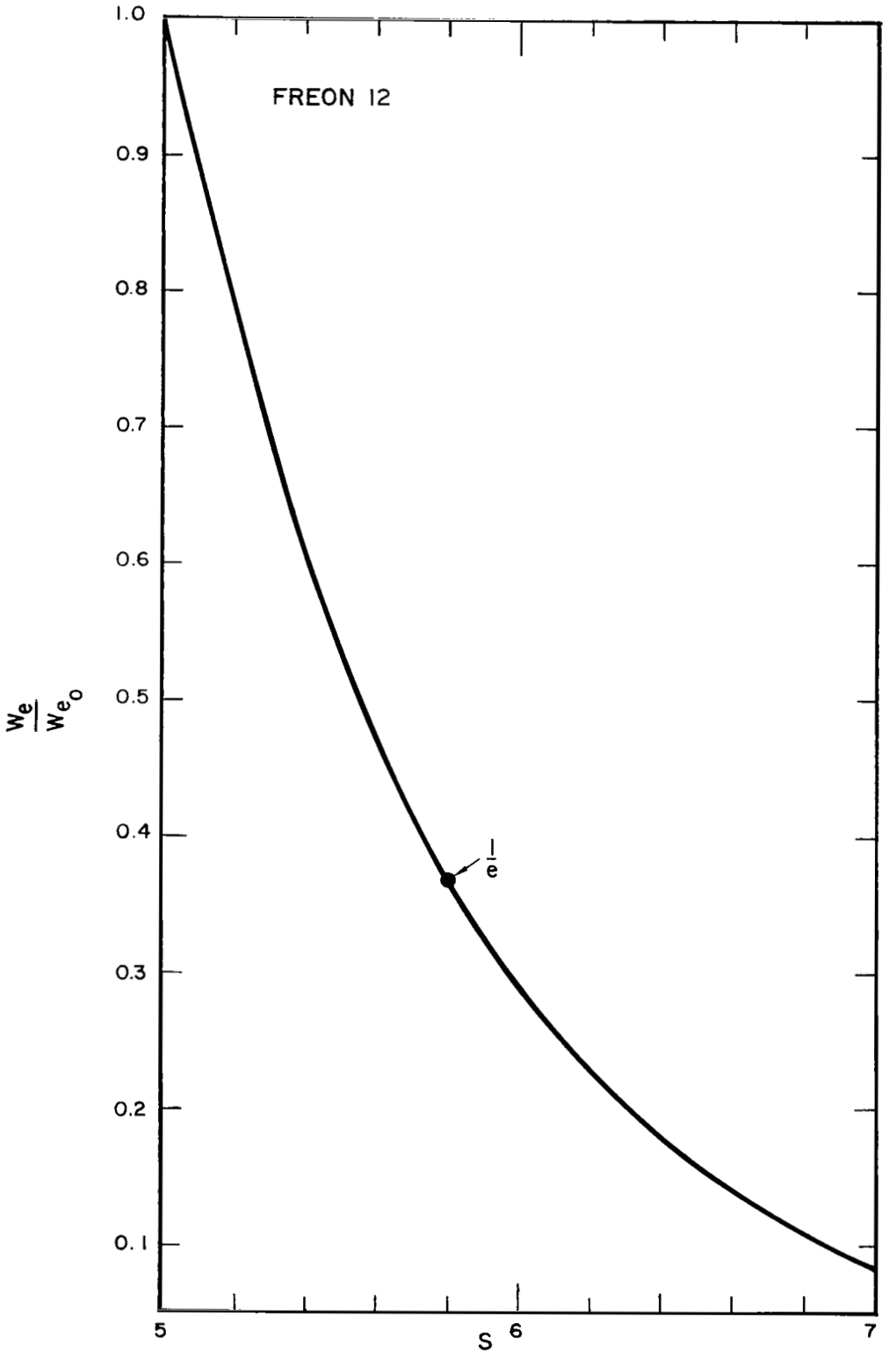

Figure 23. Rate of decrease of entrained liquid in Freon 12 boiler.

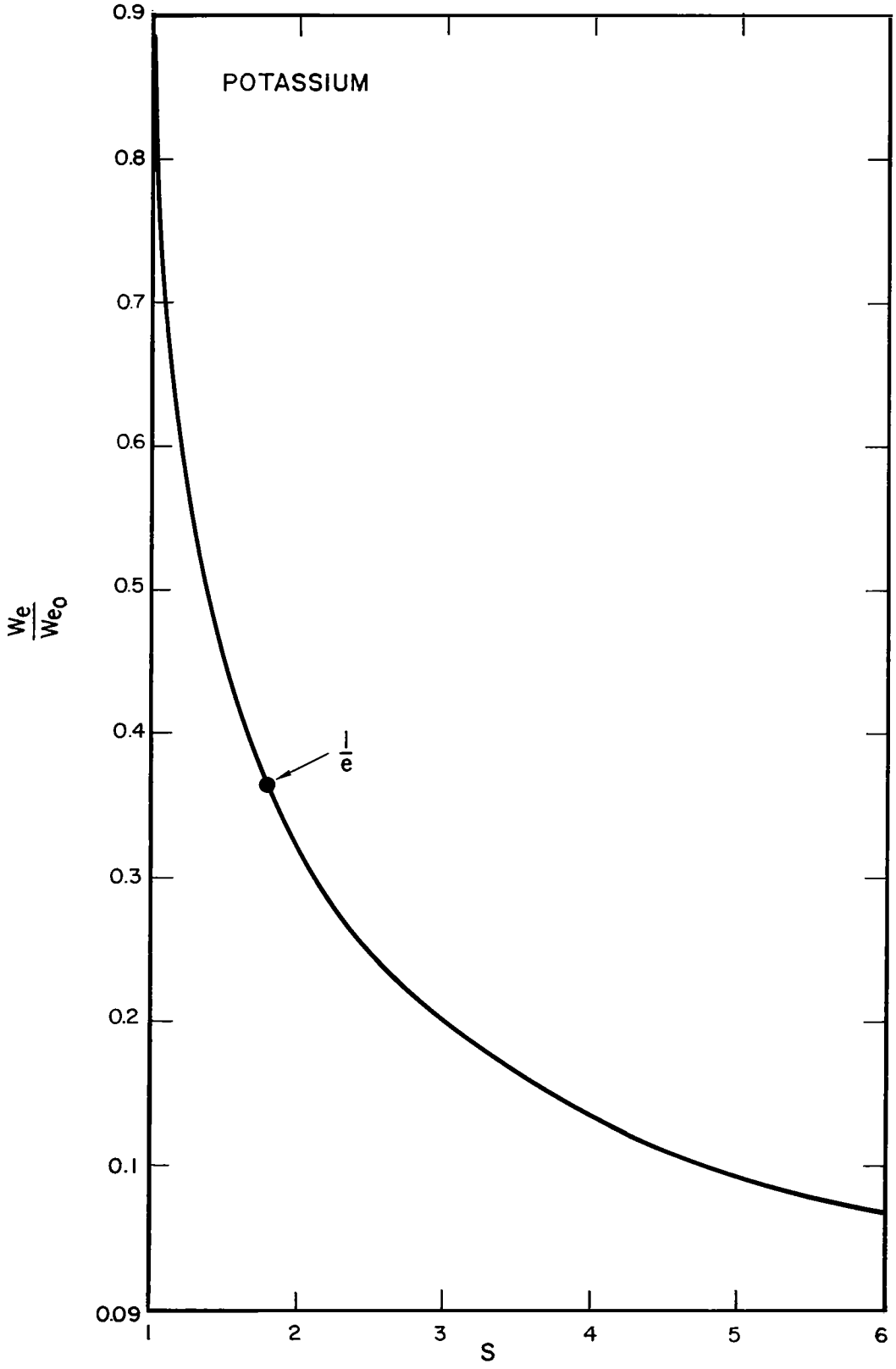

Figure 24. Rate of decrease of entrained liquid in potassium boiler.

The axial path length of droplets with transverse velocities is studied in the following paragraphs, with calculations based on velocities obtained from the ejection mechanism. Although the calculations of the mechanism are based on water observations, there is a general similarity between the surface tension and density of water and potassium, so one might expect ejection velocities of the two fluids to be similar.

Droplets ejected from an annular liquid film in forced convection nucleate boiling have a significant velocity component normal to the film surface. If the flow in the boiler tube is vertically upward, the gravitational field enters into the axial motion only, drag on the vapor is the only force acting in the transverse direction, and the transverse equation of motion is

$$-C_1 = \frac{1}{v_{tr}^2} \frac{dv_{tr}}{dt} \tag{96}$$

where v_{tr} is the transverse velocity component and the constant C_1 is defined on page 130. The appropriate initial condition is: $t = o$; $v_{tr} = v_{tro}$. This equation is easily integrated to yield the following relationship between velocity and time:

$$-C_1 t = \frac{1}{v_{tro}} - \frac{1}{v_{tr}} \tag{97}$$

A second integration yields

$$e^{C_1 \ell_t} = 1 + v_{tro} C_1 t \tag{98}$$

where ℓ_t is the transverse distance measured from the film surface.

These relationships may be easily expressed in the notation used for the analysis of accelerating droplets in a uniform heat flux boiler (Section B.3)

Equation (97) becomes

$$-\bar{t} = \frac{1}{\bar{v}_{tro}} - \frac{1}{\bar{v}_{tr}} \tag{99}$$

where

$$\bar{t} = \lambda t$$

and

$$\bar{v}_{tr} = \frac{v_t}{v_r}$$

Equation (98) becomes

$$e^{\bar{\ell}_t} = 1 + \bar{v}_{tro}\bar{t} \tag{100}$$

the maximum transverse path length is equal to the tube diameter, so that

$$\bar{\ell}_{t\,max} = \frac{D}{\ell_r}$$

With the specification of an initial transverse velocity, Equation (100) defines the maximum flight time for a droplet, and the distance the droplets are carried axially may be taken by interpolation from Figure 16. The results of such a calculation, for the same conditions as were used in Section B.3 (page 45), is given below. In the absence of any other information on the velocity of droplets ejected from nucleate boiling films, the same velocity as observed for water droplets, 4 ft/sec was used as a basis for the calculations (see page 131).

Droplet Diameter, inches	$\bar{t}$	$\bar{\ell} - \ell_o$	$\frac{\Delta\ell}{D}$
2×10^{-3}	.276	10	40
5×10^{-3}	.255	3	30
1×10^{-2}	.249	1.13	22.6
2×10^{-2}	.246	.35	14.0

As one would expect, the smallest droplets are swept the farthest downstream before impacting with the opposite wall of the tube. The two mil droplets are carried 40 diameters axially.

The two largest droplets would not have been in the stream long enough to have attained the predicted asymptotic slip. In fact, the 20 mil droplet would have only about half the velocity of the vapor at the time it impacted.

8) The Motion of Large Liquid Droplets in Helical Flow

It is usually assumed that droplets entrained in a helically flowing vapor in a boiler tube concentrate near the wall. However, droplets swept off a helical divider may take a significant amount of time to migrate to the wall, and since they travel in a spiral path to the wall, slipping with respect to the vapor and the helix, they could actually be redeposited on a helical vane rather than on the boiler tube wall. During the time they take to migrate to the wall the droplets are also swept axially downstream, and the axial flight time is also of significance. The study reported here is intended to provide some information about droplet paths in helical flow.

Idealizations which describe the model upon which the analysis is based are listed below:

1) The droplets are rigid and spherical
2) The axial vapor velocity is uniform
3) The rotational velocity field is similar to solid body rotation, so that the rotational vapor velocity is a linear function of radius
4) The droplet drag coefficient is constant
5) The liquid volume is negligible.
6) The droplet enters the flow with negligible velocity at a known point x_o, y_o, z_o
7) The droplet velocity in the transverse directions is negligible compared to the vapor velocity.

Since the axial vapor velocity is uniform, the motion in the z direction (lying along the tube axis) is independent of the x and y (transverse) motions. Therefore, only the motion in the x, y plane is considered here. The coordinate system is shown in Figure 25. The equations of motion are:

x direction

$$F_x = m \frac{d^2x}{dt^2} \tag{101}$$

where

F_x is the vapor drag force component in the x direction

m is the droplet mass

t is time

x is a transverse coordinate measured from the tube axis.

y direction

$$F_y = m \frac{d^2y}{dt^2} \tag{102}$$

where

F_y is the vapor drag force component in the y direction

y is a transverse coordinate orthogonal to the tube axis (z) and x.

The drag force components are taken to be

$$F_x = C_D A_d \frac{1}{2} \rho_v (v_{v_x})^2 \tag{103}$$

$$F_y = C_D A_d \frac{1}{2} \rho_v (v_{v_y})^2 \tag{104}$$

$$A_d = \frac{\pi}{4} D_p^2$$

and

$$m = \frac{\pi}{6} \rho_\ell D_p^3$$

where

C_D is the droplet drag coefficient

A_d is the droplet frontal area

ρ_v is the vapor density

v_{v_x} is the vapor velocity component in the x direction

v_{v_y} is the vapor velocity component in the y direction

D_p is the droplet (or particle) diameter

ρ_ℓ is the liquid density.

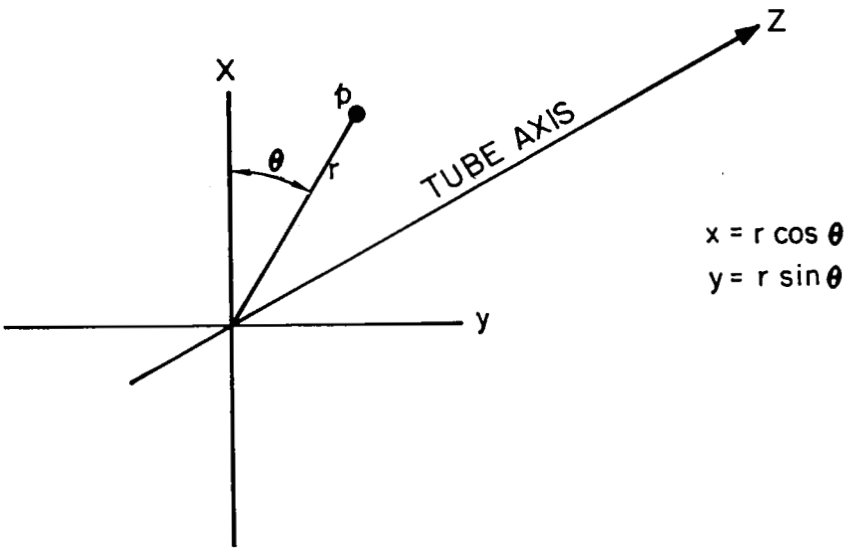

Figure 25. Coordinate system.

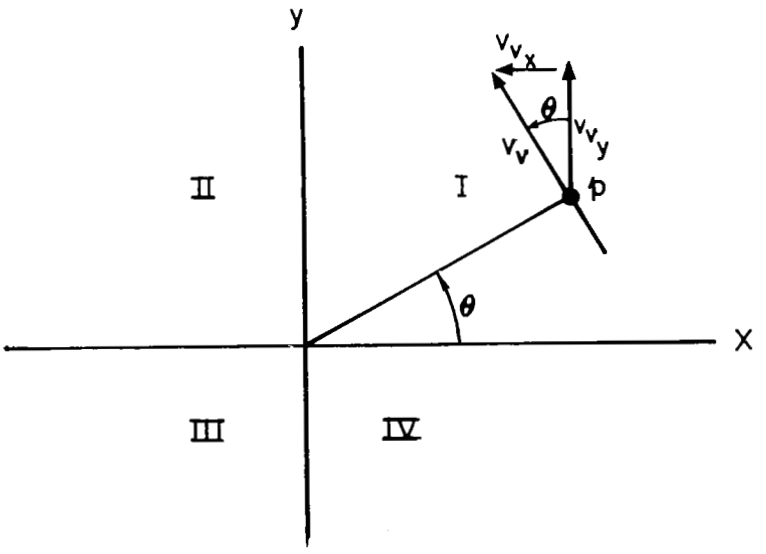

Figure 26. Vapor velocity components seen from the -Z direction (right handed helix). Helix and vapor rotation are in the $+\theta$ direction.

The vapor velocity at any point is $v_v = kr$, where r is the radius from the tube axis, k is a constant, and the velocity is in the direction normal to the radius.

Consider motion of the particle in the first quadrant, facing upstream (in the -z direction) so that the vapor rotation is counterclockwise. The droplet is at point p. A diagram of the vapor velocity components is shown in Figure 2. The signs of the drag force components are given in the following table:

Quadrant	F_x	F_y
I	-	+
II	-	-
III	+	-
IV	+	+

The vapor velocity components are given by

$$v_{v_x} = -kr\sin\theta$$

$$= -ky$$

$$v_{v_y} = kr\cos\theta$$

$$= kx$$

The constant k has the units of $(\text{time})^{-1}$, so that the characteristic time τ_r may be defined as

$$\tau_r = \frac{1}{k}$$

A convenient characteristic velocity is therefore

$$v_r = \frac{\ell_r}{\tau_r}$$

The same characteristic length used in Section B.3 appears here. It is

$$\ell_r = \left(\frac{3}{4}\frac{C_D}{D_p}\frac{\rho_v}{\rho_\ell}\right)^{-1}$$

The normalized variables are defined as

$$\bar{x} = \frac{x}{\ell_r}, \quad \bar{y} = \frac{y}{\ell_r}$$

$$\bar{v}_{v_x} = \frac{v_{v_x}}{v_r}, \quad \bar{v}_{v_y} = \frac{v_{v_y}}{v_r}$$

$$\bar{t}_r = \frac{t}{\tau_r}$$

With these definitions, the equations of motion (101) and (102) become

$$\frac{d^2\bar{x}}{d\bar{t}_r^2} = -\bar{y}^2 \tag{105}$$

and

$$\frac{d^2\bar{y}}{d\bar{t}_r^2} = +\bar{x}^2 \tag{106}$$

for the first quadrant.

These two equations are coupled and non-linear and no obvious method of obtaining a closed-form solution is available. They have been solved numerically by a tedious but straightforward iteration technique, with a single parameter, $\bar{x}_o$, the starting location. Since the vapor velocity field is axially symmetric, no loss of generality results from choosing initial locations along the x axis. A typical trajectory and useful nomenclature are presented in Figure 27. The characteristics of one specific trajectory are given in Figures 28, 29, and 30. Because of the nature of the dynamic model, one might expect that the shape of the particle trajectory in a plane normal to the tube axis would be independent of the starting location. That this is the case is demonstrated in Figure 31. In this figure, all three normalized trajectories in the $\bar{r}, \theta$ plane have been superimposed and it may be seen that aside from some scatter (probably due primarily to inaccuracies in the calculation method) the trajectories have a similar shape. The particles from different starting radii do not, however, reach similar points along the trajectory at the same times. The variation of the angle θ with time for the three starting locations is shown in Figure 32.

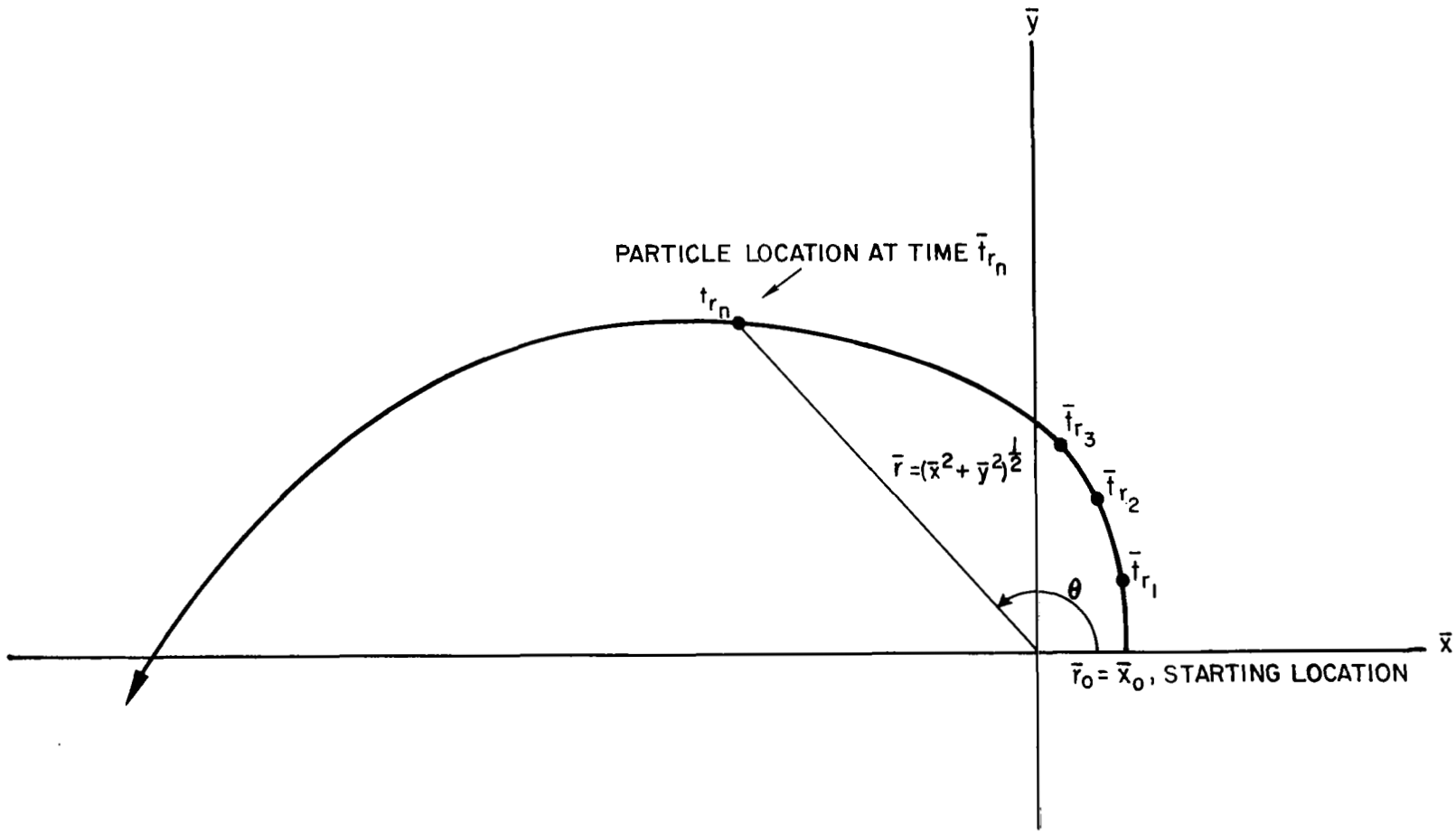

Figure 27. Schematic diagram of droplet trajectory in the directions transverse to the tube axis. Origin of coordinates fixed at the tube centerline. (Projection of helical droplet path onto a plane transverse to the tube axis.)

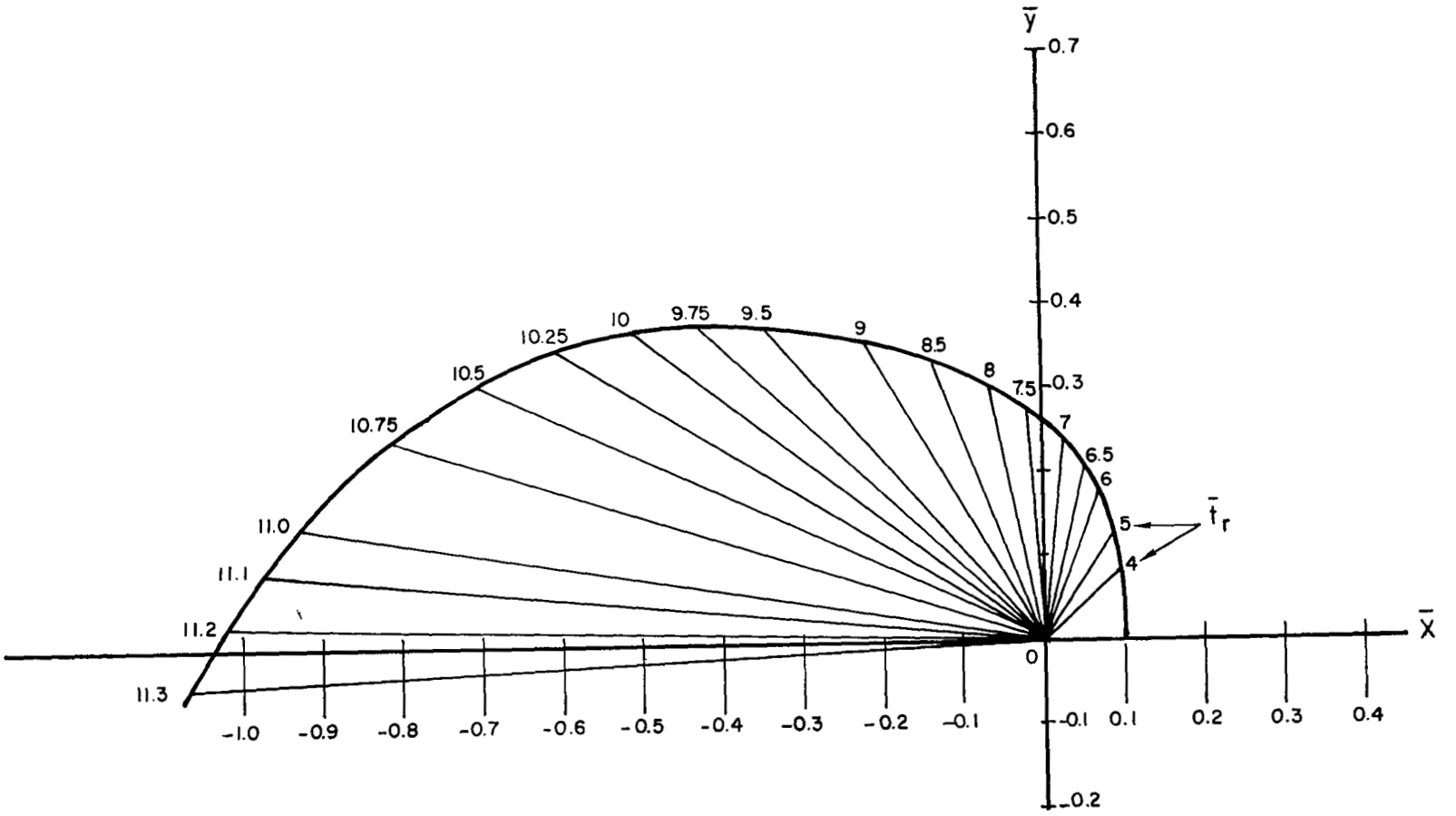

Figure 28. Motion of a droplet in helical flow, $\bar{x}_o = 0.1$.

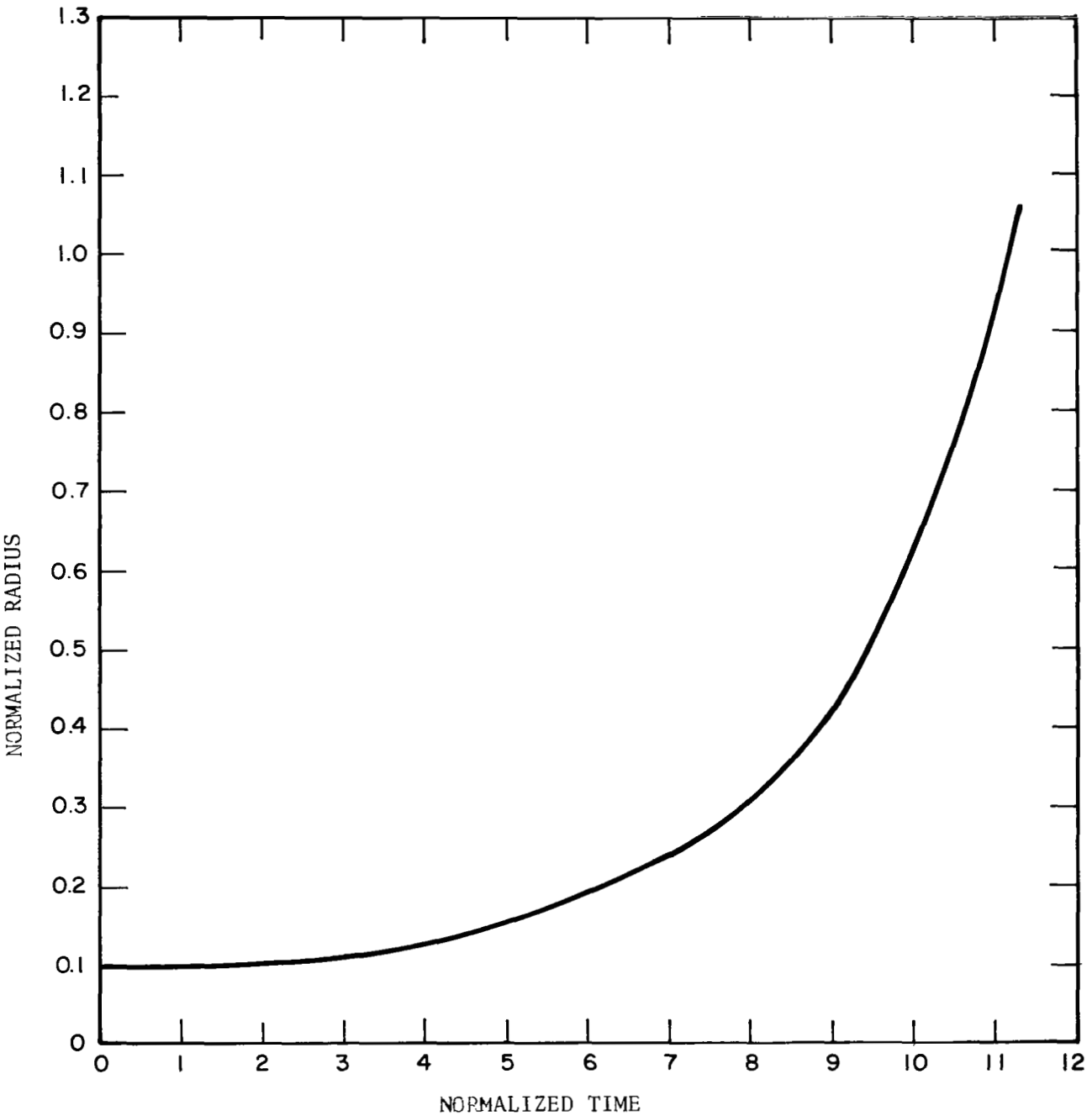

Figure 29. Radius versus time. Droplet in helical flow, $\bar{x}_o = 0.1$.

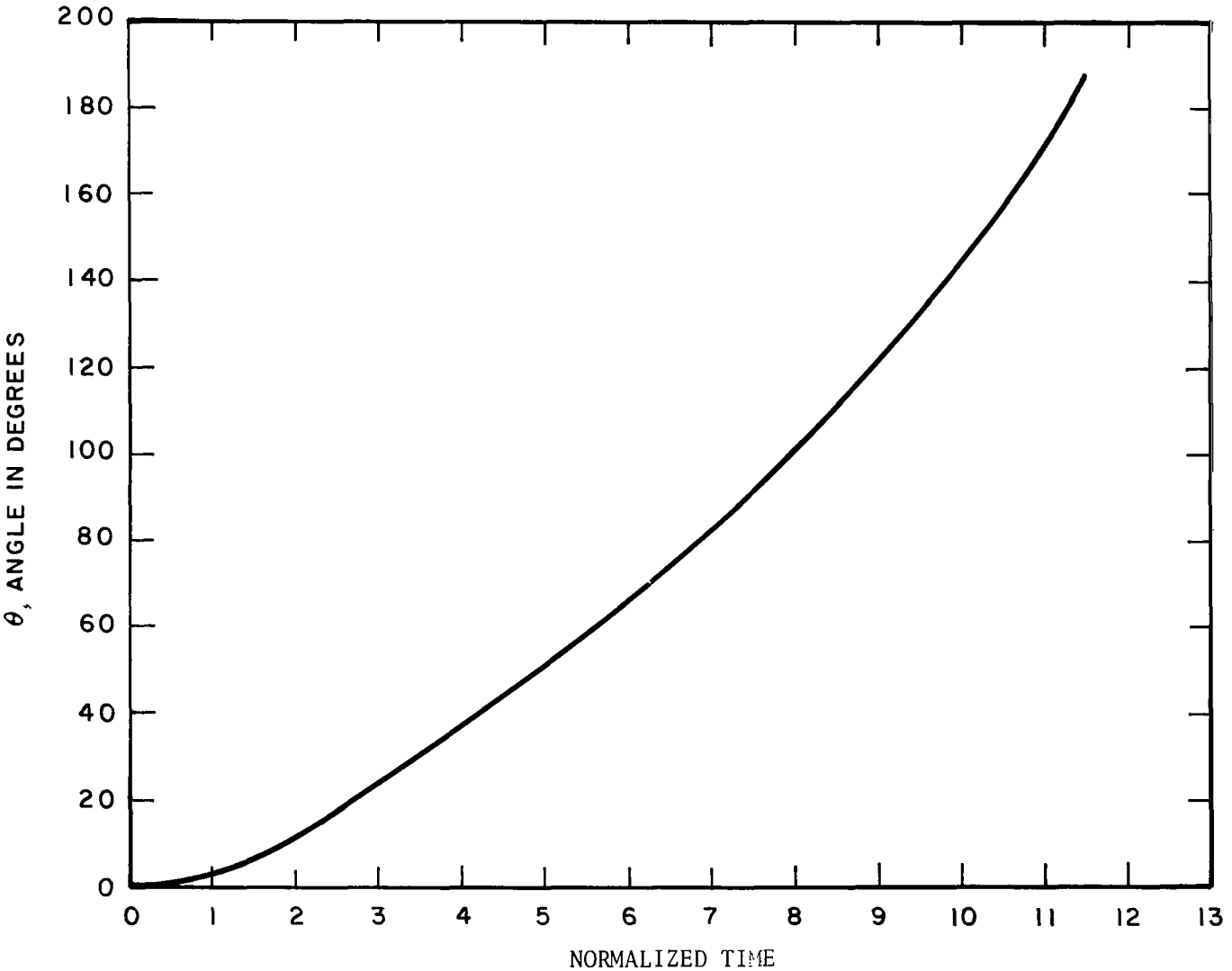

Figure 30. Angle versus time for droplet in helical flow, $\bar{x}_o = 0.1$.

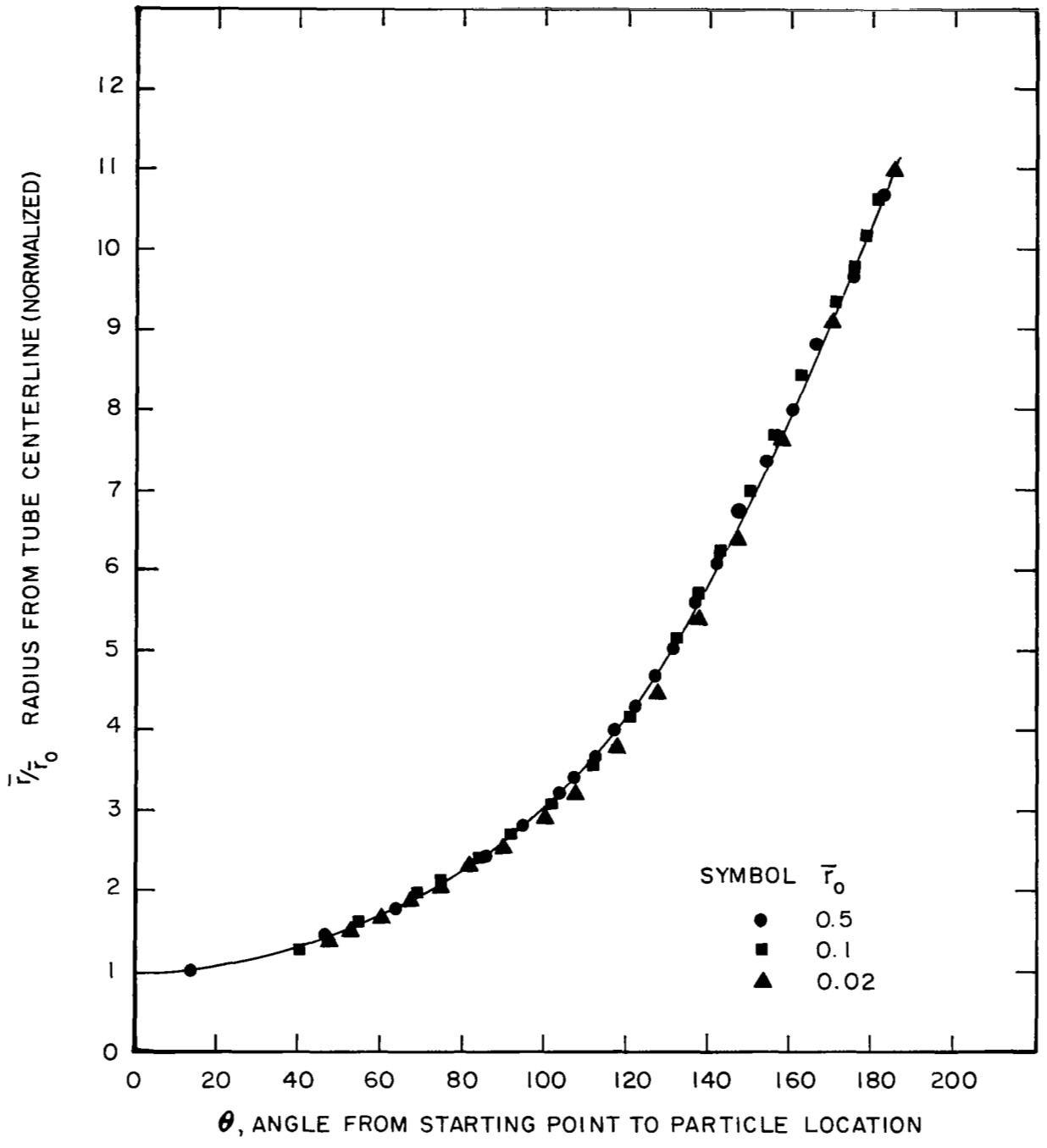

Figure 31. Comparison of computed particle trajectories for three starting locations.

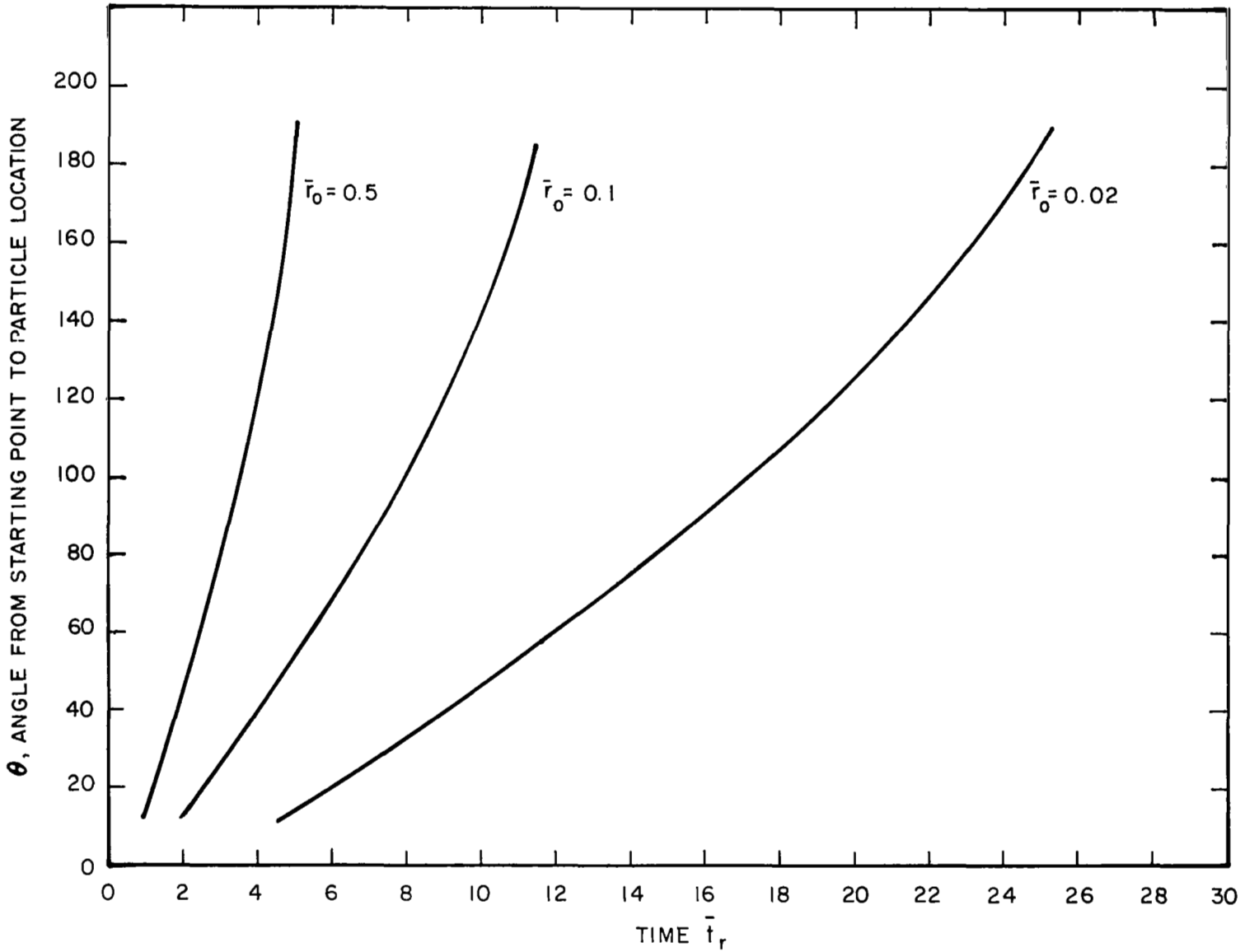

Figure 32. Angle from starting point versus time for three normalized starting locations.

9) Droplet Trajectories in a Helical Flow Boiler

The analysis of transverse motion of entrained droplets in a helical flow given in Section B.8 may be combined with any of the analyses of axial motion to compute three-dimensional trajectories. As an example of the procedure, in the following paragraphs the transverse motion has been combined with the axial motion analysis of Section B.3 (constant mass droplets, uniform heat flux). In order to illustrate the calculation method, a specific example has been carried through in detail. The boiler tube and its operating conditions are identical to those used in Section B.3 but it is assumed that a single vane helical insert with a centerbody is in the tube. A sketch of the three dimensional motion is shown in Figure 33. The conditions are:

Fluid: Potassium at 1800°F

Tube Diameter: 0.42 inch

Heat Flux (Uniform): 28 Btu/ft^2 sec

Mass Velocity G: 30 lb/ft^2 sec

Helical Insert: $\frac{p}{D} = 3.1416$

Quality X: 0.8

The calculation proceeds as follows:

vapor flow rate = GX

= 24 lb/ft^2 sec

axial vapor velocity (uniform) 160 ft/sec

vapor velocity normal to tube axis at the tube surface $= \frac{\pi D}{p} v_{axial}$

= 160 ft/sec

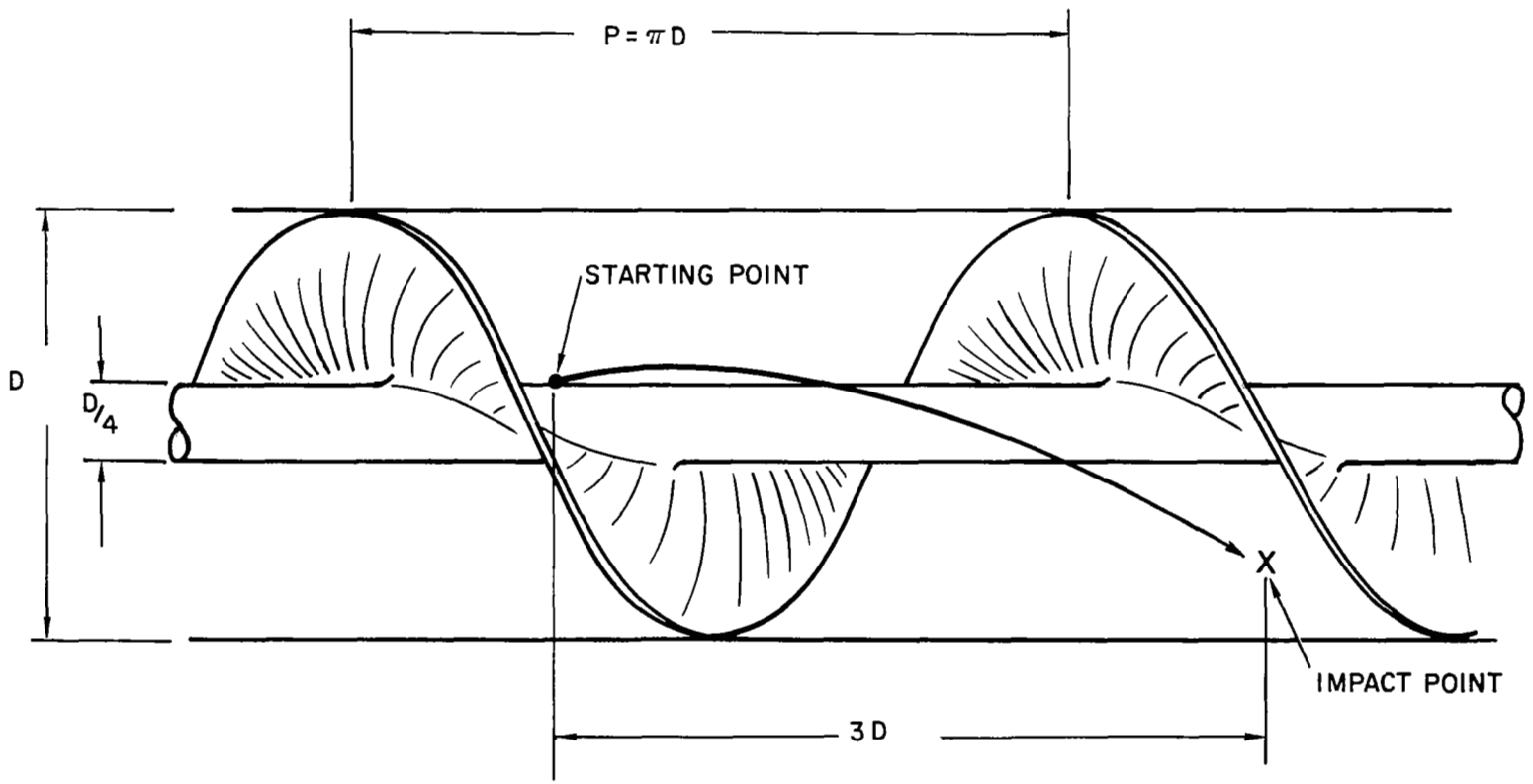

Figure 33. Sketch of droplet motion.

From Section B.8, the relationship for the vapor velocity normal to the tube axis is

$$v_v = kr$$

where

$$r = (x^2 + y^2)^{\frac{1}{2}}$$

Therefore

$$k = \frac{160 \text{ ft/sec}}{0.21 \text{ inch}}$$

$$= 9150/\text{sec}$$

Consider 1 mil diameter droplets.

From the definition of the characteristic length ℓ_r,

$$\frac{\ell_r}{D} = \frac{4 D_p}{3 D} \frac{\rho_\ell}{\rho_v} \frac{1}{C_D}$$

where

D_p is the particle (droplet) diameter

D is the tube diameter

C_D is the droplet drag coefficient (taken as 0.4)

ρ_ℓ is the liquid density

ρ_v is the vapor density.

For the conditions stated,

$$\frac{\ell_r}{D} = 2$$

The droplet for this example is injected into the stream at a radius 1/4 of the tube radius (possibly by being stripped from a centerbody of diameter $\frac{D}{4}$).

Thus

$$x_o = r_o = \frac{D}{8}$$

and

$$\bar{r}_o = \frac{\left(\frac{D}{8}\right)}{\left(\frac{\ell_r}{D}\right) D}$$

$$= \frac{1}{16}$$

The droplet collides with the wall at the point

$$\bar{r} = 4\bar{r}_o$$

$$= \frac{1}{4}$$

From Figure 31, $\frac{\bar{r}}{\bar{r}_o} = 4$ at $\Theta = 118°$.

From Figure 32, by graphical interpolation to $\bar{r}_o = 0.063$, $\bar{t}_r = 11.5$*

$$t_r = \bar{t}_r \tau_r$$

$$= \frac{\bar{t}_r}{k}$$

$$= 1.25 \text{ milliseconds}$$

From Section B.3,

$$\bar{t}_a = \lambda t$$

* In this section the normalized time $\bar{t}_r$ is used for the radial motion. The symbol $\bar{t}_a$ is used for the axial motion computed in Section B.3. The two quantities are defined using different characteristic lengths. These two time scales must therefore be kept distinct.

where

$$\lambda = \frac{4\left(\frac{q}{A}\right)}{\rho_v D L}$$

$\left(\frac{q}{A}\right)$ is the uniform heat flux

and

L is the latent heat of vaporization

For the present conditions,

$$\lambda = 27.7/\text{sec}$$

therefore,

$$\bar{t}_a = .0346$$

The axial normalized starting point in the boiler is

$$\bar{\ell}_o = \frac{\left(\frac{\ell_o}{D}\right)}{\left(\frac{\ell_r}{D}\right)}$$

The axial and radial motion characteristic lengths are identical.

The droplet injection point is at quality X = 0.8, which occurs 140 tube diameters from the onset of boiling with this heat flux. Therefore

$$\bar{\ell}_o = 70$$

By interpolation from Figure 16 of Section B.3, for the conditions $\bar{\ell}_o = 82$ and $\bar{t}_a = 0.035$

$$\bar{\ell} - \bar{\ell}_o = 1.5$$

The axial distance the one mil diameter droplet travels before impact with the wall is therefore

$$\frac{\ell - \ell_o}{D} = (\bar{\ell} - \bar{\ell}_o)\frac{\ell_r}{D}$$

$$= 3$$

The droplet travels three tube diameters downstream, and rotates an angle of 118° about the tube axis. Its distance from the tube axis, which started at D /8 has grown until it impacts with the tube wall.

This droplet may or may not impact on the helical vane. If its starting point is in roughly the first third of the distance between two successive pitches it will probably hit the wall. If the helix has two vanes (or if there is a multi-slot insert) the droplet will almost certainly hit one of the vanes, regardless of the axial location of its starting point between pitches of the helix.

A number of other specific cases of droplet motion have been worked out and are presented together with the detailed example in Table 1. Graphs of the effect of droplet diameter on axial length to impact and the effect of helix pitch length on axial length to impact have been constructed from this table and are presented in Figures 34 and 35.

TABLE 1

With the exception of droplet diameter and helix pitch, all conditions are identical to those given on page 86 of this report.

D_p	$\frac{p}{D}$	k (1)	$\frac{\ell_r}{D}$ (2)	$\bar{r}_o$	$\bar{t}_r$	t_r (3)	$\bar{t}_a$	$\bar{\ell}_o$	$\bar{\ell} - \bar{\ell}_o$	$\frac{\ell - \ell_o}{D}$
inches		sec^{-1}				sec				
$.1 \times 10^{-3}$	π	9150	.5	.25	5.7	$.62 \times 10^{-3}$	.017	280	2.5	1.25
$.5 \times 10^{-3}$	π	9150	1	.125	8	$.88 \times 10^{-3}$	.024	140	2.3	2.3
1×10^{-3}	π	9150	2	.063	11.5	1.25×10^{-3}	.035	70	1.5	3
3×10^{-3}	π	9150	6	.0208	18.5	2.02×10^{-3}	.056	23	.66	4.0
1×10^{-3}	$\pi/2$	18,300	2	.063	11.5	$.62 \times 10^{-3}$	.017	70	.81	1.62
1×10^{-3}	$\pi/4$	36,600	2	.063	11.5	$.31 \times 10^{-3}$	.0086	70	.4	.8

(1) characteristic time for radial motion

(2) characteristic length for axial and radial motions

(3) time to impact with wall (actual impact may be on helix)

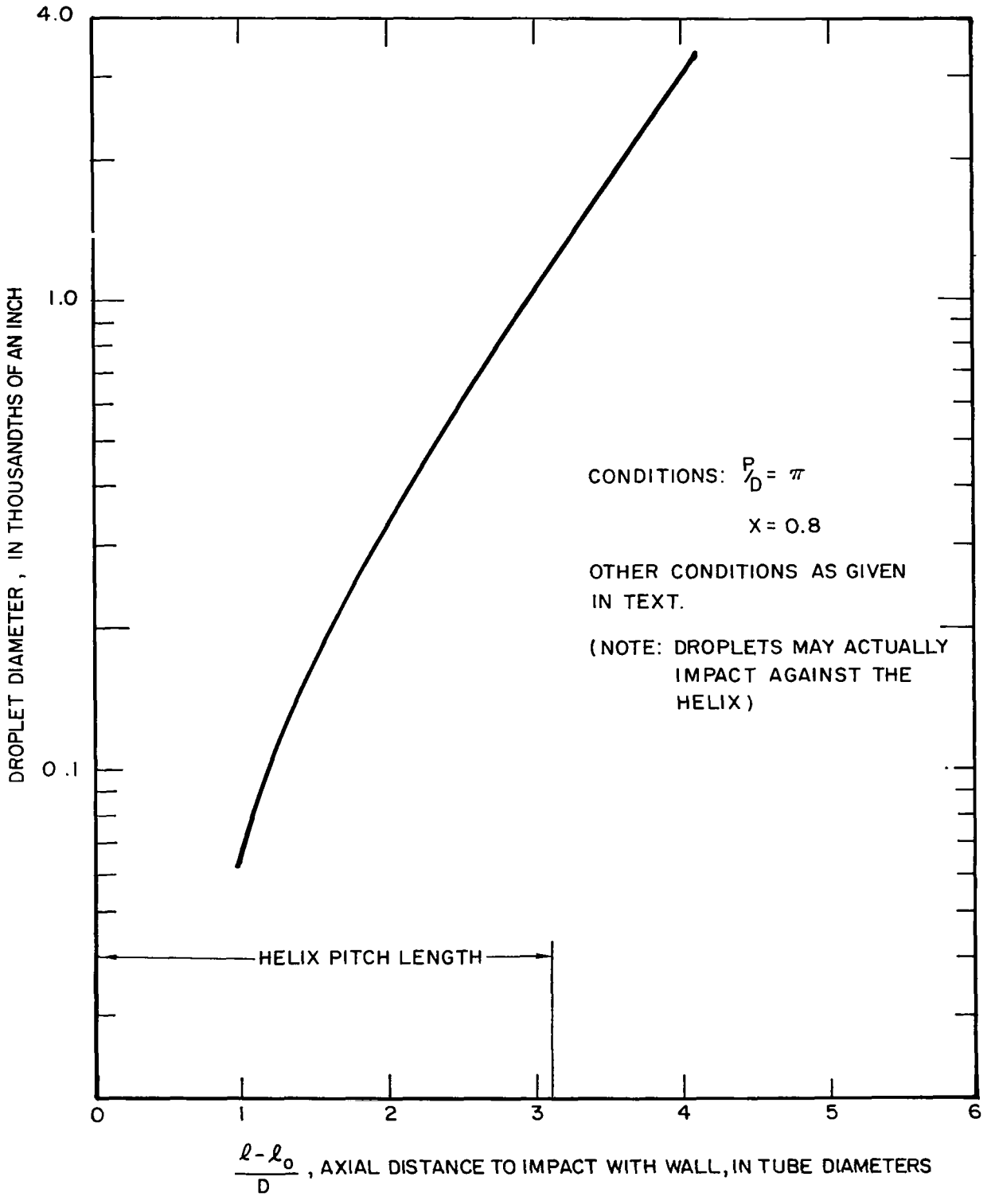

Figure 34. Axial distance to impact on tube wall for droplets shed off centerbody ¼ tube diameter.

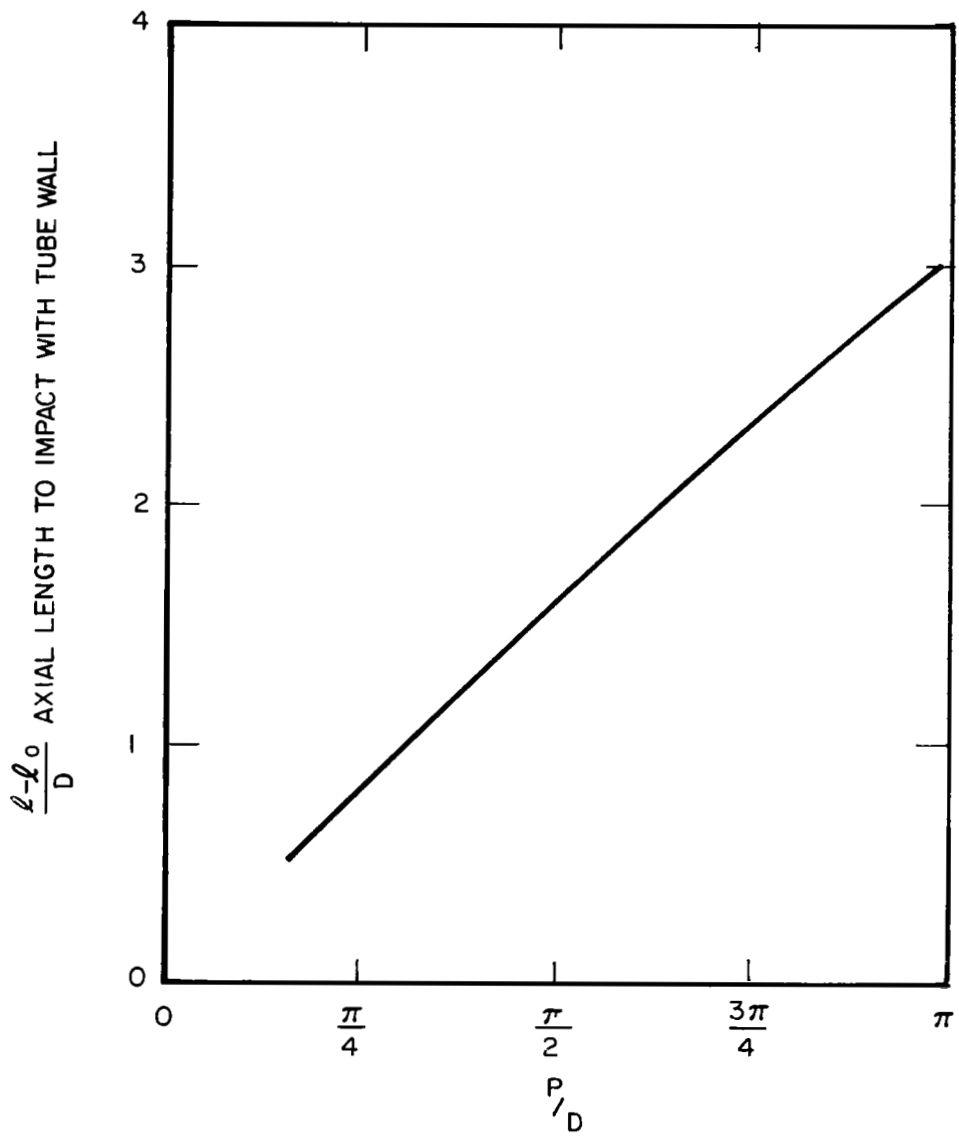

Figure 35. Axial distance to impact on tube wall for droplets shed off centerbody 1/4 tube diameter; function of helix pitch length.

10) Spacing of Sections of an Interrupted Insert

In order to remove liquid from the centerbody of a boiler helical insert, it has been proposed to interrupt the insert for an interval so that the liquid flowing along the centerbody would be shed as droplets and returned to the heat transfer wall. The analysis presented here is intended to provide information about the proper axial lengths for such insert gaps.

Several phenomena are taking place simultaneously which affect the droplet motion. The droplets, initially at rest, slip with respect to the vapor in both the axial and rotational motions, and are accelerated in a three dimensional spiral path due to drag forces. At the same time the vapor rotation, no longer maintained by the helix, begins to decay due to boiler wall friction, and the vapor axial velocity continues to increase due to vapor addition from vaporization.

In addition, the droplets may be undergoing fragmentation due to internal flow instabilities, vapor shear gradients, or other forces. In order to analyse this complex two phase flow, three major restrictions have been made, which are:

1) The axial vapor velocity change is negligible within the axial length required for the droplets to impact on the wall.

2) The vapor angular velocity change is negligible within the axial length required for the droplets to impact on the wall.

3) The droplet size is invariant during flight.

With these restrictions, the motion of the droplets may be synthesized from the helical motion computations given in Sections B.2 and B.8. A sketch of the geometry of the composite problem is shown in Figure 36.

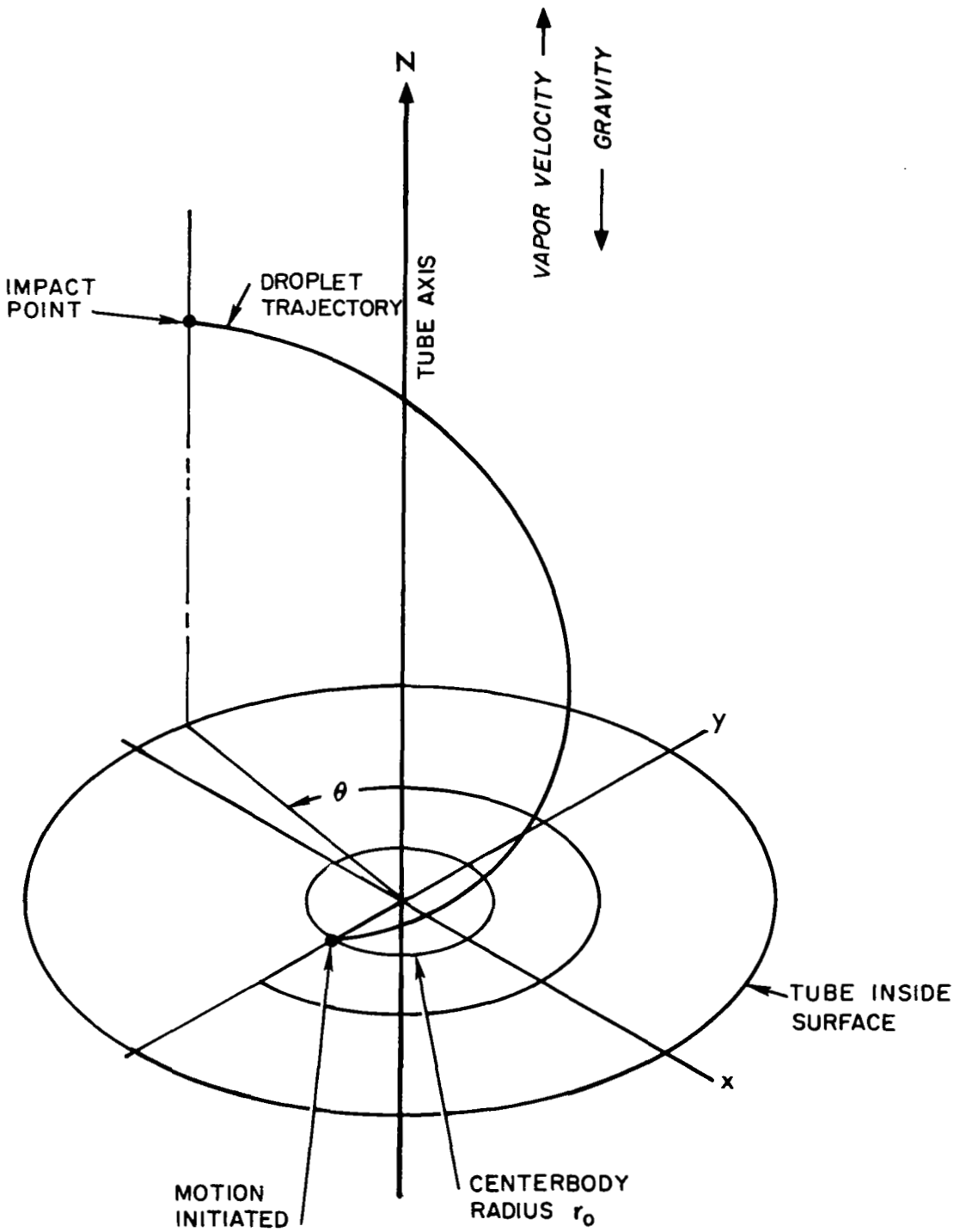

Figure 36. Sketch of droplet motion.

The analysis in Section B.8 of the motion of droplets in a helical flow yields the normalized droplet radius from the centerline as a function of angle (measured about the centerline from the position droplet motion is initiated) and normalized time, with initial normalized radius as the single parameter. Because of the nature of the analysis, the helical motion utilizes the same reference length as that which appears in the analysis of Section B.2 but a different reference time. Denote the radial normalized time by $\bar{t}_r$. The relationship between the two time scales is

$$t = \bar{t}_r \tau_r = \bar{t}_a \tau_a$$

or, by substitution of the characteristic times for the two cases

$$\frac{\bar{t}_r p}{2 v_a \pi} = \frac{\bar{t}_a}{\frac{3}{4} \frac{C_D}{D_p} \frac{\rho_v}{\rho_\ell} v_a}$$

$$\bar{t}_a = \bar{t}_r \left[\frac{3}{8} C_D \left(\frac{\rho_v}{\rho_\ell} \right) \left(\frac{p}{\pi D} \right) \left(\frac{D}{D_p} \right) \right] \tag{107}$$

Droplet helical motions were computed for three different initial radii and the trajectories were shown to be geometrically similar in Figure 31 of Section B.8. The relationships between angle and time and between normalized radius and time, not presented previously, but cross-plotted from Figures 31 and 32 are shown in Figures 37 and 38. In these figures, the normalized time is expressed as

$$\frac{\bar{t}_r}{\bar{t}_{r_{180°}}}$$

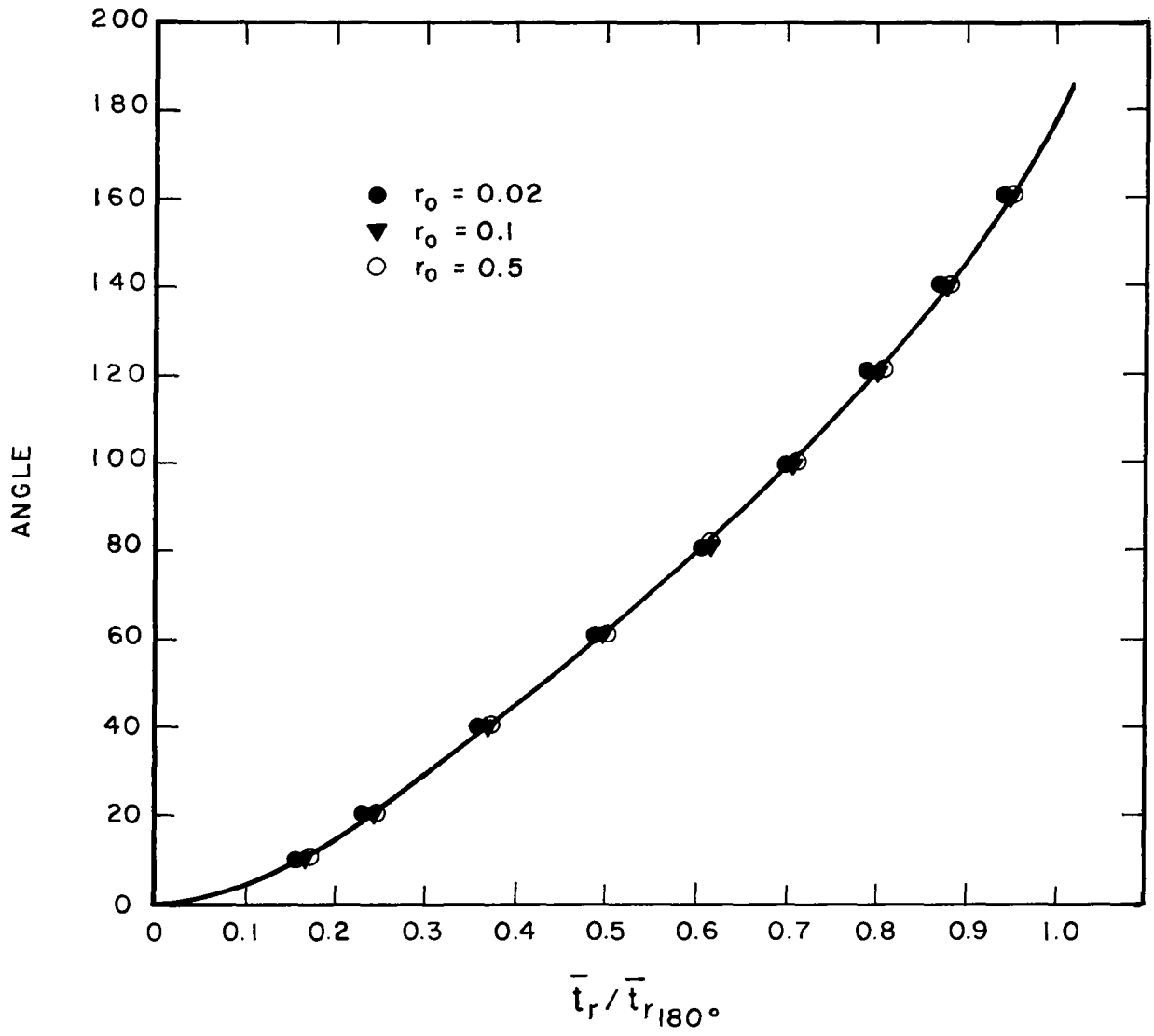

Figure 37. Helical motion of droplets: Angle θ versus time for three starting radii.

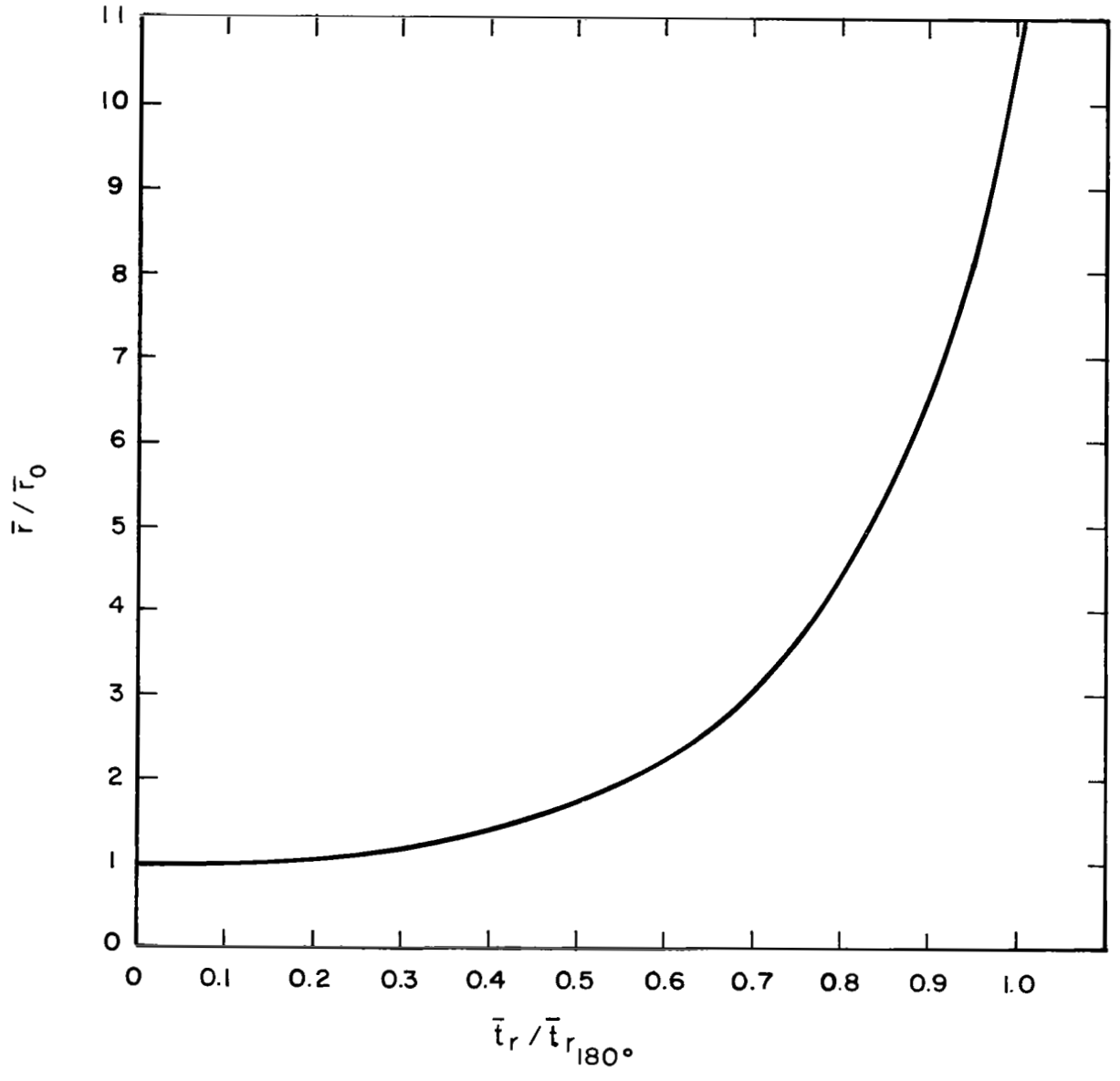

Figure 38. Helical motion of droplets: Radius ratio versus time ratio, an average trajectory for three starting radii.

where $\bar{t}_{r_{180°}}$ is the normalized time at which the droplet has traveled halfway around the tube from its starting point. Figure 39 shows the variation in time to travel halfway around the tube as a function of centerbody radius. This relationship is not as well established as the others, but the variation is probably regular enough to use for estimation of intermediate centerbody radii.

Data for a specific boiler would be

$\frac{D}{2}$, boiler tube inside radius

r_o, centerbody radius

p, pitch of the helical vane

Other known data are ρ_v, ρ_ℓ, and C_D. The latter constant may be taken as 0.4 for a wide range of conditions.

Fluid: Potassium at 1800°F saturation temperature.

$$\left(\frac{\rho_v}{\rho_\ell} = 0.04\right)$$

Particular geometrical constants required are:

$$\frac{p}{D} = 1$$

$$\frac{D}{2r_o} = 4$$

Since the droplet starts its motion at r_o, and impacts on the tube wall at the radius D/2, then $r/r_o = 4$ at impact. From Figure 38, $t_r/t_{r_{180°}} = 0.78$ at impact. From Figure 37, $\theta = 118°$ at impact.

Consider droplets of the size such that

$$\frac{D}{D_p} = 100$$

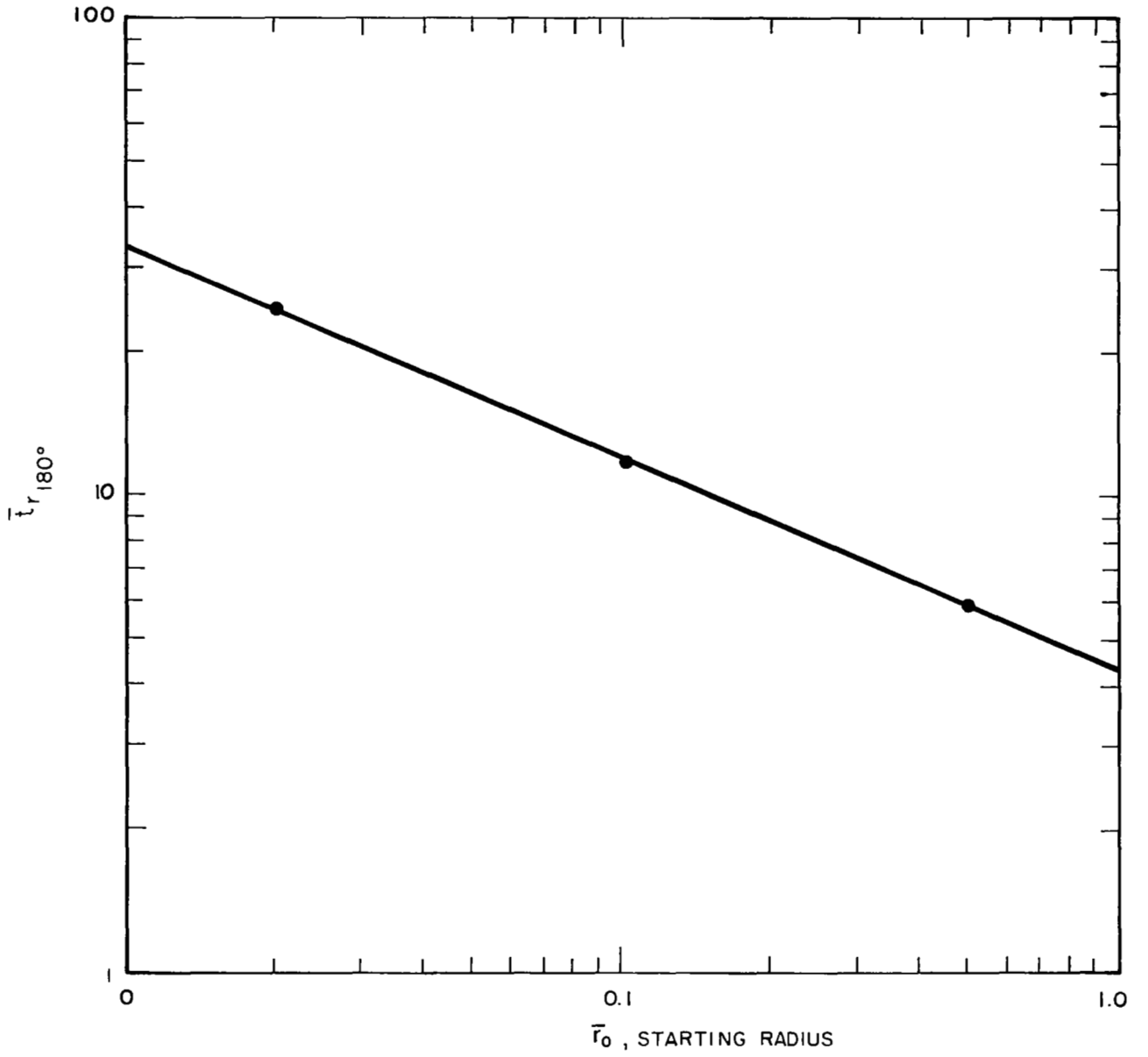

Figure 39. Helical motion of droplets: Variation in $\bar{t}_{r_{180°}}$ with $\bar{r}_o$.

For the stated conditions,

$$\bar{r}_o = \left(\frac{2r_o}{D}\right)\frac{3}{8} C_D \left(\frac{\rho_v}{\rho_\ell}\right)\left(\frac{D}{D_p}\right) \tag{108}$$

$$= 0.15$$

From Figure 39, $\bar{t}_{r_{180°}} = 10$ at impact.

The axial normalized time to impact is, from Equation (107), $t_a = 1.91$.

From Figure 11, (for g negligible) $\bar{z} = 0.8$.

From the definition of $\bar{z}$,

$$\frac{z}{D} = \frac{\bar{z}}{\frac{3}{4} C_D \left(\frac{D}{D_p}\right)\left(\frac{\rho_v}{\rho_\ell}\right)} \tag{109}$$

For the stated conditions,

$$\frac{z}{D} = .833\,\bar{z}$$

The impact point will be at an axial distance down the tube corresponding to

$$\frac{z}{D} = .667$$

An insert interruption only one tube diameter long would be adequate for this size of droplet. A graph showing the required spacing for other conditions is shown in Figure 40. It appears from these calculations that for the short pitch helical inserts generally proposed a one diameter long interruption would be adequate for even quite large droplets.

A rather striking photograph of the deposition of droplets shed from the interrupted centerbody of a helical insert is shown in Figure 41. This photograph, which supports the analysis presented here, was taken during the air-water experiments reported in Reference 3, and was provided through the courtesy of Mr. G. Converse of General Electric Missile and Space Division.

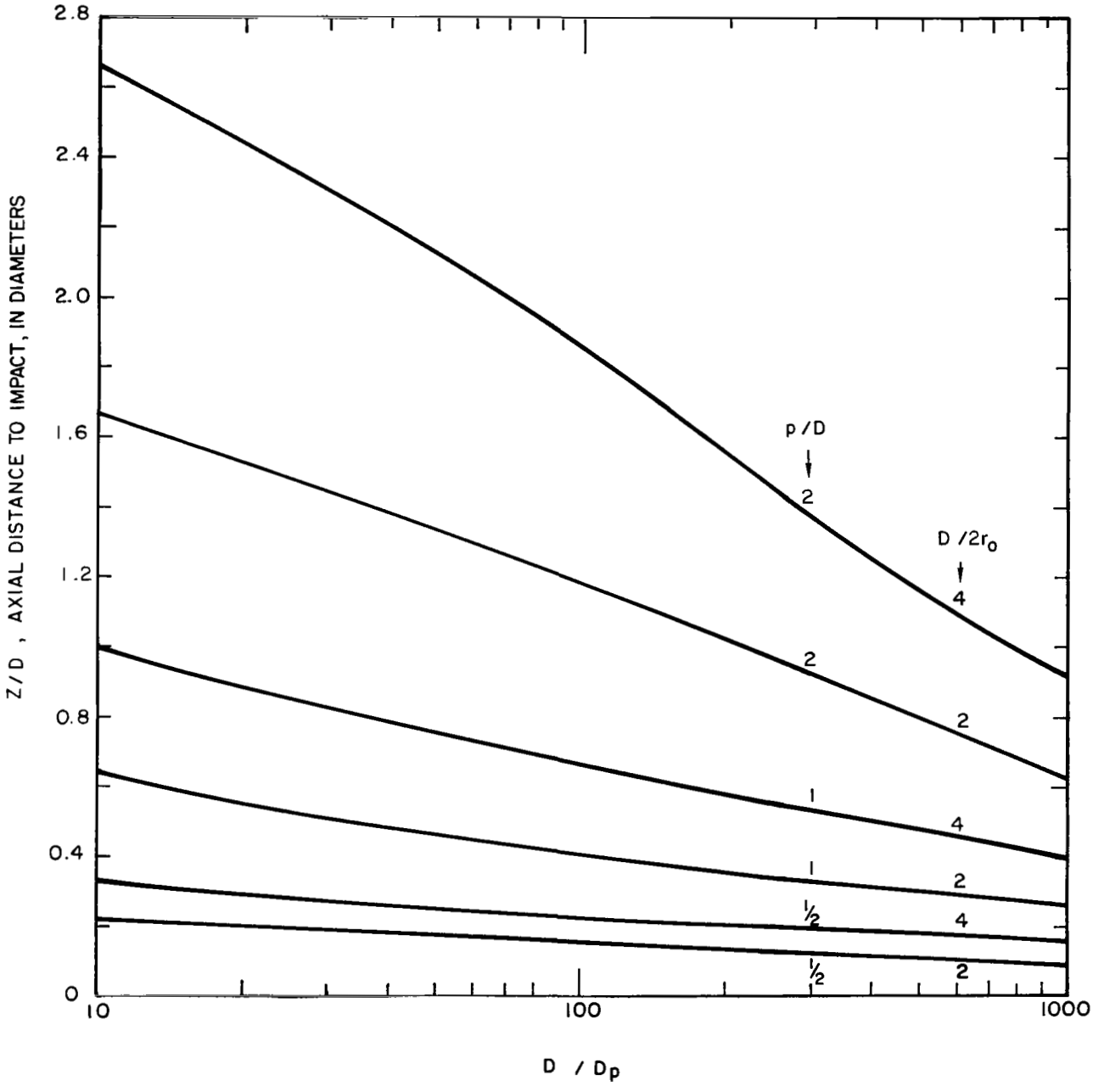

Figure 40. Axial distance to impact on wall as a function of droplet diameter helix pitch, and centerbody diameter for cases with negligible gravity field.

W_{H_2O} = 0.00217 lb/sec Tube I.D. = 0.875 in.

W_{air} = 0.050 lb/sec. x = 0.9584

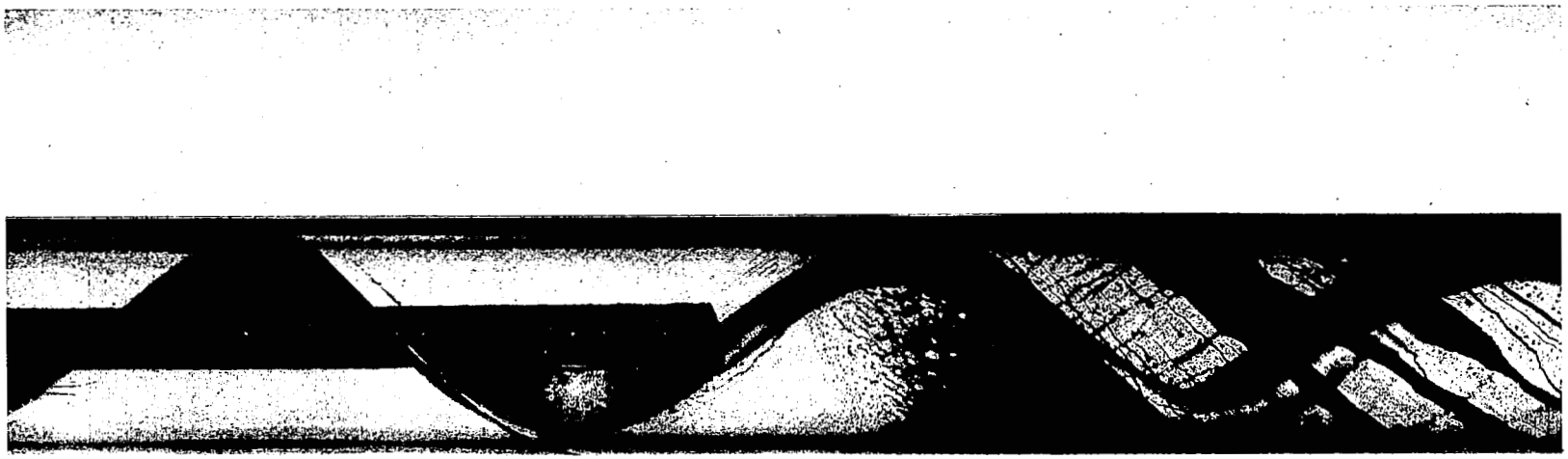

Figure 41. Droplet deposition downstream from an interrupted centerbody. (Photo courtesy of General Electric Missile and Space Division, Cincinnati, Ohio.)

11) The Motion of Very Small Droplets in Helical Flow

The motion of large droplets in helical flow has been studied analytically in Section B.2 through B.10. In these analyses the simplifying assumption was made that the velocity of the particle was small compared to that of the vapor flow. In Section B.10 it was shown that droplets large enough to satisfy that assumption are, for short p/D helical inserts and cases corresponding to actual boilers, deposited upon the tube wall in less than one tube diameter of axial length.

The large slip analysis is not valid for all droplets. It is likely that a large portion of the droplets which might be entrained in the vapor flow are small enough so that starting from rest they attain the local vapor velocity in a distance which is short compared to the tube diameter. In such cases, the droplet velocities are almost equal to the vapor velocities throughout most of the flight time of the droplet.

Such small droplets may be visualized as following the vapor flow but drifting toward the wall due to the radial force caused by helical flow. The radial motion through the vapor is opposed by drag and the droplet drifts without appreciable acceleration. The two radial forces may be equated and solved for the radial velocity as follows:

$$F_D = F_H$$

or

$$C_D A_D \frac{1}{2} \rho_v \left(\frac{dr}{dt}\right)^2 = V_D \rho_\ell \frac{v_t^2}{r} \tag{110}$$

where:

F_D is the drag force exerted on the droplet by the vapor

F_H is the radial force due to helical motion

C_D is the droplet drag coefficient, taken as a constant 0.4

A_D is the droplet frontal area

V_D is the droplet volume

ρ_v is the vapor density

ρ_ℓ is the liquid density

r is the radius at which the droplet is situated at time t

and v_t is the rotational vapor velocity.

For the idealized case of solid body rotation and uniform axial velocity,

$$v_t = \frac{\pi D}{p} v_a \left(\frac{2r}{D}\right) \tag{111}$$

where

D is the tube inside diameter

p is the helix pitch

and v_a is the axial mean velocity.

The simple differential Equation (110) may be combined with (111), the result integrated with the boundary condition $t = 0$, $r = r_o$, and rearranged to yield

$$\left(\frac{2\pi v_a}{p}\right) t = 2\left(\frac{3}{4} \frac{C_D}{D_p} \frac{\rho_v}{\rho_\ell}\right)^{\frac{1}{2}} \left(r^{\frac{1}{2}} - r_o^{\frac{1}{2}}\right) \tag{112}$$

The droplet impacts on the wall when

$$r = \frac{D}{2}$$

The principal quantity of interest in this analysis is the axial distance of travel. Since it has been assumed that the slip is negligible and that the axial velocity is uniform, time is related to axial length by

$$z = v_a t \tag{113}$$

where z is distance measured along the tube axis. Equations (112) and (113) may be combined and rearranged to yield a relationship for the axial distance traveled by a droplet drifting from the tube centerline or centerbody radius to the wall. This result is

$$\frac{z}{D} = \frac{p}{D\pi} \left[\frac{3}{8} C_D \frac{D}{D_p} \frac{\rho_v}{\rho_\ell}\right]^{\frac{1}{2}} \left[1 - \left(\frac{2r_o}{D}\right)^{\frac{1}{2}}\right] \tag{114}$$

This relationship is plotted in Figure 42, using

$$\frac{\rho_v}{\rho_\ell} = 0.04$$

which is characteristic of potassium at 1800°F.

The axial travel distance given by Equation (114) increases as the droplet size gets smaller. This is in contrast to the characteristic shown by the large slip analysis of Section B.10. However, the distance to impact for both models is of the order of one tube diameter over a large range.

Since the two analyses are based on two distinctly different idealizations, it is important to establish ranges of applicability. It is reasonable to expect that the large slip model will prevail if the velocity of a droplet is not closely accomodated to that of the vapor within one tube diameter. If the distance for velocity accomodation is short compared to one tube diameter, the small slip model will prevail.

The relationship between axial location and velocity of a droplet introduced into a uniform flow is given by combination of Equations (51) and (52) of Section B.2 and is:

$$\left(\frac{3}{4}\ \frac{C_D}{D_p}\ \frac{\rho_v}{\rho_\ell}\right) z = \frac{\frac{v_p}{v_a}}{1 - \frac{v_p}{v_a}} - \log\left(\frac{1}{1 - \frac{v_p}{v_a}}\right) \qquad (115)$$

where v_p is the absolute droplet velocity.

If adequate velocity accomodation is attained where

$$\frac{v_p}{v_a} = 0.98, \text{ then}$$

$$\frac{z}{D} = \frac{45.1}{\frac{3}{4} C_D \frac{D}{D_p} \frac{\rho_v}{\rho_\ell}} \qquad (116)$$

For potassium at 1800°F,

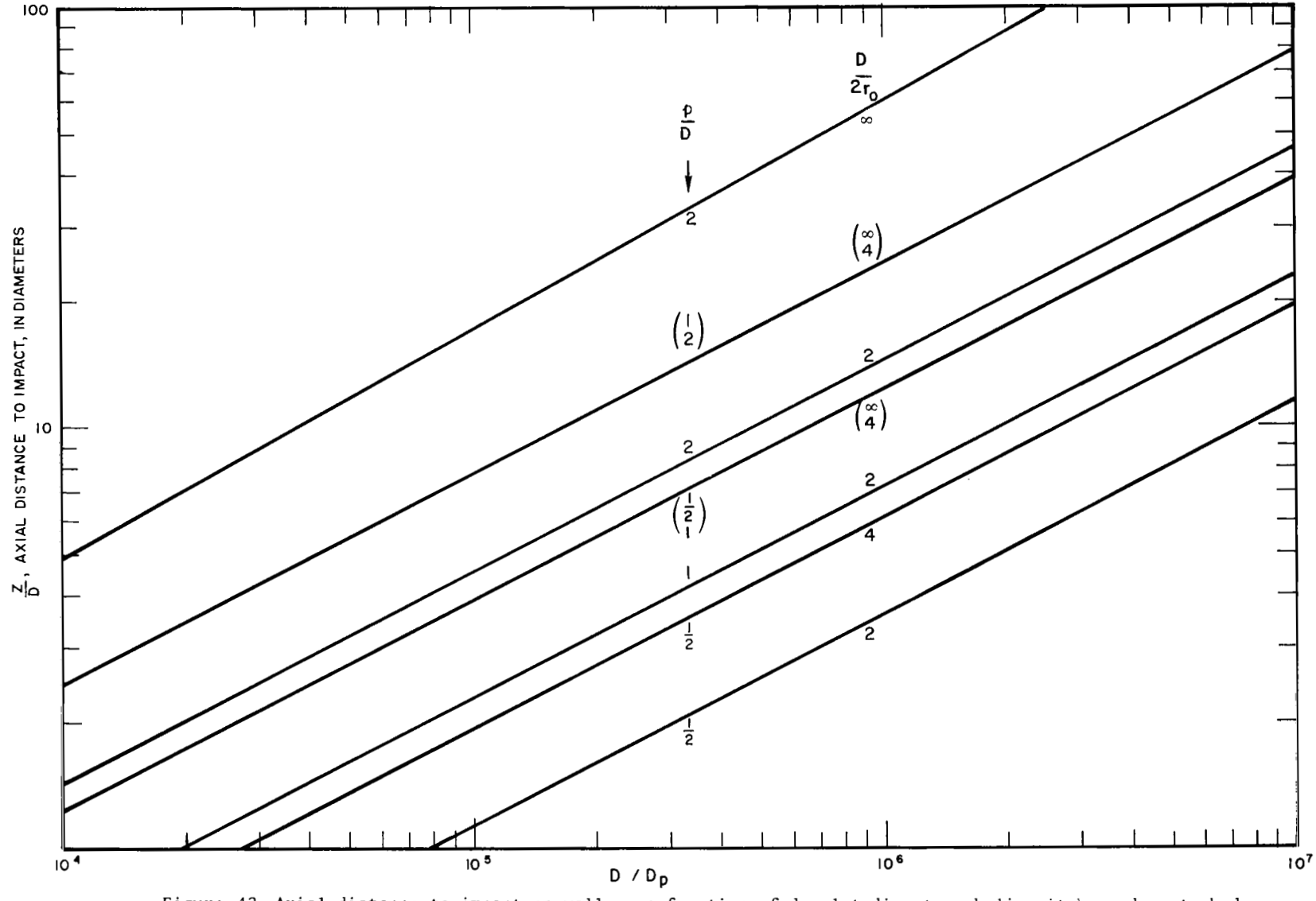

Figure 42. Axial distance to impact on wall as a function of droplet diameter, helix pitch, and centerbody radius for small slip model.

$$\frac{z}{D} = 1 \qquad \text{when } \frac{D}{D_p} = 3.8 \times 10^{3}$$

$$\frac{z}{D} = 0.01 \qquad \text{when } \frac{D}{D_p} = 3.8 \times 10^{5}$$

One would expect the large slip analysis to hold for droplets larger than 10^{-3} D, and the small slip analysis to hold for droplets smaller than about 10^{-5} D. For droplet sizes in between these two values, the axial distance to impact should be bounded by the results of the two modeis. A composite graph of the two solutions is shown in Figure 43.

In the small droplet small slip analysis only vapor rotation and vapor drag force are considered. However, these need not be the only mechanisms affecting drift of small particles. It might be supposed that the turbulent diffusion in the vapor flow, and the large secondary flows in helical systems (and other effects as well) would affect the transport of very small droplets toward the wall.

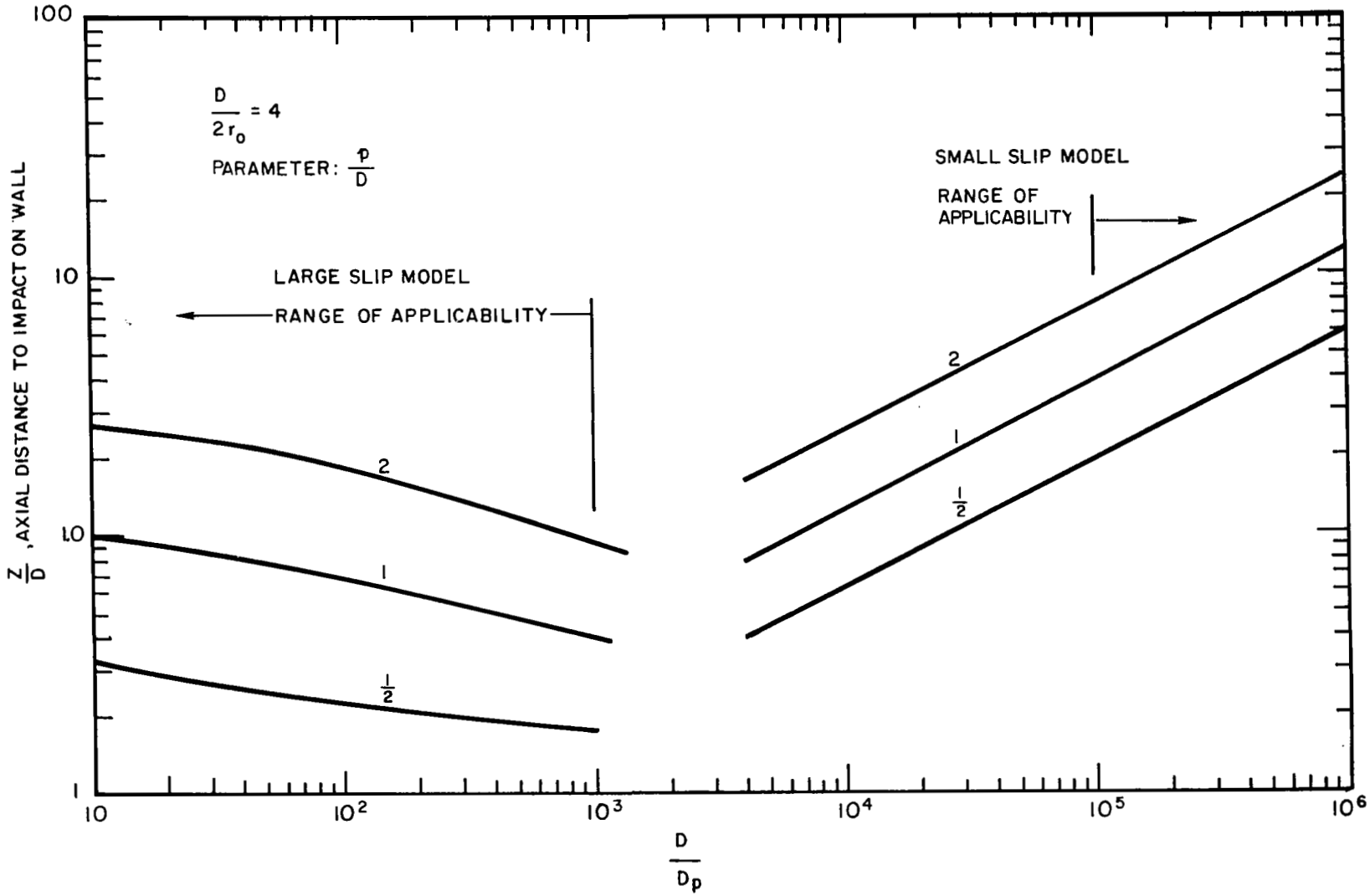

Figure 43. Axial distance to impact for droplets in helical flow: two models compared.

C. Liquid Distribution in Boilers

1) Some Aspects of Two Phase Flow in Insert Transitions

Some examples of the axial changes in boiler insert type which have been considered for use by designers are: fluted plug to helical vane, fluted plug to helical wire, and helical vane to helical wire. The vane and wire sections may or may not have a center body associated with them, and the insert pitch may or may not be the same on both sides of the insert change.

Most of these insert combinations would probably be used in regions in which the flow consists of two phases. The primary purpose of all of the inserts is to rotate the fluid, in order to separate the phases and to place the liquid component in contact with the heat transfer surface. For the purposes of this discussion it will be assumed that the upstream insert is very effective in separating the phases, so that almost all of the liquid is in a continuous liquid layer on the wall.

Consider the transition from a fluted plug to a helical vane system. If the pitches of both are the same, then the major difference between the two inserts is in the diameter of the center body, and the flow will be similar to a flow into a sudden enlargement. The vapor phase will decelerate rapidly, and there will be a recirculating stall at the base of the plug if the area change is large. The liquid layer on the wall will also tend to lose velocity and thicken, although at a lesser rate than the vapor, and if the quality change with length is high enough no significant thickening of the liquid layer will occur. No observable effect of this transition upon the heat transfer performance would be expected.

If the fluted plug and helical vane do not have the same pitch, the liquid layer will be subjected to an acceleration which will thicken it on one side

of the channel formed by the next insert and thin it on the other side. If the change in pitch is great enough, the liquid layer could separate from the vane entirely and leave a local dry spot on the heat transfer wall. This flow is identical to the open channel flow around a sharp corner, except that the gravitational field is replaced by a centrifugal acceleration field which may be many times larger than gravity.

From experience with open channel flows, one would expect that the major effects of the sharp corner turn would be obliterated within a couple of channel widths. If this transition were subjected to a high uniform heat flux a local hot spot might possibly develop at the dry spot; however, in a uniform wall temperature system, the dry spot would probably have no noticeable effect.

One would expect the presence of a liquid layer on the tube wall to have a deleterious effect upon the operation of only one of the insert types listed above, and that is the helical wire. Presuming that the liquid has by some means been deposited upon the wall, and presuming also that the liquid forms a layer which has appreciable thickness when compared to the diameter of the wire, the liquid layer will decrease the effective diameter of the wire. By the analysis of Section A2, the force tending to rotate the fluid will be decreased by the liquid layer. If the liquid layer covers the wires, no force tending to rotate the fluid will exist at all. It is true that thick liquid layers will have a very high wave structure upon them, and the wires may be partially exposed even when the average liquid thickness is greater than the diameter of the wires, but based upon the analysis cited above, the force tending to rotate the vapor phase would be small.

Consider the transition from a fluted plug or helical vane to a helical wire in the low quality region. The separation effectiveness of the plug and vane are both good so the liquid layer at the termination of these inserts may be thick. The <u>effective</u> transition the vapor phase undergoes in such a case could very well be from a helical vane (or plug) system to a very rough tube,

and one might expect the rotation to decay to virtually zero.

The heat transfer in such a transition will not necessarily be poorer than that in a helical vane. As long as the wall is completely covered, liquid-like conductances will prevail. Since centrifugal accelerations are decreasing, more liquid may be entrained in the vapor, and surface waves will also be deeper. Both of these effects thin the liquid layer, and since a large portion of the vaporization in annular flow of liquid metals occurs at the interface between the liquid and vapor, a thin layer has less heat transfer resistance than a thick one. The irregular wave motion also increases the rate of turbulent diffusion of heat through the liquid layer.

It appears that helical wires will be poor flow rotating inserts at low to intermediate vapor quality. The length of helical wire inserts in the low to intermediate quality region should be limited in length if downstream entrainment of liquid in the vapor is expected to be a problem.

2) Flow in a Curved Channel System

An analysis of heat transfer and pressure drop in a curved channel system that represents the initial boiler tube insert (helical flow in an annulus) has been made. The results may be applied to the prediction of two phase pressure drop in the multichannel plug.

The initial momentum transfer analysis is defined by separated, viscous liquid and viscous vapor flow (the liquid layer being held contiguous to the outer wall by centrifugal force). The classical shear stress-pressure gradient and viscous stress-strain equations for a curvilinear coordinate system are

$$\tau_s = \frac{1}{2} \frac{\partial p}{\partial \Theta} + \frac{\text{constant}}{r^2} \tag{117}$$

and

$$\tau_s = \mu \left(\frac{dv}{dr} - \frac{v}{r} \right) \tag{118}$$

where τ_s shear stress

Θ, angular position in the curved channel system

r, radial position in the curved channel system

v, curvilinear fluid velocity along a constant radius, r

Equations (117) and (118) were solved utilizing four boundary conditions, namely, zero velocity at the inner and outer walls and the velocity and shear stress continuity at the gas-liquid interface. The resulting velocity profile solutions

across the liquid and vapor layers are shown below:

for the outer, liquid layer,

$$v = r\left[\frac{1}{2\mu_\ell}\frac{\partial p}{\partial \theta}\ln r - \frac{C_1}{2\mu_\ell r^2}\right] + C_2 r \tag{119}$$

for the inner, vapor layer,

$$v = r\left[\frac{1}{2\mu_v}\frac{\partial p}{\partial \theta}\ln r - \frac{C_3}{2\mu_v r^2}\right] + C_4 r \tag{120}$$

where

$$C_1 = C_3 = \frac{-\frac{\partial p}{\partial \theta}\left[\frac{1}{2\mu_\ell}\ln r_2 - \frac{1}{2\mu_\ell}\ln r_i + \frac{1}{2\mu_v}\ln r_i - \frac{1}{2\mu_v}\ln r_1\right]}{-\frac{1}{2\mu_\ell r_2^2} - \frac{1}{2\mu_v r_i^2} + \frac{1}{2\mu_\ell r_i^2} + \frac{1}{2\mu_v r_1^2}} \tag{121}$$

$$C_2 = -\frac{1}{2\mu_\ell}\frac{\partial p}{\partial \theta}\ln r_2 + \frac{1}{2\mu_\ell r_2^2} C_1 \tag{122}$$

$$C_4 = -\frac{1}{2\mu_v}\frac{\partial p}{\partial \theta}\ln r_1 + \frac{1}{2\mu_v r_1^2} C_3 \tag{123}$$

A typical velocity profile together with the specific geometrical and fluid conditions is shown in Figure 44. This solution can be used to estimate the frictional pressure drop in a helical flow annulus (for a viscous-viscous flow). Addition of momentum and frictional pressure drop terms yield the total

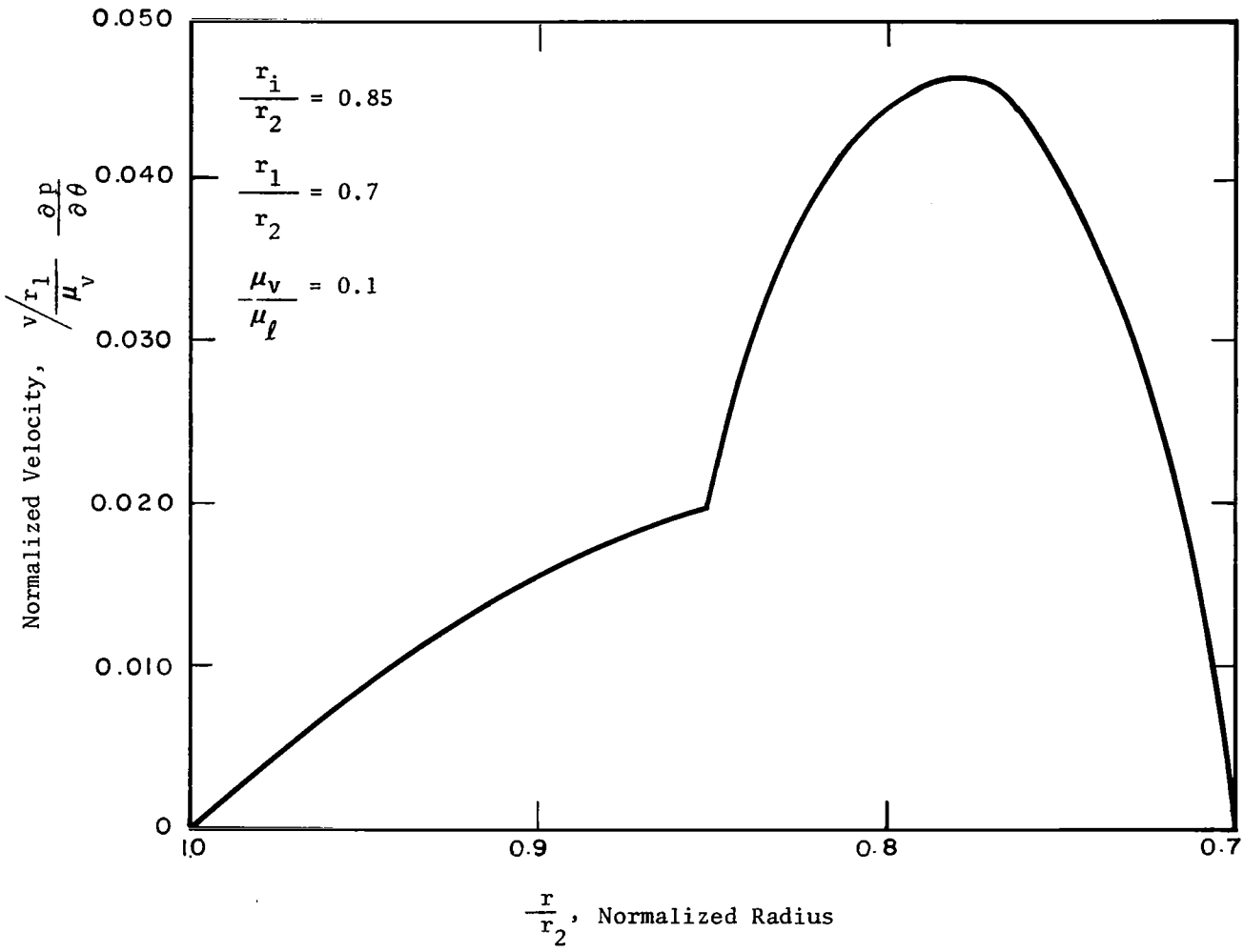

Figure 44. Typical velocity profile in two-phase flow in a curved channel.

pressure loss. The heat transfer for this system can be represented by conduction through a superheated liquid layer or by the volume heat sink representation presented previously for annular flow in a tube (Reference 14).

This same model is extended to the case in which the vapor phase is in turbulent flow in the following paragraphs.

Integration of the shear stress-pressure and viscous shear stress-strain equations leads to the velocity equation for the viscous layer, namely,

$$v = r\left(\frac{1}{2\mu_\ell}\frac{\partial p}{\partial \theta}\ell n\, r - \frac{C_1}{2\mu_\ell r^2}\right) + C_2 r \qquad (124)$$

where C_1 and C_2 are constants determined from the boundary conditions, r is radial position, μ_ℓ is the viscosity of the liquid, p is pressure and θ is angular position. For the turbulent layer, the shear stress-pressure and shear stress-strain equations are again integrated, but in the latter equation this viscosity is replaced by an eddy diffusivity that is dependent on the mean velocity and radial position, namely,

$$\epsilon = \mu_v + B(v)\,(r_i - r)\,(r - r_1) \qquad (125)$$

where μ_v, is the viscosity of the vapor, B is a parameter that relates the turbulence level to the mean layer velocity and r_i is the radial distance to the liquid vapor interface and r_1 is the radius of the inner channel wall. The radius function in Equation 125 approximates the radial eddy diffusivity distribution. The previously indicated integration for the turbulent vapor layer velocity profile is

$$v = \frac{1}{2}\frac{\partial p}{\partial \theta}\, r\int \frac{1}{r}\,\frac{dr}{\left[\mu_v + B(v)\,(r_i - r)\,(r - r_1)\right]} + r\int \frac{C_3\, dr}{r^3\left[\mu_v + B(v)\,(r_i - r)\,(r - r_1)\right]} + C_4 r \qquad (126)$$

The four constants, C_1, C_2, C_3, and C_4 in Equations 124 and 126 are evaluated from the four boundary conditions,

$$v(r_2) = 0$$

$$v(r_1) = 0$$

$$v(r_i^+) = v(r_i^-)$$

$$\tau_s(r_i^+) = \tau_s(r_i^-)$$

where r_2 is the radius of the outer channel wall and τ_s is the shear stress.

The results are:

$$C_3 = \frac{-\frac{1}{2\mu_\ell}\frac{\partial p}{\partial \theta}\ln r_2 + \frac{a}{2\mu_\ell r_2^2} + \frac{1}{2\mu_\ell}\frac{\partial p}{\partial \theta}\ln r_i - \frac{1}{2r_i}\frac{\partial p}{\partial \theta}F_2(r_i) - \frac{a}{2\mu_\ell r_i^2} + \frac{1}{2}\frac{\partial p}{\partial \theta}\frac{F_2(r_1)}{r_1}}{\frac{-b}{2\mu_\ell r_2^2} + \frac{b}{2\mu_\ell r_i^2} + \frac{F_3(r_i)}{r_i} - \frac{F_3(r_1)}{r_1}} \tag{127}$$

$$C_1 = a + b\,C_3 \tag{128}$$

$$C_2 = -\frac{1}{2\mu_\ell}\frac{\partial p}{\partial \theta}\ln r_2 + \frac{C_1}{2\mu_\ell r_2^2} \tag{129}$$

$$C_4 = -\frac{1}{2}\frac{\delta p}{\partial \theta}\frac{F_2(r_1)}{r_1} - \frac{F_3(r_1)}{r_1}C_3 \tag{130}$$

where

$$a = \frac{1}{2}\frac{\partial p}{\partial \theta}\mu_v r_i\left(\frac{dF_2(r_i)}{dr} - \frac{F_2(r_i)}{r_i}\right) - \frac{1}{2}\frac{\partial p}{\partial \theta}r_i$$

$$b = \mu_v r_i\left(\frac{dF_3(r_i)}{dr} - \frac{F_3(r_i)}{r_i}\right)$$

$$F_2(r) = r\int \frac{dr}{r(\mu_v + B(v)(r_i-r)(r-r_1))}$$

$$F_3(r) = r\int \frac{dr}{r^3(\mu + B(v)(r_i-r)(r-r_1))}$$

The integral in $F_2(r)$ is of the form $\int \frac{dx}{x(c_1 + c_2x + c_3x^2)}$ and the integral in $F_3(r)$ is of the form $\int \frac{dx}{x^3(c_1 + c_2x + c_3x^2)}$; they are expressible in long, known closed form algebraic equations available in standard integral tables. This solution can be used to estimate the frictional pressure loss in the initial boiler tube insert (helical flow in an annulus). The solution also relates vapor quality to liquid layer thickness which can be used in a heat transfer analysis of the type described in Reference 14.

3) A Criterion for the Onset of Entrainment Due to Vapor Shear at the Liquid-Vapor Interface in Annular Flow Boiling

One of the important mechanisms causing the entrainment of liquid into the vapor phase from the liquid layer in annular flow boiling is shear entrainment. It appears that most of the shear entrainment is from the peaks of large "breaking" waves, which have a height above the average liquid layer thickness of the same order as the layer thickness itself[15]. There is no agreement as to the conditions upon which the onset of roll waves occurs. However, there has been a correlation published for the onset of spray entrainment from these waves which is purported to give good agreement with data for adiabatic two-fluid systems (probably air and water). This correlation is[12]:

$$\frac{v_c \mu_g}{\sigma}\left(\frac{\rho_g}{\rho_\ell}\right)^{\frac{1}{2}} = 2.46 \times 10^{-4} \qquad (131)$$

where

v_c is the critical velocity for the onset of entrainment

μ_g is gas (or vapor) phase viscosity

σ is liquid surface tension

ρ_g is gas (or vapor) density

ρ_ℓ is liquid density

Although this correlation may give good results for the systems tested, and is claimed to represent systems with varied physical properties, it is easy to demonstrate that this correlation gives absurd results for some very important cases.

Consider, for example, Freon 12 vapor and liquid at 155 psia. The critical velocity predicted by the correlation is 0.59 ft/sec. The dynamic head for Freon 12 vapor at this velocity is about 2×10^{-2} lb/ft^2, which is clearly far too low to entrain liquid from large waves.

The corresponding predicted critical velocity for an air-water system at room temperature where one would expect the correlation to apply, is 78.5 ft/sec, leading to a dynamic head of 10 lb/ft^2, a reasonable value.

It is possible to devise a simple model for the removal of liquid droplets from roll waves. Presume that the waves already exist on the liquid surface, and that the flow is upward. The removal of a droplet is probably due to the drag of the vapor upon the tip of an irregularity in the wave. A schematic drawing

of this model is shown in Figure 45a. The force system acting upon the wave tip is indicated in Figure 46b. Clearly the restraining force on the wave tip decreases and the drag force increases rapidly after a "neck" appears, and a droplet is almost certain to be pulled off. A force balance may be written for the droplet when it is still attached to the wave tip.

$$F_D = F_g + F_\sigma \tag{132}$$

The forces are approximately

$$\left.\begin{aligned} F_D &= C_D \frac{\pi}{4} D_p^2 \frac{1}{2} \frac{\rho_v}{g_c} v_v^2 \\ &\text{where } v_v \text{ is the local vapor velocity relative to the liquid} \\ F_g &= \frac{g_e}{g_c} \rho_\ell \frac{\pi}{6} D_p^3 \\ F_\sigma &= \pi D_p \sigma \end{aligned}\right\} \tag{133}$$

Combination of Equations (1) and (2) and rearrangement yields

$$v_v = \frac{2\sqrt{3}}{3} \left\{ \frac{g_e \frac{\rho_\ell}{\rho_v} D_p + \frac{6\sigma g_c}{\rho_v D_p}}{C_D} \right\}^{\frac{1}{2}} \tag{134}$$

Evaluation of Equation (134) requires estimation of the droplet diameter and the drag coefficient for the wave tip.

The droplet diameter is probably of the same order as the height of the wave tip above the mean liquid layer thickness. For a typical air-water system, the mean liquid layer must be at times in the order of 0.1 inch. The wave amplitude might be (as stated before) twice this value. So a droplet diameter of 0.1 inch would be a plausible value.

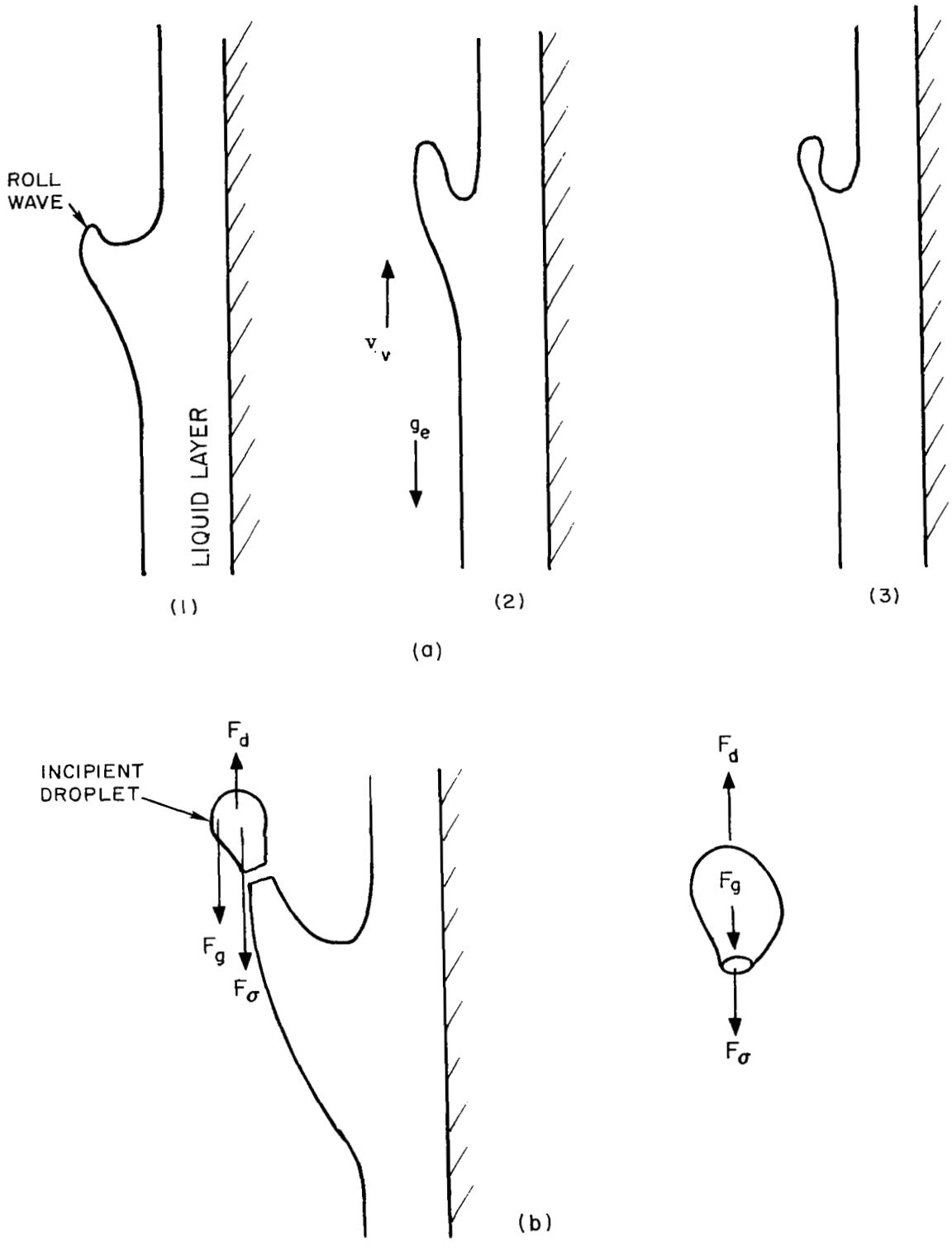

Figure 45. Liquid and vapor in upward flow.

The drag coefficient for a cylindrical object with a rounded downstream end is in the order of 0.25.

Evaluating Equation (134) with these estimates and the other required constants

$$\sigma_{H_2O} = 5 \times 10^{-3} \text{ lb}_f/\text{ft}$$

$$\rho_v = 0.1 \text{ lb/ft}^3$$

$$\rho_\ell = 62.4 \text{ lb/ft}^3$$

The predicted value of critical air velocity is

$$v_v = 1.15 \left\{ 670 + 4650 \right\}^{\frac{1}{2}} \text{ ft/sec}$$

$$= 84 \text{ ft/sec}$$

This is close to the value predicted by the experimental correlation. By use of the same droplet diameter and drag coefficient, a prediction may also be made for Freon 12 at 155 psia. The resulting critical velocity is

$$v_v = 1.15 \left\{ 27.5 + 13.0 \right\}^{\frac{1}{2}}$$

$$= 6.8 \text{ ft/sec}$$

This is certainly a more reasonable number than before. The dynamic pressure in the vapor based on this velocity is 2.3 lb_f/ft^2. It is interesting that the gravity term which is small in the case of water with its high surface tension, is the larger term in the case of Freon 12.

The predicted entrainment criterion can be put into the same form as the experimental correlation. The result is

$$\frac{v_v \mu_v}{\sigma} \left(\frac{\rho_v}{\rho_\ell} \right)^{\frac{1}{2}} = \frac{2\sqrt{3}}{3} \mu_v \left\{ \frac{g_e}{\sigma^2} \frac{D_p}{C_d} + \frac{6 g_c}{\sigma \rho_\ell C_D D_p} \right\}^{\frac{1}{2}} \tag{135}$$

The right hand side replaces the experimental constant in the correlation. Using the same physical constants as before, the right hand side has the value for air and water: 2.8×10^{-4}

The experimentally determined value is 2.46×10^{-4}. Such good agreement is probably fortuitous, since the model presented is simple and the phenomenon treated is quite complex.

In the absence of a comprehensive theory of entrainment, the results of this model have been used to make predictions for the boundaries of shear entrainment in a boiling system. These predictions are described in the next section.

4) Estimated Limits for Shear Entrainment in Annular Flow Wetted-Wall Boiling Systems

The mean thickness of the turbulent annular film in a forced convection boiler may be predicted by means of mathematical models available in the technical literature (see for example Reference 14).

The principal parameters upon which the liquid layer thickness depends are: vapor quality, vapor-to-liquid density ratio, wall friction factor, liquid-vapor interface friction factor, and tube diameter.

The turbulent annular film may be expected to have a complex wave structure superimposed upon it, so that under some conditions large roll waves may occur and these large roll waves are apparently the source of liquid droplets entrained by shear. Since the "breaking" waves are of the order of twice the liquid layer thickness in height, it may be expected that the diameter of the sheared-off fragments is approximately the same as the mean liquid layer thickness. By combining the shear entrainment criterion presented in the preceding section with the annular flow liquid film thickness predictions a map of conditions under which shear entrainment would be expected results. Several

such maps have been constructed. These are presented in Figures 46, 47, 48, and 49.

As an example of the interpretation of these figures, consider the graph for Freon 12 flowing in a .45 inch tube, Figure 46. By hypothesis the film thickness must be at least equal to the droplet diameter for entrainment to occur. Therefore, a given size droplet will only be entrained into the vapor at qualities for which the film thickness is greater than that drop size. However, the vapor velocity must be high enough to entrain droplets of that size so the entrainment region lies above the line representing the entrainment criterion. Conditions for entrainment of 0.05 inch Freon droplets exist above the graph of the shear entrainment criterion, and below the 0.05 inch film thickness line, in the cross hatched area. The interpretation of the figures for the other fluids is the same except that they are complicated by lines representing the entrainment criterion for various sized droplets. By inspection of Figure 47, one would conclude that shear entrainment will only occur for potassium in a 0.42 inch tube at low qualities and mass velocities far larger than those encountered in experimental boilers. Figure 48 indicates that shear entrainment can occur more readily in a potassium flow in a 0.92 inch tube. Figure 49 which is constructed for wetting flow mercury indicates that shear entrainment is extremely unlikely under conditions of practical importance.

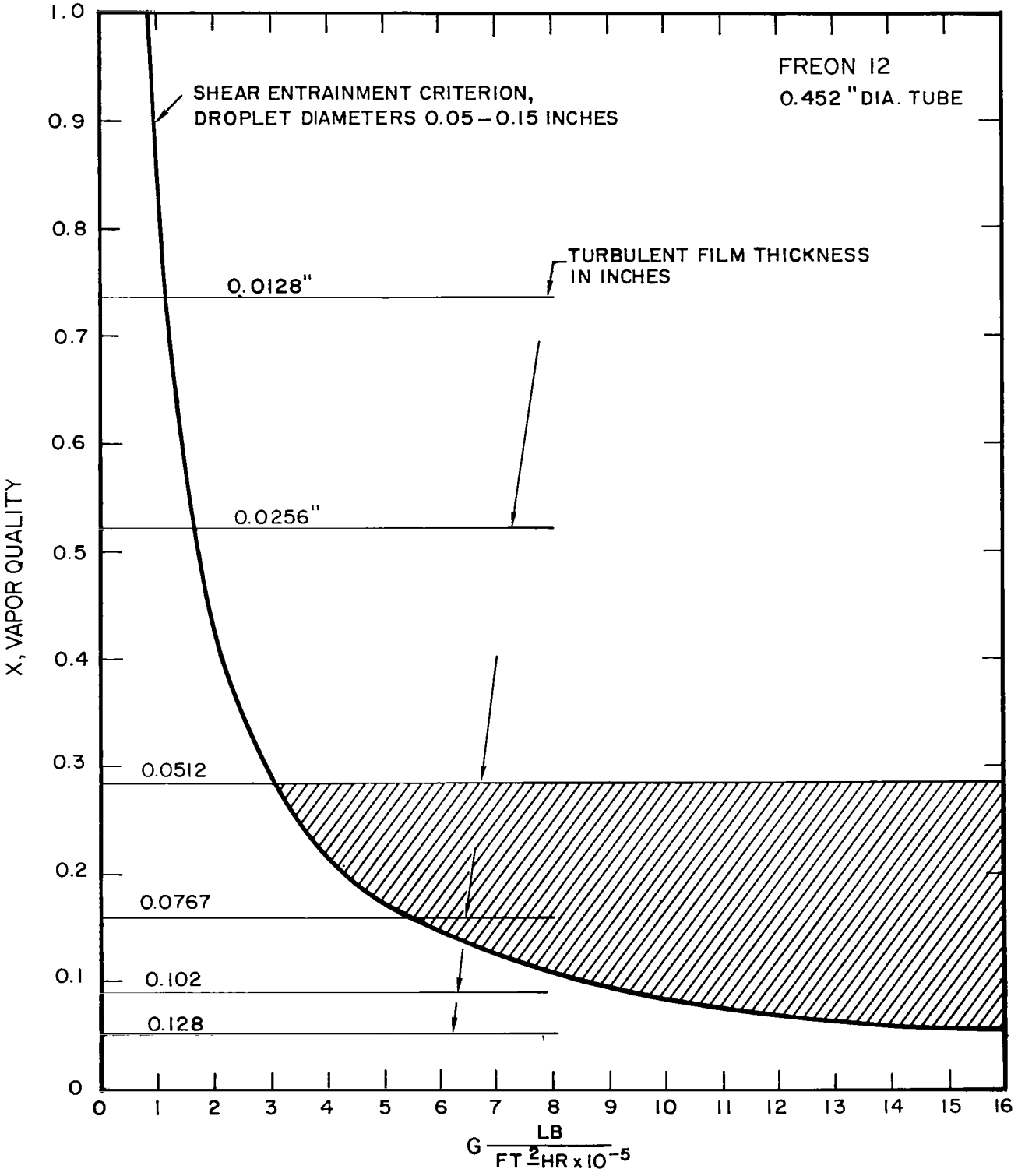

Figure 46. Boundaries for onset of entrainment due to shear.

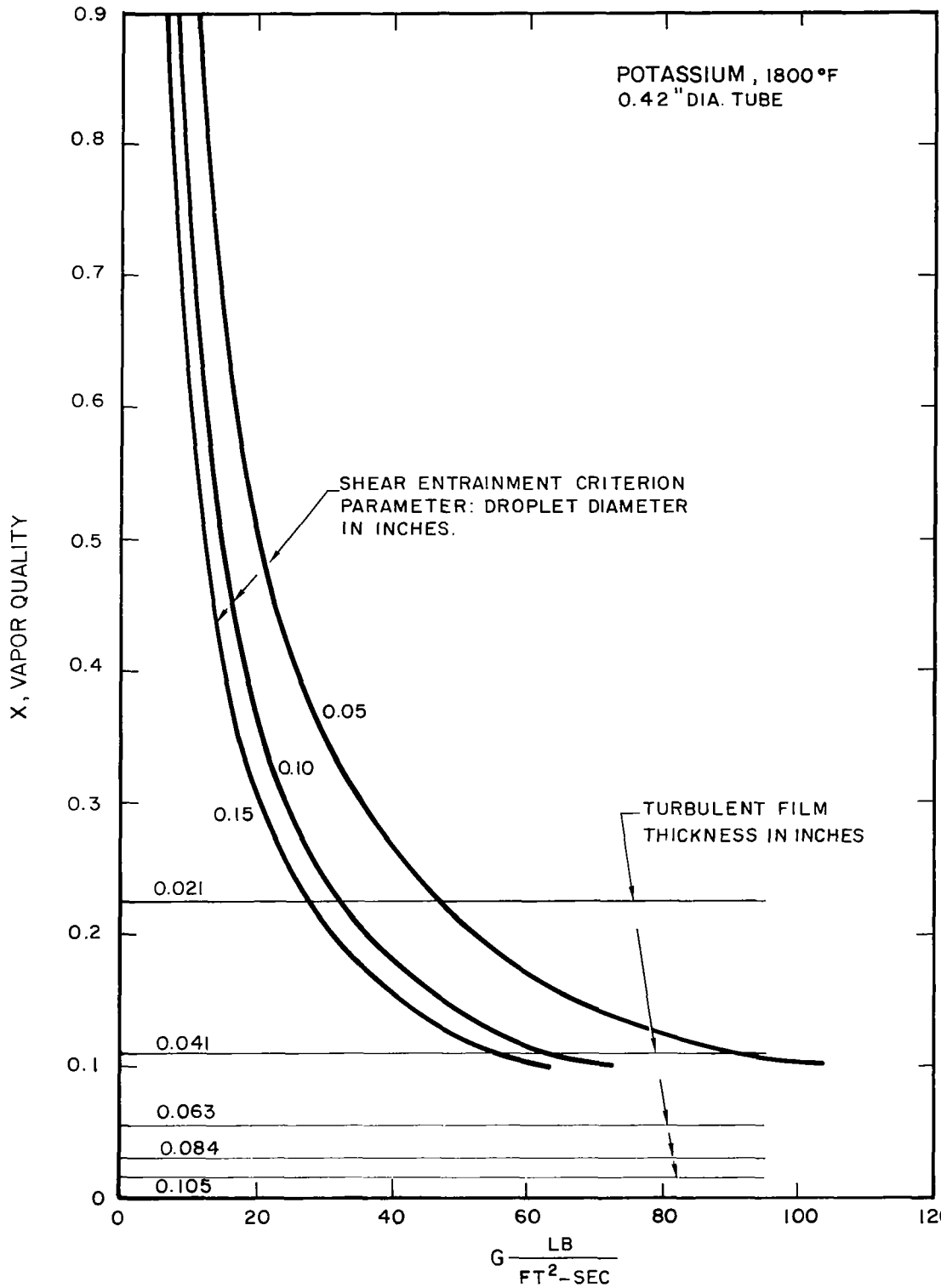

Figure 47. Boundaries for onset of entrainment due to shear.

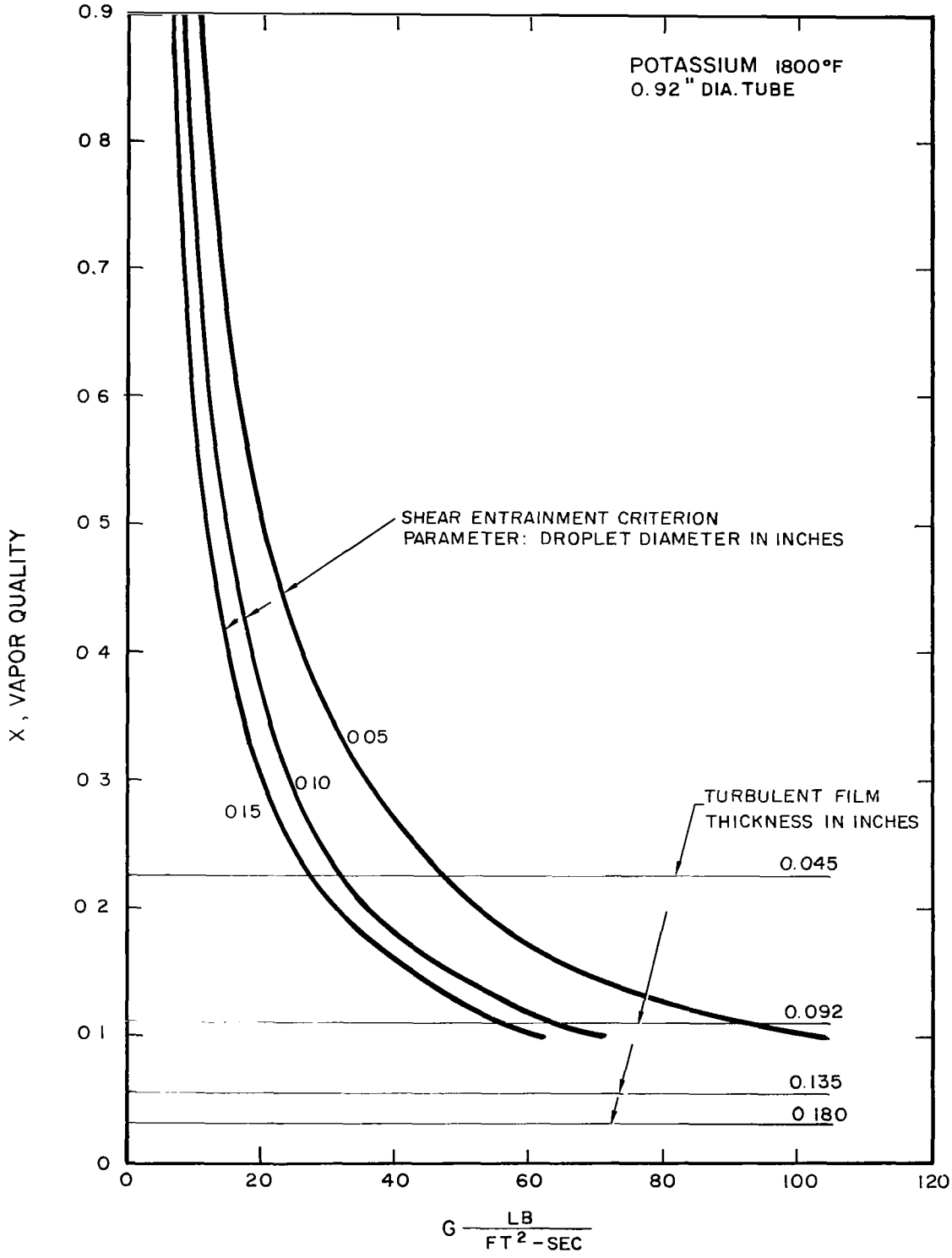

Figure 48. Boundaries for onset of entrainment due to shear.

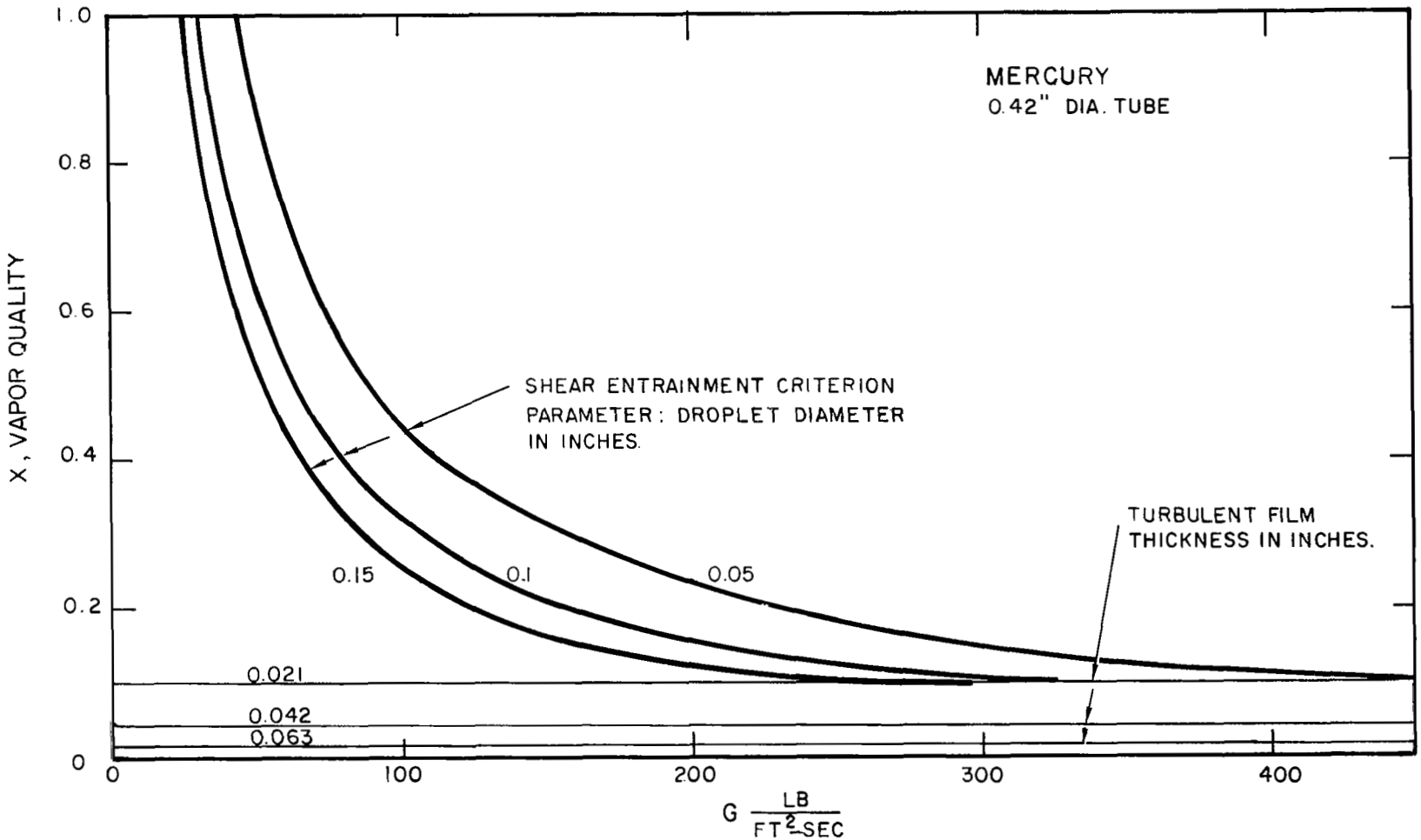

Figure 49. Boundaries for onset of entrainment due to shear.

5) A Mechanism for Spray Generation in Nucleate Boiling

There are several plausible mechanisms which may be proposed for the generation of spray by nucleate boiling. Careful observations of Freon 11 in forced convection, water in pool boiling, and air bubbles rising in water have shown that one particular process occurs in a significant number of cases. In this process, bubbles rise to the surface and are caught in the surface layer where they form a blister. After remaining in the surface layer for a small length of time (up to ~10 seconds) they burst, and a small droplet is ejected from the surface. It seems reasonable to suppose that since the bubbles remain in the surface layer for a finite length of time any upward momentum associated with the rising bubble does not contribute significantly to the momentum of the ejected drop.

The liquid layer covering the "blister" appears thinnest at the center, and it is reasonable to suppose that the surface ruptures at this point. One can therefore imagine a spherical cavity in the surface collapsing upon itself due to surface tension forces, and in the case of a gravitational field normal to the surface, due to energy in the ring-shaped wave formed by the broken bubble. When the bubble collapses upon itself, instantaneous pressures at the center must be high enough to eject a small amount of liquid from the surface.

In the case of air bubbles in water, 1/8 inch diameter bubbles eject droplets to a height of two to three inches above the surface. These droplets appear to be in the order of 10^{-2} inches in diameter.

Although no analytical description of the processes in the liquid layer following the fracture of the bubble seem to be presently available, the trajectory of the liquid fragment ejected can be analyzed readily.

Consider a spherical fragment leaving the surface vertically upward at the initial velocity v_o. The equation of motion of this particle is

$$-(F_D + g_e m) = m \frac{dv}{dt} \tag{136}$$

A first integration of this equation yields the following relationship between velocity and time:

$$t = C_3 - \frac{1}{\sqrt{C_1 C_2}} \tan^{-1}\left(\sqrt{\frac{C_1}{C_2}}\, v\right) \tag{137}$$

where

$$C_1 = \frac{F}{m v^2}$$

$$C_2 = g_e$$

$$C_3 = \frac{1}{\sqrt{C_1 C_2}} \tan^{-1}\left(\sqrt{\frac{C_1}{C_2}}\, v_o\right)$$

At the maximum altitude, v = o, so that

$$t_{\ell\, max} = C_3$$

A second integration of this equation yields the following relationship between distance (from the surface) and time:

$$-\ell = C_4 - \frac{1}{C_1} \log \cos\sqrt{C_1 C_2}\; t_d \tag{138}$$

where

$$t_d = C_3 - t$$

and

$$C_4 = \frac{1}{C_1} \log \cos\sqrt{C_1 C_2}\; C_3$$

From these relationships,

$$-\ell_{max} = \frac{1}{C_1} \log \cos \tan^{-1} \sqrt{\frac{C_1}{C_2}}\; v_o \tag{139}$$

It may be shown that in the case of the water droplet ejected vertically the frictional drag term is small compared to the gravity term. This is, of course, not true for a nucleation bubble in a vertically oriented film in forced convection. The constant C_1, is

$$C_1 = \frac{F_D}{m v^2}$$

$$= \frac{3}{4} \frac{C_D}{D_p} \frac{\rho_v}{\rho_\ell}$$

This will be recognized as the reciprocal of the characteristic length for droplet acceleration used in several analyses in Section B of this report.

For the water droplet observations described in this section,

$$D_p = .010 \text{ inch}$$

$$\ell_{max} = 3 \text{ inches}$$

so that

$$C_1 = \frac{0.036}{\text{inches}}$$

$$\sqrt{C_1 C_2} = \frac{3.74}{\text{sec}}$$

$$\sqrt{\frac{C_1}{C_2}} = .965 \times 10^{-2} \ \frac{\text{sec}}{\text{inch}}$$

v_o, the initial velocity of the water droplet as it leaves the surface may be computed from these constants and Equation (139). From this calculation:

$$v_o = 4.23 \text{ ft/sec}$$

A droplet traveling upward three inches in a drag-free environment would have an initial velocity of 4.01 ft/sec.

6) A Discussion of the Mechanism by Which Liquid Collects on a Helical Flow Center Body

A number of investigations, including recent ones at General Electric performed under Contract NAS 3-9426,[3] have shown that despite rather large radial accelerations because of rotational flow, a significant amount of liquid can collect on the center body of a helical flow system. Figure 50 clearly shows this center body flow. A qualitative description of the hydrodynamic causes for such a phenomenon follows. Included are suggestions for some simple modifications which can be made to the helical vane system to alleviate or completely eliminate such undesirable effects. A flow with curved streamlines has a pressure gradient normal to the streamlines. In a rotational flow system the flow streamlines are curved, and the pressure difference between the center body and the outside wall is given by

$$p_w - p_c = \int_{r_t}^{r_c} \rho_v \frac{v_v^2}{r}\, dr \qquad (140)$$

A sketch of the geometry is given in Figure 51. This pressure difference would be uniform around the circumference of the tube if the velocity field were axially symmetric. There would also be no secondary flows. However, the vanes which maintain the flow rotation have boundary layers on either side and the value of the integral giving the pressure difference between the center body and outside wall tends toward zero as the vane is approached. There must therefore, be a pressure gradient component on the inside tube surface in the Θ direction, and strong secondary flows.

An estimate of the pressure gradient on the tube wall in the Θ direction may be made. By consideration of Figure 52,

W_{H_2O} = 0.00685 lb/sec Tube I.D. = 0.875 in.

W_{air} = 0.0323 lb/sec C.B. = 0.25 in.

x = 0.8250 p/D = 3.0

Figure 50. Two-phase flow in a tube containing a helical insert. Liquid layer on centerbody can be clearly seen. (Photo courtesy of General Electric Missile and Space Division, Cincinnati, Ohio.)

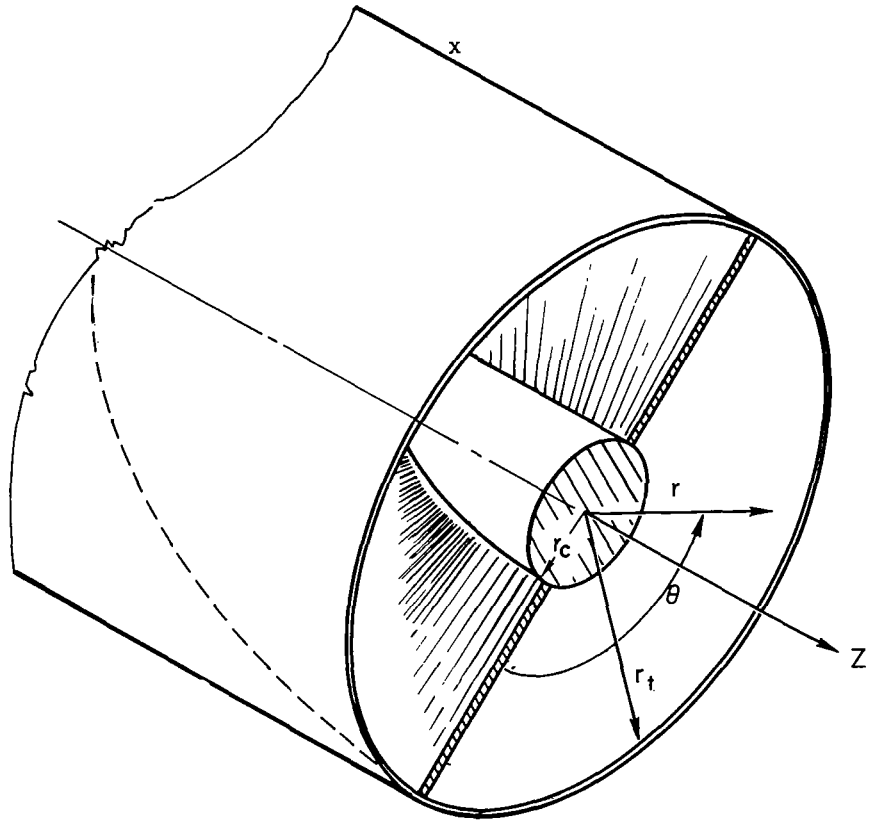

Figure 51. Geometry and notation.

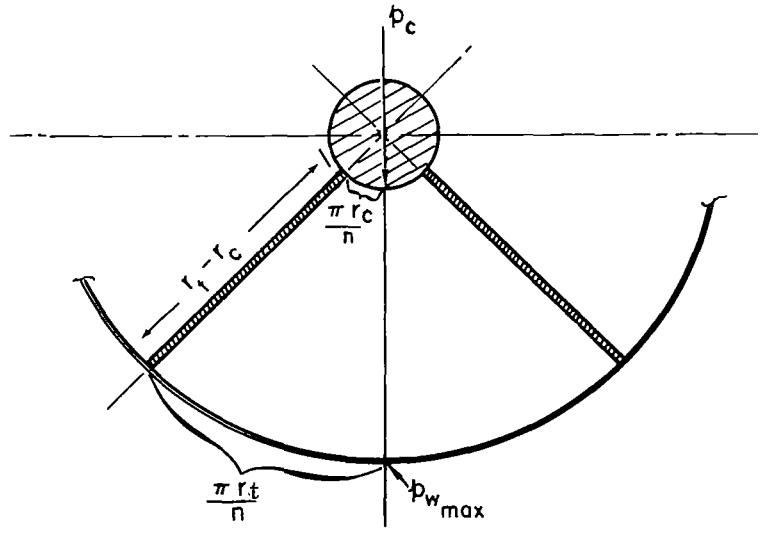

Figure 52. Path length for secondary boundary layer flows.

$$\frac{1}{r_t}\frac{dp}{d\Theta} \sim \frac{p_{w_{max}} - p_c}{\frac{\pi}{n}(r_w + r_c) + r_w - r_c} \qquad (141)$$

where n is the number of vanes on the helix.

Clearly the pressure gradient gets larger as the number of vanes increases, and one would expect stronger secondary flows in multivane systems than in single vane systems. The secondary flows in tubes with helices have been investigated for single phase systems. As one might expect, the flow patterns are qualitatively as shown in Figure 53.

Liquid droplets entrained in the vapor flow in a helical flow boiler are accelerated toward the outer wall and deposited there. The liquid flowing along the wall in a helical system has small velocity compared to the vapor and is propelled primarily by shear forces from the adjacent vapor flow. The boundary layer vapor flow, therefore, moves the fluid toward the vane and across the center body, and one observes a liquid rivulet in locations where transverse flows are low velocity; i.e., on the center body at the stagnation region. In a boiler tube, the fluid which is not vaporized on the tube wall (the heat transfer surface) probably eventually migrates to the center body. Because there is no heat generated on this surface, and there is no local force field strong enough to strip the fluid away from the center body, it simply migrates along the center body in the direction of the local shear forces.

The flow toward the centerbody is difficult to show in photographs of a helical vane system. However, there is an insert system which has been tested by General Electric which demonstrates the flow toward the centerbody quite clearly. Figure 55 is a photograph of a tube containing helical wire flow rotator and a centerbody. These two objects are not in contact with each other, but a welded strut supports the centerbody at intervals. These struts provide a flow path for the liquid to cross over to the centerbody. The support strut near the left hand side of the photograph clearly has a stream of liquid flowing up it from the helical wire to the centerbody.

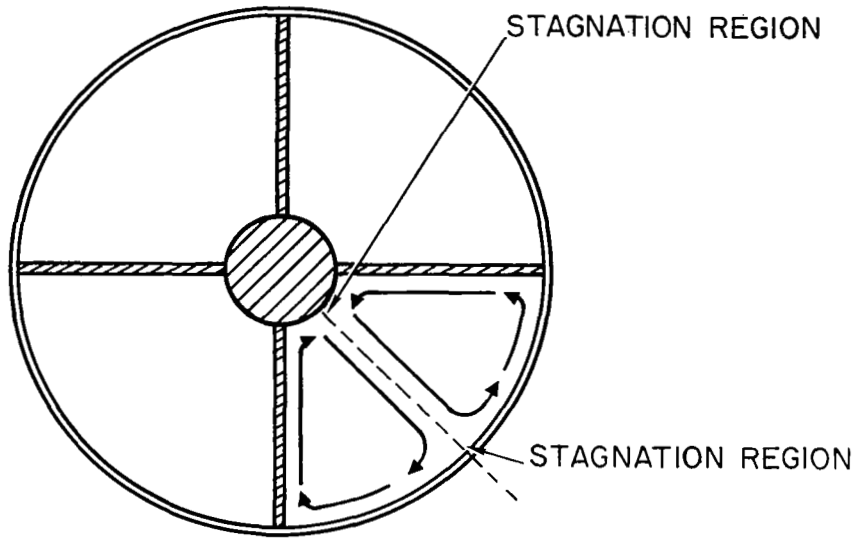

Figure 53. Secondary flow circulation pattern.

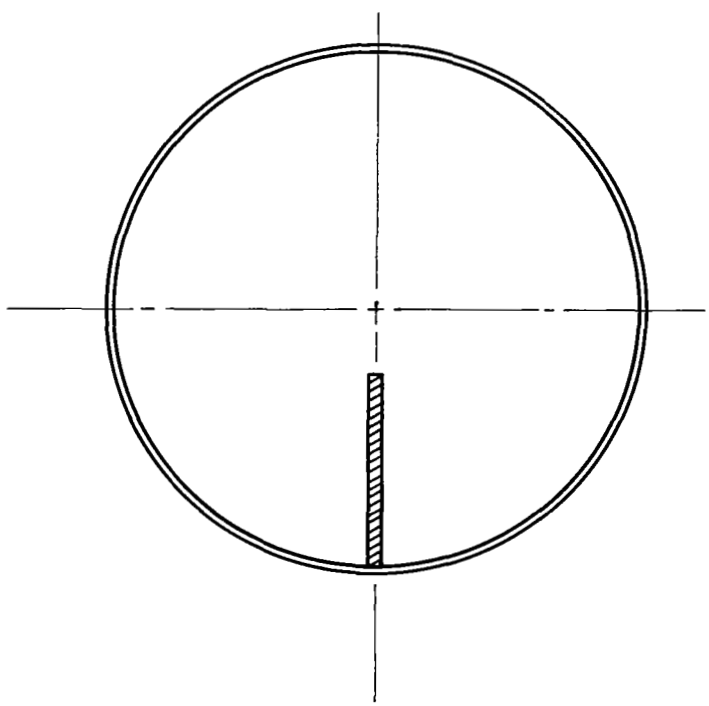

Figure 54. Short single vane helix.

W_{H_2O} = 0.00217 lb/sec

W_{air} = 0.050 lb/sec

x = 0.9584

Tube I.D. = 0.875 in.

C.B. = 0.25 in.

Wire Dia. = 3/16 in.

p/D = 3.0

d/D = 0.214

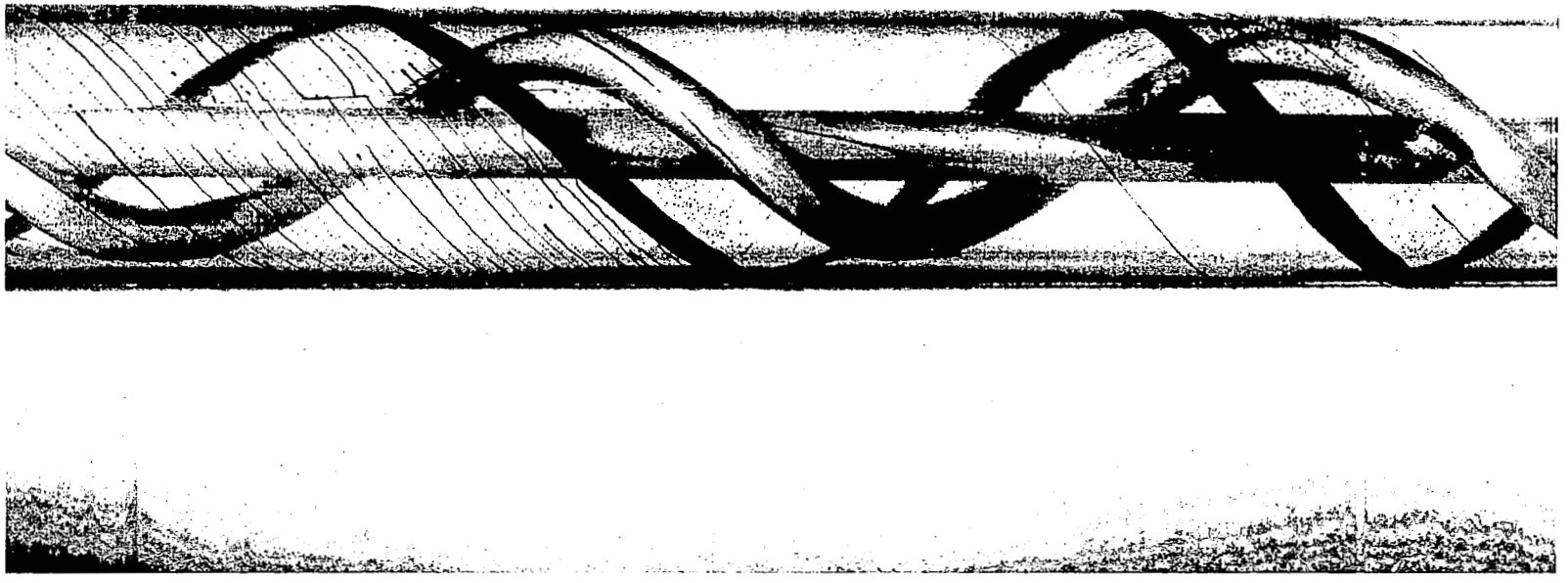

Figure 55. Two phase flow in a tube with helical wire and centerbody. (Photo courtesy of General Electric Missile and Space Division, Cincinatti, Ohio.)

There are several obvious methods of alleviating this effect. One suggestion is to keep the number of vanes to a minimum (one) since in addition to causing the secondary flows, the vanes provide the path to the centerbody. A multichannel plug which has many paths to the centerbody available, would be expected to have a larger portion of the fluid on the centerbody than would a tube with a single vane. Observations of the SNAP-8 mercury boiler inlet plug, which has many small channels, have shown that the main portion of liquid leaving the plug is very effectively atomized. If this fluid were on the tube wall at the exit of the plug, which presumably is a region of fairly rapid vapor deceleration (due to the increased flow area) one would not expect atomization to occur. On the other hand, a stream of relatively slowly moving liquid injected into the dividing line between a vapor jet and a strong recirculating eddy (which would be found at the base of the plug) would be atomized. One might, therefore, surmise that a large portion of the liquid leaving the SNAP-8 inlet plug may be on the center body rather than the tube wall.

A method for further alleviating this effect would be to remove the center body entirely and terminate the vane short of the centerline, as shown in Figure 54. The fluid would migrate to the inner edge of the vane, and probably form into droplets which would be stripped off and redeposited on the heat transfer surface. A large diameter helical wire would effectively approximate this geometry. Elimination of secondary flows would be accomplished by use of interrupted vanes, or propellers at intervals along the tube. A method of alleviating the collection of liquid on the center body while retaining the center body would be to put a skirt at intervals on the center body normal to the helical vane. These skirts would force the rivulets to form droplets on the downstream edge from which they would be stripped by the vapor flow. A sketch of the conceptual operation is shown in Figure 56. The possibility of using guide vane materials that do not make direct contact (wet) with the drops should also be considered; drop stripping by the vapor stream would probably be improved.

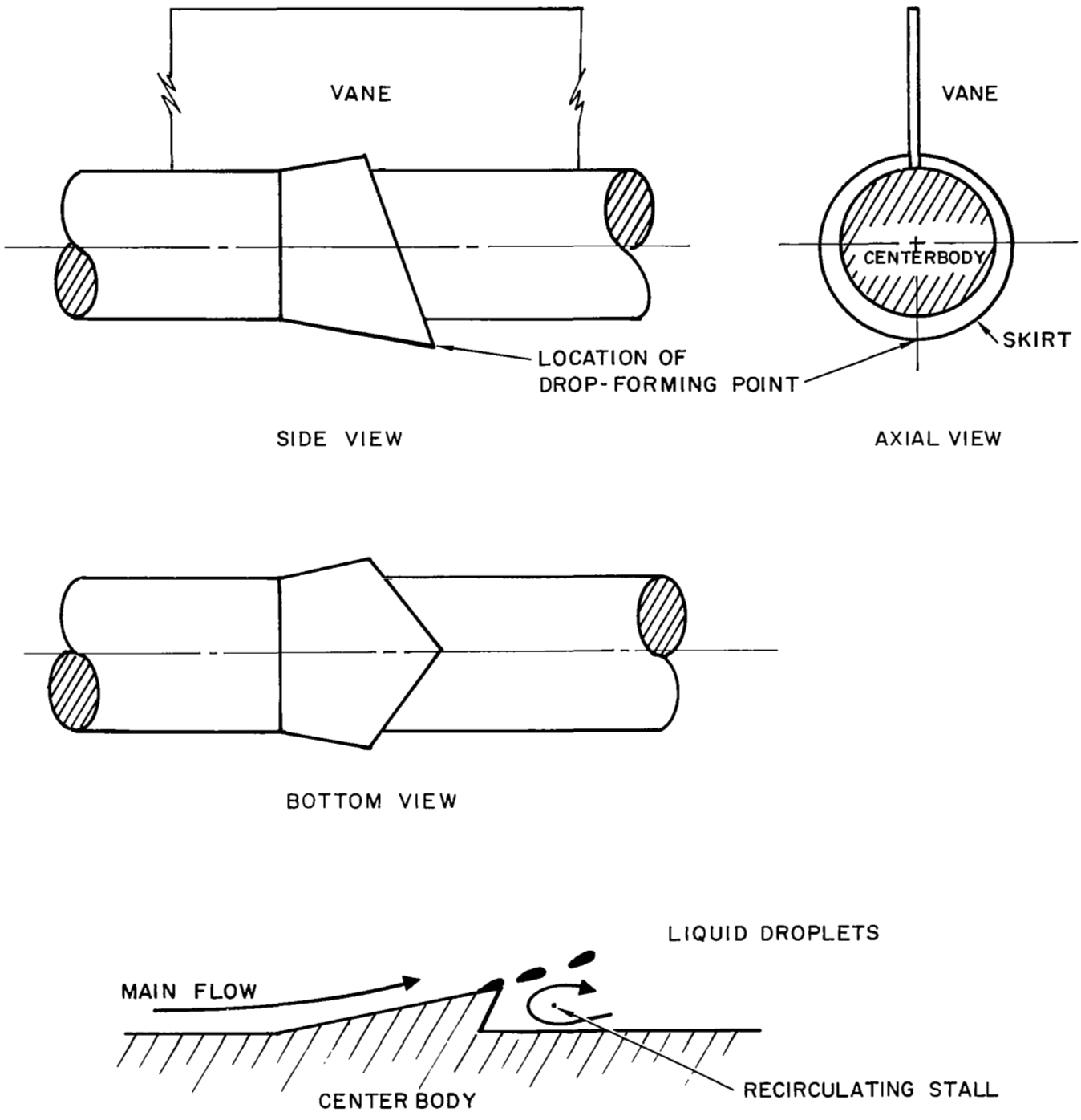

Figure 56. Drop-forming skirt for helix center body.

7) Motion of Wetted Liquid Films on Helical Vanes

a) Secondary Vapor Flow Velocities

It has been shown in the preceeding section that the longitudinal boundary layers on helical flow dividers provide the driving force for secondary flows. By consideration of the forces on a cross-section of the fluid, it is possible to estimate the velocities in the secondary flows. Such an estimate is made in the following paragraphs.

Consider the idealized secondary flow depicted in Figure 57. The rotating fluid in the secondary flow has a center of motion about which it turns with a velocity profile approximating solid body rotation, but with a superposed boundary layer against the solid surfaces. Idealizations necessary to perform the analysis are:

1. The flow is incompressible,
2. The frictional effects perpendicular to the tube axis and parallel to the tube axis are independent,
3. Liquid layers which may be present on the walls have negligible velocity,
4. Boundary layers in the tube may be approximated by one-seventh power velocity profiles,
5. The secondary flows have no effect upon the idealized solid body rotation (with boundary layers) of the mean flow about the tube axis, which is caused by the helical divider.

The pressure difference between the tube centerline and the tube outside wall caused by the helical flow rotation, is given by

$$\Delta p = \rho_v \int_o^{r_t} \frac{v_t^2}{r} \, dr \qquad (142)$$

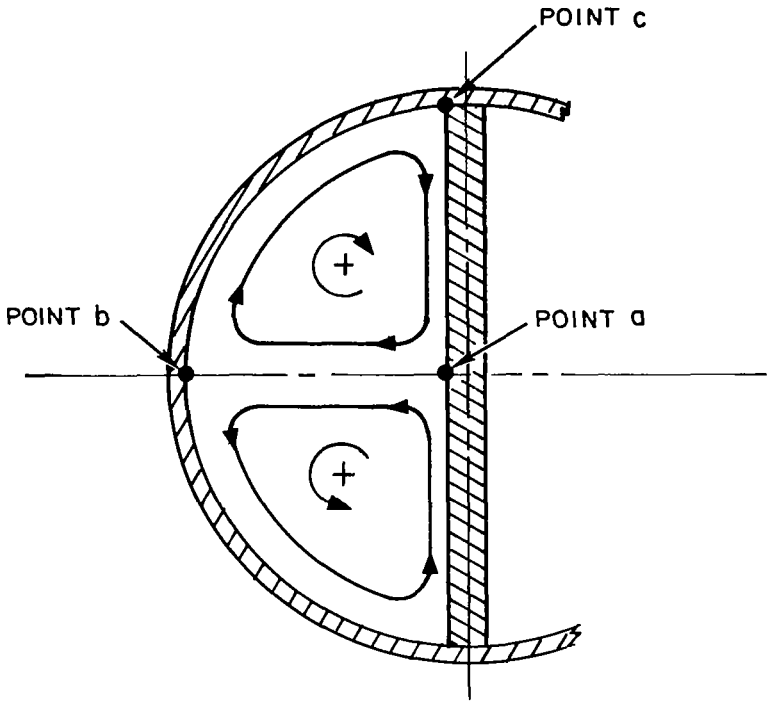

Figure 57. Idealized flow patterns in tube with twisted tape.

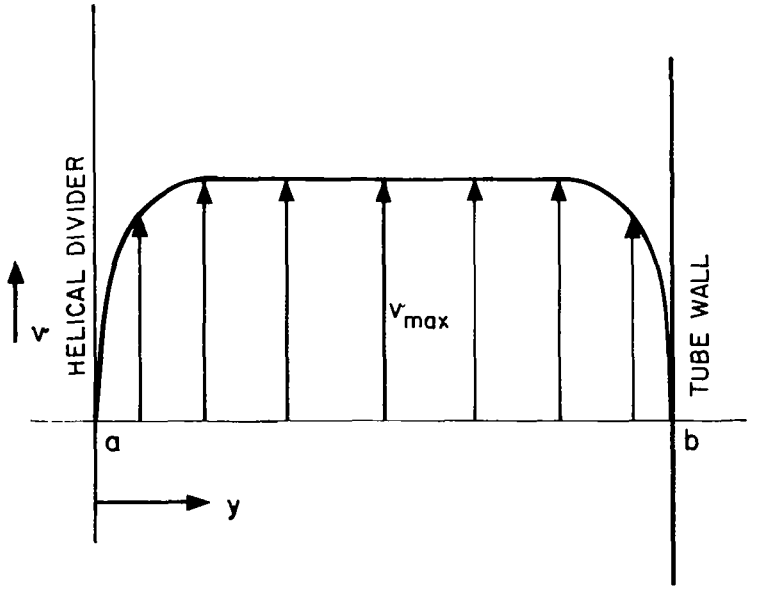

Figure 58. Axial velocity component along line a-b.

where r_t is the tube radius

v_t is the velocity component about the tube axis

r is radius from the centerline

and ρ_v is vapor density

with the solid body rotation idealization,

$$v_t(r, y) = \frac{\pi D}{p} \; v_\ell(y) \frac{r}{r_t} \tag{143}$$

where $v_\ell(y)$ is the local axial velocity.

If one visualizes a conventional one-seventh power boundary layer to exist upon the helical divider, as shown in Figure 58, then

$$v_\ell(y) = v_{max} \left(\frac{2y}{D_e}\right)^{\frac{1}{7}} \tag{144}$$

where y is distance from the divider

D_e is the passage equivalent diameter for turbulent helical flow

v_{max} is the maximum velocity (axial)

By combination of equations (142) through (144) and integration, the radial pressure difference may be shown to be* (neglecting the effect of boundary layer on the tube wall)

$$\Delta p(y) = \frac{1}{2} \rho_v \left[\frac{\pi D}{p} v_{max} \left(\frac{2y}{D_e}\right)^{\frac{1}{7}}\right]^2 \tag{145}$$

---

*The integrations are not truly radial, but are taken parallel to the helical divider, which lies along a tube diameter. Geometrical inaccuracies such as this are probably negligible compared to other simplifications.

The mean axial velocity component is

$$v_a = \frac{w_v}{\rho_v A_T} \tag{146}$$

where w_v is the vapor phase flow rate

ρ_v is vapor density

and A_T is the flow cross-section area.

The mean and maximum velocities are simply related [11].

$$v_a = .817\ v_{max} \tag{147}$$

One may then write

$$\frac{\Delta p(y)}{\frac{1}{2}\rho_v v_a^2} = \left(\frac{1}{.817}\right)^2 \left(\frac{\pi D}{p}\right) \left(\frac{2y}{D_e}\right)^{\frac{2}{7}} \tag{148}$$

This equation describes the pressure along the tube wall extending away from point c , as it is affected by the axial boundary layer along the divider between points a and c.

The pressure integral along the line a - b, where there is no boundary layer in the axial flow, is

$$\frac{\Delta p_{a-b}}{\frac{1}{2}\rho_v v_a^2} = \left(\frac{1}{.817}\right)^2 \left(\frac{\pi D}{p}\right)^2 \tag{149}$$

The usual equation used by most authors which neglects tube boundary layers is

$$\frac{\Delta p_{a-b}}{\frac{1}{2}\rho_v v_a^2} = \left(\frac{\pi D}{p}\right)^2 \tag{150}$$

Although this latter equation gives excellent results, the form Equation (149) containing the correction for maximum velocity with a boundary layer is used here to be consistent with other equations in the analysis.

The boundary layer on the vane causes a pressure defect along the tube wall, and this pressure defect may be integrated along the wall away from the vane to obtain a net radial inward force being exerted on the fluid. The magnitude of this force driving the secondary flows per unit of tube axial length, is

$$\frac{F_s}{\frac{D_e}{4}\rho_v v_a^2} = \left(\frac{1}{.817}\right)\left(\frac{\pi D}{p}\right)^2 \left[1 - \int_o^{\frac{D_e}{2}} \left(\frac{2y}{D_e}\right)^{\frac{2}{7}} dy\right] \tag{151}$$

$$= \left(\frac{1}{.817}\right)^2\left(\frac{\pi D}{p}\right)^2 \left[\frac{2}{9}\right] \tag{152}$$

This force, with the appropriate moment arm around the center of secondary flow rotation, provides a torque on the fluid which is restrained by the secondary flow shear stresses along the tube wall and helical vane (see Figure 59) and by turning losses due to eddying in the corners. The restraining forces per unit of tube length are in the order of:

$$F_r = \underbrace{\frac{1}{8}\xi\rho_v v_s^2 \frac{D}{2}\left[\frac{\pi}{2} + 1\right]}_{\text{shear}} + \underbrace{3\left[\frac{D_e}{4}\frac{1}{2}\rho_v v_s^2\right]}_{\text{turning losses}} \tag{153}$$

where v_s is the velocity of the secondary flow, measured normal to the tube axis just outside of the secondary flow boundary layer.

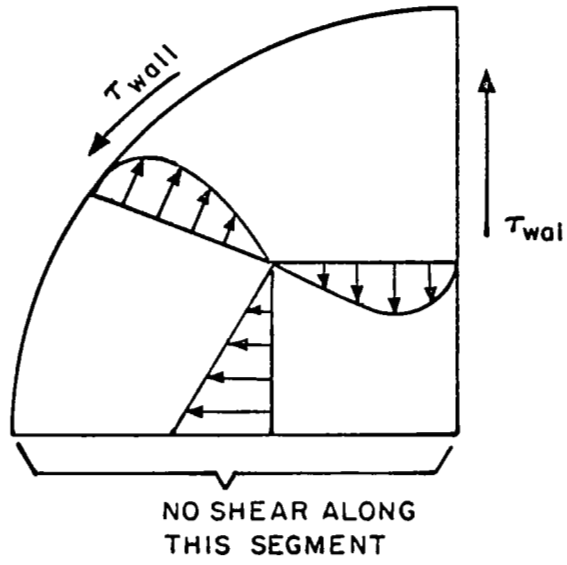

Figure 59. Transverse velocity profiles in secondary flow cell.

The turning losses are taken to have a loss coefficient of one, there are effectively three corners, and the effective width of the turning stream is estimated at $\frac{D_e}{4}$.

For equilibrium secondary flows, these forces may be equated (since the moment arms are of equal length) and solved for the secondary flow velocity. These operations yield

$$\frac{v_s}{v_a} = \left\{ \frac{\frac{2}{9}\left(\frac{\pi D}{p}\right)^2}{(.817)^2\left[\frac{1}{4}\xi\frac{D}{D_e}\left(\frac{\pi}{2}+1\right)+\frac{3}{2}\right]} \right\}^{\frac{1}{2}} \qquad (154)$$

$\frac{D_e}{D}$ for a twisted divider is a function of $\frac{\pi D}{p}$ but for values of this parameter characteristic of tight twisted dividers[14], a typical value is

$$\frac{D_e}{D} \sim .5$$

for a typical ξ value of 0.02 the denominator bracket terms are

$$\left[0.06 + 1.5\right]$$

Equation (154) reduces to

$$\frac{v_s}{v_a} = 0.47\left(\frac{\pi D}{p}\right) \qquad (155)$$

This simple relationship is based upon what is considered to be a reasonable flow model, so that although the coefficient is only an estimate, the functional form is probably correct to the first order.

Seymour[16] has made extensive measurements of secondary flows in systems containing twisted tapes of quite long pitch. For a tape of $\frac{D}{p} = 0.105$, his measurement yielded $v_s = 25$ ft/sec, $v_a = 208$ ft/sec, so that

$$\left(\frac{v_s}{v_a}\right)_{\text{experimental}} = 0.12$$

From Equation (155), the predicted value would be

$$\left(\frac{v_s}{v_a}\right)_{\text{analytical}} = 0.155$$

The agreement is reasonable.

The predicted pressure rise (from centerline to wall), computed from Equation (150), does not include the effects of boundary layers. Boundary layers would be expected to increase the measured pressure rise by increasing the maximum velocity and by decreasing the tube radius at which the maximum velocity occurs. Why this is so may be seen from Equation (142). It is worthwhile to assess the magnitude of this effect. For this calculation, suppose the axial component to be modified by a one-seventh power velocity profile on all surfaces. A mass flow integration over the half tube has been performed numerically to determine v_{max}. The result of this calculation is:

$$\frac{v_{max}}{v_a} = 1.33.$$

This compares with the full tube value

$$\frac{v_{max}}{v_a} = \frac{1}{.817}$$

$$= 1.22$$

Using the hypothetical one-seventh power profile with a maximum velocity of $1.33\ v_a$, the pressure rise along a radius was computed numerically, by use of Equations (142) and (143). The result was:

$$\frac{(\Delta p)_{\text{boundary layers}}}{(\Delta p)_{\text{no boundary layers}}} = 1.13$$

It appears that differences between the ideal relationship Equation (150) and actual measurements will not be very large.

b) Force Systems Acting on the Liquid Film

Consider a wetted liquid film on a helical vane (or twisted tape) in a tube with a vapor flow. The film is driven in motion by shear from the vapor flow. This shear has two components, one at constant radius from the tube centerline and directed downstream, and one directed inward along the tube radius. The second component is due to the secondary flows in the tube. The liquid film moves along the vane due to the axial shear, and as it moves it rotates about the tube axis, so that there is a centrifugal force on the liquid tending to accelerate it toward the tube wall. Both radial and axial motion are opposed by friction between the vane and the liquid film. A schematic representation

of this force system is shown in Figure 60. The purpose of this analysis is to determine under what conditions the liquid film will flow toward the center-body. The flow and force systems in the axial and radial directions are considered to be independent of each other.

A boundary layer analysis of the flow in the direction of constant radius yields (see, for example, reference 17) for a laminar film,

$$v_x = \frac{F_x}{\mu_\ell} \quad y \tag{156}$$

where

v_x is the velocity in the film in the direction of constant radius

F_x is the vapor shear force in the x direction

y is the distance from the vane surface (within the film)

μ_ℓ is liquid viscosity

The radial acceleration to which the film is subjected is

$$a_r = \frac{v_x^2}{r} \tag{157}$$

$$= \left(\frac{F_x}{\mu_\ell} \; y\right)^2 \; \frac{1}{r} \tag{158}$$

The radial flow equation, which includes this body force, is

$$\frac{d^2 v_r}{dy^2} + \frac{a_r \rho_\ell}{\mu_\ell} = 0 \tag{159}$$

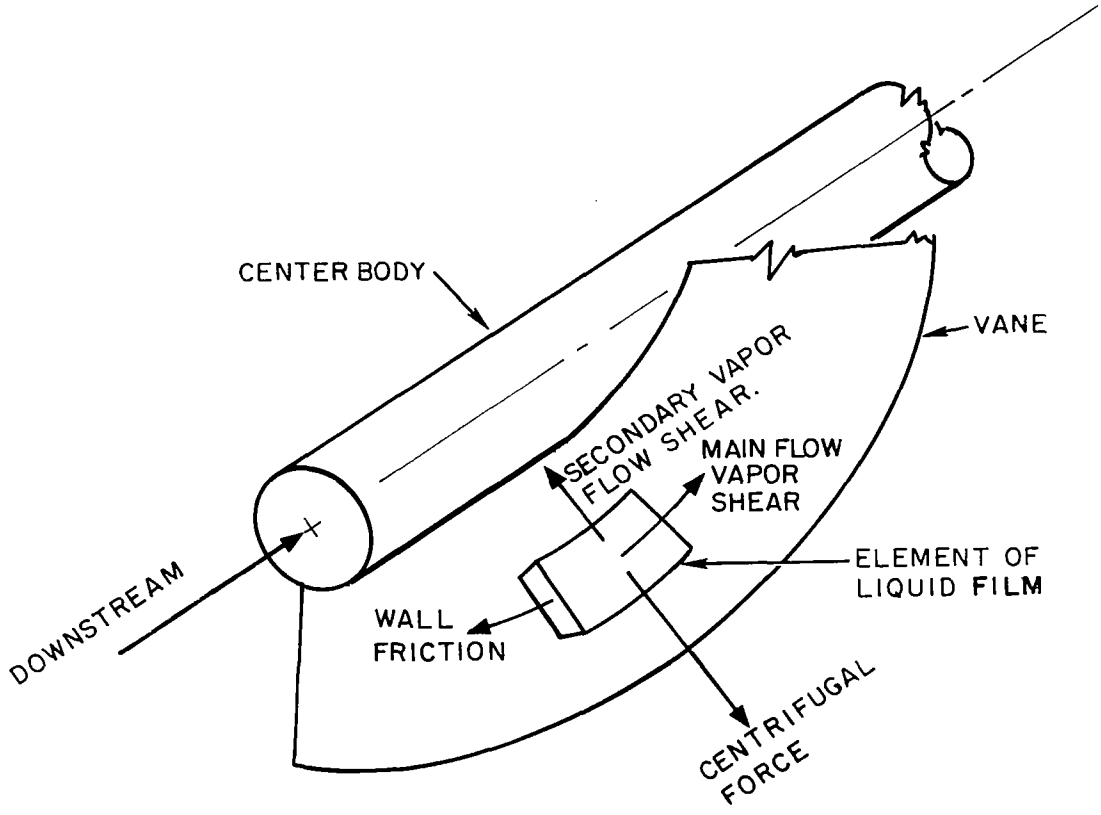

Figure 60. Forces acting on an element of the liquid layer.

where

v_r is velocity in the radial direction

ρ_ℓ is liquid density

The appropriate boundary conditions are

$$y = \delta:$$

$$\mu_\ell \frac{dv_x}{dy} = F_r \tag{160}$$

and

$$y = 0$$

$$v_x = 0$$

where

δ is the film thickness

F_r is the radial shear force due to secondary flows.

By integrating twice, and applying the boundary conditions, one obtains

$$\bar{v}_r = -\frac{1}{12}\bar{y}^4 + \left(\frac{1}{3} - \frac{F_r \delta}{\mu_\ell \kappa}\right)\bar{y} \tag{161}$$

where

$$\bar{y} = \frac{y}{\delta}, \quad \bar{v}_r = \frac{v_r}{\kappa},$$

and

$$\kappa = \frac{F_x^2 \delta^4 \rho_\ell}{\mu_\ell^3 r}$$

The quantity of interest is the net flow of fluid in the radial direction. This flow, per unit of vane length, is

$$w_r = \rho_\ell \int_o^\delta v_r \, dy \tag{162}$$

$$= \rho_\ell \kappa \delta \int_o^1 \bar{v}_r \, d\bar{y} \tag{163}$$

From which

$$\frac{w_r}{\rho_\ell \kappa \delta} = \frac{9}{60} - \frac{F_r \delta}{2 \mu_\ell \kappa} \tag{164}$$

The radial flow <u>outward</u> goes negative when the second term is greater than $\frac{9}{60}$, and the net flow is toward the centerbody.

The vapor shear stress due to secondary flows is (from part a) of this section)

$$F_r = \xi \rho_v v_s^2$$

$$= \xi \rho_v (.47)^2 \left(\frac{\pi D}{p}\right)^2 v_a^2$$

$$F_x = \xi \rho_v v_a^2$$

then

$$\frac{F_r \delta}{2 \mu_\ell \kappa} = \frac{(.47)^2 \left(\frac{\pi D}{p}\right)^2 \mu_\ell^2 r}{2 \xi \rho_v v_a^2 \delta^3 \rho_\ell} \tag{165}$$

It is clear from inspection that there is always a value of δ, the film thickness, small enough so that Equation (165) will be greater than 9/60, regardless of the values of the other parameters.

The net-flow of a "thick" film is outward, the net flow of a "thin" film is inward. One may conclude that when the liquid wets the wall, there will always be a net flow of liquid toward the centerbody in a two-phase helical flow system.

8) Criteria for the Existence of the Liquid Phase on Boiler Tube Centerbodies

The criteria for the existence of liquid phase on centerbodies in boiler tubes can best be outlined by grouping the processes into hypothetical steps.

First, it is postulated that a liquid layer exists on the centerbody as well as on the boiler tube wall. In this case vapor flows between the two liquid layers. Linear and curved channel three-layer flow analyses similar to the two-layer solutions previously discussed can be made. From resulting liquid film thicknesses on the centerbody, tests on liquid film rupture can be made and the fraction of centerbody area covered by rivulets determined (following the procedure used for the boiler tube wall). In the case of curvilinear flow, however, the previous analysis for the rivulet profile would have to be generalized.

Specifically, a centrifugal force as a result of rivulet flow around the centerbody would be added to the force equation. As the centrifugal force term increases in strength, the rivulet profile will become thicker and eventually the centrifugal force will exceed the surface tension force and the rivulet will leave the surface or rupture. This simple criterion suggests practical ways of reducing the liquid flow on centerbodies. If the contact angle for a given liquid metal and surface combination were to be increased by choosing an appropriate material for the centerbody, rivulets would be removed from the surface or their density decreased at reduced vapor flow rates or qualities.

D. Temperature Distributions in Boiler Tube Walls

It is of technical interest to be able to describe quantitatively the peripheral variation in wall temperature in a boiler tube that contains discontinuous liquid layers. These layers may be in direct contact with the wall or be separated from the wall by a vapor film. The difference in heat transfer between the liquid cooled zone and the vapor cooled zone contiguous to it causes a temperature asymmetry. An analytical solution has been derived for a thin-walled system; the details and results are given below. Analog solutions for temperature distributions in thick-walled boiler tubes subjected to several liquid distributions are presented later in this section.

1. Temperature Distributions in a Thin-Walled Tube with Internal Conductance Discontinuities

The idealized boiler tube system is shown in Figure 61 and the postulates that define the system follow:

a) The boiler tube wall is thin; thus, the temperature drop across the wall is small and negligible compared to peripheral temperature drops.

b) The ends of the one-dimensional wall element shown in Figure 61 are insulated.

c) A step function conductance profile exists on the boiling side, simulating the rivulet and vapor zones.

d) A uniform conductance distribution exists on the hot fluid side.

e) Steady state exists.

A heat rate balance on a differential wall element (which accounts for convection and conduction into and out of the element) yields,

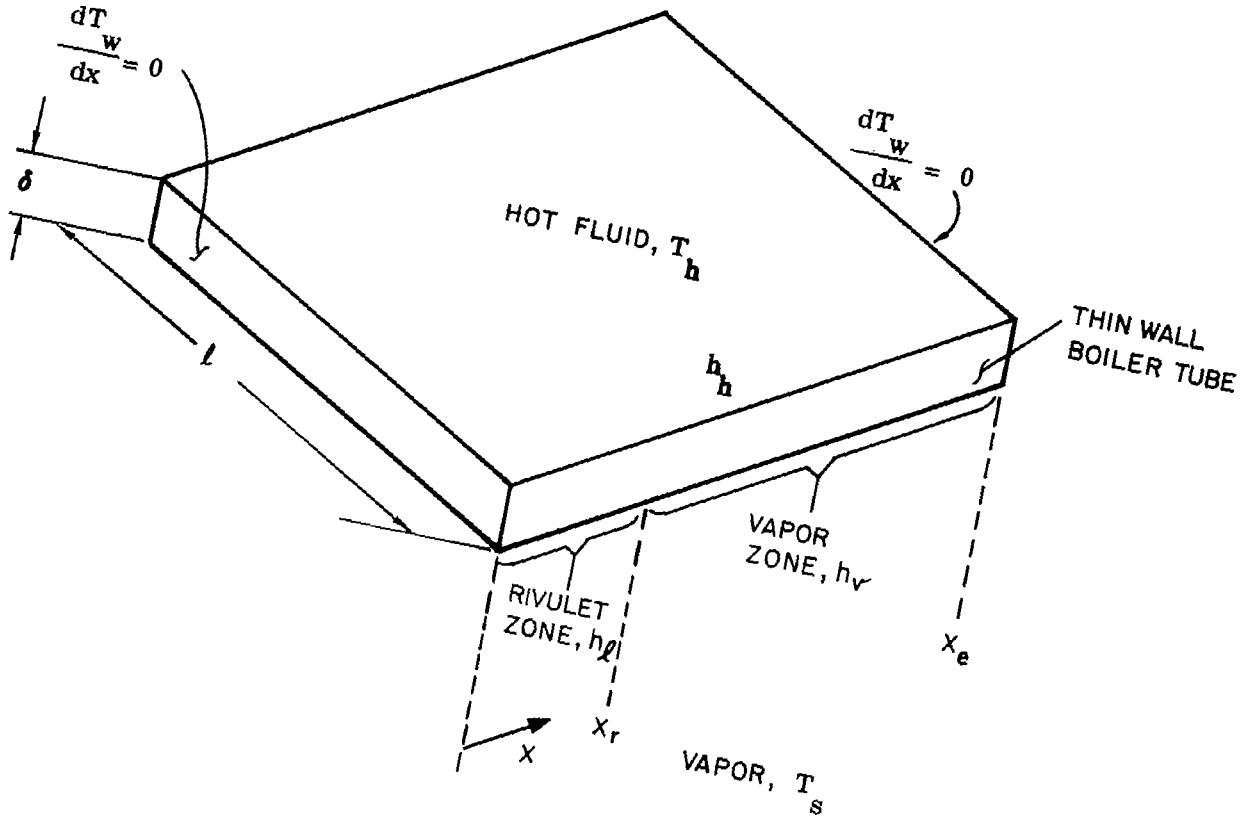

Figure 61. Idealized thin wall boiler tube - rivulet system.

for $0 < x < x_r$

$$\frac{d^2T_w}{dx^2} = \left(\frac{h_h + h_\ell}{k_w \delta}\right) T_w - \left(\frac{h_h T_h + h_\ell T_s}{k_w \delta}\right)$$

$$= \alpha_1 \left(T_w - \frac{n_1}{\alpha_1}\right) \tag{166}$$

for $x_r < x < x_e$

$$\frac{d^2T_w}{dx^2} = \left(\frac{h_h + h_v}{k_w \delta}\right) T_w - \left(\frac{h_h T_h + h_v T_s}{k_w \delta}\right)$$

$$= \alpha_2 \left(T_w - \frac{n_2}{\alpha_2}\right) \tag{167}$$

The solutions of Equations (166) and (167) are, respectively,

for $0 < x < x_r$

$$T_w - \frac{n_1}{\alpha_1} = C_1 e^{-\sqrt{\alpha_1} x} + C_2 e^{\sqrt{\alpha_1} x} \tag{168}$$

for $x_r < x < x_e$

$$T_w - \frac{n_2}{\alpha_2} = C_3 e^{-\sqrt{\alpha_2} x} + C_4 \sqrt{\alpha_2} x \tag{169}$$

where:

C_1, C_2, C_3, C_4, equation constants (see derivation)

h_h, convective conductance on hot fluid side, Btu/hr ft^2 °F

h_v, vapor convective conductance, Btu/hr ft^2 °F

h_ℓ, rivulet vaporization conductance, Btu/hr ft^2 °F

k_w, wall thermal conductivity, Btu/hr ft °F

n_1, n_2, α_1, α_2, system parameters (see derivation)

T_w, boiler wall temperature at position x, °F

x, peripheral distance along boiler tube (origin at rivulet center), ft

x_r, half width of rivulet, ft

x_e, peripheral distance from rivulet center to point where the peripheral temperature gradient is zero, ft

δ, boiler tube wall thickness, ft

T_h, mixed mean temperature of the hot fluid, °F

and

T_s, saturated vapor temperature, °F

From the boundary condition, $\frac{dT_w}{dx} = 0$ at $x = 0$, it can be shown that

$$C_1 = C_2 \tag{170}$$

From the boundary condition, $\frac{dT_w}{dx} = 0$ at $x = x_e$, it can be shown that

$$C_3 = C_4 e^{2\sqrt{\alpha_2}x_e} \tag{171}$$

From the boundary conditions, $T_{w+} = T_{w-}$ and $\left(\frac{dT_w}{dx}\right)_+ = \left(\frac{dT_w}{dx}\right)_-$ at $x = x_r$, two equations in two unknowns (C_1 and C_3) result,

$$\frac{n_1}{\alpha_1} + C_1 \left(e^{-\sqrt{\alpha_1}x_r} + e^{\sqrt{\alpha_1}x_r}\right) = \frac{n_2}{\alpha_2} + C_4 \left(e^{2\sqrt{\alpha_2}x_e} e^{-\sqrt{\alpha_2}x_r} + e^{\sqrt{\alpha_2}x_r}\right) \tag{172}$$

$$-C_1 \left(\sqrt{\alpha_1} e^{-\sqrt{\alpha_1}x_r} - \sqrt{\alpha_1} e^{\sqrt{\alpha_1}x_r}\right) = -C_4 \left(e^{2\sqrt{\alpha_2}x_e} \sqrt{\alpha_2} e^{-\sqrt{\alpha_2}x_r} - \sqrt{\alpha_2} e^{\sqrt{\alpha_2}x_r}\right) \tag{173}$$

The solution of Equations (172) and (173) yields

$$C_4 = \frac{\frac{n_2}{\alpha_2} - \frac{n_1}{\alpha_1}}{\frac{N_2 N_4}{N_3} - N_1} \tag{174}$$

$$C_1 = \frac{\frac{n_2}{\alpha_2} - \frac{n_1}{\alpha_1} + C_4 N_1}{N_4} \tag{175}$$

where

$$\left.\begin{aligned}
N_1 &= e^{2\sqrt{\alpha_2}x} e^{-\sqrt{\alpha_2}x_r} + e^{\sqrt{\alpha_2}x_r} \\
N_2 &= e^{2\sqrt{\alpha_2}x} e^{\sqrt{\alpha_2}} e^{-\sqrt{\alpha_2}x_r} - \sqrt{\alpha_2}\, e^{\sqrt{\alpha_2}x_r} \\
N_3 &= \sqrt{\alpha_1}\, e^{-\sqrt{\alpha_1}x_r} - \sqrt{\alpha_1}\, e^{\sqrt{\alpha_1}x_r} \\
N_4 &= e^{-\sqrt{\alpha_1}x_r} + e^{\sqrt{\alpha_1}x_r} \\
n_1 &= \frac{h_h T_h + h_\ell T_s}{k_w \delta} \\
\alpha_1 &= \frac{h_h + h_\ell}{k_w \delta} \\
n_2 &= \frac{h_h T_h + h_v T_s}{k_w \delta} \\
\alpha_2 &= \frac{h_h + h_v}{k_w \delta}
\end{aligned}\right\} \tag{176}$$

Thus the solution to the boundary value problem described above is given by Equations (168), (169), (170), (171), (174), (175), and (176).

The solution has been evaluated for three specific examples. The results of the three sets of calculations are shown in Figures 62, 63, and 64 to demonstrate how the shapes of the wall temperature profiles can vary as the system parameters are changed. The thermal conductivities of the boiler tube wall range from 0 to ∞ and fractions of the wall covered by a rivulet of 0.1 and 0.5 are considered. The vapor conductance in the boiler tube, h_v, varies from 10 to 100 Btu/hr ft^2 °F. The hot fluid T_h is constant at 1300°F and the saturated vapor temperature in the boiler tube, T_s, is constant at 1000°F. The hot fluid conductance, h_h, and the rivulet conductance in the boiler tube, h_ℓ, are both set equal to 10,000 Btu/hr ft^2 °F. The boiler tube wall thickness, δ, is equal to 0.004 ft. The specific variations considered in Figures 62, 63, and 64, are given in the legends.

2. Temperature Distributions Due to Axial Discontinuities in the Internal Liquid Film in a Thick-walled Boiler

Boilers which are wet by the vaporizing liquid in the low quality region all undergo a transition at some quality in which the wall ceases to be completely wetted by liquid. If this point occurs at a quality of less than one, the remaining liquid may be in rivulets on the wall, (which is locally wet) rivulets separated from the wall by a vapor film, droplets or masses of liquid throughout the bulk of the vapor, or combinations of these distributions.

Consider the point at which the liquid film ends, so that the wall cooling is discontinuous on the inner surface. If the wall conductivity in the direction normal to the discontinuity is significant then heat will flow along the wall toward the high conductance (low temperature) region, increasing the local temperature difference in the well cooled portion near the discontinuity. The magnitude of the inner wall heat flux and temperature variations are of interest.

The solution for the temperature and heat flux distribution in a thermal conductor subjected to the appropriate boundary conditions is not easily obtained by analytical means, and the required information was obtained by a two-

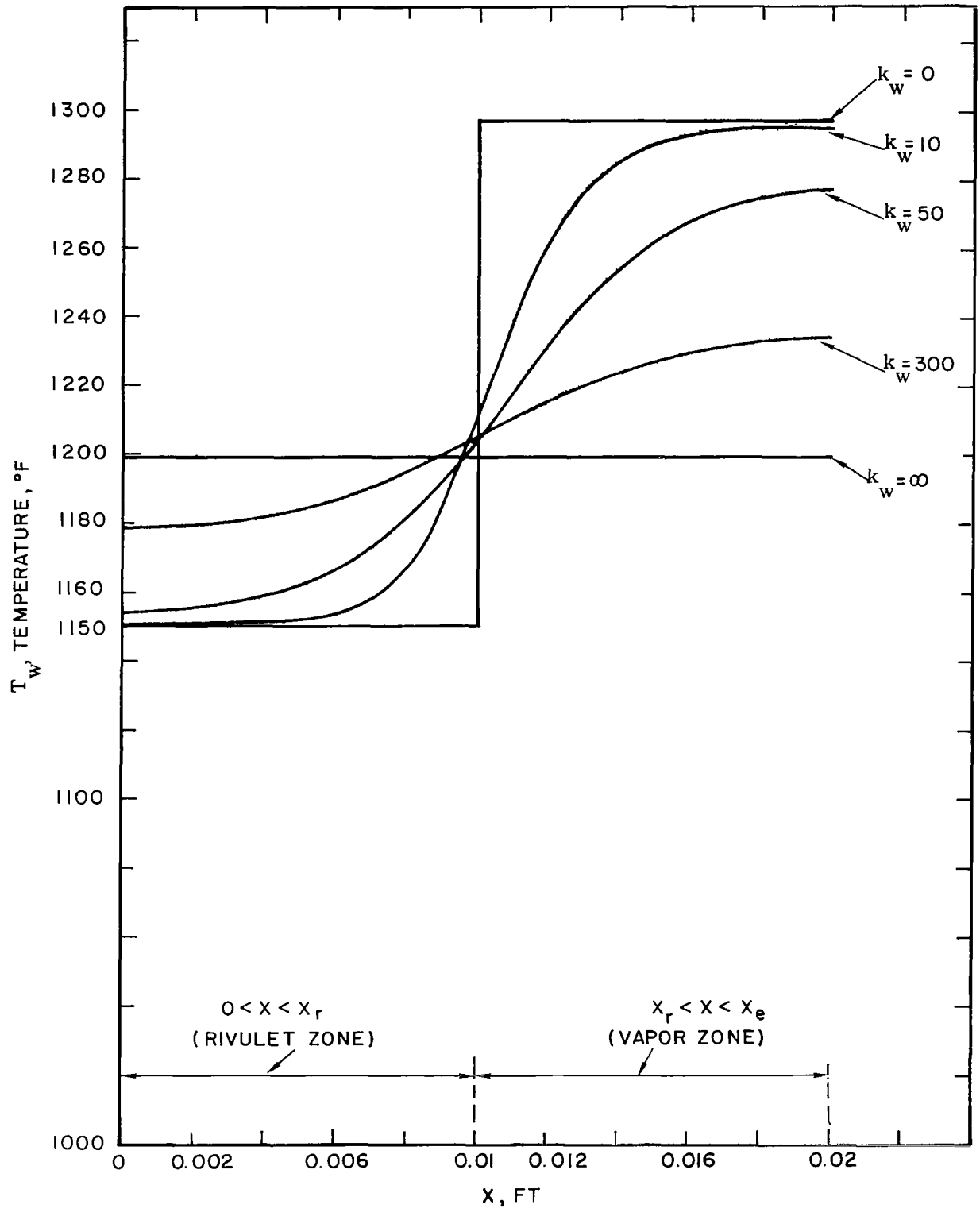

Figure 62. Temperature profiles for a thin wall boiler tube with a rivulet, (X_r= 0.01', X_e = 0.02', h_v = 100 Btu/hr ft^2 °F.)

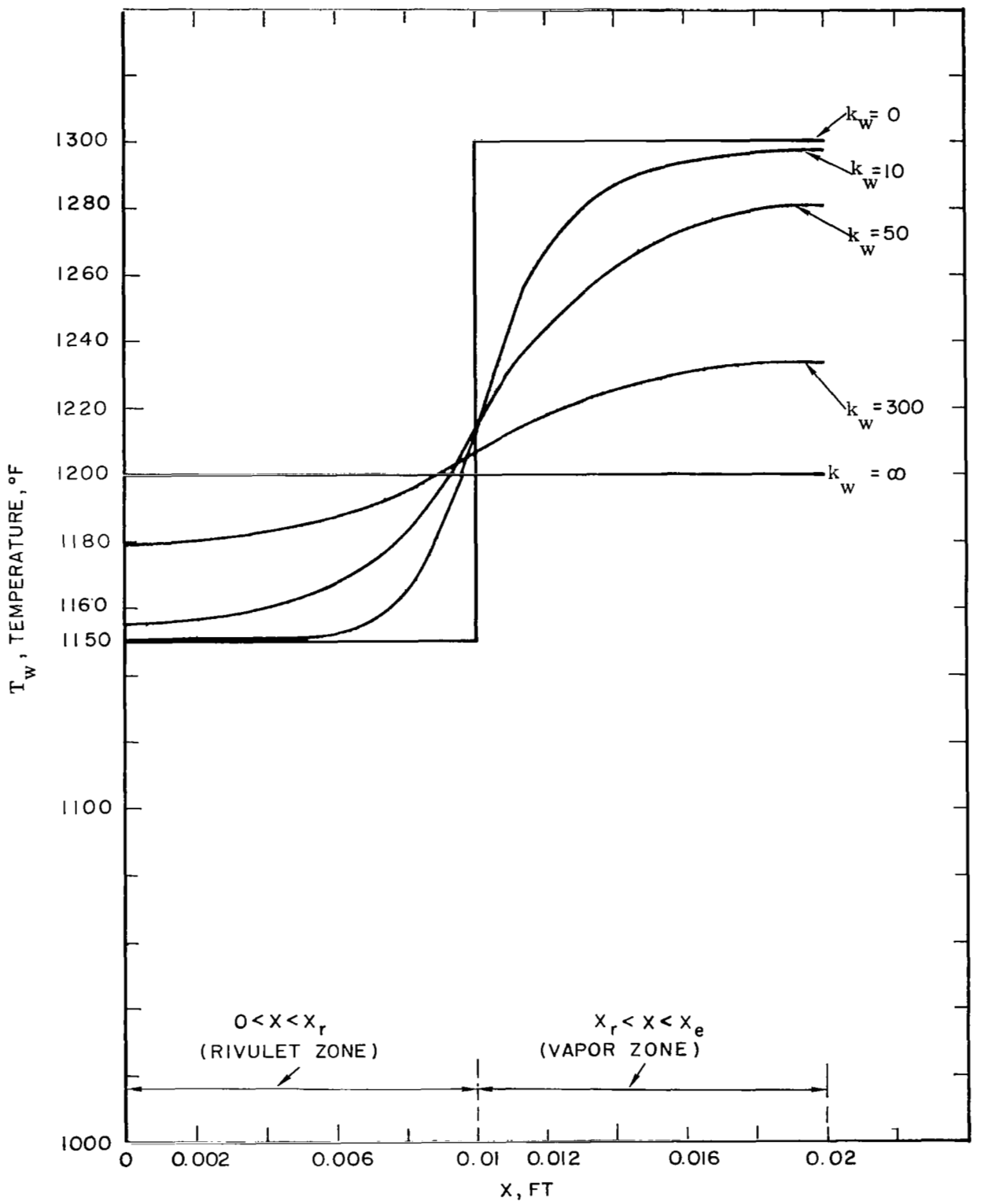

Figure 63. Temperature profiles for a thin wall boiler tube with a rivulet, (X_r=0.01', X_e=0.02', h_v=10 Btu/hr ft^2 ^oF)

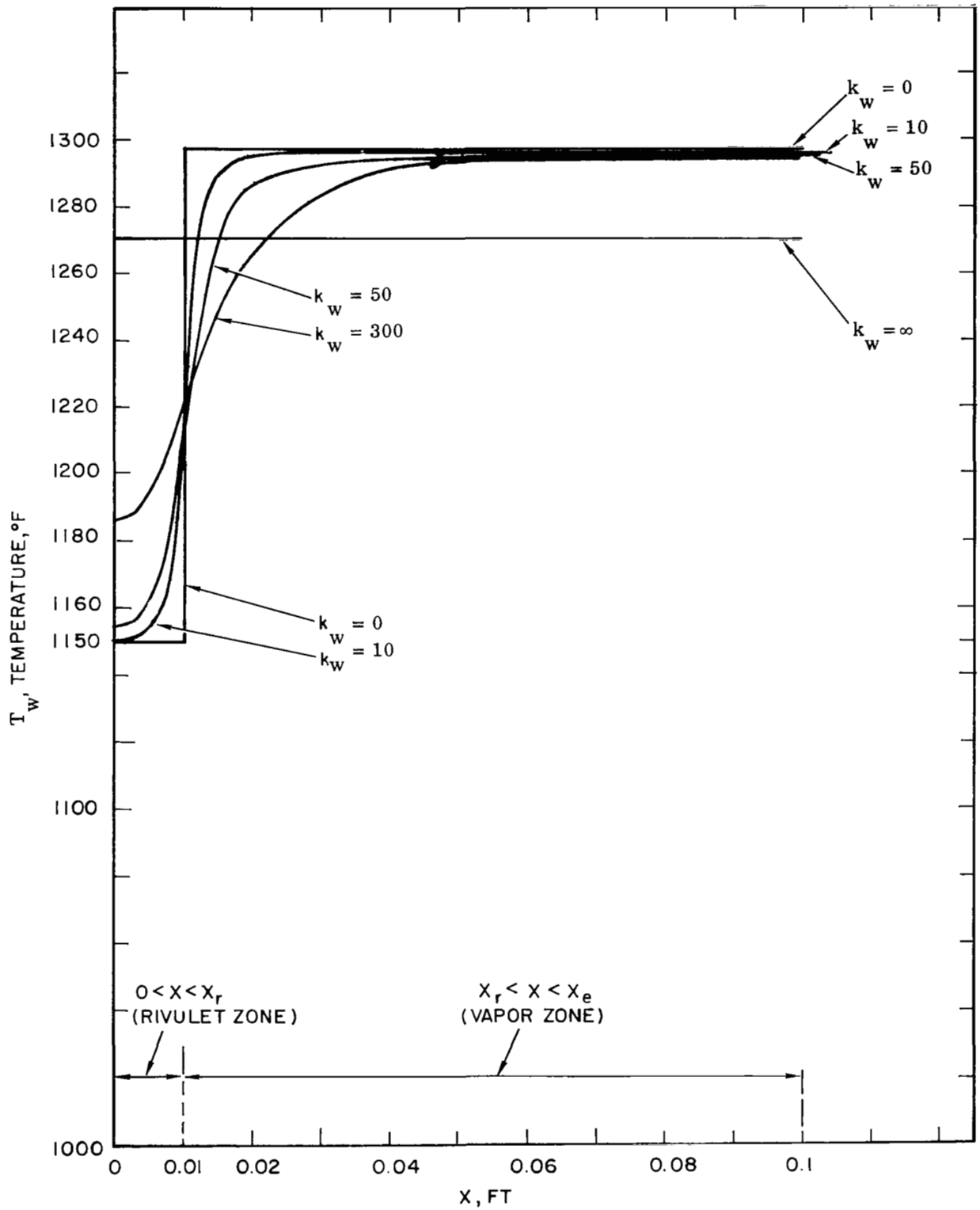

Figure 64. Temperature profiles for a thin wall boiler tube with a rivulet, (X_r=0.01', X_e=0.10', h_v=100 Btu/hr ft^2 °F)

dimensional electric analog, using Teledeltos (Western Electric Company) conductive paper. The circuit used is shown in Figure 65. A photograph of the apparatus is shown in Figure 66. A tube cross section model for study of temperature under rivulets, which is the case discussed in the next section, is shown in the photograph.

All of the model work was done using the uniform outside wall heat flux boundary condition because this condition is frequently used in 'critical heat flux' boiling experiments and also because it eliminates the outside wall conductance as a parameter.

The two parameters used are,

$$\frac{h_\ell}{\frac{k_w}{\delta}}$$

which is the ratio of the 'wet wall' conductance to the reciprocal of boiler wall resistance and

$$\frac{h_\ell}{h_v}$$

which is the ratio of the 'wet wall' conductance to the 'dry wall' conductance. h is the heat transfer conductance, k_w is the wall thermal conductivity and δ is the wall thickness.

Two typical wall temperature distribution plots are shown in Figures 67 and 68. It is clear from these plots that although the outside wall heat flux is uniform, the inside wall heat flux is highly non-uniform for many wall thicknesses in either direction from the discontinuity. At large distance from the discontinuity the isotherms lie parallel to the wall edges. In the portions of the models shown, the isotherms lie almost perpendicular to the wall edges, showing that the major portion of the heat is flowing along the wall. In Figure 69 the variation in inside wall temperature at the conductance discontinuity is shown as a function of the two parameters.

These results may be related to an actual boiler tube under uniform heat flux conditions as follows. The wall temperature drop at $x = \pm \infty$ is

$$\Delta T_w = \frac{(q/A)}{(k_w/\delta)} \qquad (177)$$

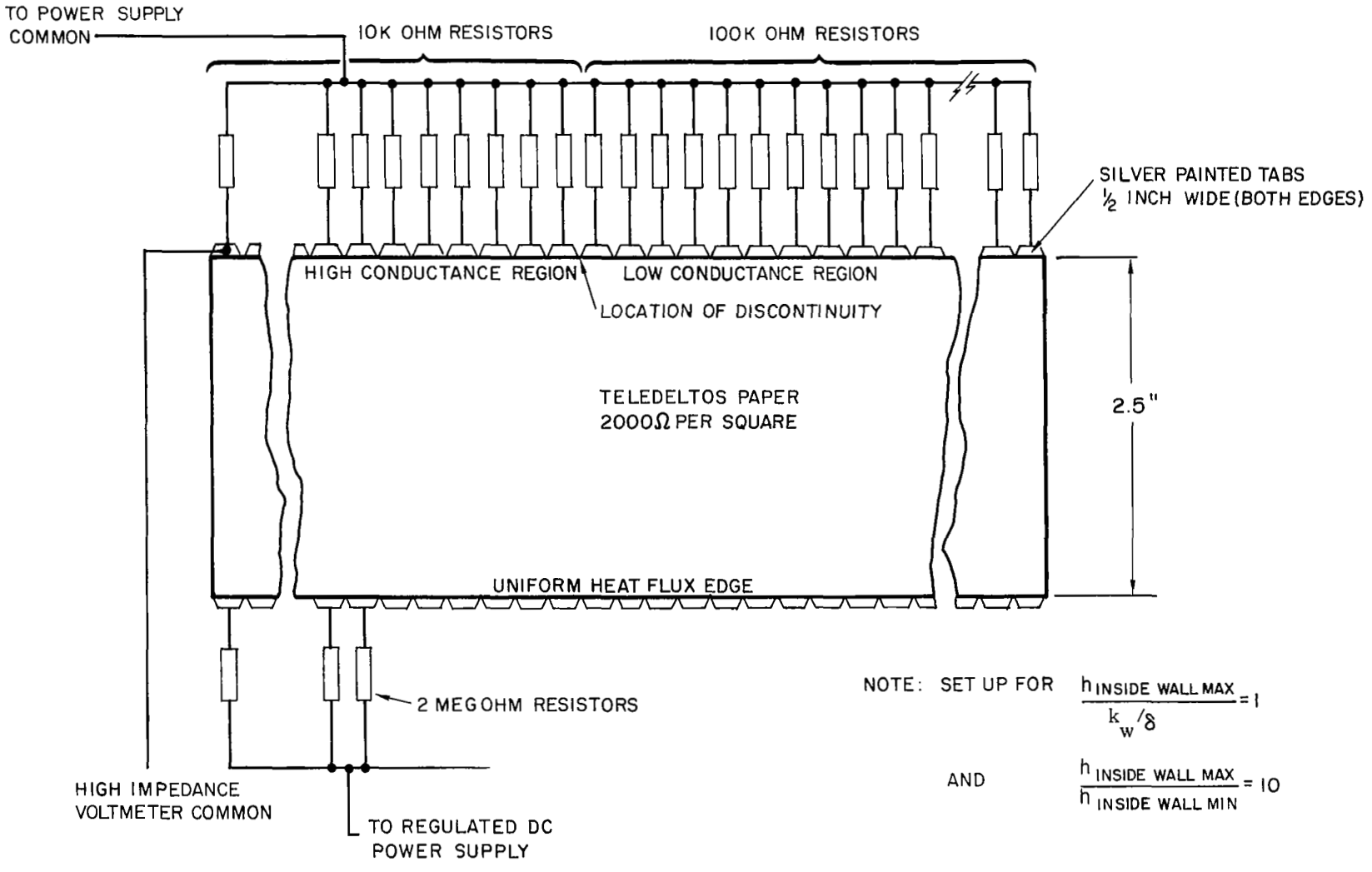

Figure 65. Circuit for flux plotting apparatus.

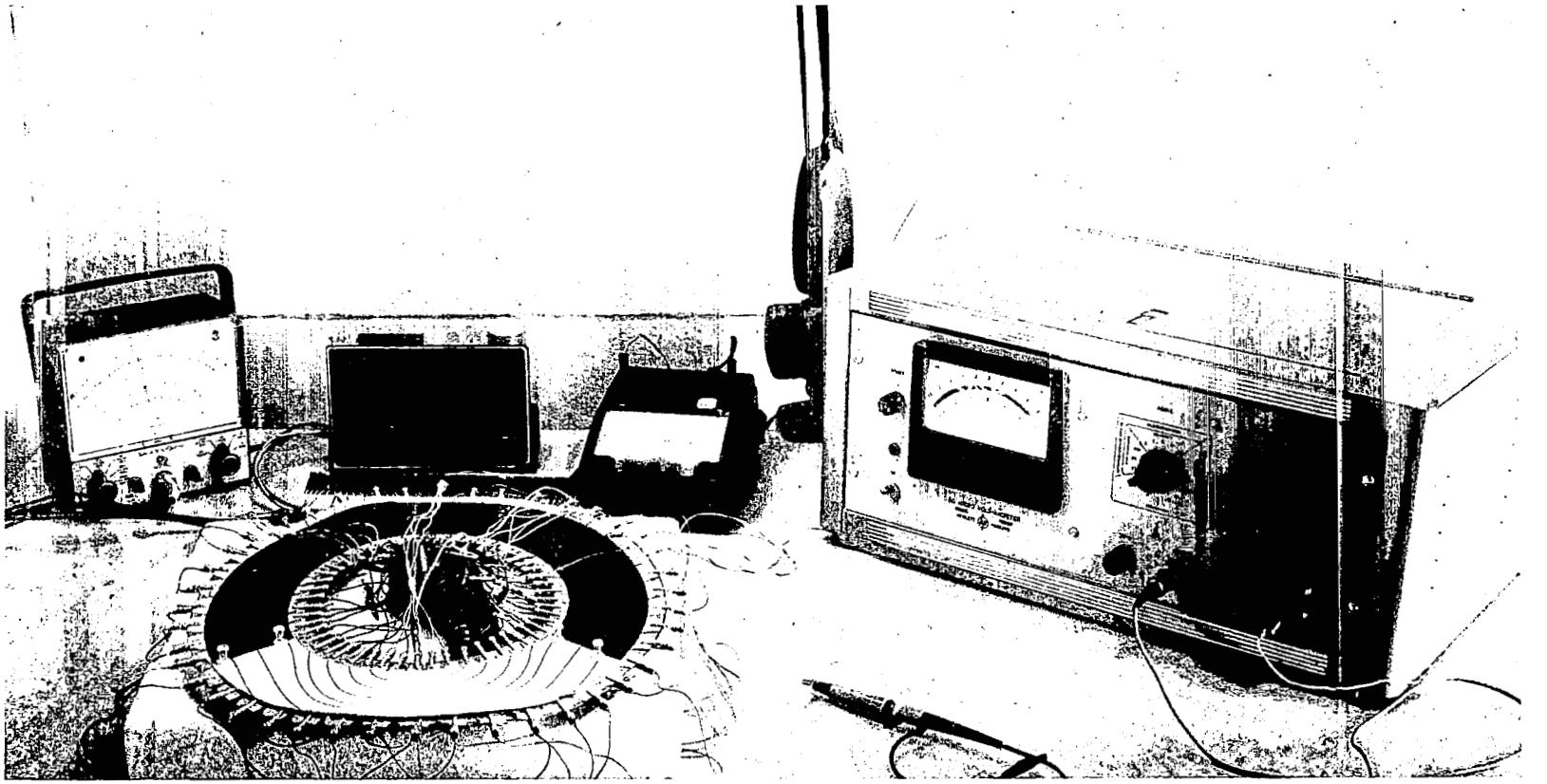

Figure 66. Photograph of the flux plotting apparatus, showing boiler tube cross section model in place.

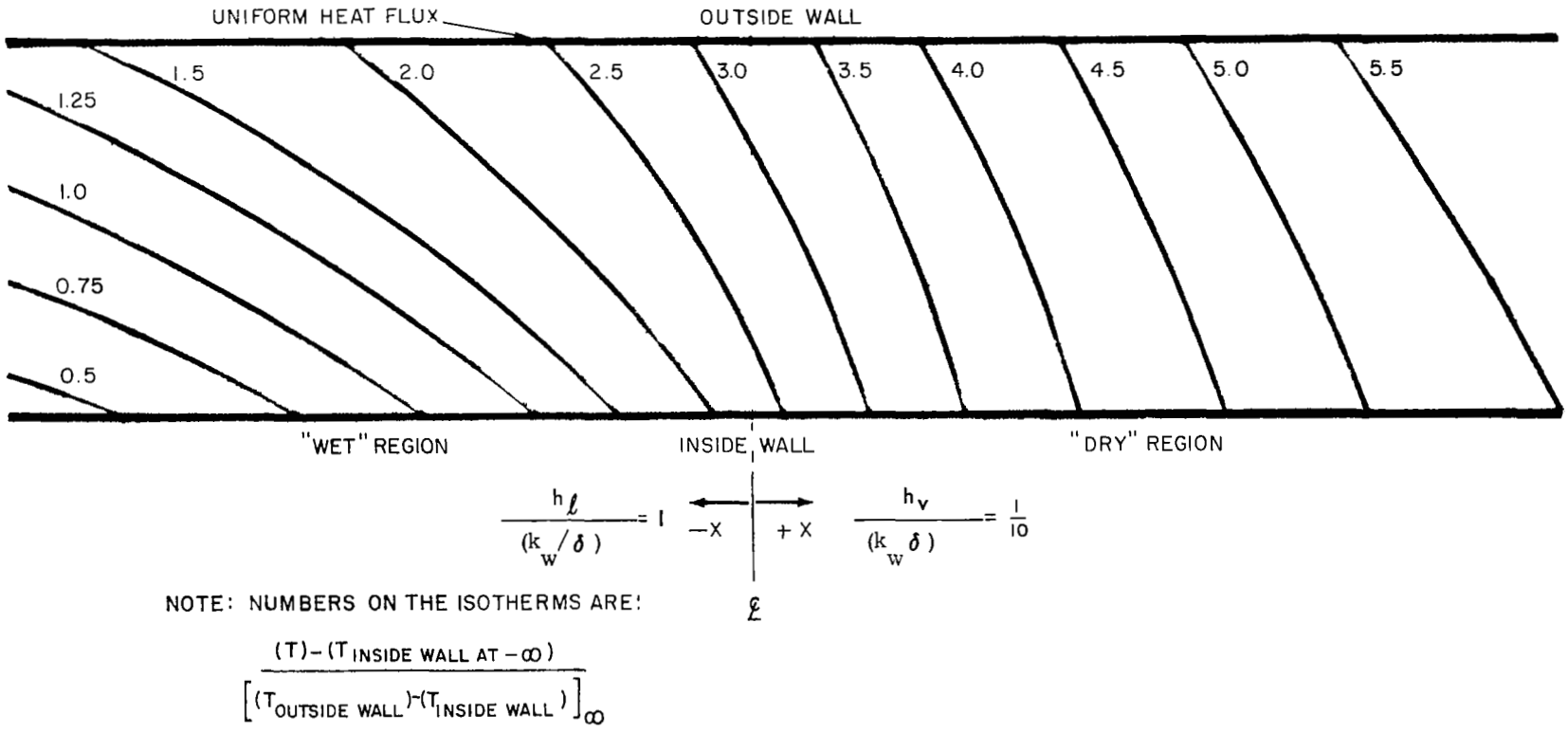

Figure 67. Temperature distribution in wall near conductance discontinuity.

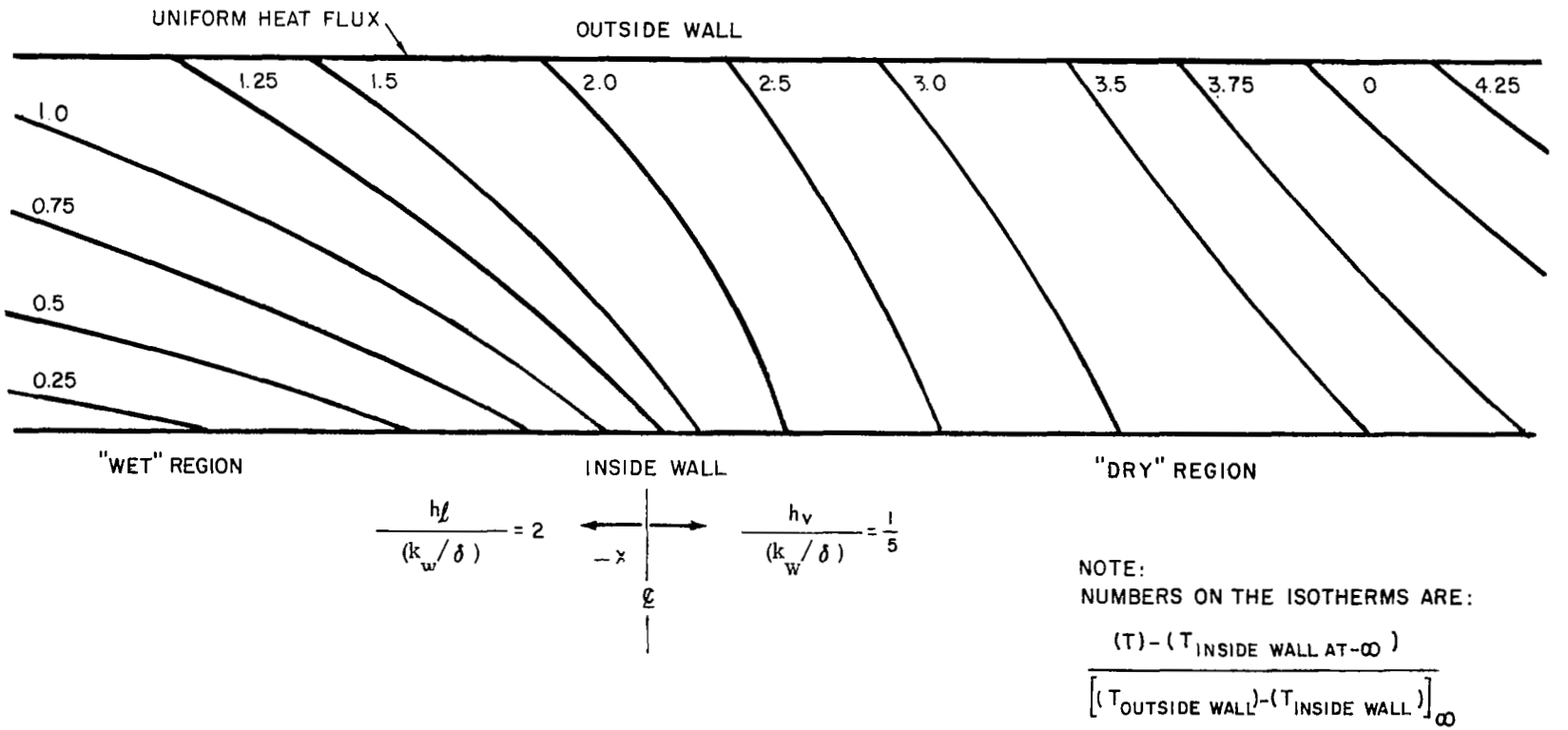

Figure 68. Temperature distribution in wall near conductance discontinuity.

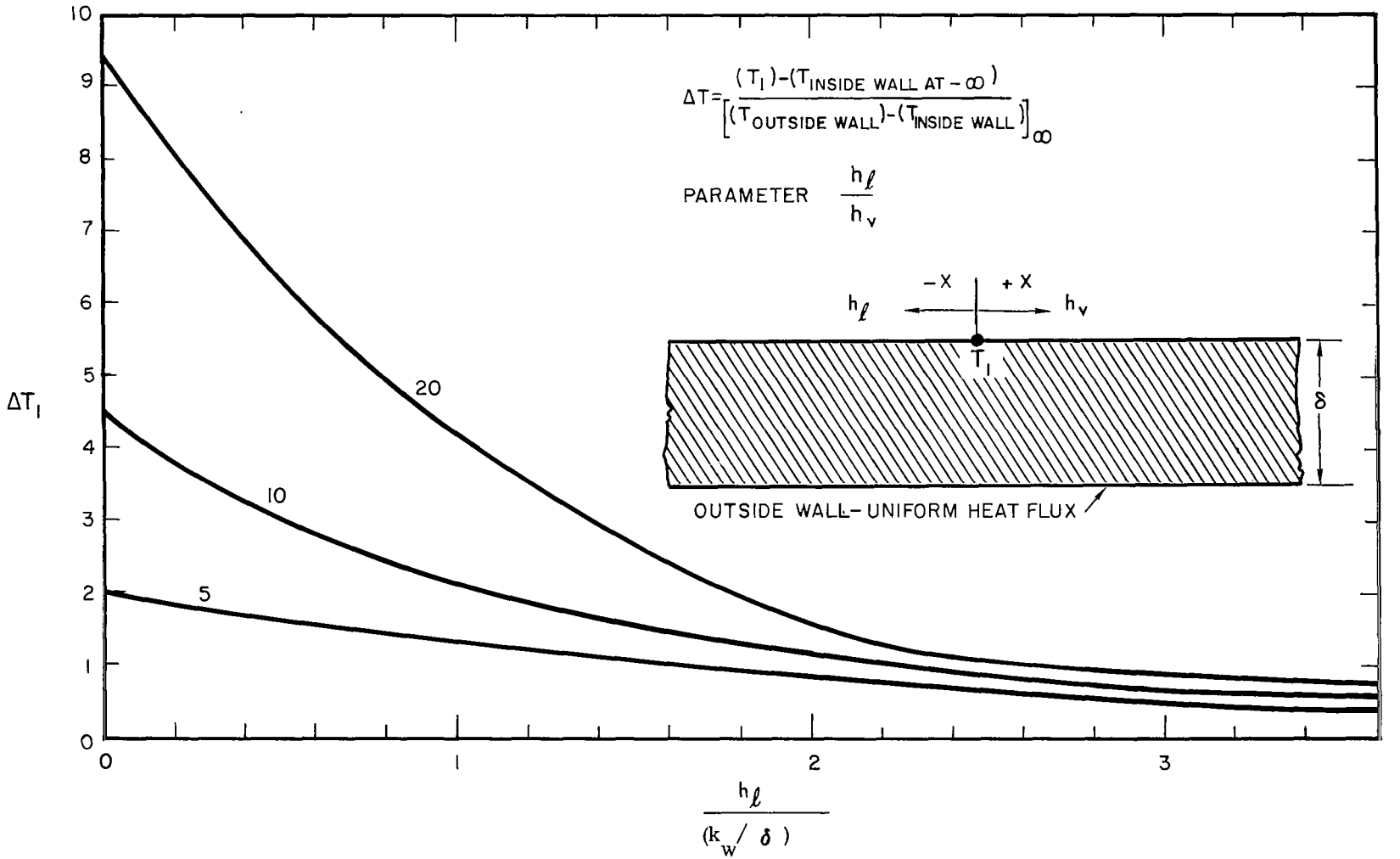

Figure 69. Normalized temperature at conductance discontinuity.

The temperature of the inside wall at $-\infty$ (the 'wet wall' end) is given by,

$$(T_{\text{inside wall at } -\infty}) = T_s + \frac{q/A}{h_\ell} \tag{178}$$

The temperature T_1 is given by

$$T_1 = \Delta T_1 \frac{(q/A)}{(k_w/\delta)} + \frac{q/A}{h_\ell} + T_s \tag{179}$$

where T_s is the saturation temperature.

3. Temperature Distributions in a Thick-Walled Tube with Internal Rivulet Flows

a) Number of Rivulets Variable

A plausible internal phase distribution can be visualized in which the axial variation in inside conductance is negligible, but in which the azimuthal variation is large, due to wetted liquid rivulets running along the inner wall of the tube. In general, the significant parameters in this hypothetical flow distribution are: boiler wall thickness δ, wall thermal conductivity k_w, wetted wall conductance h_ℓ which may be a function of location in the rivulet, 'dry wall' conductance h_v which may be a function also of azimuthal position, inside to outside tube radius ratio, ratio of rivulet width to inside circumference, number of rivulets, and probably others as well. The general case contains too many parameters to present concisely, and a fairly specific case has been investigated. General Electric Company SPPS performed experiments with a 3/8 schedule 80 (IPS) columbium - 1% zirconium boiler tube under NASA contract NAS 3-2528, and this boiler tube was chosen to model with the flux plots. Radius ratio, wall thickness, wall thermal conductivity are all fixed. In addition, fixed representative values of 'wetted wall' conductance and 'dry wall' conductance were chosen. The inside conductances were idealized as uniform within their respective areas. A single rivulet was taken to be 1/10 of the inside circumference. The only variable then considered was the number

of rivulets on the inside wall. The fixed parameters are

tube radius ratio = 0.63

δ = 0.126 inch

$$k_w = 31.5 \frac{\text{Btu}}{\text{ft}^2\text{hr}\ (^\circ\text{F/ft})}$$

$$h_\ell = 12{,}000 \frac{\text{Btu}}{\text{ft}^2\text{hr}\ ^\circ\text{F}}$$

$$h_v = 600 \frac{\text{Btu}}{\text{ft}^2\text{hr}\ ^\circ\text{F}}$$

Based on these values, the parameters used in the flux plot work were taken as

$$\frac{h_\ell}{k/\delta} \sim 4$$

$$\frac{h_\ell}{h_v} = 20$$

Flux plots were made for cases of 1, 2, 3, and 5 idealized rivulets. The case in which all the wall is wetted except for one dry strip 1/10 of the inside circumference wide was also plotted.

The 5 flux plots resulting from this work are given in Figures 70, 72, 74, 76, and 78 of this report. The outside and inside wall temperature variations for these same cases are given in Figures 71, 73, 75, 77, and 79. In all cases the temperature distributions have been normalized upon the temperature drop across the wall which would have existed had the inside wall cooling been uniform.

Inside wall to saturated fluid temperature differences for the center and edge of the rivulet are given in Figure 80. These temperatures have been normalized by dividing by the temperature difference which would have existed had the entire inside of the tube been wetted. Outside wall maximum and minimum temperatures are given in Figure 81.

Although this model is rather specific several general conclusions can be drawn from the results. One conclusion is that when wetted rivulet flow exists in a boiler tube, very large scatter in the conductance data could occur if the conductances are computed from a single outside thermocouple. A second conclusion is that onset of film boiling of the rivulets could occur at smaller apparent inside wall to fluid temperature differences than one might expect. Under conditions of non-uniform cooling the boiler tube may be subjected to considerable thermal stresses and transverse warping might also occur.

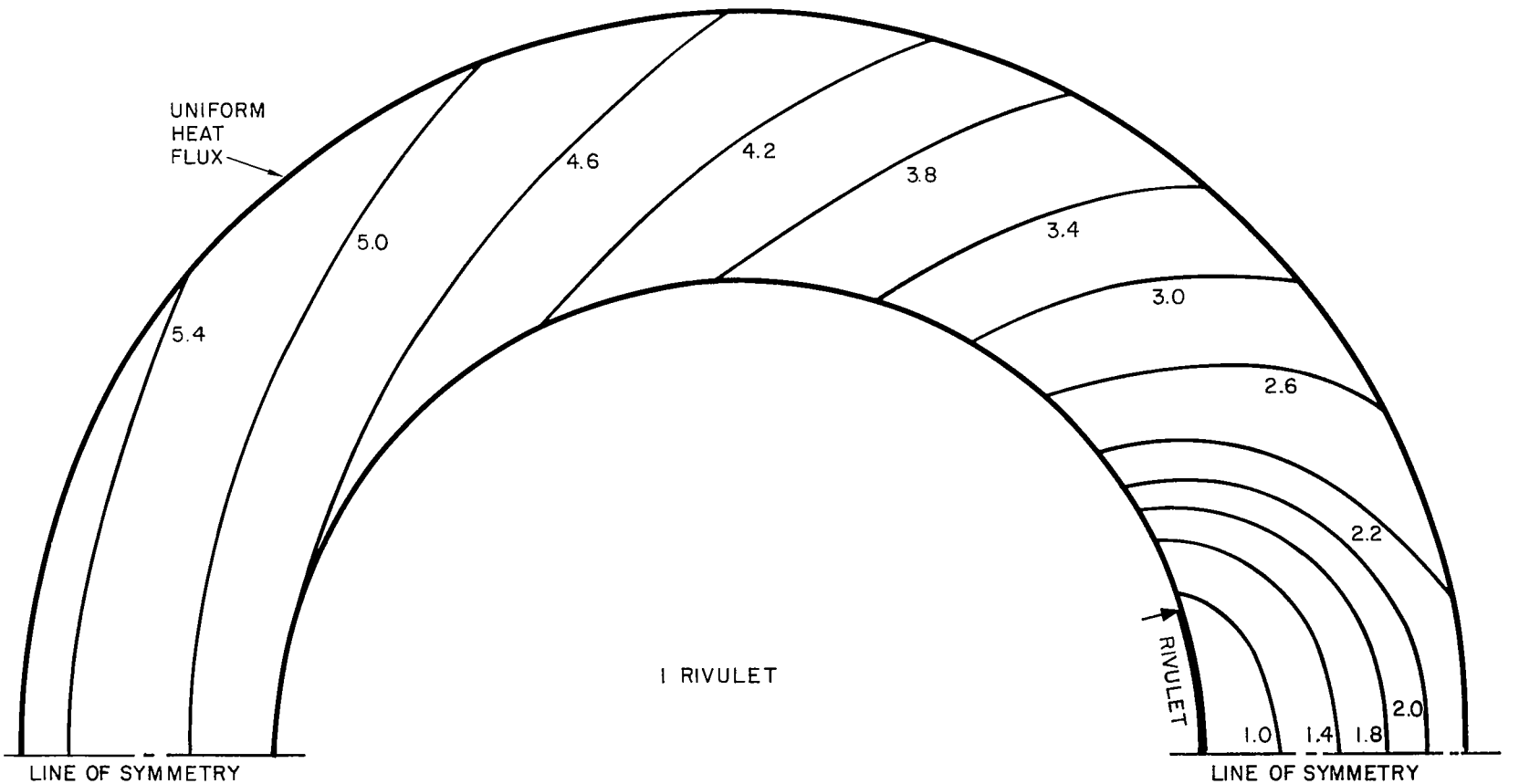

$\frac{h_\ell}{h_v} = 20$, $\frac{h_\ell}{(k_w/\delta)_{WALL}} = 4$, TUBE DIA. RATIO = 0.63 ($\frac{3}{8}$ SCH 80 PIPE)

Figure 70. Isotherms in boiler wall.

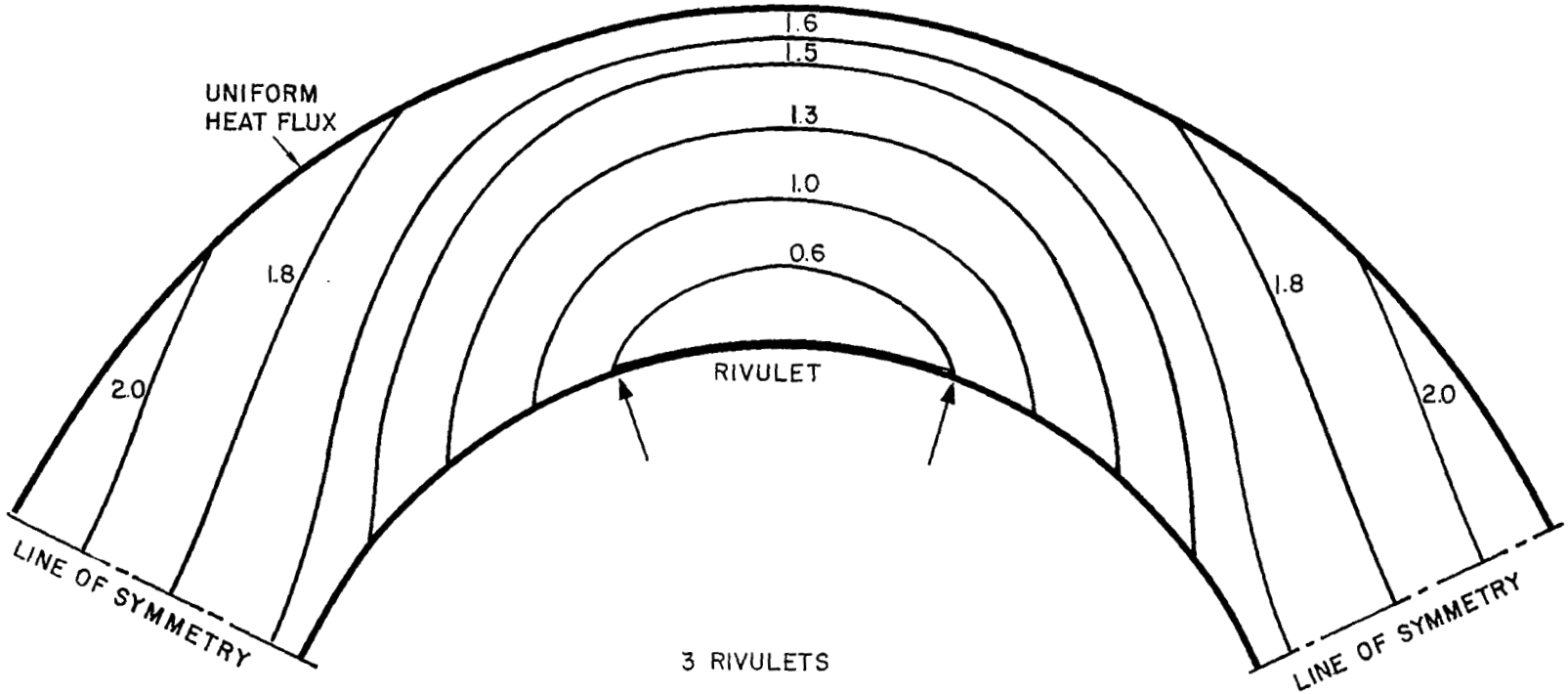

$$\frac{h_\ell}{h_v} = 20 \;,\; \frac{h_\ell}{(k_w/\delta)_{WALL}} = 4 \;,\; \text{TUBE DIA. RATIO} = 0.63 \left(\tfrac{3}{8} \text{ SCH 80 PIPE}\right)$$

Figure 71. Isotherms in boiler tube wall.

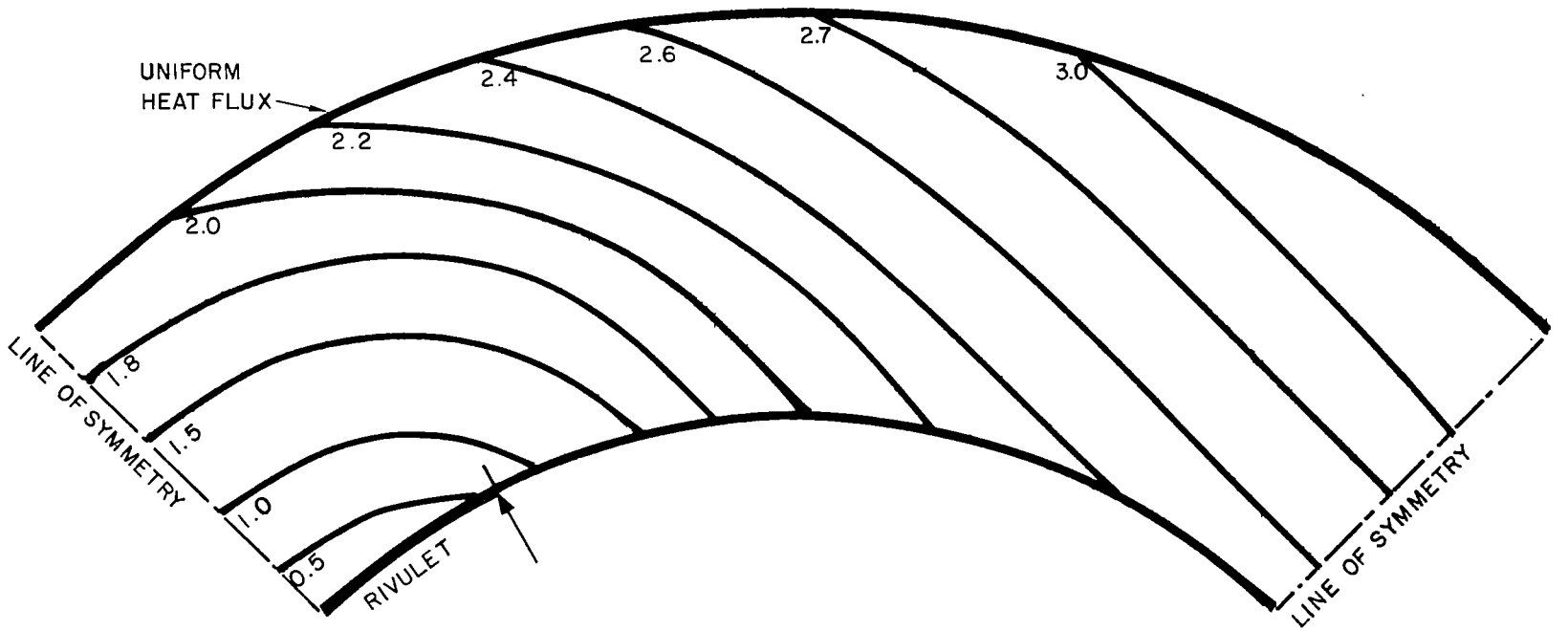

2 RIVULETS

$\frac{h_\ell}{h_v} = 20$, $\frac{h_\ell}{(k_w/\delta)_{WALL}} = 4$, TUBE DIA. RATIO = 0.63 ($\frac{3}{8}$ SCH 80 PIPE)

Figure 72. Isotherms in boiler tube wall.

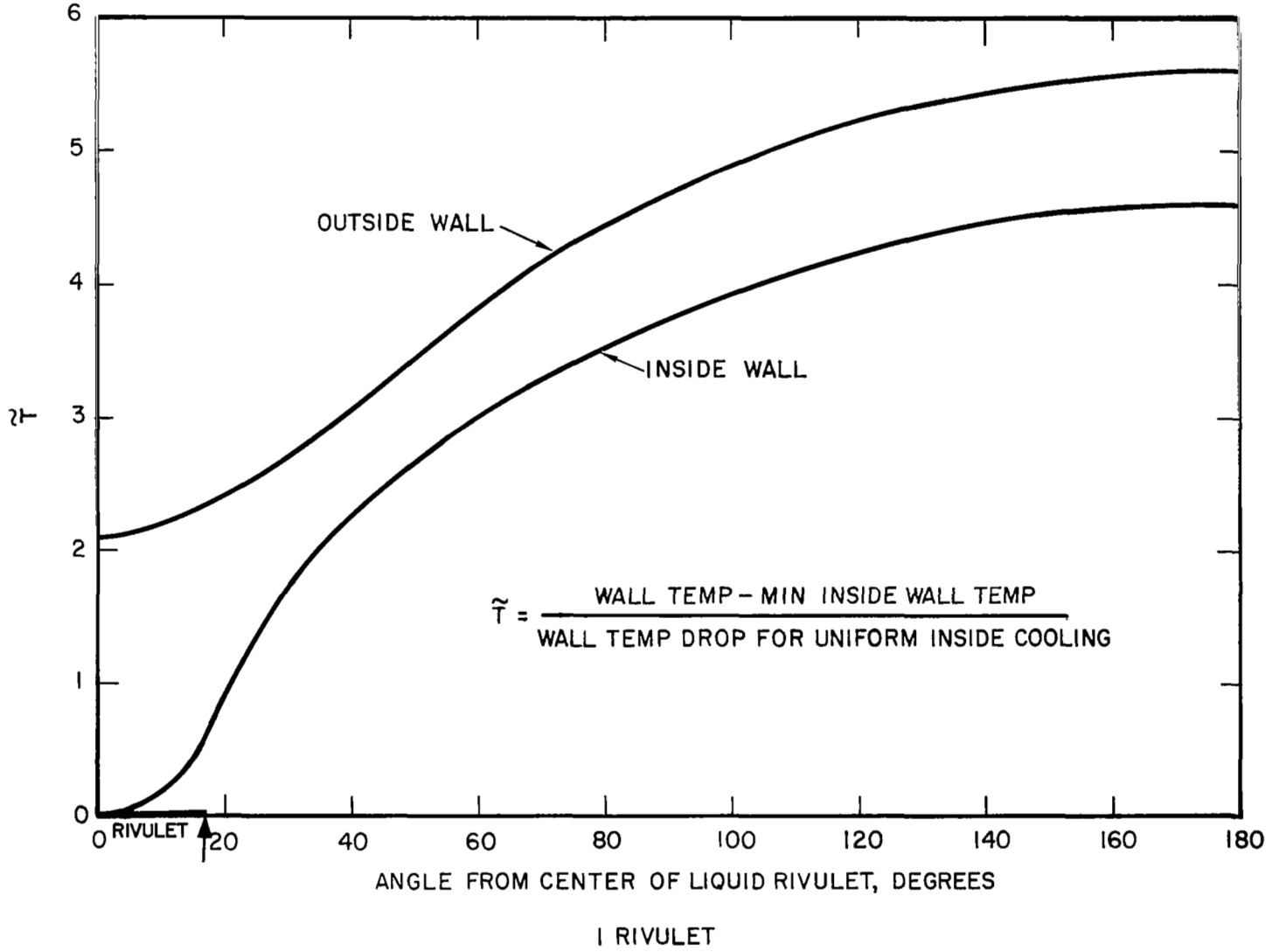

Figure 73. Boiler surface temperatures.

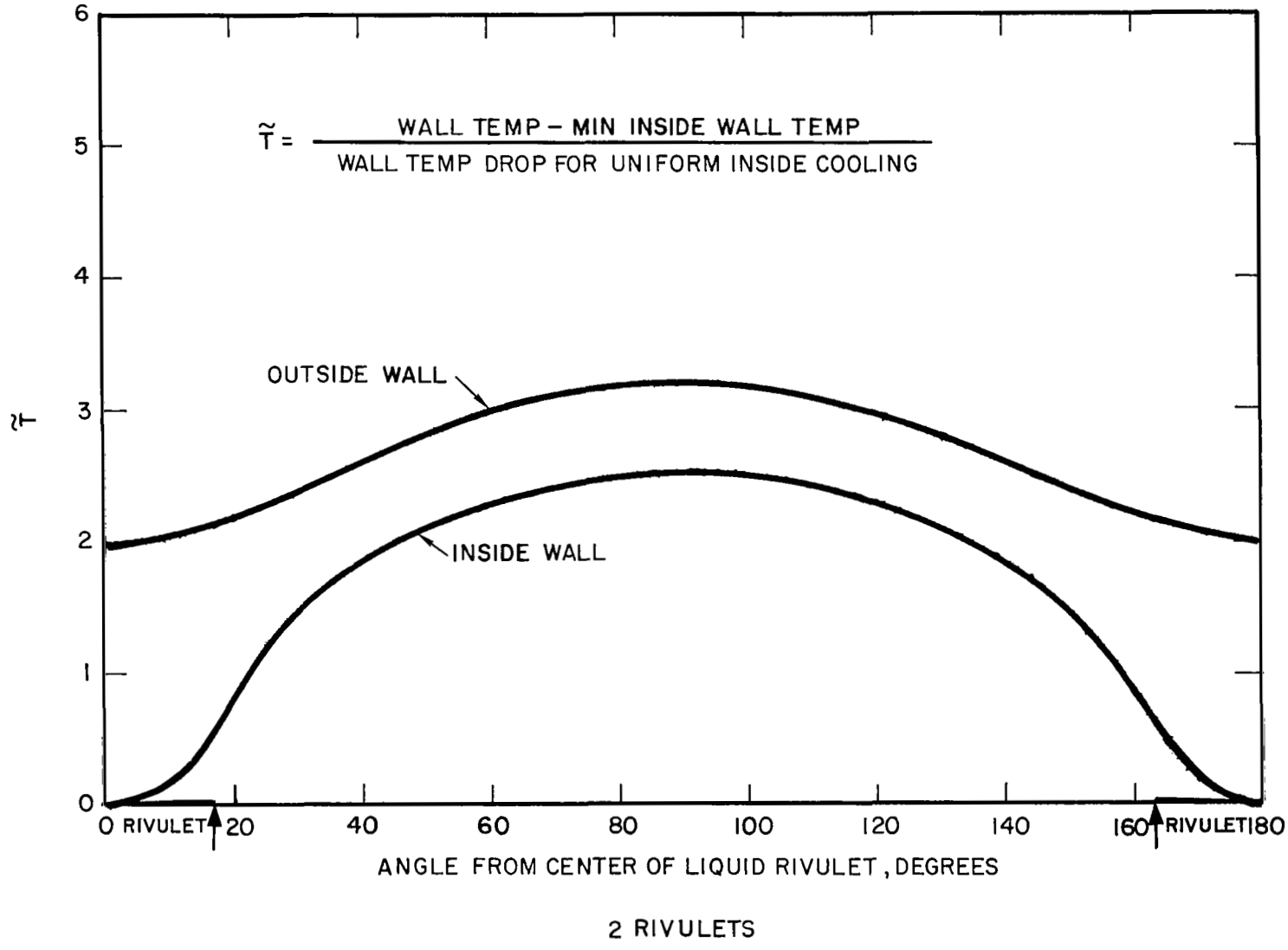

Figure 74. Boiler surface temperatures.

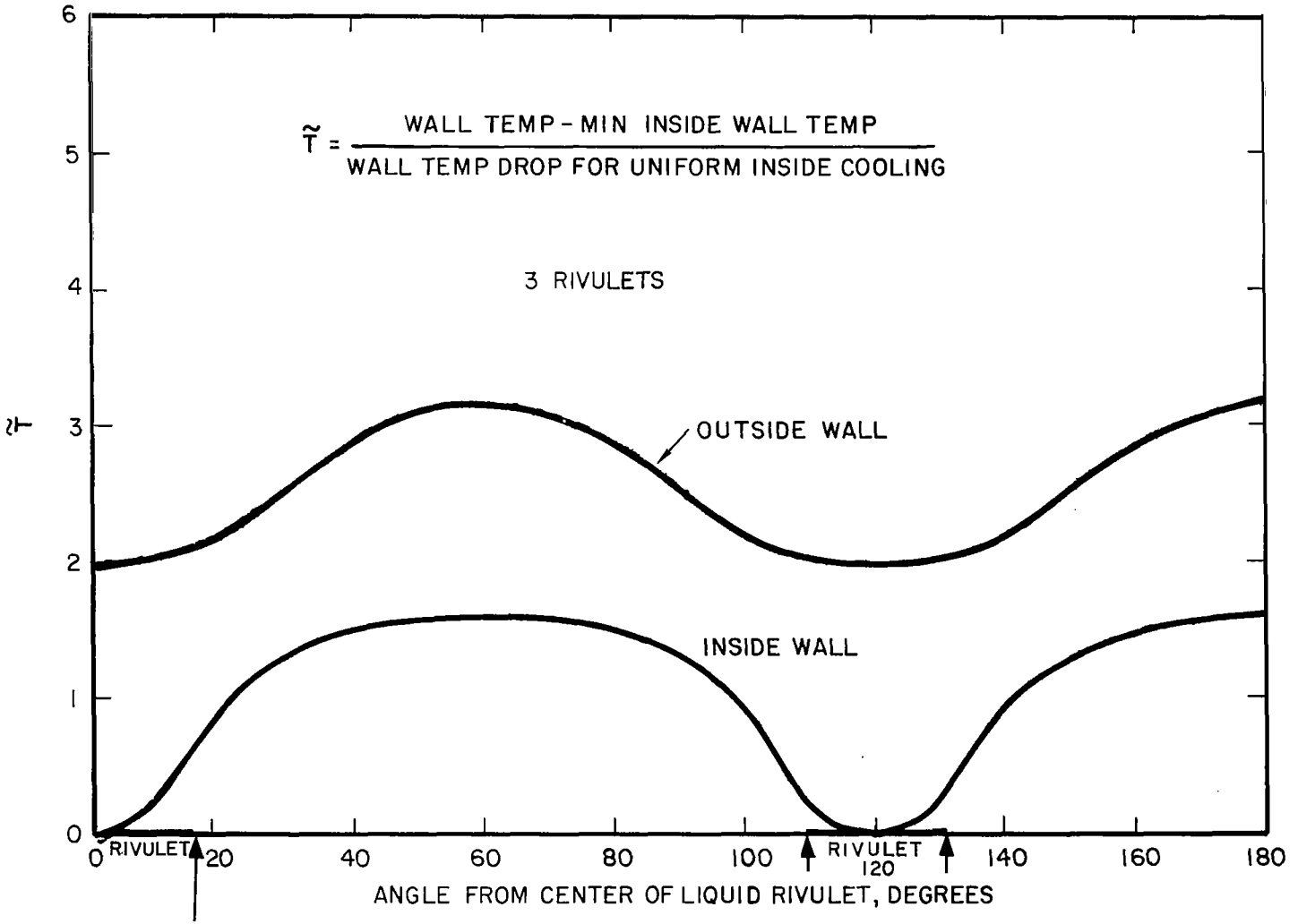

Figure 75. Boiler surface temperatures.

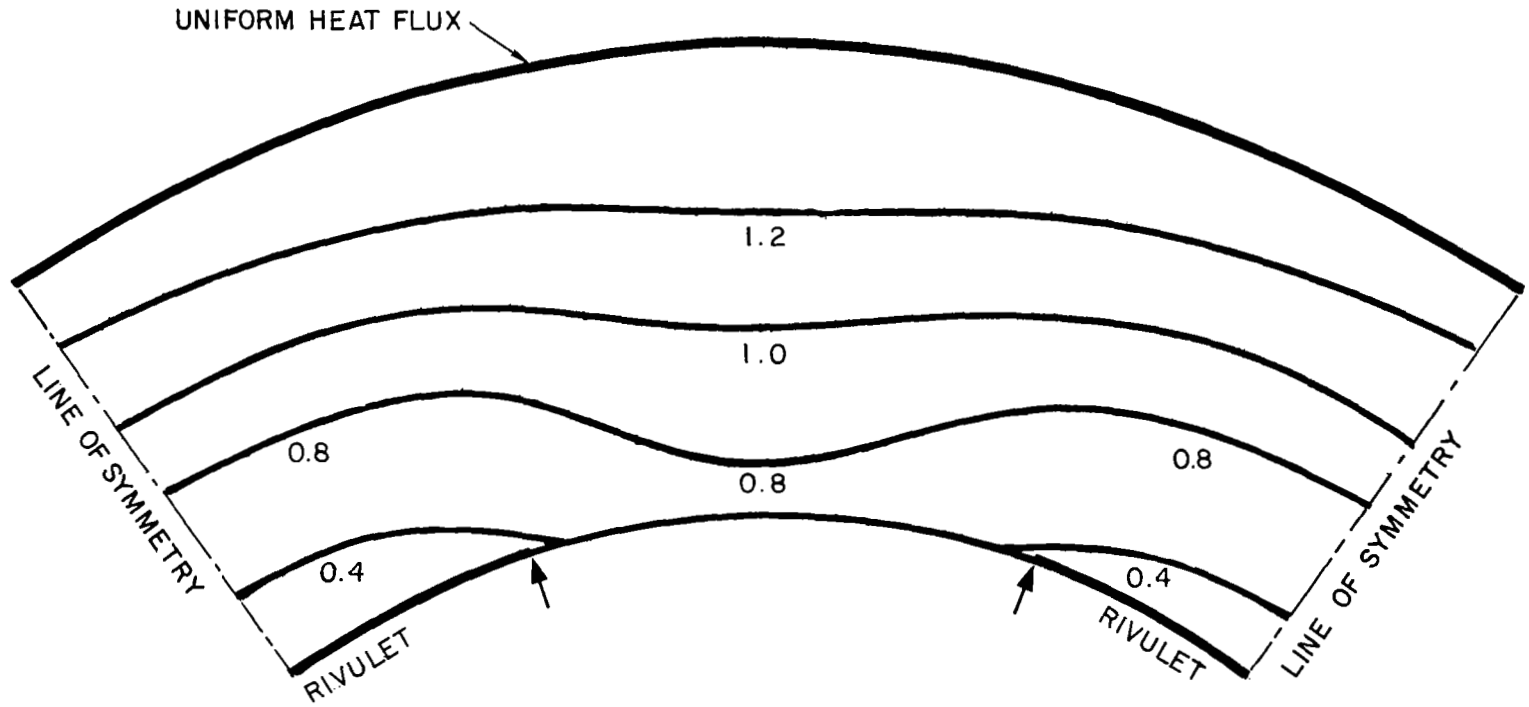

5 RIVULETS

$\frac{h_\ell}{h_v} = 20$, $\frac{h_\ell}{(k_w/\delta)_{WALL}} = 4$, TUBE DIA. RATIO = 0.63($\frac{3}{8}$ SCH 80 PIPE)

Figure 76. Isotherms in boiler tube wall.

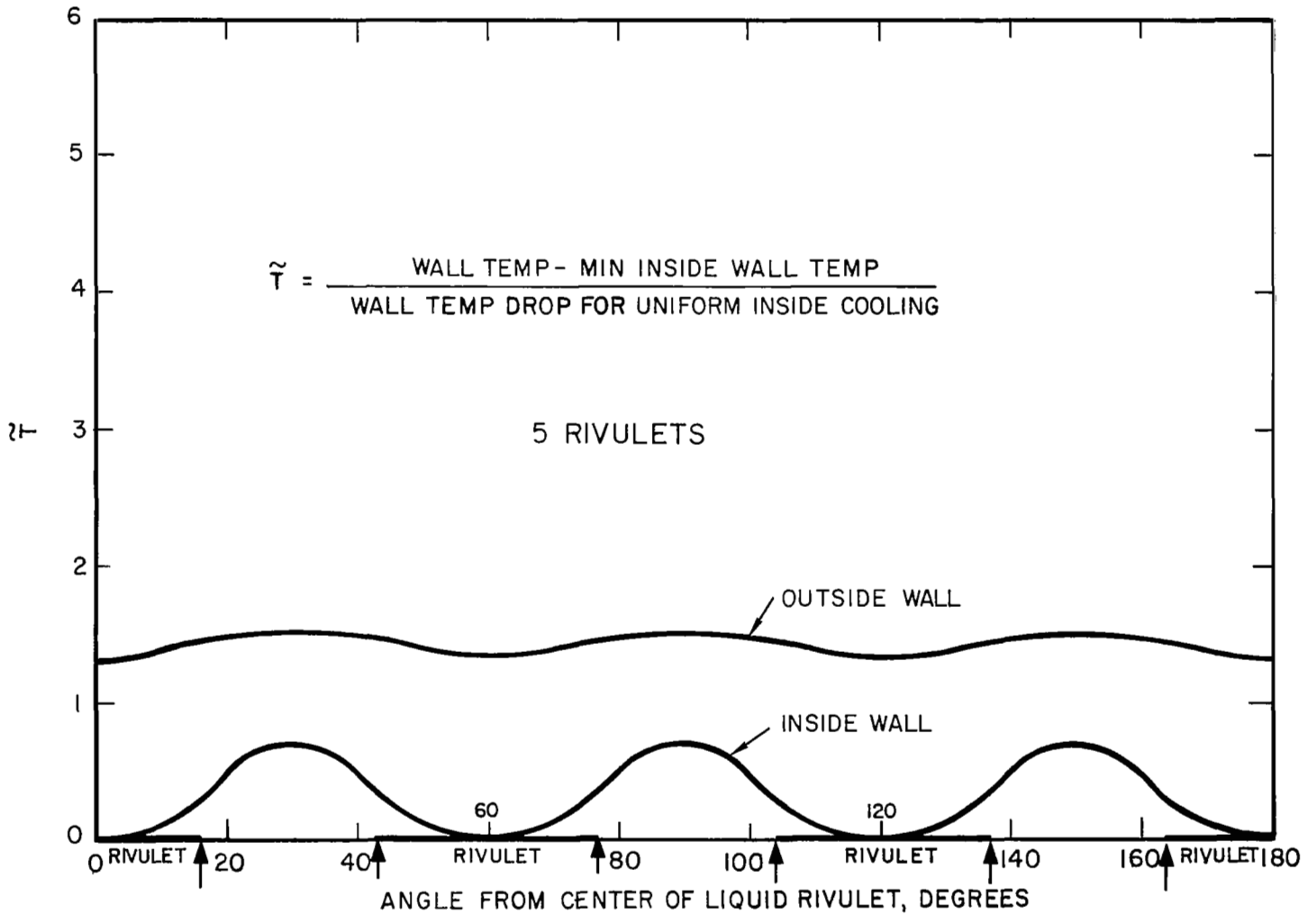

Figure 77. Boiler surface temperatures.

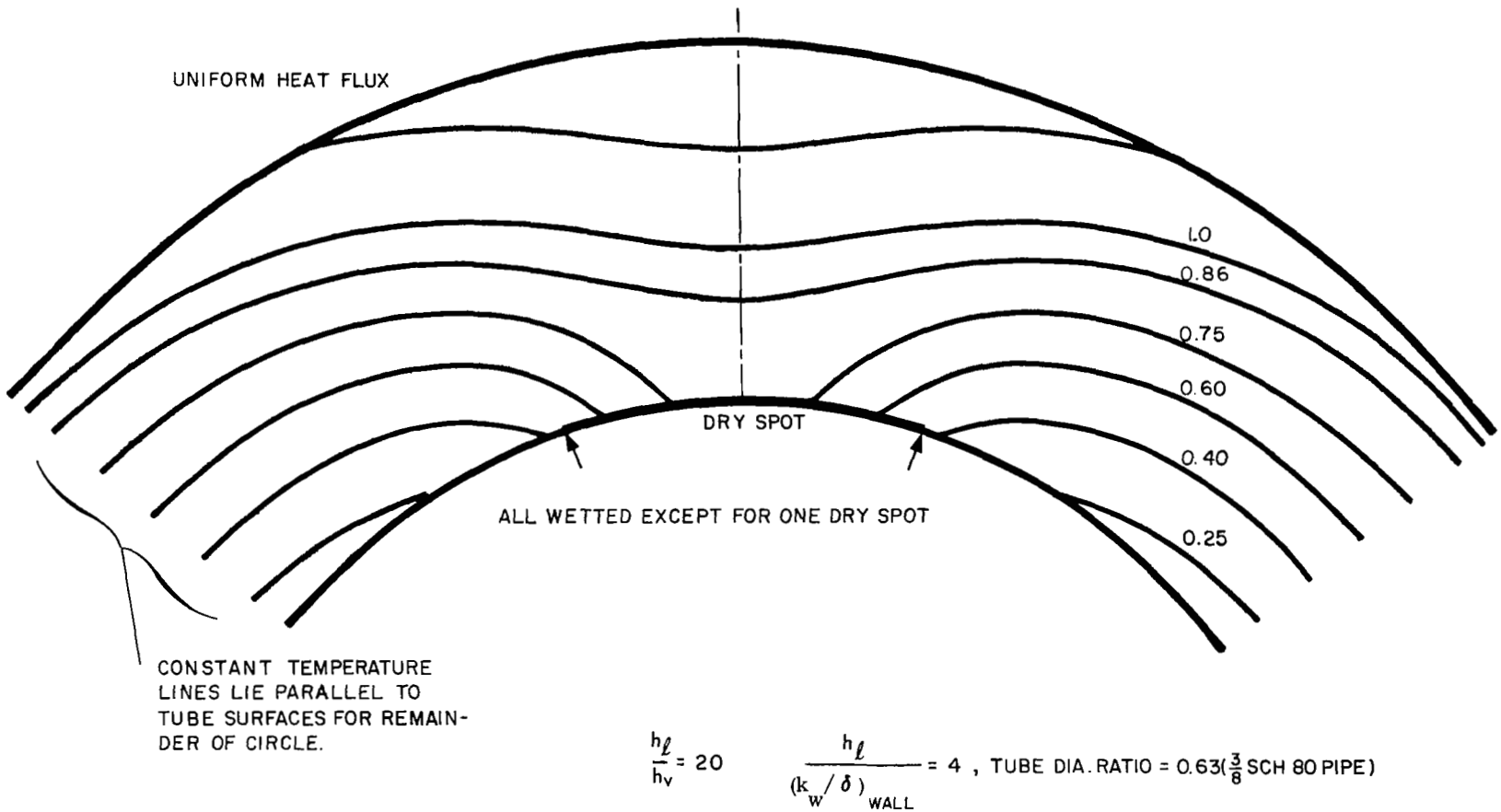

Figure 78. Isotherms in boiler tube wall.

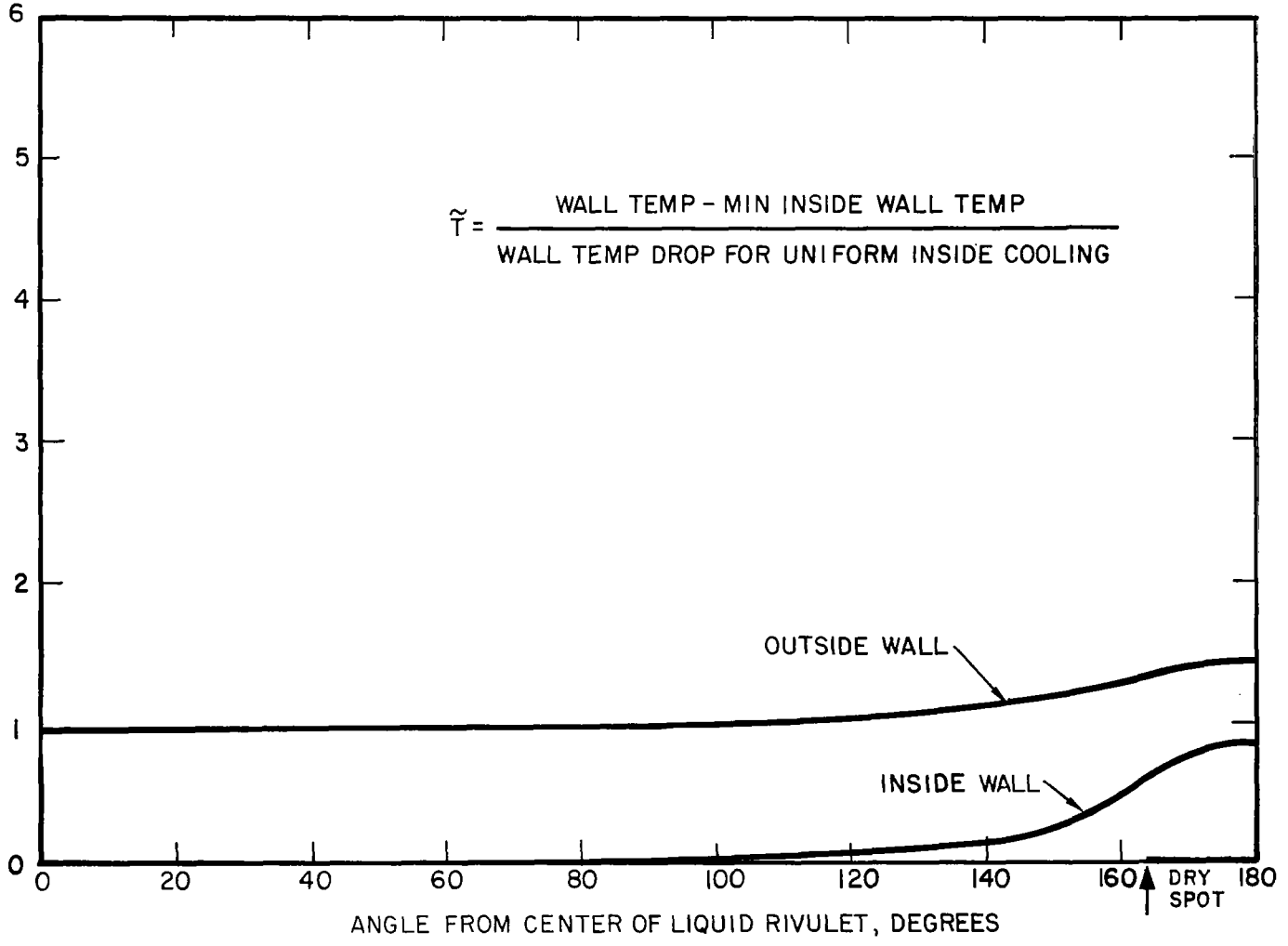

Figure 79. Boiler surface temperatures.

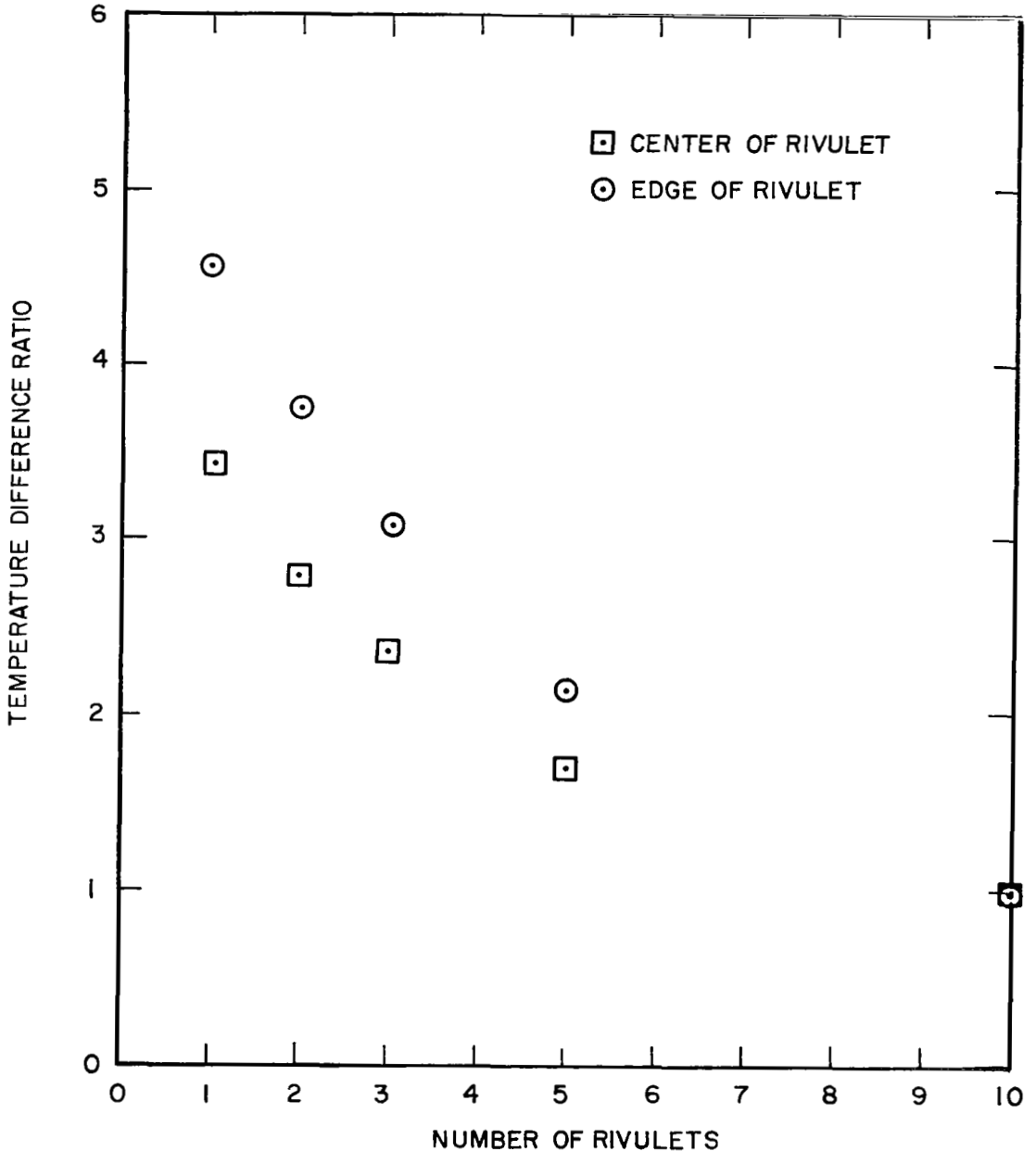

Figure 80. Local inside wall to saturated fluid temperature differences, normalized on uniform "wet wall" cooling temperature difference.

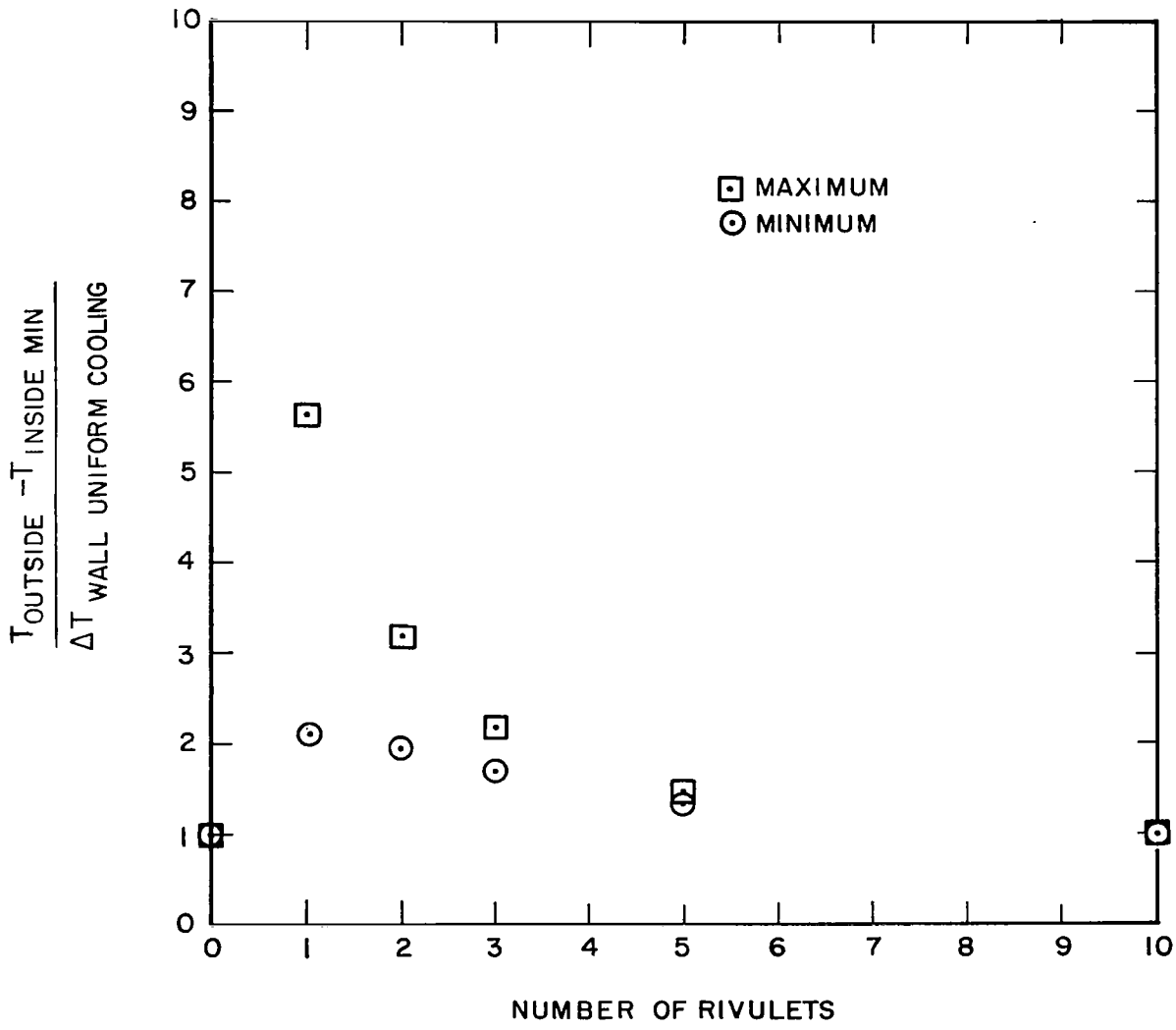

Figure 81. Outside wall temperature maxima and minima.

b) Width of Rivulets Variable

In the preceeding section surface and interior wall temperature distributions were presented for cases in which the maximum and minimum inside conductances and hypothetical rivulet width were held constant. The number of rivulets was the only variable. Since general results cannot be obtained in a problem with as many variables as are present in rivulet flow heat transfer, another specific case is presented here for comparison with the preceeding one in order to test the generality of the conclusions. In the present case, the geometry and conductances are identical to those in Section C.3.a), but the number of rivulets is held at two and the width of the rivulets is allowed to vary.

The normalized wall temperature distributions on the inside and outside surfaces are shown in Figure 82. The variation of maximum and minimum wall temperatures with amount of inside area wetted are shown in Figures 83 and 84.

In Figure 81, the number of rivulets corresponds to the percentage area covered by liquid, so that two rivulets, for example, correspond to 20% wetted area or 80% dry. Then by comparing Figures 81 and 83, it may be seen that the variations in outside wall maxima and minima are similar for the two cases, and it may be possible to generalize the conclusions to arbitrary liquid rivulet distributions.

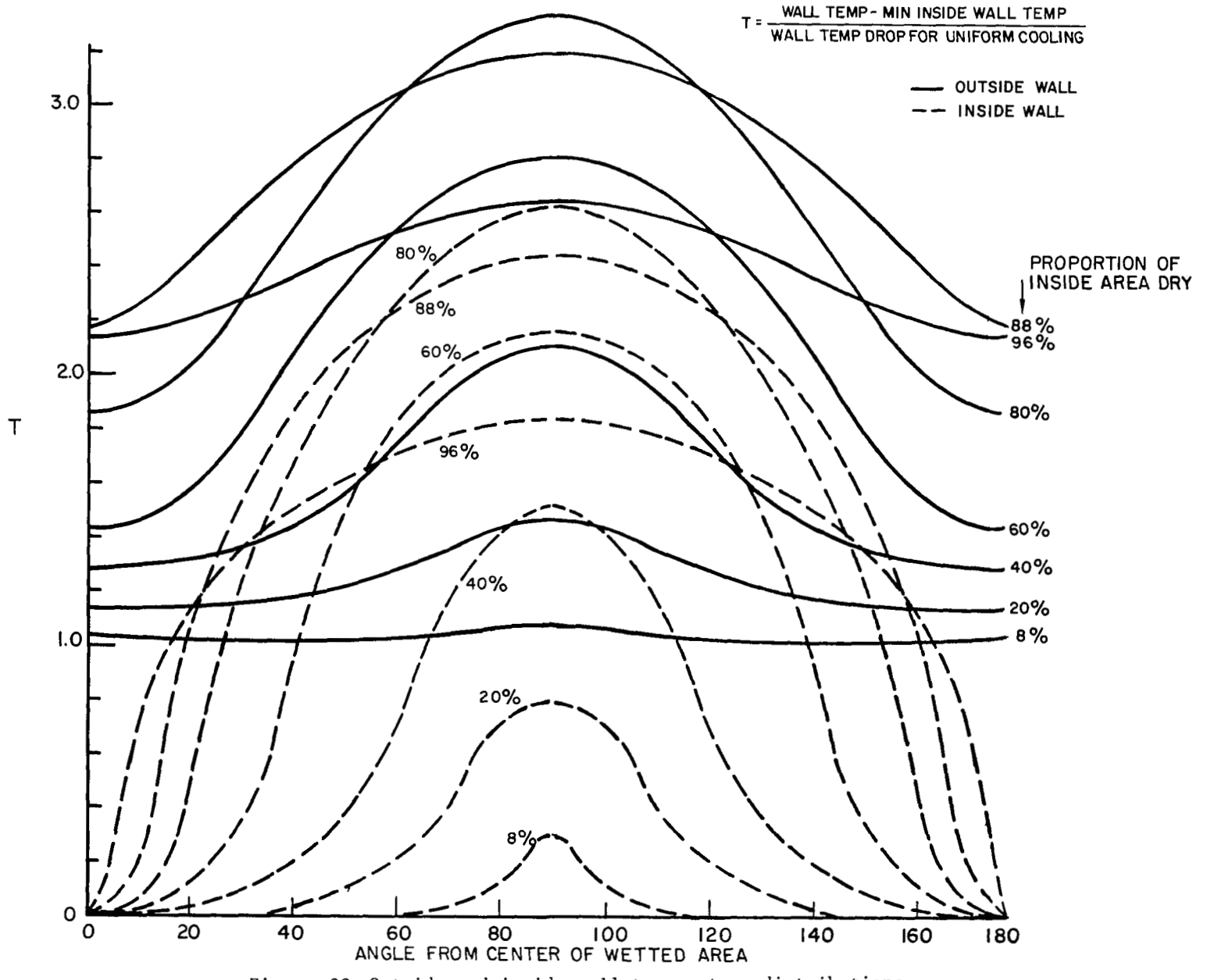

Figure 82. Outside and inside wall temperature distributions.

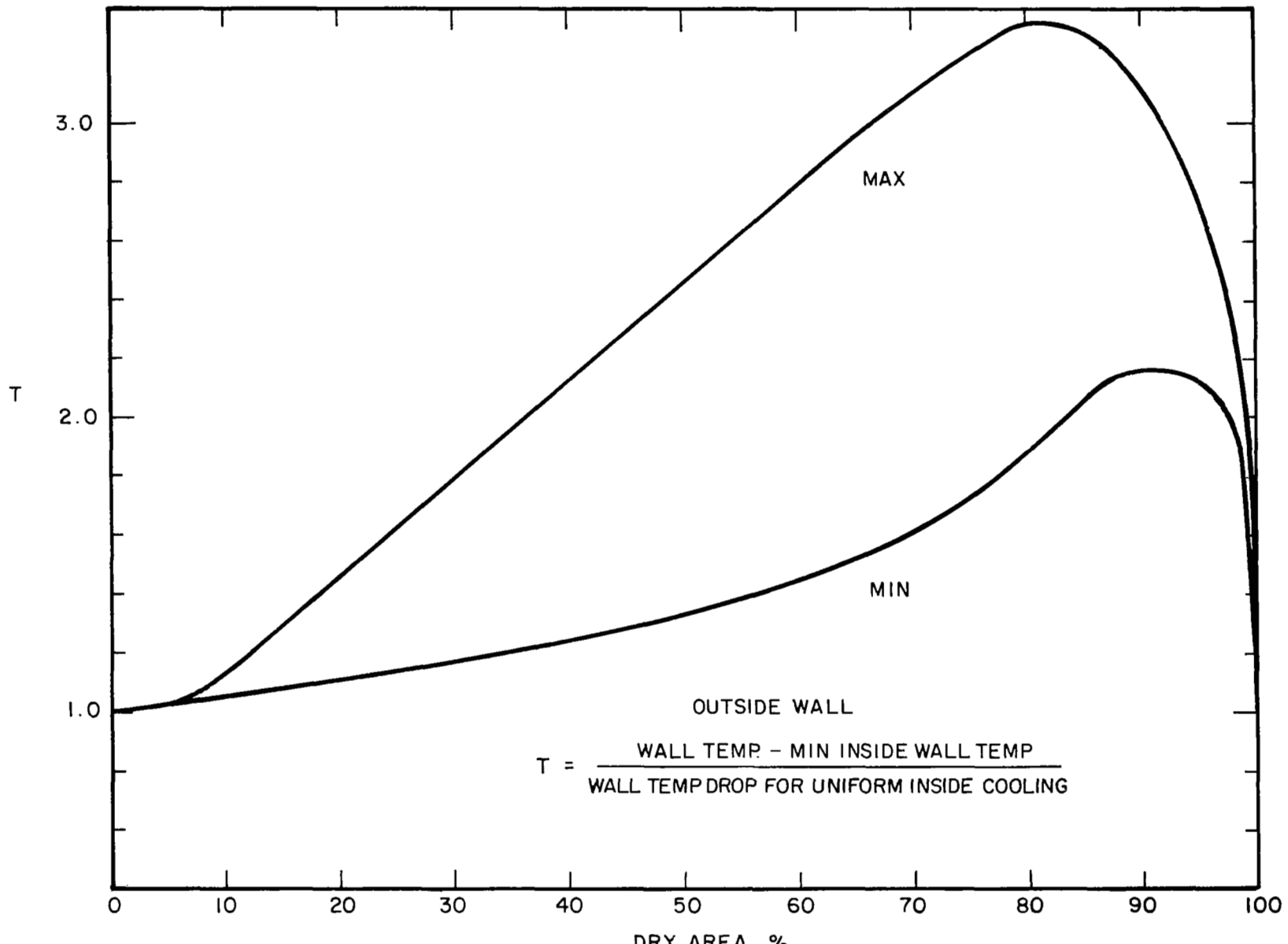

Figure 83. Outside wall maximum and minimum temperatures.

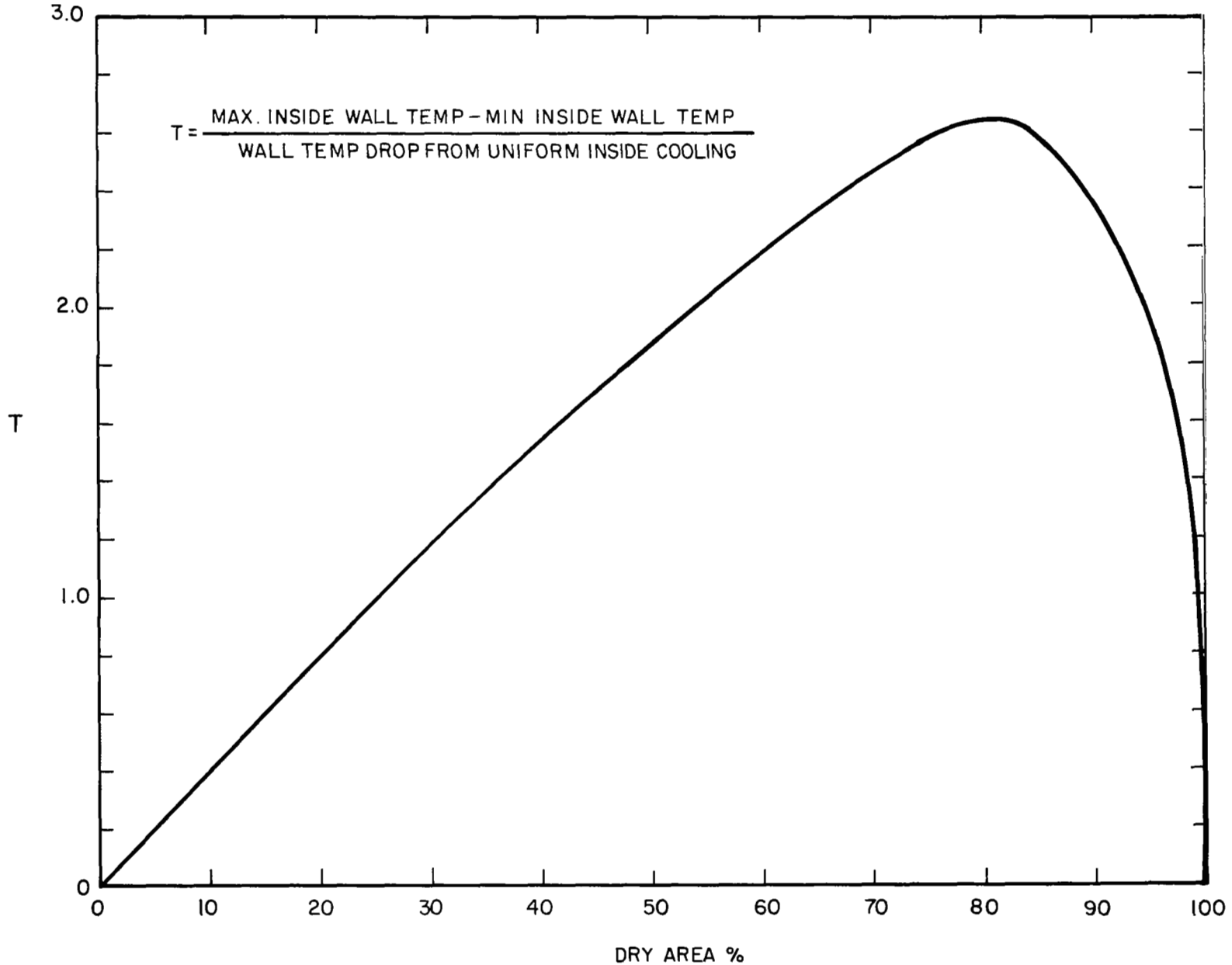

Figure 84. Inside wall maximum temperatures.

4) Apparent Heat Transfer Conductances in a Boiler Tube Containing Rivulet Flows

Heat transfer conductances measured for boiling flows are usually based on data obtained at the outside wall of the boiler tube, so that both the heat flux and wall temperature calculations for the inside wall require a correction for changes across the wall. For lack of other information, this correction is based on the assumption that the heat flow is purely radial. It has been shown in the preceeding sections that in the presence of rivulet flow, or near the termination of annular flow, large variations in heat flux distribution can occur on the inside surface even if the flux on the outside is precisely uniform. The conductances inferred are therefore incorrect and it is useful to assess the magnitude of this error.

Consider a boiler tube containing a rivulet flow and subjected to a uniform outside heat flux. The rivulets are considered to be axially uniform so that all variations are two dimensional. The conductance between the rivulet and the wall is h_ℓ, the conductance between the vapor and the wall is h_v, and the portions of the inside tube area covered by the rivulets and vapor are A_ℓ and A_v respectively. The apparent conductance on the inside wall, based on outside wall data, is

$$h_a = \frac{(q/A)_o \, (A_o/A_i)}{T_o - T_s - \Delta T_w} \tag{180}$$

where $(q/A)_o$ is the uniform outside heat flux

A_o is outside wall area

A_i is inside wall area

T_o is outside wall temperature (this varies with angular position and is assumed to be measured from a single, arbitrarily placed thermocouple)

T_s is saturation temperature

ΔT_w is wall temperature drop

For usual boiler tube geometries, ΔT_w is probably adequately determined by

$$\Delta T_w = (q/A)_o \left(\frac{2A_o}{A_i + A_o} \right) \frac{\delta}{k} \tag{181}$$

where k is the wall thermal conductivity

δ is the wall thickness

The actual mean conductance on the inner wall is

$$h_m = \frac{h_\ell A_\ell + h_v A_v}{A_i} \tag{182}$$

or, because of the known relationships between A_ℓ, A_v, and A_i

$$h_m = h_\ell - (h_\ell - h_v) \frac{A_v}{A_i} \tag{183}$$

For cases in which the rivulet conductance is much larger than the vapor conductance, this relationship reduces to

$$h_m \sim h_\ell \frac{A_\ell}{A_i}$$

The maximum and minimum possible apparent conductances have been computed from the wall temperature distributions of Section c.3.b), using Equations (180) and (181). These have been normalized using Equation (183), and are presented in Figure 85. It may be seen that the possible scatter band in the apparent conductance with this thick boiler tube is only about 40% wide and a randomly placed thermocouple would be expected to yield a conductance below the true mean value.

The maximum and minimum conductances based on the data of Section C.3.a) for constant width rivulets of varying number, are shown in Figure 86. A continuous curve is not valid for this case, but it may be seen that the maximum expected error is about the same and again the randomly placed thermocouple would usually yield a low conductance.

One would expect that scatter in mean conductance would be increased for thinner walled boilers in spite of the smaller heat conduction around the wall. For a vanishingly thin wall, where the heat flow is purely radial, the scatter in mean conductance inferred from a randomly placed thermocouple would be as large as the maximum and minimum conductances themselves.

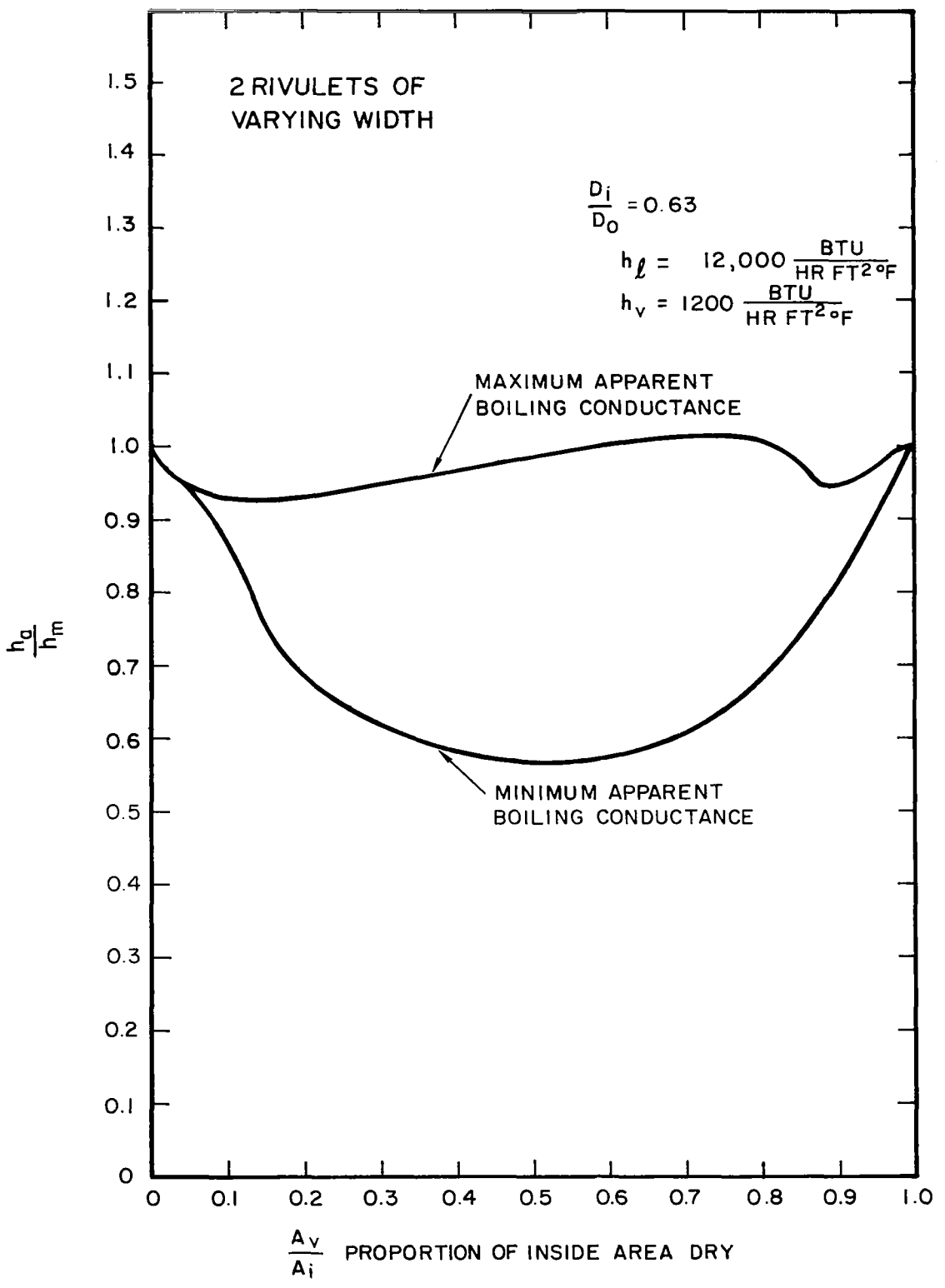

Figure 85. Error in rivulet flow boiling conductance inferred from outside wall data, columbium boiler.

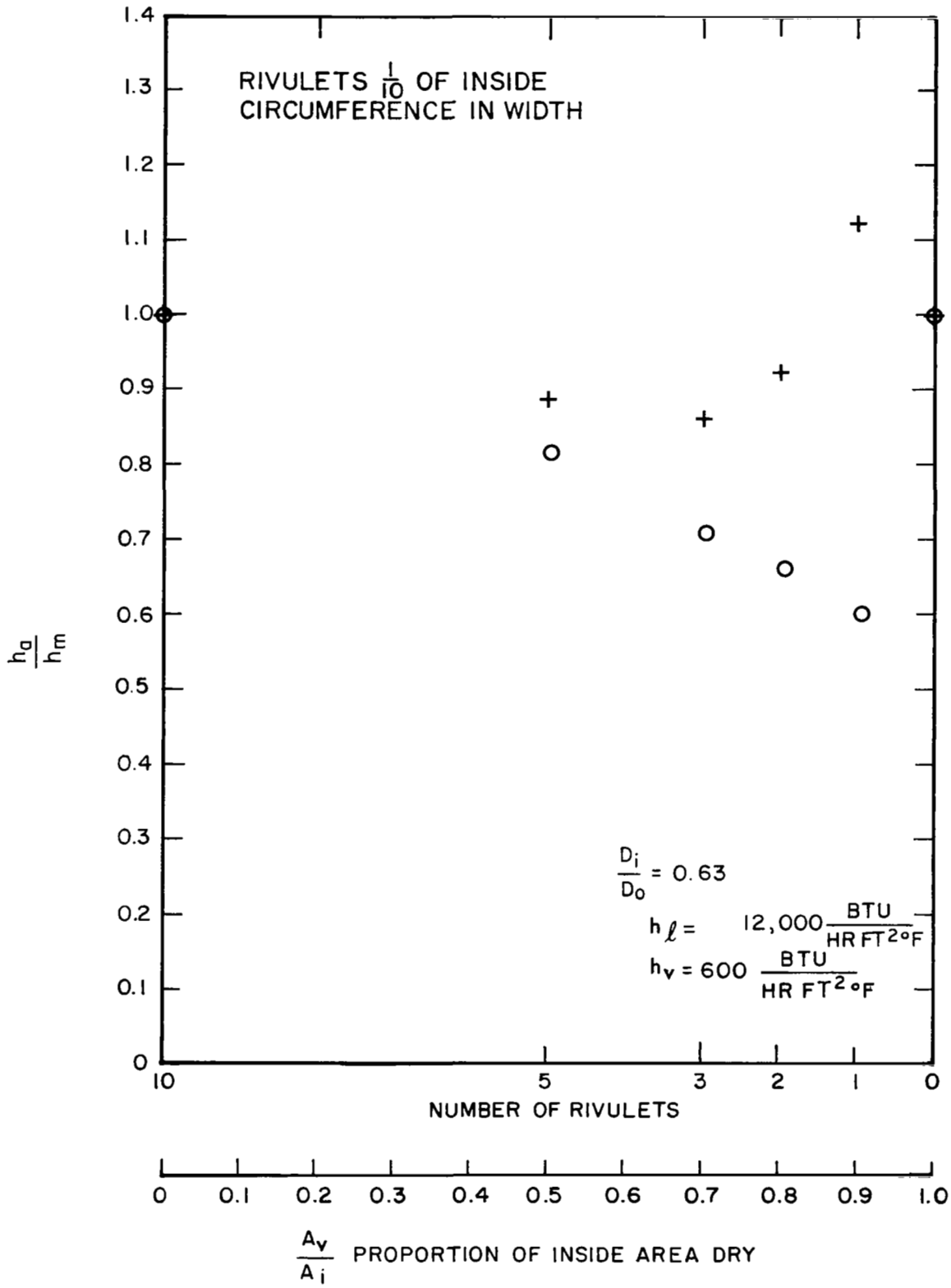

Figure 86. Error in rivulet flow boiling conductance inferred from outside wall data, columbium boiler.

E. Mechanisms of Heat Transfer Regime Change

Analyses and experimental data are available for prediction of heat transfer in many of the flow regimes known to exist in forced convection boilers. It is not always clear however, which of the many possible flow patterns will occur at a given point in a boiler. The analyses in this section have been worked out in order to provide some information about which flow regime might be expected under a given set of circumstances.

1) Hydrodynamics of Linear Wetting Flow Boiling "Burnout"

The term "burnout", as it is usually used in reference to forced convection boiling of wetting fluids in vertical linear flow systems, is assumed by most workers to coincide with the end of the annular liquid film. Observations made with Freon 11 in a glass test section at Geoscience Limited (Reference 14) support this interpretation of "burnout". These observations, taken under uniform heat flux conditions, demonstrate a very large and discontinuous decrease in heat transfer conductance at an axial location which coincides with the termination of the annular film. The "burnout heat flux" data obtained from these experiments coincide with the experimental critical heat flux data reported by Kirby (Reference 12) for Freon 12. These latter data are reproduced in Figure 87. One may conclude that in Kirby's data, which were taken in an opaque test section, the "burnout quality" coincides

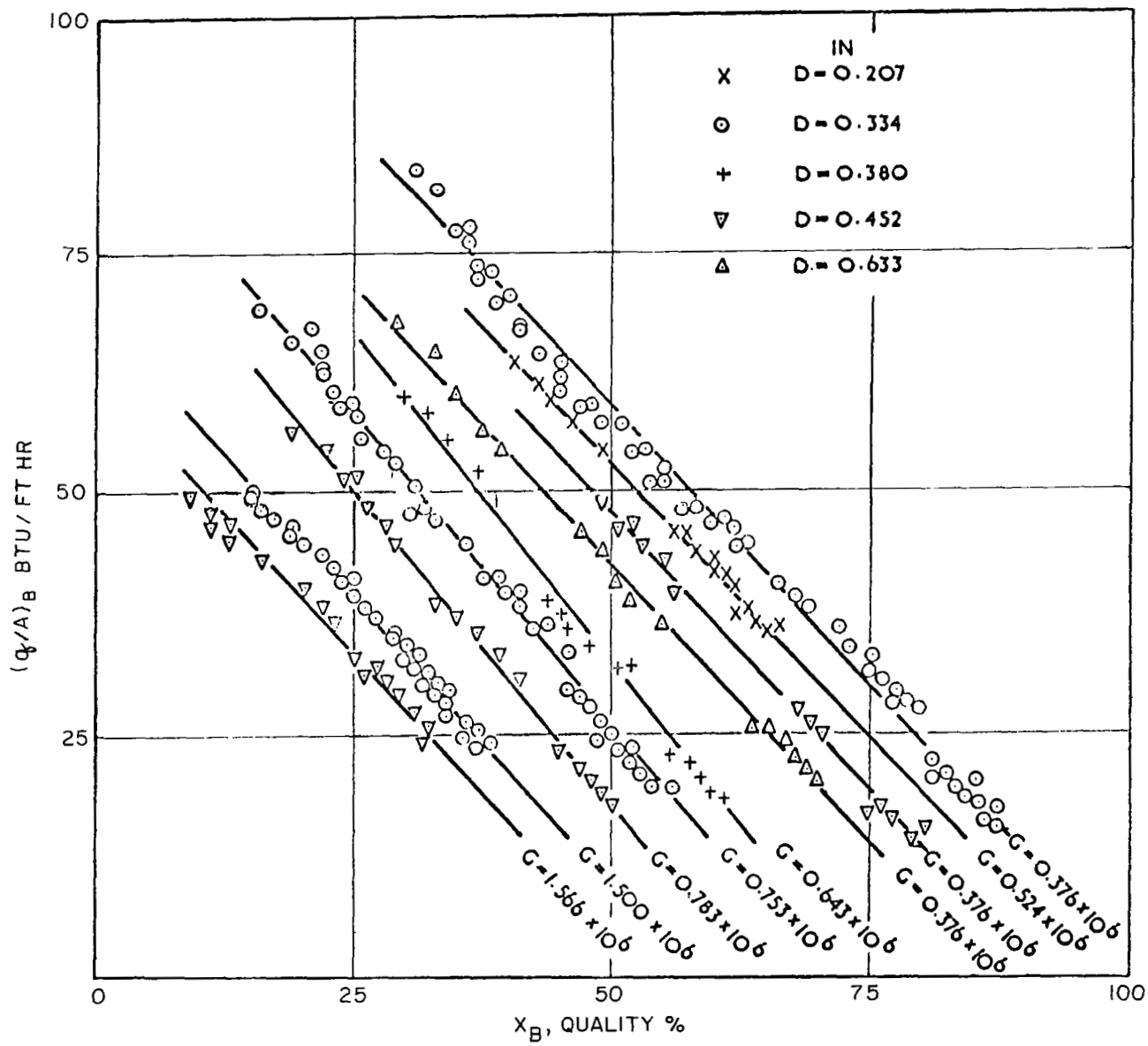

Figure 87. Freon 12 linear flow "burnout" data. (From Reference 12)

with the downstream termination of the liquid film.

As has been pointed out by Kirby, the rate of change of the liquid flow in the film is determined by a mass balance between the liquid evaporated, the entrained liquid deposited from the vapor flow, and the film liquid entrained into the vapor flow. The liquid entrained from the film is usually supposed to be removed from the film by two mechanisms; namely stripping of liquid from wave peaks, and ejection of liquid by breaking of bubbles generated in the film due to boiling. If such a picture of the annular film is actually true, then the mechanisms controlling the flow rate in the annular film are largely hydrodynamic. One might expect that the liquid film flow rate at any point in the boiler is determined by the processes occurring upstream; the rate of deposition, the rate of entrainment, the rate of change of vapor velocity all contribute to the liquid film flow. One might also expect that there are many different combinations of processes which would give virtually the same liquid flow rate at a particular point.

The annular film is very thin near its end so that bubble nucleation and wave motion are probably both suppressed. If such is the case, then the principal mass fluxes in and out of the annular film near its termination are due to evaporation and deposition. When the end of the annular film occurs at a quality less than one, the remainder of the liquid must certainly be entrained in the vapor flow. Due to diffusion, the fine droplets in the vapor eventually settle out on the walls and evaporate. The longer is the boiler, the smaller the entrained flow at the end will be. This deposition of entrained liquid from the vapor flow onto the walls would not be expected to be greatly affected by the presence of a thin liquid film on the wall, so that the deposition process may be considered without regard to the presence of a liquid film.

In a uniform heat flux boiler, length, quality, and heat flux bear a simple relationship to each other, namely

$$X = \frac{\left(\frac{q}{A}\right)\pi D \ell}{W_t L} \tag{184}$$

It is clear that for a fixed flow rate, a low heat flux boiler is a long boiler. If entrainment rates are not too high, a long boiler has proportionately less entrained liquid at a given quality, and one would expect that the end of the annular film would occur at higher quality for a low flux (long) boiler than for a high flux (short) boiler.

Some conclusions may be drawn concerning the nature of "burnout heat flux" experimental determinations in linear flow. One is that variations upon the conventional straight, vertical, continuously-heated tube geometry may be expected to change the deposition and entrainment rates. These variations will therefore change the resulting "critical" heat flux. Thus a curved, or unheated section in the two phase region would be expected to decrease the amount of entrained fluid, thicken the film, modify the entrainment rate, and change the quality at which the end of the annular film occurs. Another conclusion is that regardless of tube diameter, liquid flow rate, or other conditions, the end of the annular film will occur at $X = 1$ for vanishingly small heat flux.

Some of the observations made above may seem rather obvious. However, they are appropriate to use as a guide for the interpretation of "burnout" data. For example, the plot of Figure 87, showing Freon 12 burnout data, indicates a linear relationship between $(q/A)_B$ and X_B over a wide range of test conditions. From the physical arguments just given, it may be concluded that all of the data lines must pass through the point $(q/A)_B = 0, X_B = 1$. Since this is the case, only one of the lines in Figure 87 can be straight at substantially lower flux than the data cover. All of the remainder must curve at low heat flux. Since this is the case, extrapolation of these data to lower fluxes

than the range of the data is completely unwarranted. The data of Figure 87, plotted on semi-logarithmic coordinates, are shown in Figure 88. It is clearer in this plot that the data do tend toward zero heat flux at X = 1. The solid lines indicate the actual range of the data. The dotted lines indicate where one might expect data taken over a wider range of heat fluxes to lie. These same data have been replotted as functions of length by use of Equation (184), and are presented in Figure 89. In this figure it may be seen that the boiler length required to maintain the annular film at high quality increases rapidly for high mass flow rates.

One of the unexpected aspects of these burnout data is the amount of liquid entrained in the vapor flow at high mass flow rates. As stated earlier, all of the remaining liquid is entrained at the end of the film. Thus, the entrained liquid plot of Figure 90 has been constructed from the data of Figure 89 by use of the relationship

$$\frac{W_e}{W_t} = 1-X_B \tag{185}$$

where W_e is the entrained liquid flow rate and W_t is the total flow. From Figure 90 it can be seen that for high flows and fluxes as much as 90% of the flow can be entrained. When studying these data, it is well to keep in mind that these graphs of entrained liquid do not represent variation of entrainment with length in a single boiler at a given condition, but represent instead the entrainment at the end of the annular film in tubes of fixed diameter and flow rate but of many different lengths (heat fluxes).

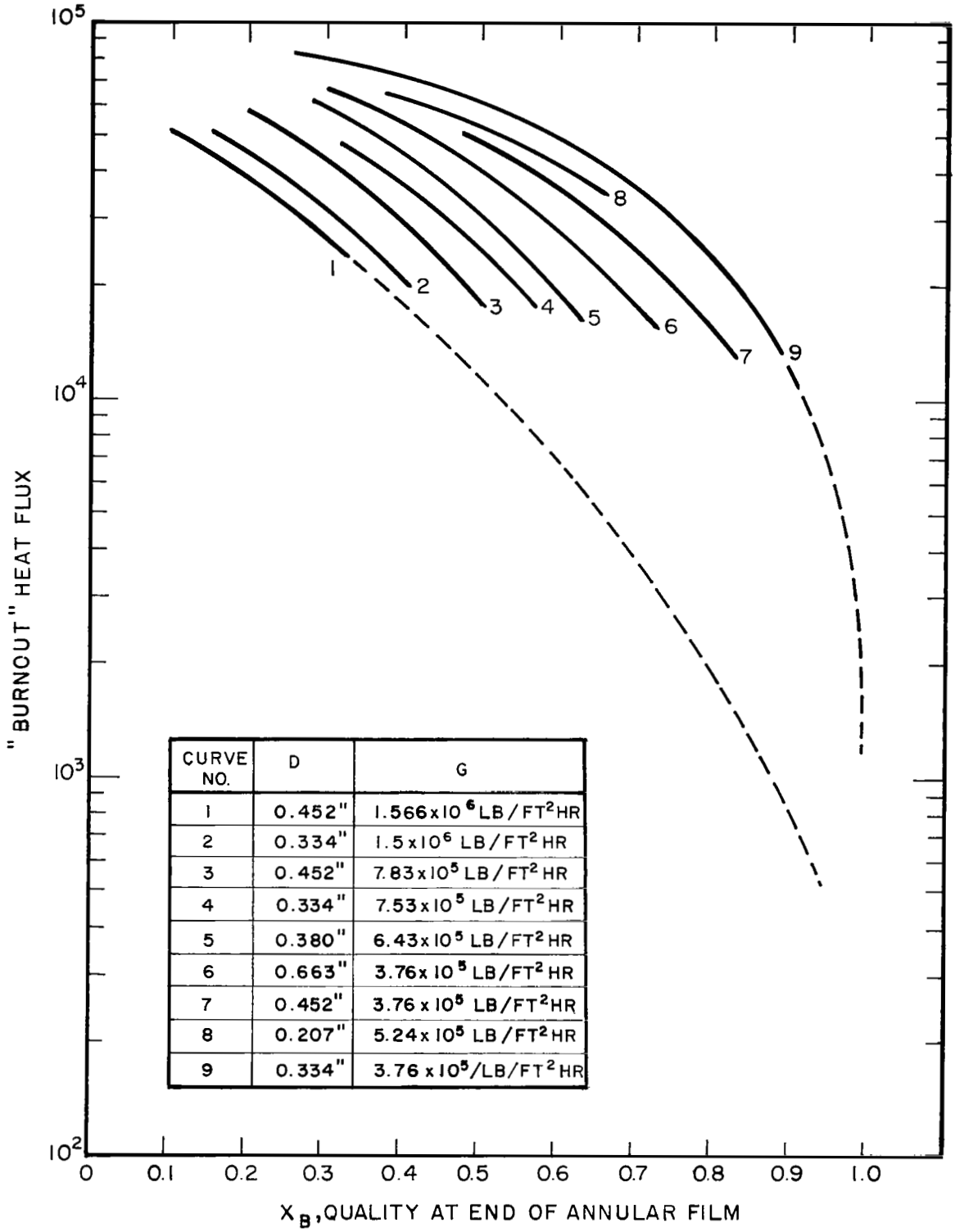

CURVE NO.	D	G
1	0.452"	1.566×10^6 LB/FT^{2}HR
2	0.334"	1.5×10^6 LB/FT^{2}HR
3	0.452"	7.83×10^5 LB/FT^{2}HR
4	0.334"	7.53×10^5 LB/FT^{2}HR
5	0.380"	6.43×10^5 LB/FT^{2}HR
6	0.663"	3.76×10^5 LB/FT^{2}HR
7	0.452"	3.76×10^5 LB/FT^{2}HR
8	0.207"	5.24×10^5 LB/FT^{2}HR
9	0.334"	3.76×10^5/LB/FT^{2}HR

Figure 88. Freon 12 linear flow "burnout" data. (From Reference 12)

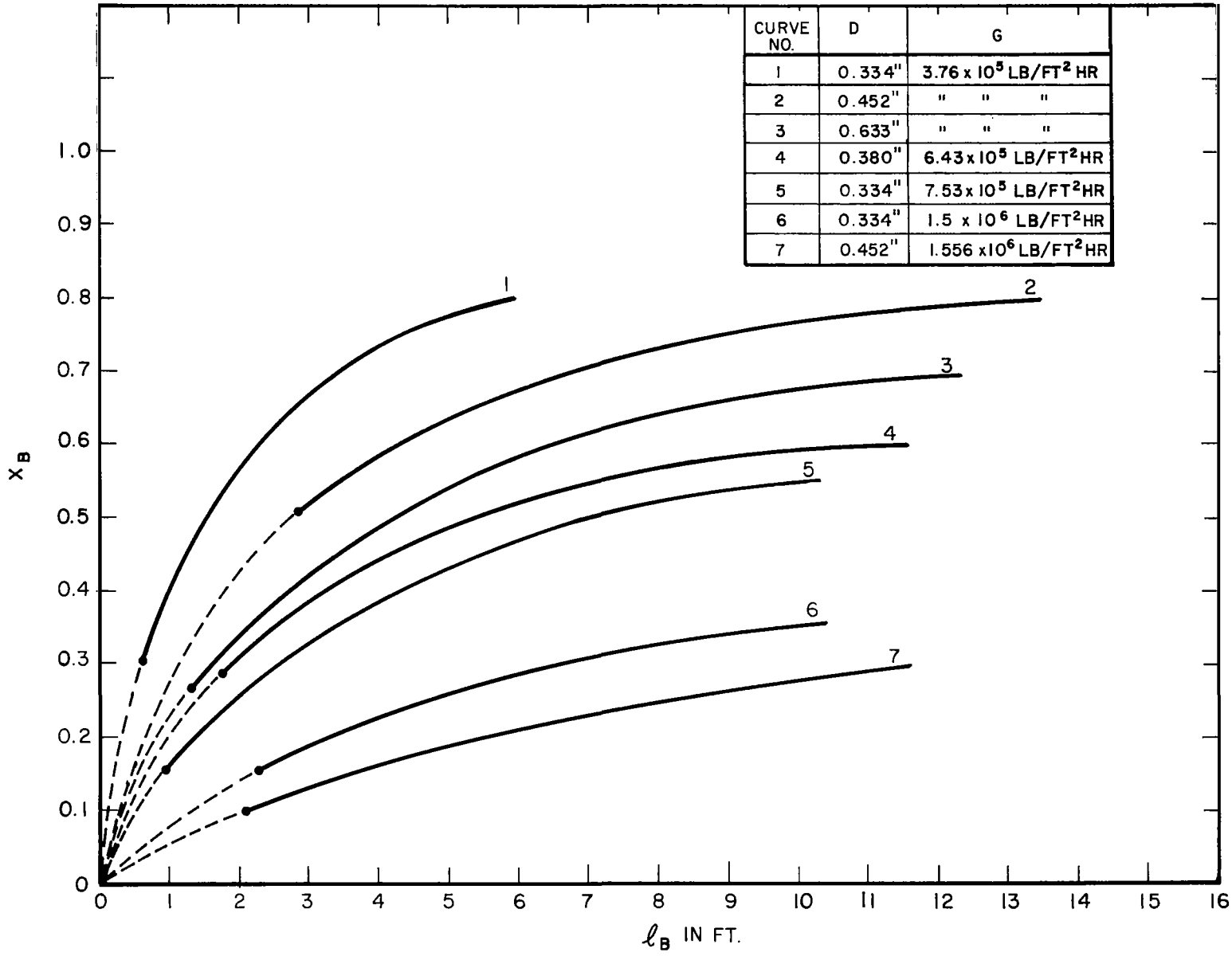

Figure 89. Freon 12 linear flow "burnout" data. (From Reference 12)

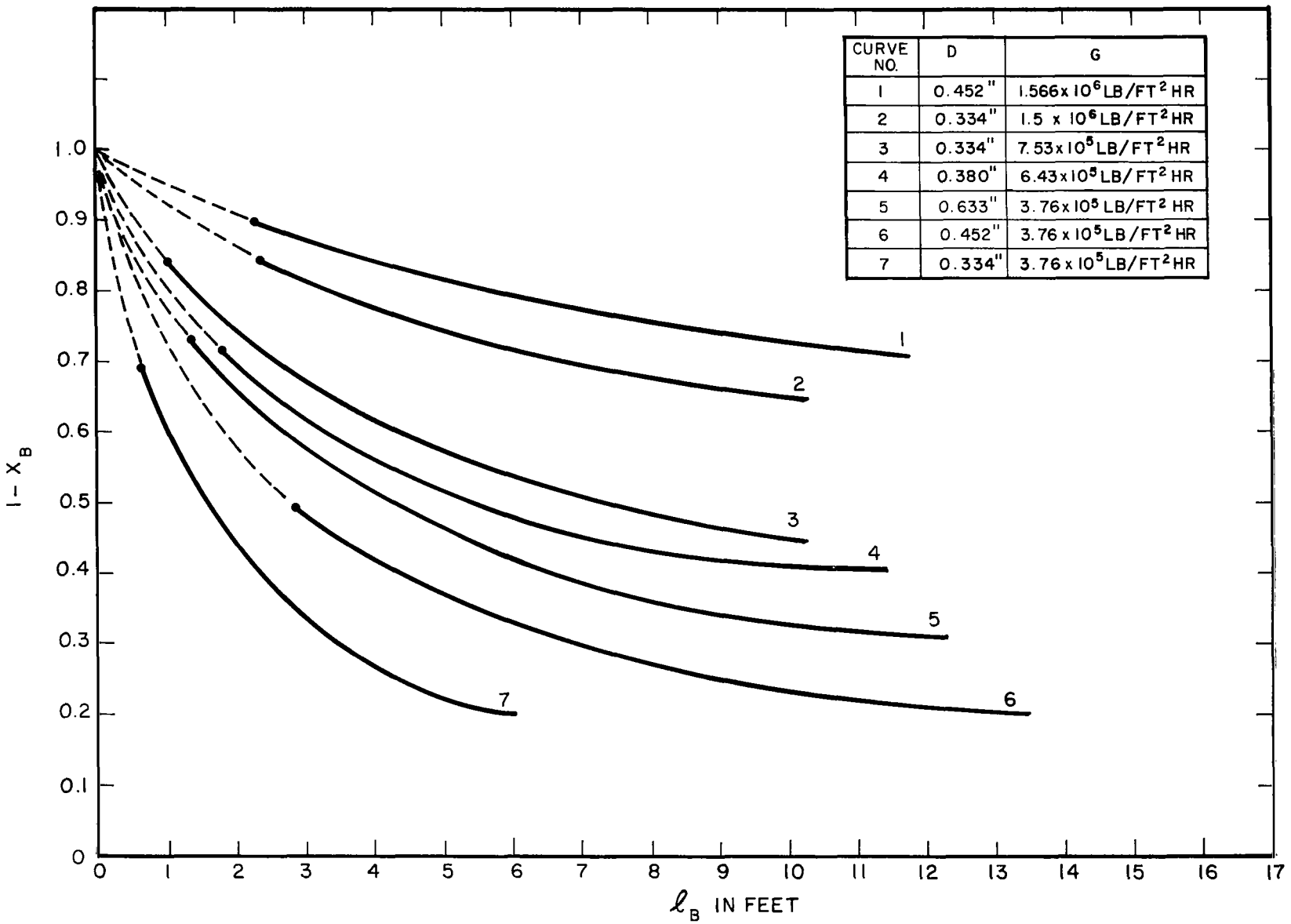

Figure 90. Entrained liquid at end of annular film - Freon 12.

2. A Criterion for the Onset of Nucleate Boiling in a Forced Convection System With an Annular Liquid Film

The phenomenon of nucleate boiling in conventional pool boiling systems is usually attributed to minute cavities with residual gas trapped inside. These minute cavities form the visible nucleation sites which are the source of vapor bubbles in the pool. Water usually boils in metal containers with only a degree or two of superheat at the wall. However, it has the ability to superheat in the liquid phase to almost 150°F above the saturation temperature if carefully degassed and heated in a system which has been evacuated to remove the trapped gas from the cavities in the heated surface. In contrast to metal, glass usually has few cavities in the surface which can act as nucleation sites. Boiling chips, which contain many microscopic cavities, are frequently added to glass boiling systems to reduce liquid superheating with its accompanying violent change of phase.

Consider the boiling process in a forced convection system containing an annular film. If nucleate boiling does not occur then heat which is added to the annular film at the wall must be conducted across the liquid layer so that vaporization occurs on the inner surface at the interface between the liquid and the vapor. Since this interface must be at or above the local saturation temperature, the liquid in contact with the heated wall must be superheated. One would expect that in the absence of nucleation sites, the onset of nucleate boiling would be dependent upon the maximum superheat temperature which the fluid can sustain without changing phase. In the forced convection experiments of Reference 18, Freon 22 was vaporized in three tubes of identical geometry and under very nearly identical conditions, except that two of the test sections were metal and the third was glass. The glass test section was heated by electrical conduction through a transparent metal film on the inside and was used for flow visualization. Some of the data from these experiments are reproduced in Figures 91 and 92. Clearly in these data the glass has a much lower boiling heat transfer conductance than the two metal tubes. Since this difference must be related to the surface material, it is a plausible conclusion that the difference is in the availability of nucleation sites in the metal and their absence in the glass test section. Since the glass test section by hypothesis does not have as many nucleation sites as the metal tube, more superheat of the liquid at the wall would be required to bring on vapor generation in the liquid bulk.

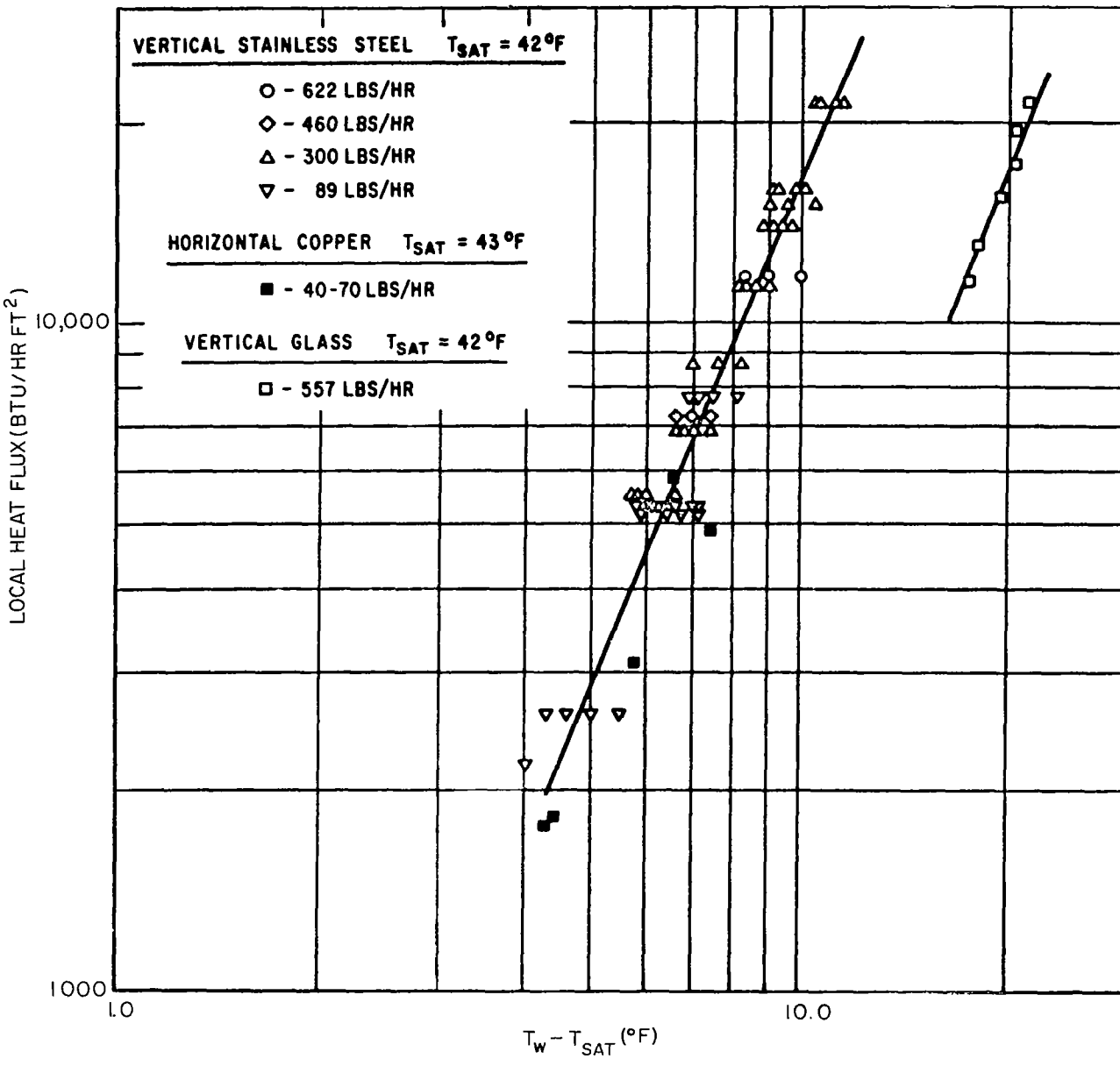

Figure 91. (Reproduced from Figure 8, Reference[18]) Heat transfer data for refrigerant -22 at a reduced pressure of 0.12. Range of vapor qualities from 0.01 to 0.60.

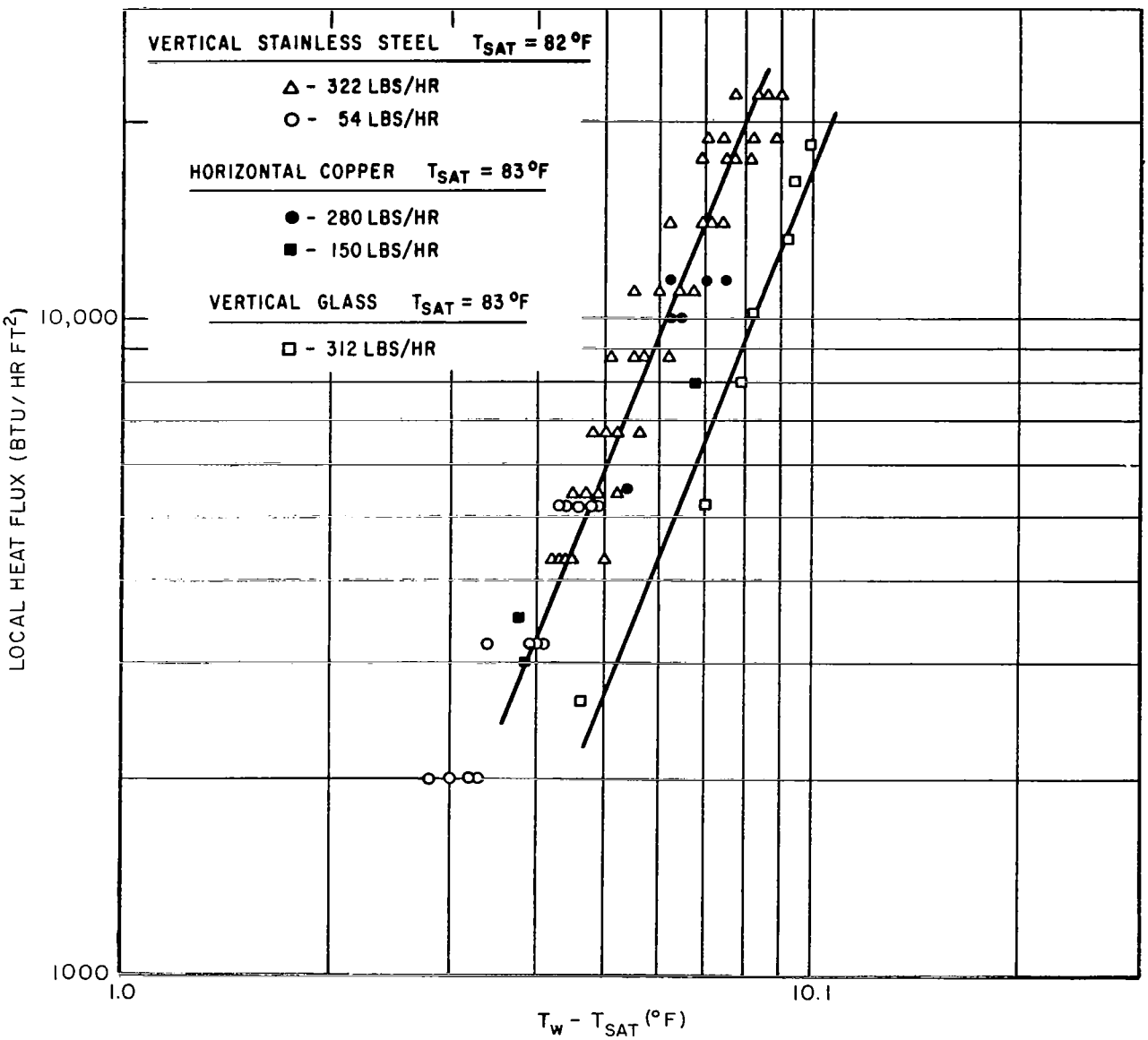

Figure 92. (Reproduced from Figure 9. Reference [18]) Heat transfer data for refrigerent -22 at a reduced pressure of 0.22. Range of vapor qualities from 0.01 to 0.60.

they are charged with the working fluid. This procedure is in contrast to that used in conventional fluid systems. The evacuation is required in order to prevent chemical reactions or oxidation of the working fluid. Since the removal of inert or noncondensible gases from the system by evacuation may destroy the effectiveness of small surface cavities as nucleation sites, one would expect that superheating of the liquid metal would occur readily in liquid metal systems. Many workers have reported and described this phenomenon.

In the complete absence of nucleation sites it is possible to estimate the amount of superheat required to bring on the formation of vapor cavities in the liquid. Predictions have been made for water, potassium, and sodium in Reference 19. These results are reproduced in Figure 93. In the absence of nucleate boiling, (which acts as a volume heat sink within the liquid film), all of the heat added to the annular film at the wall must be conducted or convected across the liquid layer to vaporize fluid at the inner surface. Since the liquid metals have very high thermal conductivity, convection may be neglected and the temperature drop across the liquid layer computed on the basis of conduction alone. With this simple model, graphs for the minimum heat flux required to bring on nucleate boiling have been computed for potassium and Freon 12 and are shown in Figures 94 and 95 assuming that the interface between liquid layer and vapor core is at the saturation temperature. The curve for Freon is, of course, hypothetical since with its low thermal conductivity turbulent convection in the liquid layer certainly predominates.

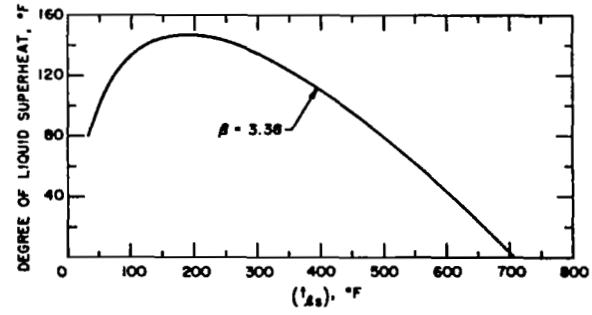

(a.) WATER

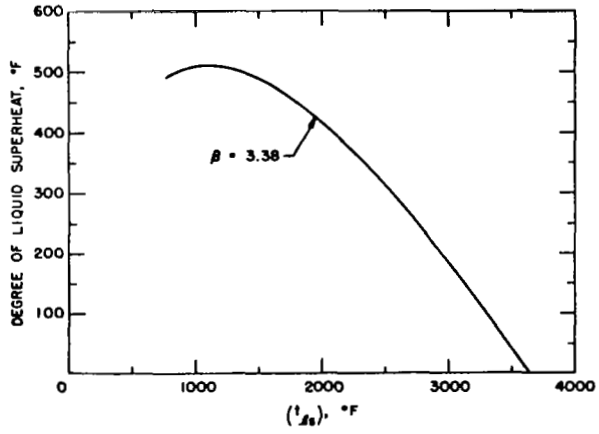

(b.) SODIUM

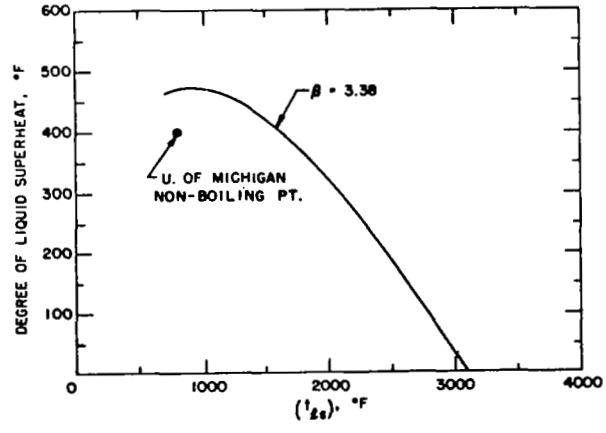

(c.) POTASSIUM

Figure 93. Liquid superheat predictions from Reference 19)

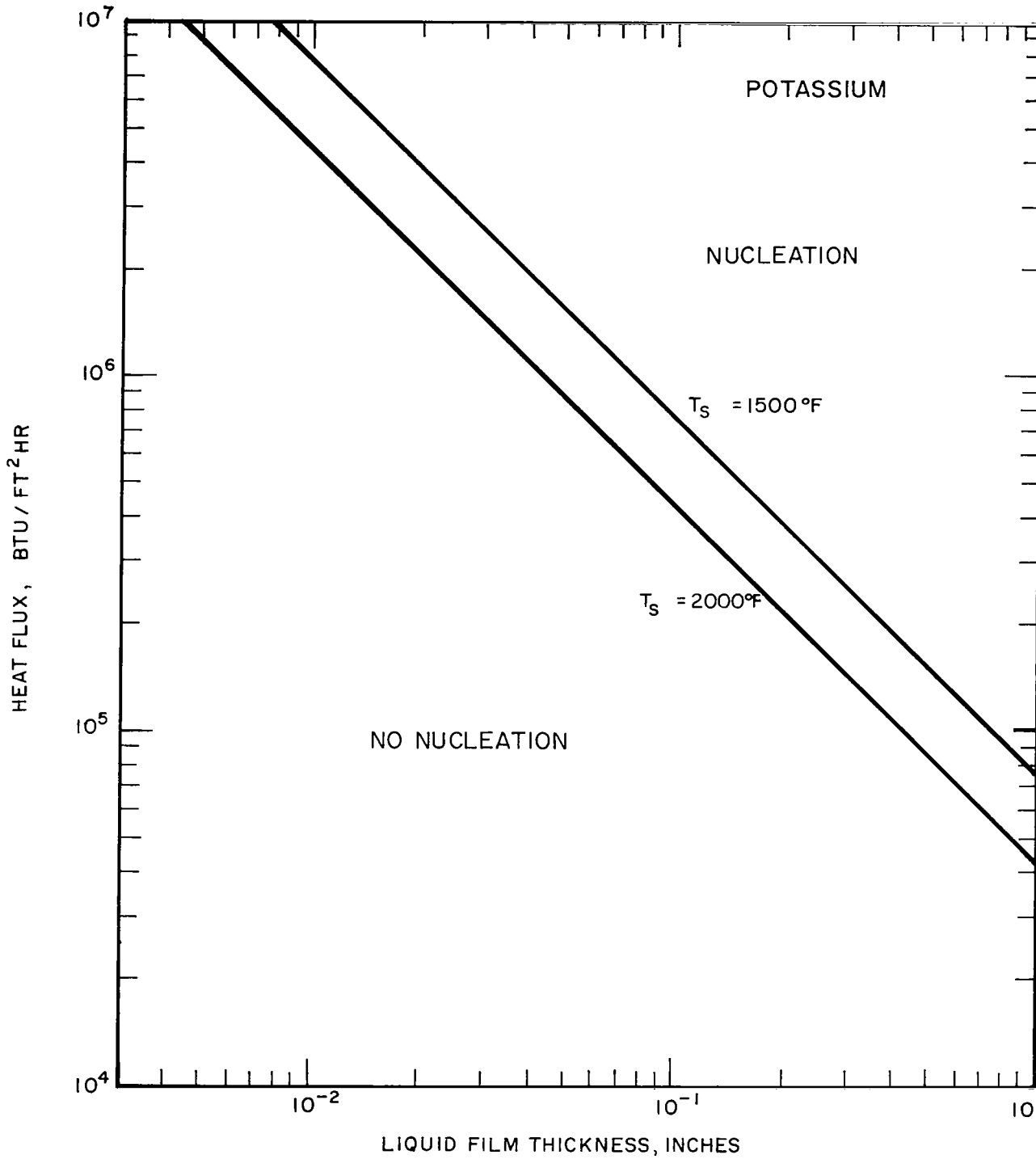

Figure 94. Heat flux required to initiate nucleate boiling in an annular flow without nucleation sites.

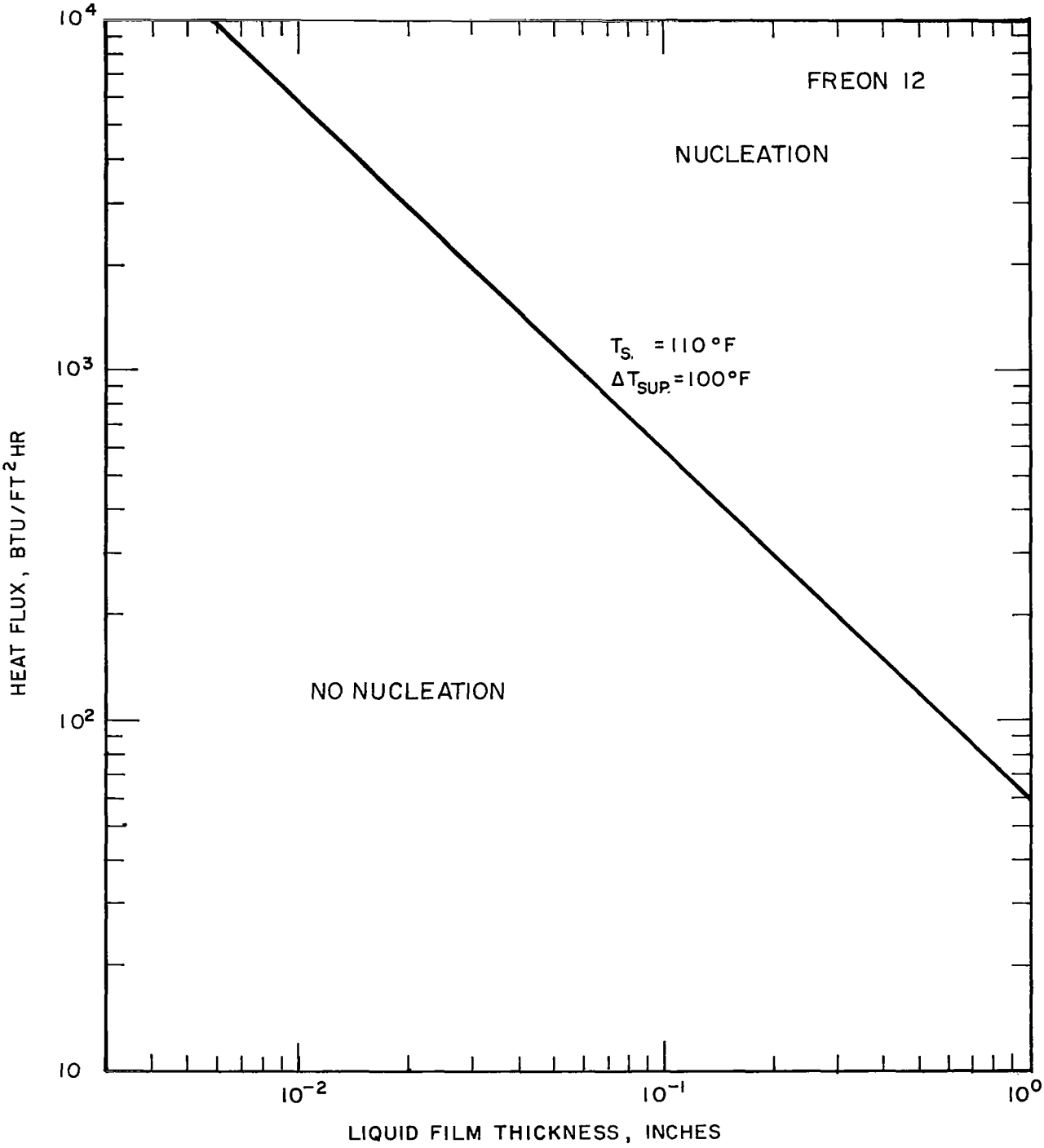

Figure 95. Heat flux required to initiate nucleate boiling in an annular flow without nucleation sites.

3. Criteria for the Rupture of a Liquid Film on a Boiler Tube Surface

It can be shown analytically and experimentally that there are significant differences between surface vaporization or wetted wall boiling, film boiling droplet or rivulet flow and linear slug flow boiling[14]. A major question that arises is, which of these modes of boiling heat transfer is in operation for a given set of parameters. One approach to this difficult area is to review a number of possible criteria that assist in defining conditions under which a liquid film that is in complete contact in a boiler tube (under surface vaporization conditions) ruptures. A number of obvious criteria are listed below and discussed briefly.

Consider a perfectly smooth boiler tube surface upon which a liquid is vaporizing. It is postulated that the liquid is in direct contact with the surface and the boiling consists of surface vaporization or some volume boiling but no film boiling. If the contact angle between the liquid and the wall is zero degrees, then hypothetically, there will be a complete annular liquid film at the wall from qualities ranging from zero to 100 percent. If the contact angle (which is defined by the liquid-vapor, solid-vapor, solid-liquid surface forces) is greater than zero, the width of a liquid rivulet for that particular profile area defined by the contact angle and vapor quality must be compared to the inner circumference of the boiler tube. If the rivulet width is greater than the tube circumference then the liquid film would not rupture. If the rivulet width is less than the tube circumference, then the liquid film would be separated.

Consider a rough boiler tube surface on which a liquid is vaporizing. Several possible processes can probably occur. For example, if the heights of the surface asperities are greater than the thickness of the liquid film, the contact area of the liquid film will be reduced. If the surface roughness is due to non-homogeneous structure such as oxide deposits or large metallic grains, changes in local contact angles can also cause local rupture of the liquid film, hence, reducing the contact area. Finally, as a result of surface pits or local areas of non-wetting, film boiling can occur at such points resulting in reduced superheat temperature differences at which surface vaporization ends and transition boiling begins. This change in boiling heat transfer mode is associated with a rupture of the liquid film.

4. Critical Contact Angle at Film Rupture

If a complete liquid annulus exists at a boiler tube wall and the liquid is in direct contact with it, the boiling conductance is high and increases with vapor quality. The heat transfer process involved is surface vaporization at the liquid-vapor interface or volume boiling. The important question of whether the liquid annulus is complete or not can hypothetically be answered by comparing the width of an axial rivulet relative to the boiler tube perimeter. Further, the fraction of the boiler tube area covered with the direct-contact rivulet and the corresponding heat transfer are dependent upon the rivulet contact angle (defined by the liquid-vapor, solid-vapor and solid-liquid surface forces) and the vapor quality.

Consider a liquid axial rivulet in a boiler tube. As the contact angle is decreased for a given liquid cross sectional area, the rivulet width increases and finally attains a value equal to the inner perimeter of the boiler tube. At this point the two edges of the rivulet meet and a complete liquid annulus is generated. The particular contact angle under this condition can be called the critical rupture angle (i.e., if the angle is increased slightly, a hydrodynamic or surface disturbance could cause the annular film to rupture). The critical angle can be calculated in the following way. It is postulated that the rivulet profiles are controlled only by surface tension forces (all gravitational forces are presumed to be small). Consequently, the rivulet cross sections are circular in shape. A second approximation involves the cross sectional area of a rivulet. It is postulated that the rivulet cross sectional area is the same as the value for a complete liquid annulus. From a previous Geoscience study, a liquid annulus boiling model has been developed that relates liquid film thickness at the boiler tube wall (or cross sectional area) and the heat transfer conductance to vapor quality[14]; the results of that work are used in the present study.

Consider the idealized rivulet system in Figure 96. The width of the rivulet at the critical contact angle is equal to the perimeter of the boiler tube,

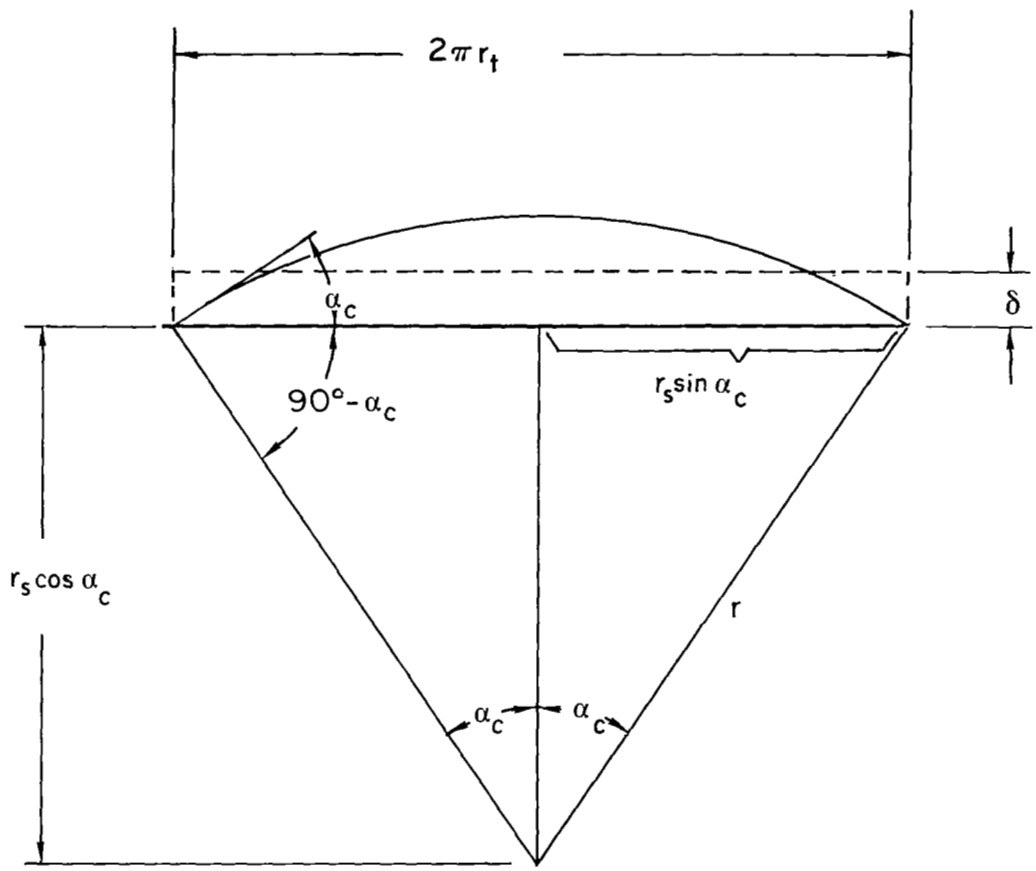

Figure 96. Geometrical parameters for the case of annular film rupture.

$$2r_s \sin \alpha_c = 2\pi r_t \tag{186}$$

where

r_s radius of curvature of rivulet surface

α_c, critical contact angle at film rupture

r_t, inside radius of the boiler tube.

The rivulet cross sectional area is,

$$\pi r_s^2 \frac{2\alpha_c}{2\pi} - \frac{1}{2}(2r_s \sin \alpha_c \; r_s \cos \alpha_c) = 2\pi r_t \delta \tag{187}$$

where δ is the thickness of the annular liquid film (a contact angle of zero or complete wetting). The solution of the two algebraic Equations (186) and (187) two unknowns (α_c and r) yields a relation for the critical contact angle,

$$\frac{2\delta}{\pi r_t} (\sin \alpha_c)^2 = (\alpha_c - \frac{1}{2} \sin 2\alpha_c) \tag{188}$$

A calculation of the critical contact angle, based on this model and on the annular flow analysis of Reference 14, is presented at the end of the next section (page 213).

5. Rivulet Widths (Portion of Boiler Wall Covered by a Direct Contact Rivulet)

Consider the case where the rivulet contact angle lies in the region $\alpha_c \leq \alpha < 90°$ (see Figure 97). If, as in the preceeding section, it is postulated that the liquid rivulet cross sectional area is equivalent to the cross sectional area for the case of complete wetting (annular liquid film) at a specific vapor quality,

$$\pi r_s^2 \frac{2\alpha}{2\pi} - \frac{1}{2}(2r_s \sin\alpha \; r_s \cos\alpha) = 2\pi r_t \delta \tag{189}$$

where r_s is the unknown and α is known for a given liquid, surface and temperature level. The fraction of the boiler tube area covered by a rivulet is,

$$F = \frac{2r_s \sin\alpha}{2\pi r_t} \tag{190}$$

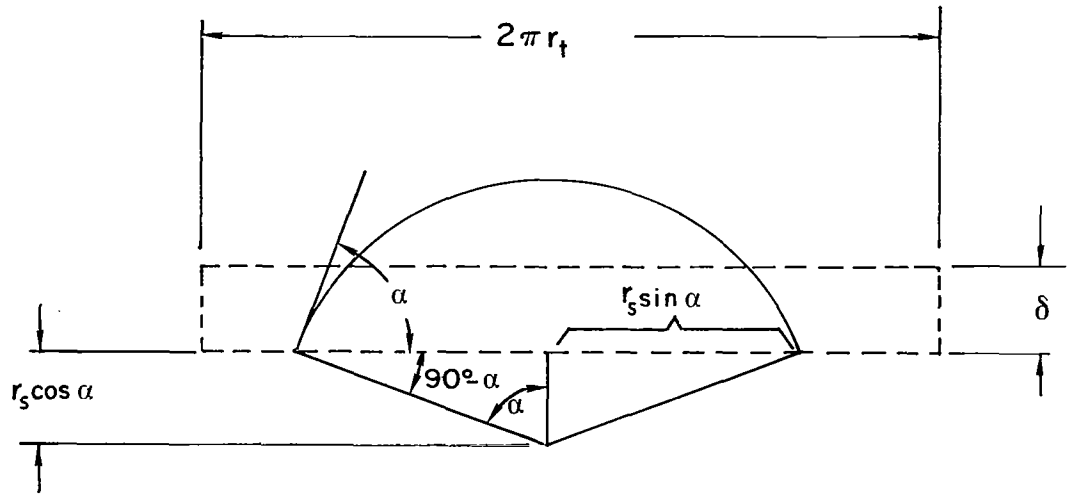

Figure 97. Geometrical parameters for the case where $\alpha_c < \alpha < 90°$.

Upon solving for r_s in Equation (189) and substituting it into Equation (190) there results

$$F = \frac{\sin\alpha}{\pi r_t} \sqrt{\frac{2\pi r_t \delta}{\alpha - \frac{1}{2}\sin 2\alpha}} \tag{191}$$

A similar analysis for the case $90 < \alpha < 180°$ yields

$$F = \frac{\sin(\pi - \alpha)}{\pi r_t} \sqrt{\frac{2\pi r_t \delta}{\alpha + \frac{1}{2}\sin(\pi - \alpha)}} \tag{192}$$

As an illustrative example of the use of this analysis, consider a viscous-viscous annular flow pressure drop and heat transfer case from the analysis of Reference 14. Results for δ and $h_{an.\ film}$ (based on surface vaporization at the film-vapor interface) obtained as a function of vapor quality, are listed in Table II. It should be noted that for the postulated viscous-viscous flow model, the working fluid flow rate does not enter the solution and is hence not needed.

Table II.

vapor quality, X	δ, ft	$h_{an.film}$, Btu/hr ft^2 °F
0.1	0.0052	3,270
0.2	0.0037	4,590
0.3	0.0029	5,860
0.4	0.0024	7,090

Figure 98 shows the results of critical rupture contact angle α_c as a function of vapor quality for the conditions of the illustrative example. For each vapor quality listed in Table II, a critical contact angle was calculated from Equation (188). If actual contact angles for the system fall below the critical values, the annulus film would not rupture; if the actual contact angles fall above the critical values, film rupture occurs. Note that critical contact angles decrease with increasing vapor quality. Thus for invariant actual contact angles, one would expect the annular film to rupture at higher vapor qualities.

Figure 99 presents the function F versus vapor quality for contact angles greater than the critical angles for rupture. These values were calculated from Equations (191) and (192).

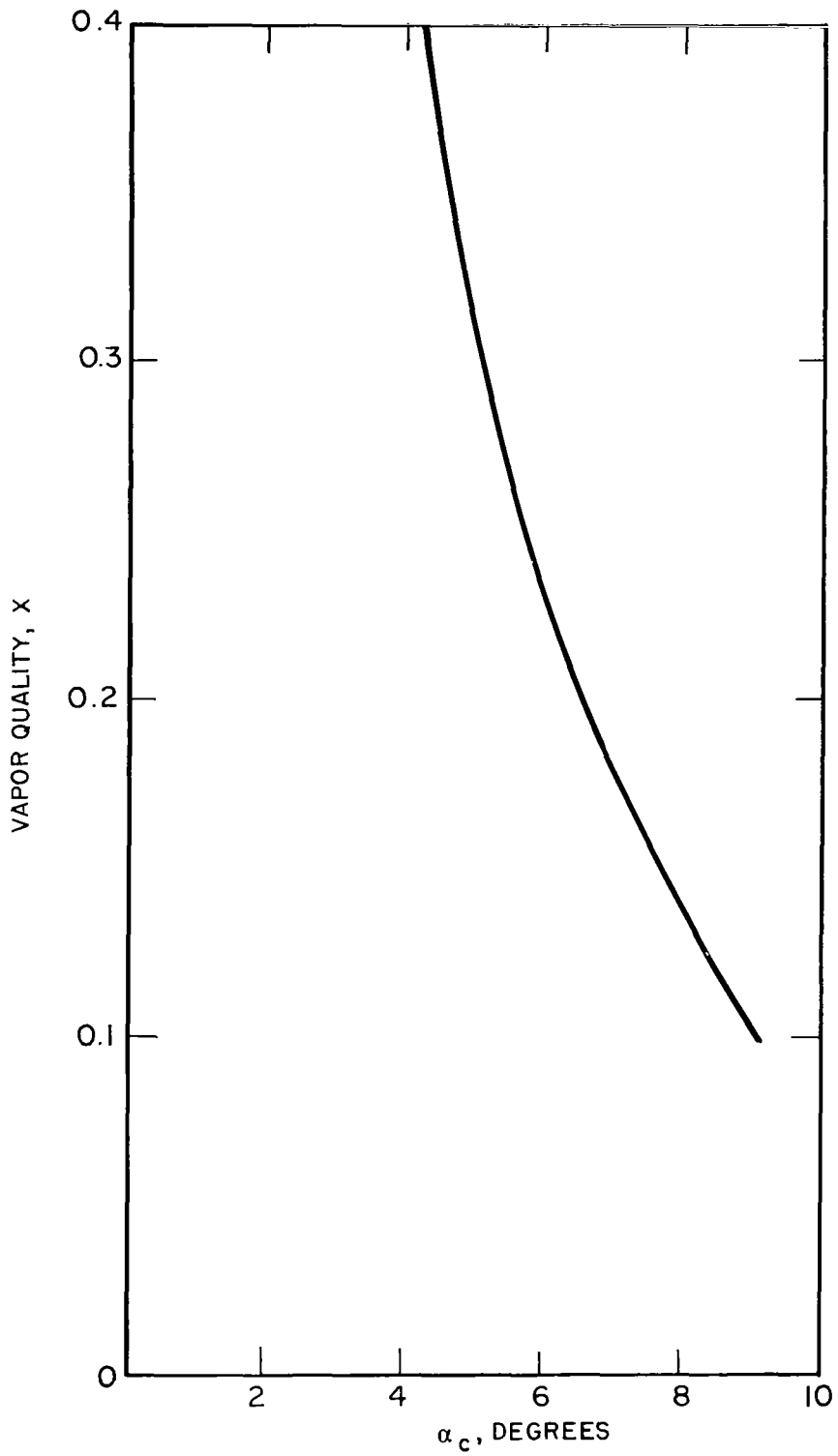

Figure 98. α_c versus vapor quality for a potassium system (illustrative example).

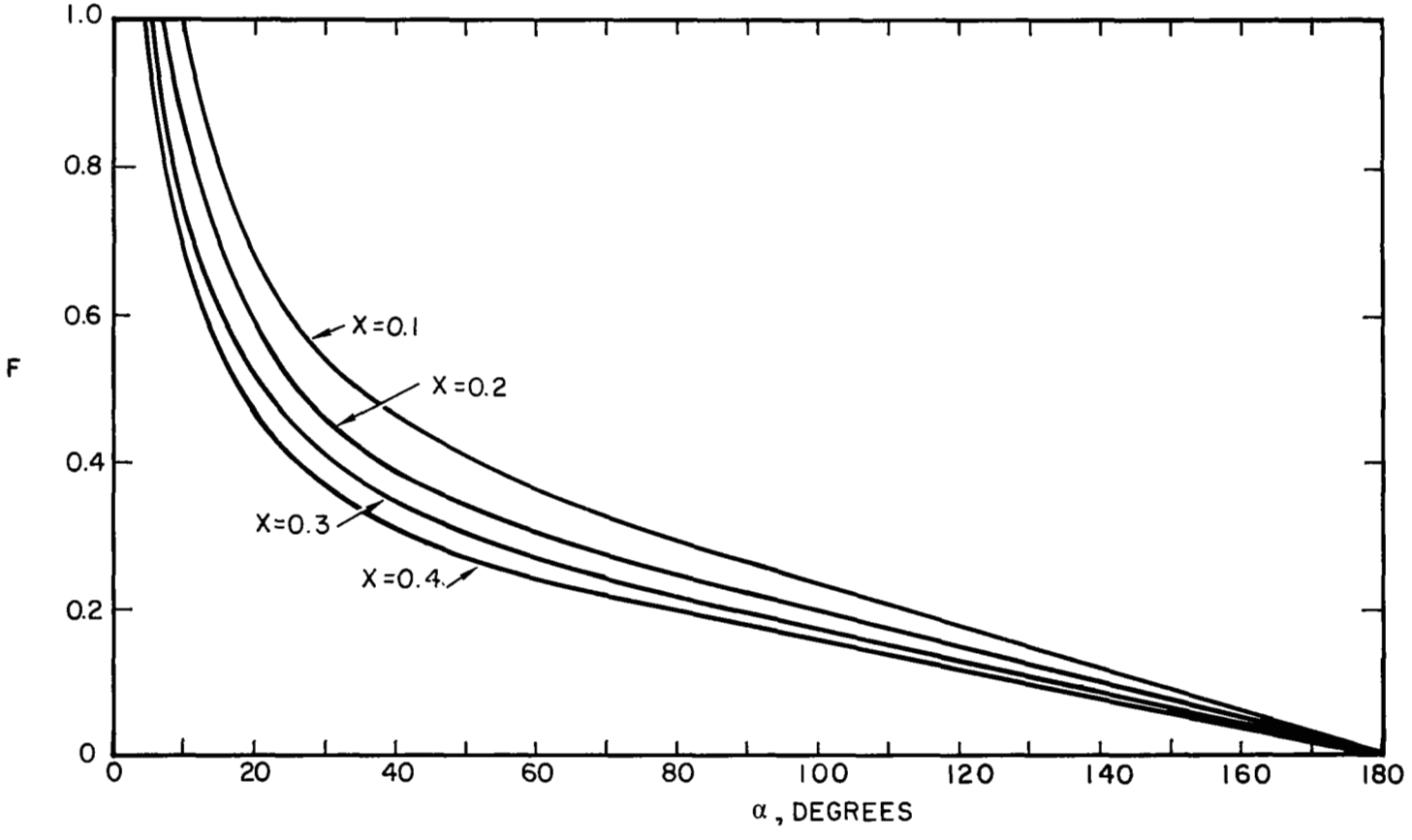

Figure 99. Function F versus vapor quality and contact angle for a potassium system (illustrative example).

6. Effect of Boiler Wall Thermal Conductivity on the End of the Wetted Film in a Boiler Tube

Many experiments have shown that the onset of film boiling occurs when the superheat of the wall surface above the liquid saturation temperature reaches a certain temperature level.

It was shown in Section D of this report that local heat fluxes and wall temperatures are much higher than the average values near discontinuities in the inner wall conductances. One might expect that when the surface temperature under the edge of the liquid film reaches a critical level local "vapor blanketing" will occur, and the end of the liquid film will move upstream.

It might appear that in a uniform flux boiler the temperature under the edge would not change as the film edge moved upstream, and therefore the wall would dewet all the way to the beginning of the boiler. There is at least one plausible reason why this need not be the case. As stated in Section E.1, the unboiled liquid not carried in the liquid film is entrained in the vapor. The rate at which the entrained liquid is deposited on the wall is dependent on its concentration in the vapor, and the closer to the beginning of the boiler the film ends the higher the droplet concentration and the deposition rate must be. The impinging droplets do not wet the wall according to the model under discussion but they still contribute significantly to the wall cooling. The ratio of the 'wetted wall' heat transfer conductance to the 'dry wall' conductance would therefore be expected to decrease as the end of the film moves toward the boiler inlet. As is shown in Figure 69, the decrease in this ratio causes a lowering of the wall temperature at the edge of the film, so that at some point the edge becomes stable and ceases to move. Given a fixed value of wall to saturated fluid for which the onset of film boiling occurs, the maximum heat flux for which the end of the annular liquid layer is stable is given by

$$(q/A)_{max} = \frac{\left(T_1 - T_s\right)_{max}}{\frac{\Delta T_1}{(k/\delta)} + \frac{1}{h_\ell}} \qquad (193)$$

where $(T_1-T_s)_{max}$ is the temperature difference at which "vapor blanketing" occurs. Consider the application of this criterion to a potassium boiler. Suppose that for a specific case good estimates for h_ℓ, h_v, and k/δ have been made and that the values are

$$h_\ell = 2 \times 10^4 \text{ BTU/ft}^2 \text{ hr } ^\circ\text{F}$$

$$h_v = 2 \times 10^3 \text{ BTU/ft}^2 \text{ hr } ^\circ\text{F}$$

$$k/\delta = 1 \times 10^4 \text{ BTU/ft}^2 \text{ hr } ^\circ\text{F}$$

Suppose also that the maximum superheat for which a wet wall may be maintained $(T_1-T_s)_{max}$, is 50°F. From the specified conditions and by use of Figure 69,

$$\Delta T_1 \approx 1.1$$

so that

$$(q/A)_{max} = 31 \times 10^4 \text{ BTU/ft}^2 \text{ hr}$$

The specific case chosen corresponds to the temperature distribution given by Figure 67.

The isotherm labeled 1.0 has a temperature $(q/A)/(k/\delta)$ above that of the inside wall at $x=-\infty$. For the maximum heat flux this temperature difference is 31°F. This is also the temperature drop across the wall at a large distance from the discontinuity in either direction.

Several conclusions may be made about the onset of film boiling as described by this model. One is that a thick walled or high conductivity boiler decreases the likelihood that the annular liquid layer will be removed by film boiling. Another conclusion is that film stability studies, such as that of Reference 20, in which the attempt is made to describe analytically the conditions under which dry or wet spots will be maintained on a boiler wall, are not com-

plete unless they include the effects of wall heat conduction. Still a third conclusion is that very rapid regime changes in a boiler tube might be interpreted as fairly gradual ones under some circumstances, if inside wall conductances are inferred from outside wall temperatures and fluxes. An example of such an interpretation may well occur in the boiling Freon data of Reference 21. Their data, obtained with a (high conductivity) copper tube, show a change from the maximum near the end of the annular film to the minimum in the fog flow region which is quite gradual, while the data for Freon given in Reference 22, obtained with an aid of flow visualization in a (low conductivity) glass test section show a discontinuous transition between the two regimes. A comparison of these data is shown in Figure 100.

If instead of an annular liquid layer wetted liquid rivulets occur on the inside of the tube, as described in Section C., lower outside heat flux would probably be required to bring on film boiling, since the variations in the local inside temperature differences are larger for rivulet flows than for discontinuous annular flows.

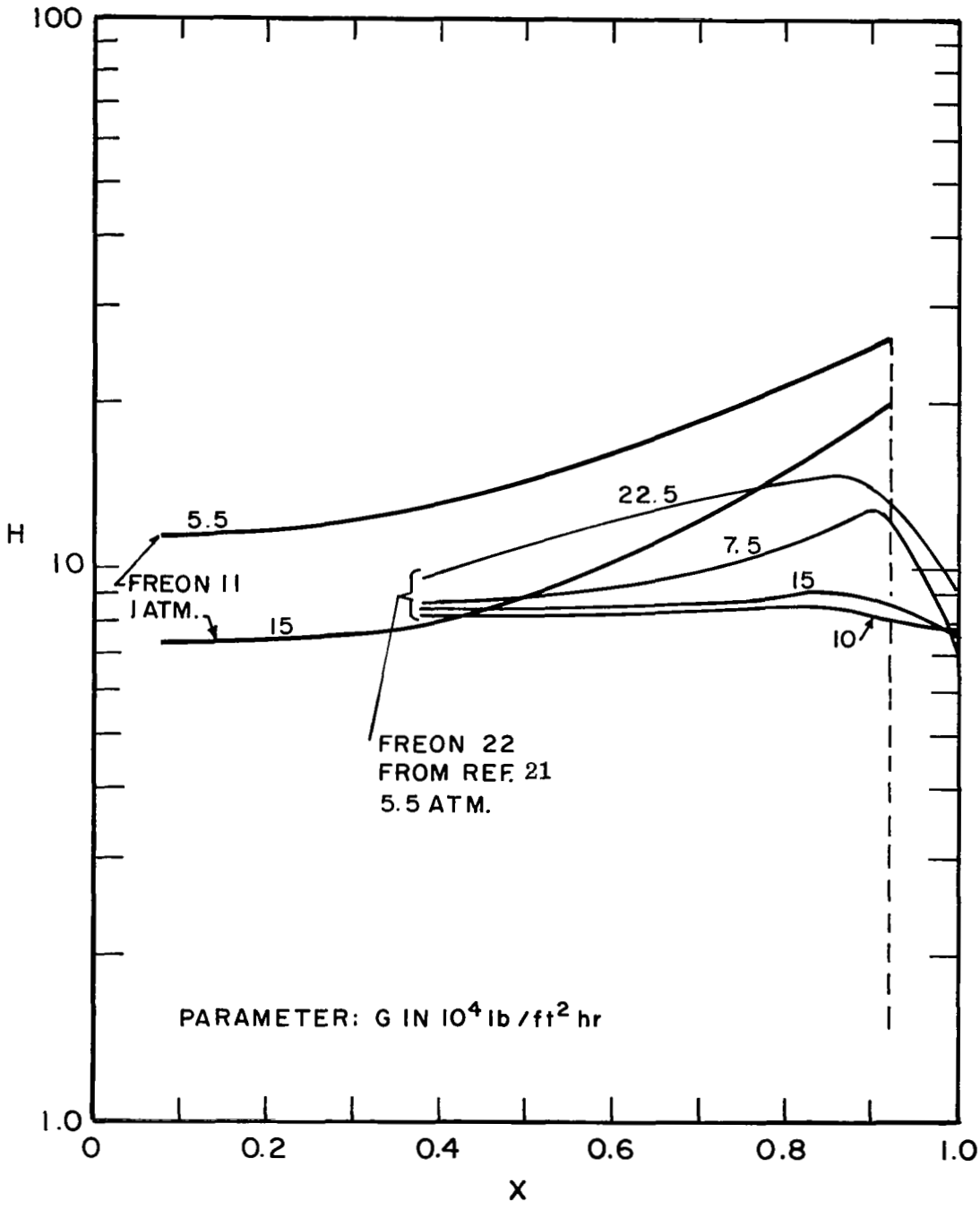

Figure 100. Linear forced convection boiling data for Freon 11 and 22.

F. Heat Transfer in Boiler Tubes

1. Direct Contact Rivulet Heat Transfer

The mean boiling heat transfer conductance in a boiler tube with a direct-contact axial rivulet can be expressed as

$$h_b = h_\ell \; F + h_v \; (1 - F) \tag{194}$$

where F is the fraction of the tube wall covered by liquid, h_ℓ is the liquid rivulet vaporization conductance, and h_v is the convective conductance for the dry areas in the boiler tube. The rivulet conductance can be defined in terms of the mean thickness of the rivulet, $\overline{\delta}_{riv}$, and the rivulet thermal conductivity, k_ℓ.

$$h_\ell = \frac{k_\ell}{\overline{\delta}_{riv}} \tag{195}$$

An alternate way in which to express the rivulet conductance is in terms of the conductance for a complete annular film and the function F, which is given on page 213. Thus,

$$h_\ell = \frac{k_\ell}{\delta} \cdot \frac{\delta}{\overline{\delta}_{riv}}$$

$$= \frac{k_\ell}{\delta} \cdot \frac{2 r_s \sin\alpha}{2\pi r_t}$$

$$= h_{an.film} \; F \tag{196}$$

Combination of Equations (196) and (194) yields

$$h_b = h_{an.film} \; F^2 + h_v \; (1 - F) \tag{197}$$

The elementary heat transfer analysis presented above for a smooth boiler tube may be applied to an illustrative example. Consider the case of potassium forced flow boiling in a 3/4 inch ID tube, under the same conditions as were used to calculate the conditions of Table II on page 213.

Figure 101 shows how the boiling conductance function is degraded as the liquid annular film is ruptured and the rivulet contact area F is decreased. There is evidence in the case of a number of mercury experiments that this phenomenon plays a major role in controlling the boiling heat transfer[23].

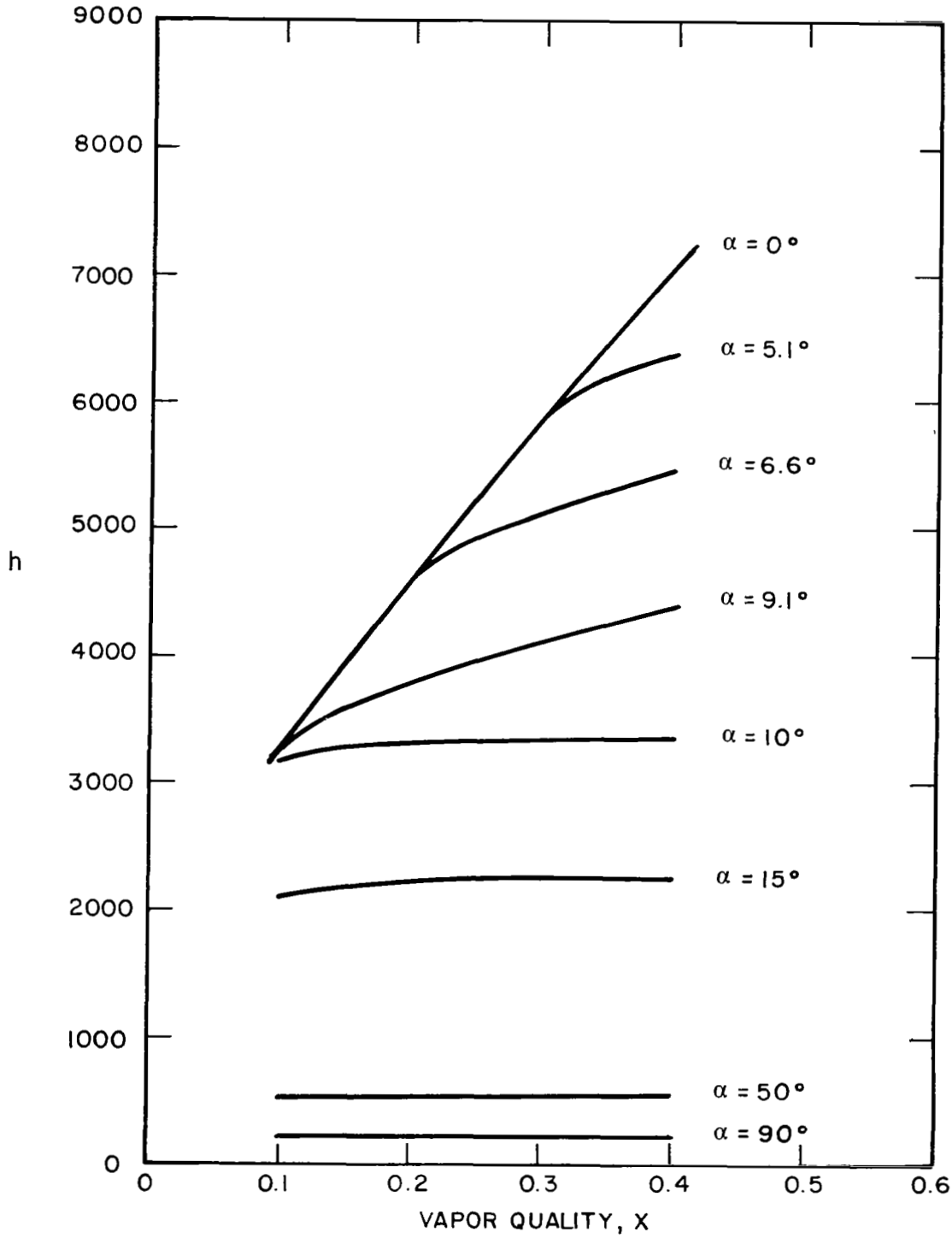

Figure 101. Boiling conductances versus X and α for a potassium system (illustrative example).

2. Effect of Surface Tension and Gravity on Rivulet Heat Transfer

In the preceeding section, wherein surface vaporization heat transfer from liquid rivulets making direct contact with the boiler tube wall was considered, it was postulated that only surface tension forces were in operation to control the rivulet profiles. In the case of a high surface tension liquid such as mercury, this postulate seems to be reasonable. Under high velocity rotational flow conditions, however, a centrifugal force field is acting on a rivulet or droplet moving helically along the boiler tube surface. Therefore, it is desirable to calculate under what conditions the centrifugal acceleration field will significantly change the rivulet profile from what it would be if only surface tension were effective. The effect of gravitational forces (or centrifugal forces due to rotation) previously excluded are added in the rivulet profile analysis given below.

From classical physics, the differential equation that describes the force balance between surface tension and gravitational forces for a rivulet (two dimensional system shown in Figure 102) is

$$\frac{p\,dp}{\left[1 + p^2\right]^{3/2}} = \frac{4}{c^2}\,y\,dy$$

where

$$p = \frac{dy}{dx}$$

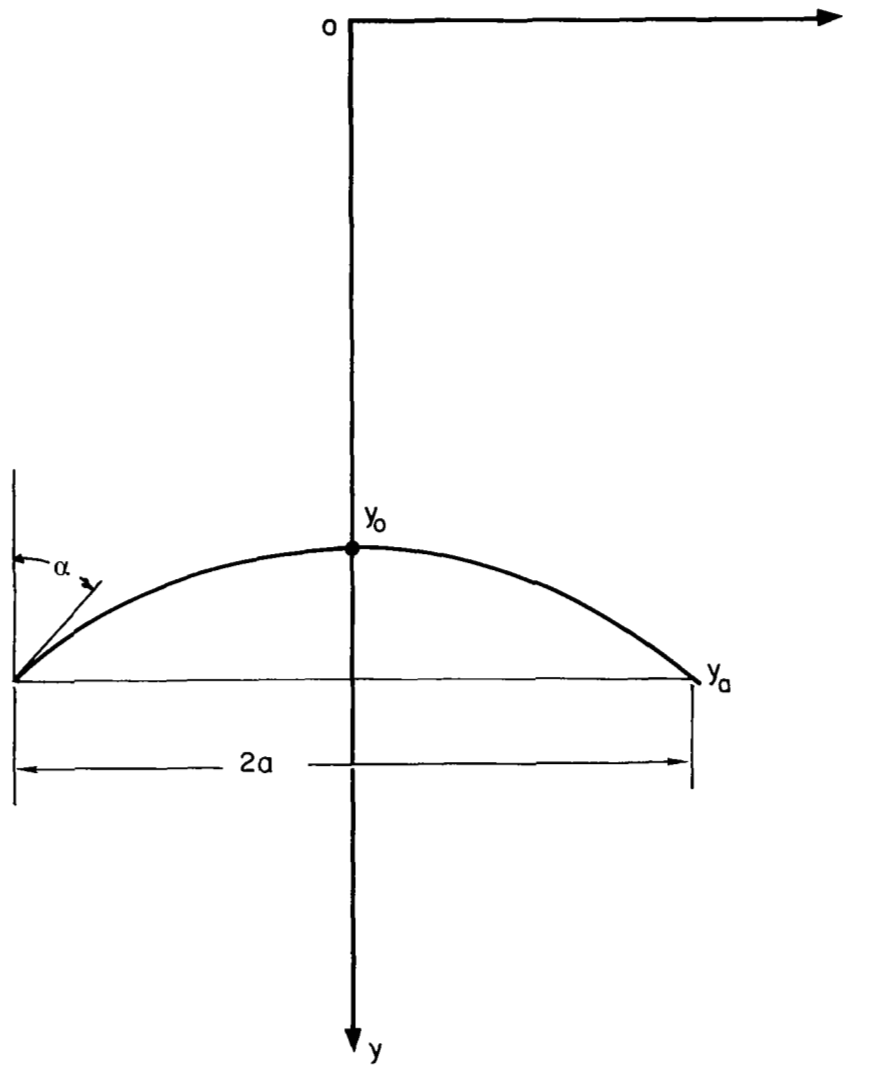

Figure 102. Rivulet coordinate system.

where

y, vertical rivulet surface coordinate (from plane of zero pressure)

x, horizontal rivulet surface coordinate (from rivulet center)

$$c = \sqrt{\frac{\sigma}{\rho_\ell g}}$$

σ, surface tension

ρ_ℓ, density

g, acceleration of gravity

Two boundary conditions define the system, namely,

$\frac{dy}{dx} = 0$ at the rivulet center ($x = 0$, $y = y_.$)

and $\frac{dy}{dx} = \cot \alpha$ at the rivulet edge ($x = a$, $y = y_a$)

α, complement of the contact angle

a, half width of rivulet

y_a, vertical coordinate at edge of rivulet

The first integration of Equation (198) together with the first boundary condition yields

$$dx = \frac{c^2 - 2(y^2 - y_o^2)}{2\sqrt{c^2(y^2 - y_o^2) - (y^2 - y_o^2)^2}}\, dy \qquad (199)$$

The final integration is facilitated by making the change of variable

$$y^2 - y_o^2 = c^2 \cos^2 \phi \qquad (200)$$

Upon substituting Equation (200) into Equation (199) together with the definition, $k^2 = c^2/(y_o^2 + c^2)$, there results,

$$dx = \frac{c^2 - 2c^2 \sin^2 \phi}{\frac{2c}{k}\sqrt{1 - k^2 \sin^2 \phi}}\, d\phi$$

$$dx = \left(\frac{ck}{2} - \frac{c}{k}\right) \frac{d\phi}{\sqrt{1 - k^2 \sin^2 \phi}} + \frac{c}{k} \sqrt{1 - k^2 \sin^2 \phi}\, d\phi \qquad (201)$$

Because $\phi = \pi/2$ when $y = y_o$ or $x = 0$, the limits of integration are x to 0 and ϕ to $\pi/2$. The resulting solution can be shown to be

$$x = \frac{c}{k}\left[\left(1 - \frac{k^2}{2}\right)\Big(K(k) - F(k,\phi)\Big) - \Big(E(k) - E(k,\phi)\Big)\right] \qquad (202)$$

where the functions K(k), F(k,ϕ), E(k) and E(k,ϕ) are the classical elliptic integrals. It is noted that both k and ϕ in Equation (202) are dependent upon x. It is necessary to use the second boundary condition to complete the solution. Specifically, the value of ϕ at $x = a$, $y = y_a$, is given by

$$\cos \phi_1 = \frac{\sqrt{y_a^2 - y_o^2}}{c} \qquad (203)$$

But since $p = \cot \alpha$ when $y = y_a$, it can be shown that

$$\frac{\sqrt{y_a^2 - y_o^2}}{c} = \frac{1 - \sin \alpha}{2} \qquad (204)$$

Thus, Equation (203) can be expressed as

$$\cos \phi_1 = \sqrt{\frac{1 - \sin \alpha}{2}} \qquad (205)$$

Also Equation (202) becomes

$$a = \left(\frac{c}{k} - \frac{ck}{2}\right)\Big[K(k) - F(k,\phi_1)\Big] - \frac{c}{k}\Big[E(k) - E(k,\phi_1)\Big] \qquad (206)$$

The solution for the profile of a rivulet is then obtained as follows. First, the value of k is determined from Equation (206), after substitution of the constants ϕ_1 (from Equation (205) and c. The value for y_o is next determined from the definition of the term k. Finally, the values for x and y are given in terms of parameter ϕ by

Equation (202) and (200) respectively. The vertical coordinate at the edge of the rivulet, y_a, is given by Equation (204).

The cross sectional profile area of the rivulet is obtained for the complete solution outlined above by the relationship

$$A = 2a\,y_a - 2\int_0^a y\,dx$$

In order to compare this result to the analysis for which gravity was neglected, the width of a rivulet with a circular cross section (which neglects gravitational effects) has to be determined. That result is then compared to the exact value, 2a.

The solution presented in this section has been evaluated for a number of specific mercury flow cases. Figure 103 shows a plot of the profile of a 1.27 cm wide mercury rivulet under a one earth gravity field condition and a contact angle of ten degrees. The area under the curve was integrated and the result used to obtain a rivulet profile with a circular shape (no gravitational forces considered) with a contact angle of ten degrees. A second evaluation (Figure 104) pertains to a condition where a one hundred fold earth gravity field was in operation on a 1.27 cm wide mercury rivulet with a ten degree contact angle.

Note the drastic changes in the rivulet profiles for these specific conditions. These results, which are particularly applicable to rivulet flow on the inside of a boiler tube wall with linear or helical flow, show that as one might expect, significant flattening of the rivulets occurs under high gravitational fields. At one earth gravity field, the ratio of rivulet width to the corresponding value for a zero gravitational field is 1.17. At one hundred earth gravity fields, the ratio of rivulet width to the corresponding value for a zero gravity field is 1.78. These results can be used to refine the rivulet heat transfer model presented in Section E.5.

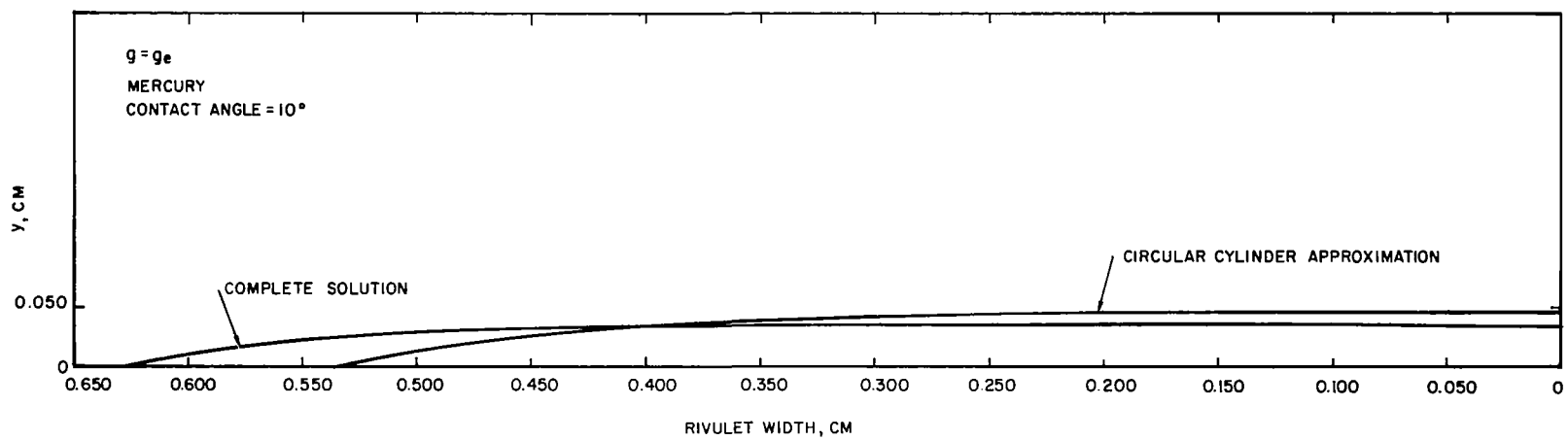

Figure 103. Mercury rivulet profile ($g=g_e$ and a=10 degrees).

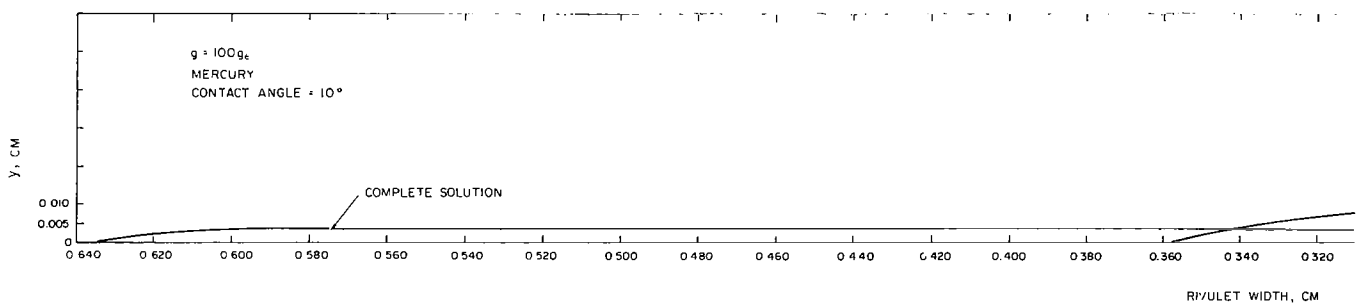

Figure 101. Mercury rivulet profile ($g = 100g_e$ and $\alpha = 10$ degrees).

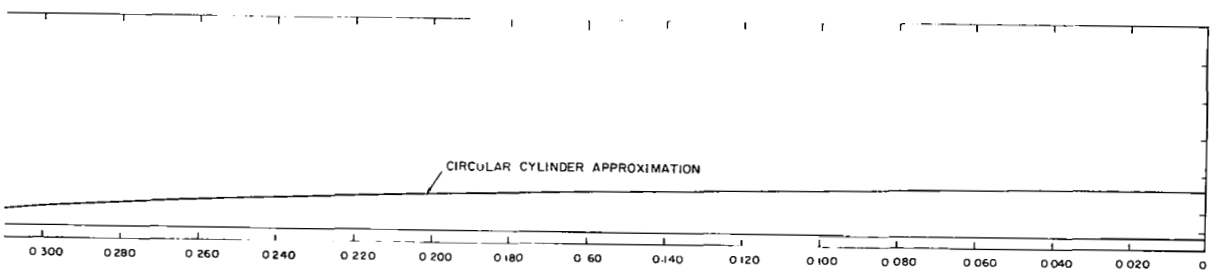
CIRCULAR CYLINDER APPROXIMATION
0 300
0 280
0 260
0 240
0 220
0 200
0 180
0 60
0 140
0 120
0 100
0 080
0 060
0 040
0 020
0

3. Heat Transfer with Film Boiling Entrained Droplets in Helical Flow

A recapitulation of Geoscience's boiling potassium and mercury measurements in a boiler tube with a twisted divider indicated that the boiling conductances generally decreased from predictable entrance values (at a vapor quality of zero percent) to predictable helical vapor flow exit values (at a vapor quality of one hundred percent); these changes in conductance were found to be two to three orders of magnitude (Reference 14). Some typical data are shown in Figure 105.

The boiling heat transfer in the vapor quality region, $0.5 < x < 1.0$, may be examined on the basis of two models previously proposed by Geoscience. One model postulates the presence of droplets or rivulets at the duct wall with a helically flowing gaseous core. A second model presumes that the drops are very small and distributed in the form of fog within the helically flowing superheated gaseous core. Both models require that the liquid phase distribution and droplet size be known. On the basis of some earlier experimental measurements with mercury and air, some data on the droplet number per diameter length of boiler tube are available for helical flow; information on fog particle size and distribution is only qualitative, however.

Consider the case where droplets and vapor are flowing helically in a boiler tube. Heat transfer from the wall to the working fluid consists of both gaseous forced convection and droplet vaporization. Because the mechanisms are operating in parallel, the corresponding conductances can be added,

$$h_b = h_{conv} + h_{vap} \tag{208}$$

where h_b, total boiling conductance

h_{conv}, convective conductance

h_{vap}, droplet vaporization conductance

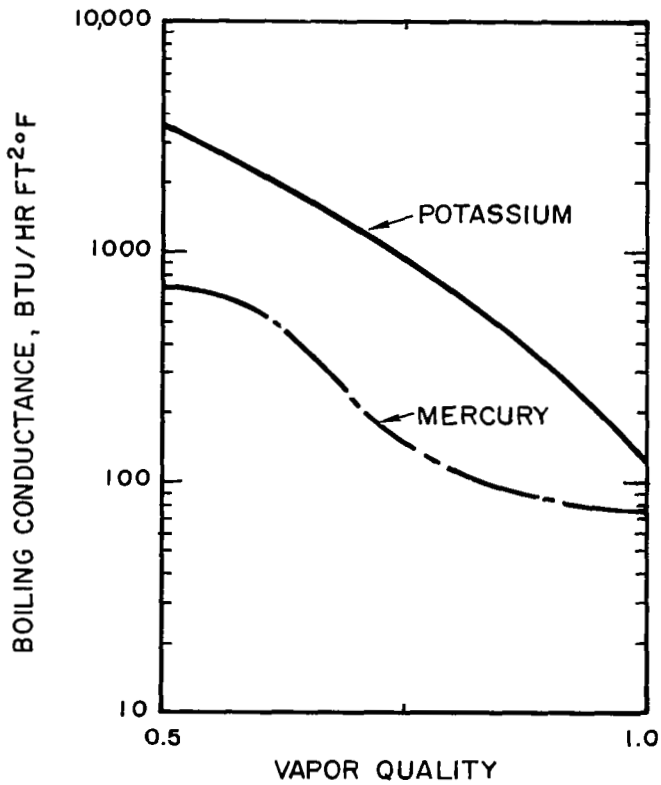

Figure 105. Some typical potassium and mercury boiling conductance data in the high vapor quality region (helical flow).

From the forced flow drop vaporization model derived earlier[14], it was shown that

$$\frac{h_{vap}\, D}{k_v} = \frac{6.61\, n \left(\frac{Y_\ell}{8n}\right)^{8/15}}{B^{2/3}} \tag{209}$$

$$\text{where } B = \frac{k_v\, \Delta t}{L\, \rho_d^{1/2}\, \rho_v^{1/2}\, U_{tv}^{3}} \tag{210}$$

$$U_{tv} = \frac{\pi D}{p}\, \frac{x\, W_t}{A_c\, w_v} \tag{211}$$

$$Y_\ell = \frac{1 - x}{1 + \left(\frac{w_\ell}{w_v} - 1\right) x} \tag{212}$$

Upon substituting Equations (210), (211), and (212) into (209) and simplifying, there results,

$$h_{vap} = \frac{6.6\, k_v\, \pi^{6/5}\, n^{7/15}\, L^{2/5}\, \rho_d^{1/5}\, \rho_v^{1/5}\, W_t^{6.5}}{8^{8/15}\, D\, k_v^{2/5}\, \Delta t^{2/5} \left(\frac{p}{D}\right)^{6/5} A_c^{6/5}\, w_v^{6/5}} \left(\frac{1 - x}{1 + \left(\frac{w_\ell}{w_v} - 1\right) x}\right)^{8/15} x^{6/5} \tag{213}$$

The quantity n varies with tube vapor quality because the vapor volume increases thereby increasing the distance between the droplets. It can be shown that,

$$n = \frac{n_o\, x_o}{x} \tag{214}$$

where n_o, number of droplets per diameter of tube length at vapor quality, x_o

x_o, vapor quality near tube entrance

Upon substitution of Equation (214) into (213) and simplifying Equation (212) for $x \geq 0.01$ and $w_\ell / w_v \sim 4000$, one obtains,

$$h_{vap} = \left[\frac{6.6\, L^{0.4}\, \rho_d^{0.2}\, \rho_v^{0.2}\, k_v^{0.6}\, W_t^{1.2}}{8^{8/15}\, \Delta t^{0.4} \left(\frac{p}{D}\right)^{1.2} \left(\frac{D^2}{4}\right)^{1.2} D\, w_v^{1.2}} \right] \left(\frac{w_v}{w_\ell}\right)^{8/15} (1 - x)^{8/15}\, x^{1/5} \tag{215}$$

The convective conductance term in Equation (208) has previously been expressed as

$$h_{conv} = h_{forced} + h_{free} \tag{216}$$

The conductances can be expressed in terms of the Nusselt modulus (Reference 14;

$$Nu_{forced} = Nu_{lin.\,turb.\,vap.} \left[1 + \left(\frac{\pi}{p/D}\right)^2 \right]^{0.4} \left(\frac{D_h}{D_e}\right)^{0.8} \tag{217}$$

$$Nu_{free} = Nu_{lin.\,turb.\,vap.} \left[7.1\, \frac{(\beta\, \Delta t)^{1/3}}{Re_\ell^{0.13}\, Pr^{0.07}} \right] \left(\frac{\pi}{p/D}\right)^{2/3} \left(\frac{D_t}{D_e}\right)^{2/3} \tag{218}$$

Substitution of Equations (215), (216), (217) and (218) into Equation (208) gives an equation for the total boiling heat transfer conductance. Equation (208) has been compared in Figure 106 to some experimental boiling potassium data obtained previously at Geoscience; the defining conditions for the forced, helical flow boiling are noted in the figure. The

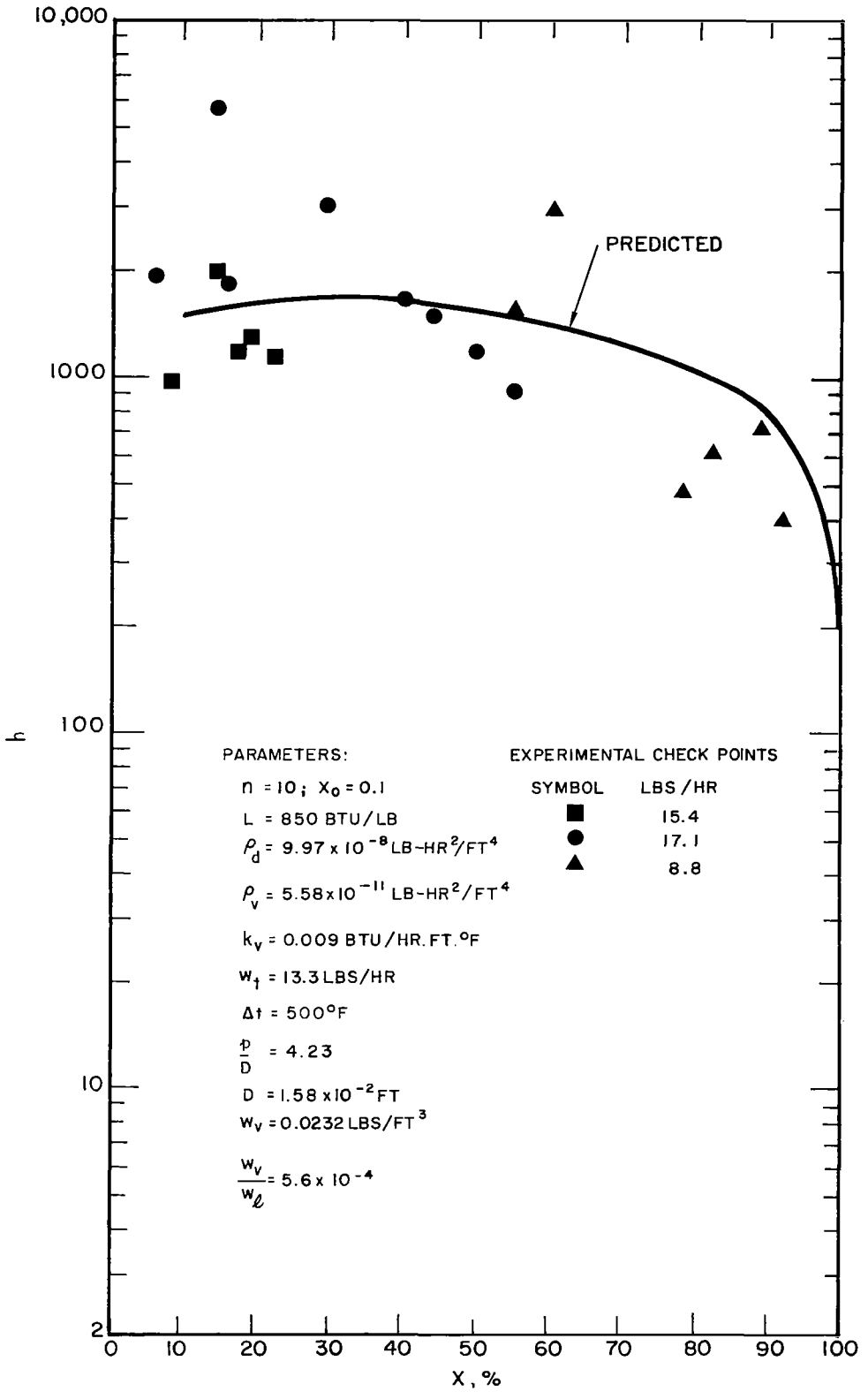

Figure 106. Predicted and experimental helical flow boiling potassium results.

predicted and experimental data have similar profiles and magnitudes. The calculations were made for the case, $n_o = 10$ and $x_o = 0.1$; these values were estimated on the basis of adiabatic mercury-air flow experiments in a glass tube[24].

4. Effects of Droplet Bouncing on Film Boiling in Helical Flow

Previous Geoscience studies of the film boiling droplet vaporization regime indicated that a tiny droplet that was vaporizing in the steady state regime could, at times, suddenly begin to oscillate (to a height equal to, or greater than, ten times the diameter of the droplet)[24]. When this process occurs (for reasons not completely clear), the corresponding vaporization lifetimes are found to be as much as fifty percent greater than those predicted for steady state film boiling. It is noted that the steady state predictions were usually in good agreement with steady state experimental droplet film boiling. Since the analysis in the preceeding section is based upon an analysis of steady state droplet vaporization, it is important to assess the effect of bouncing upon the helical flow film boiling analysis.

The bouncing droplet dynamics in the film boiling state have previously been discussed in Geoscience reports[24,25]. In the present section, two simple analyses have been made of the effect of a rotational force field on a droplet that leaves the surface of a boiler tube with a given, invariant velocity. The solutions obtained can be used to calculate the reduction in the height to which a bouncing droplet will rise for constant escape velocity at the wall. The results of the two analyses are outlined below, together with several restricting postulates.

This complicated dynamics problem was idealized to the case of a simple bouncing sphere having a coefficient of restitution equal to unity and an invariant initial velocity (not related to the gravitational force field strength). It is recognized that these conditions may be too limiting for the purpose of drawing general conclusions at this time.

First the classical situation of a uniform gravitational force field (with elevation) is considered. The highest point in the trajectory, y_1, for this condition is

$$y_1 = \frac{\dot{y}_o^2}{2g} \tag{219}$$

or

$$\frac{y_1}{\dot{y}_o^2/2g_e} = \frac{1}{g/g_e} \tag{220}$$

where

$\dot{y}_o$, invariant initial velocity at y = 0

g_e, acceleration of the earth's gravity field

g, acceleration of gravity for system

A graph of Equation (220) is shown in Figure 107; note that for the postulated conditions, the absolute and dimensionless highest point in the trajectory varies inversely with the gravity field. Therefore, in a boiler tube with high velocity rotational flow, the high-amplitude bouncing droplet mode observed in the one-gravity droplet vaporization apparatus is not expected to be as prevalent.

It is likely that the gravitational field independent of height is too restrictive for the present purposes, so a second analysis was made for the case of a variable gravitational force field as found in a boiler tube having helical flow. The general force equation on the droplet is

$$\frac{W}{g(y)} \ddot{y} = - W \tag{221}$$

where

W, weight of the droplet

g(y), variable acceleration field

$\ddot{y}$, second derivative of y with respect to time

t, time

Upon expressing the first derivative of y with respect to time as the variable p, Equation (221) is transformed to

$$p \frac{dp}{dy} = - g(y) \tag{222}$$

This equation may be integrated twice to yield

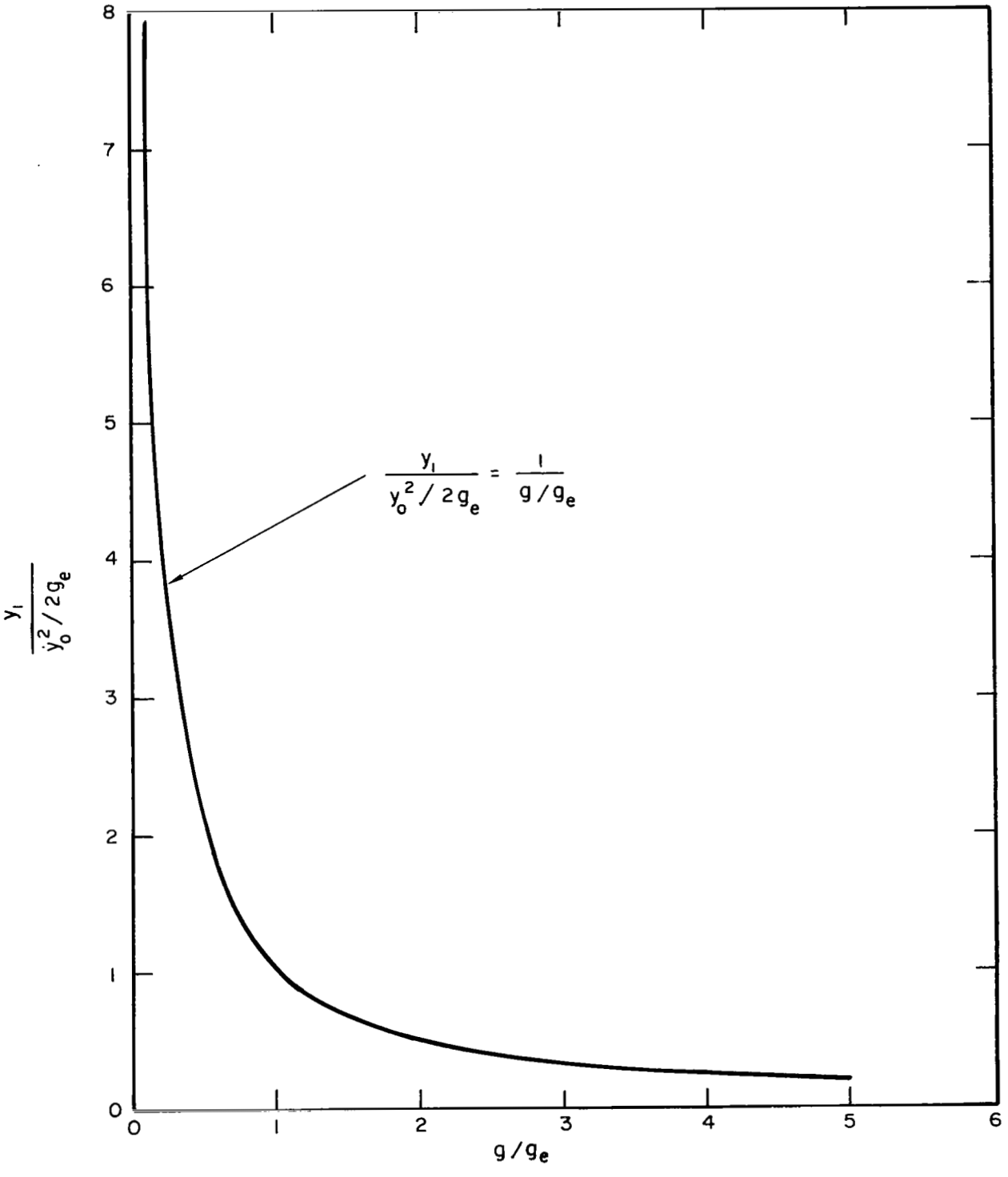

Figure 107. Normalized trajectory amplitude versus acceleration of gravity.

(Uniform Gravitational Field Analysis)

$$\int \frac{dy}{\sqrt{-2\int g(y)\,dy + 2C_1}} = \int dt + C_2 \qquad (223)$$

From the condition $\dot{y} = \dot{y}_o$ at $t = 0$, it can be shown that the constant $C_1 = 1/2\,(\dot{y}_o)^2$. From the condition $y = 0$ at $t = 0$, it can be shown that the constant $C_2 = 0$. From the first derivative of y with respect to t, the amplitude of the trajectory, y_1, can be found from the equation

$$2\int_0^{y_1} g(y)\,dy = \dot{y}_o^{\,2} \qquad (224)$$

For helical flow in a boiler tube the tangential velocity, v_t, can be approximated by

$$v_t = b_1 (r_t - y) \qquad (225)$$

where

b_1, a constant dependent on the axial flow rate

r_t, boiler tube radius

y, radial distance from the tube wall

The centrifugal acceleration term is considered to control the acceleration g(y) for most practical cases; thus,

$$g(y) = \frac{v_t^{\,2}}{r_t - y} = \frac{b_1^{\,2}(r_t - y)^2}{r_t - y} = b_1^{\,2}(r_t - y) \qquad (226)$$

Substitution of Equation (226) into Equation (224) leads to

$$2b_1^{\,2}\left(r_t y_1 - \frac{y_1^{\,2}}{2}\right) = \dot{y}_o^{\,2} \qquad (227)$$

The solution of this quadratic equation for the region $0 < y_1/r_t < 1$ is,

$$\frac{y_1}{r_t} = 1 - \sqrt{1 - \frac{\dot{y}_o^2}{(b_1 r_t)^2}}$$

$$= 1 - \sqrt{1 - \left(\frac{\dot{y}_o}{v_{t_o}}\right)^2} \qquad (228)$$

where the quantity, y_o/v_{t_o}, is the ratio of vertical to tangential velocities at the boiler tube wall. A graph of Equation (228) is shown in Figure 108. Note that the trajectory amplitude of a droplet decreases as the tangential velocity (acceleration field) increases. This is in agreement with the result of the analysis for a uniform force field, the results for which are given in the preceeding figure.

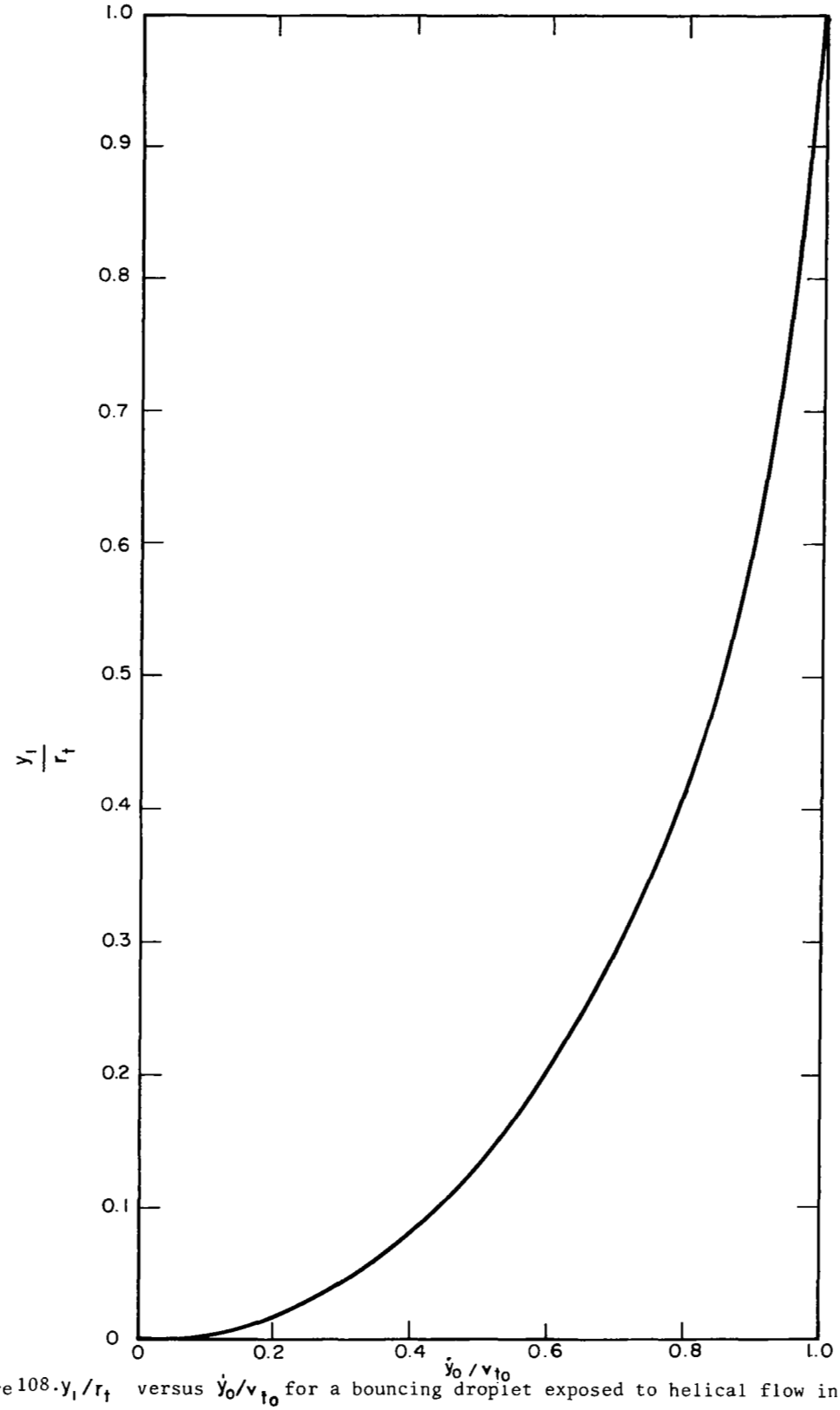

Figure 108. y_1/r_t versus $\dot{y}_0/v_{t0}$ for a bouncing droplet exposed to helical flow in a pipe.

5. Heat Transfer with Deposition and Vaporization of Entrained Droplets

One possible mechanism for the heat transfer behavior in the "transition boiling" region which occurs downstream of the end of the annular film, is spray cooling of the wall by wetting evaporation of droplets deposited from the entrained flow.

An analysis has been presented for the rate of deposition of entrained droplets in Section B.6. If one postulates that the wall is locally wetted by the impinging droplets, and that they are completely vaporized on the wall, then a computation may be made of the effect the droplet deposition will have on the mean temperature of the vapor flow in the tube. The temperature of interest here is the mixed mean temperature of the vapor phase only. The droplets entrained in the vapor flow are at saturation. The idealizations upon which the analysis is based are:

(1) The annular film has ended

(2) There are no rivulets; all of the remaining liquid is entrained in the vapor flow

(3) Deposition follows the relationships given in Section B.6

(4) The droplets wet the wall and vaporize completely

(5) The wall is subjected to a uniform heat flux

(6) The vapor temperature is initially at saturation

(7) No significant vaporization occurs in the entrained flow.

A simple energy balance based on these idealizations leads to the following equation for the mixed - mean vapor temperature:

$$\bar{T} = \frac{\left[(s-s_o)k_2\right] - \left[1 - \frac{w_{e(s)}}{w_{eo}}\right]}{\frac{w_t}{w_{eo}} - \frac{w_e}{w_{eo}}} \qquad (229)$$

where

$$\bar{T} = \frac{T_v - T_s}{\frac{L}{c_p}}$$

$$k_2 = \frac{q/A \, \pi \, D\ell_r}{L \, w_{e_o}}$$

L = latent heat of vaporization, c_p = vapor specific heat, and s_o and w_{eo} are the normalized boiler length and the entrained liquid flow at the end of the annular film. The other symbols are defined in section B.6.

Inspection of Equation (229) shows that in the absence of deposition, the mixed mean vapor temperature rises linearly, consistent with the idealizations. Physically the smallest value of $\bar{T}$ which may occur is zero, and this value will occur if the deposition (and vaporization) rate is large enough to require all of the heat provided to the wall. Mathematically, the value of $\bar{T}$ can be negative, since the mathematical relationships can specify a deposition rate larger than that which can be completely vaporized. In this latter case, a liquid film would form on the wall, which is a violation of the postulates.

Two cases have been computed, one for Freon 12 and one for potassium. These cases correspond to the ones chosen for the deposition rate calculations presented in section B.6. The results are presented in Figures 109 and 110.

The negative temperature in Figure 109 shows that according to the model a liquid film re-forms on the wall. Since the case chosen corresponds to a "burnout" point presented by Kirby (Reference 12) and therefore according to experiment the annular film has in fact ended, it is clear that the deposition rate is too high, (by at least a factor of four).. The most likely reason

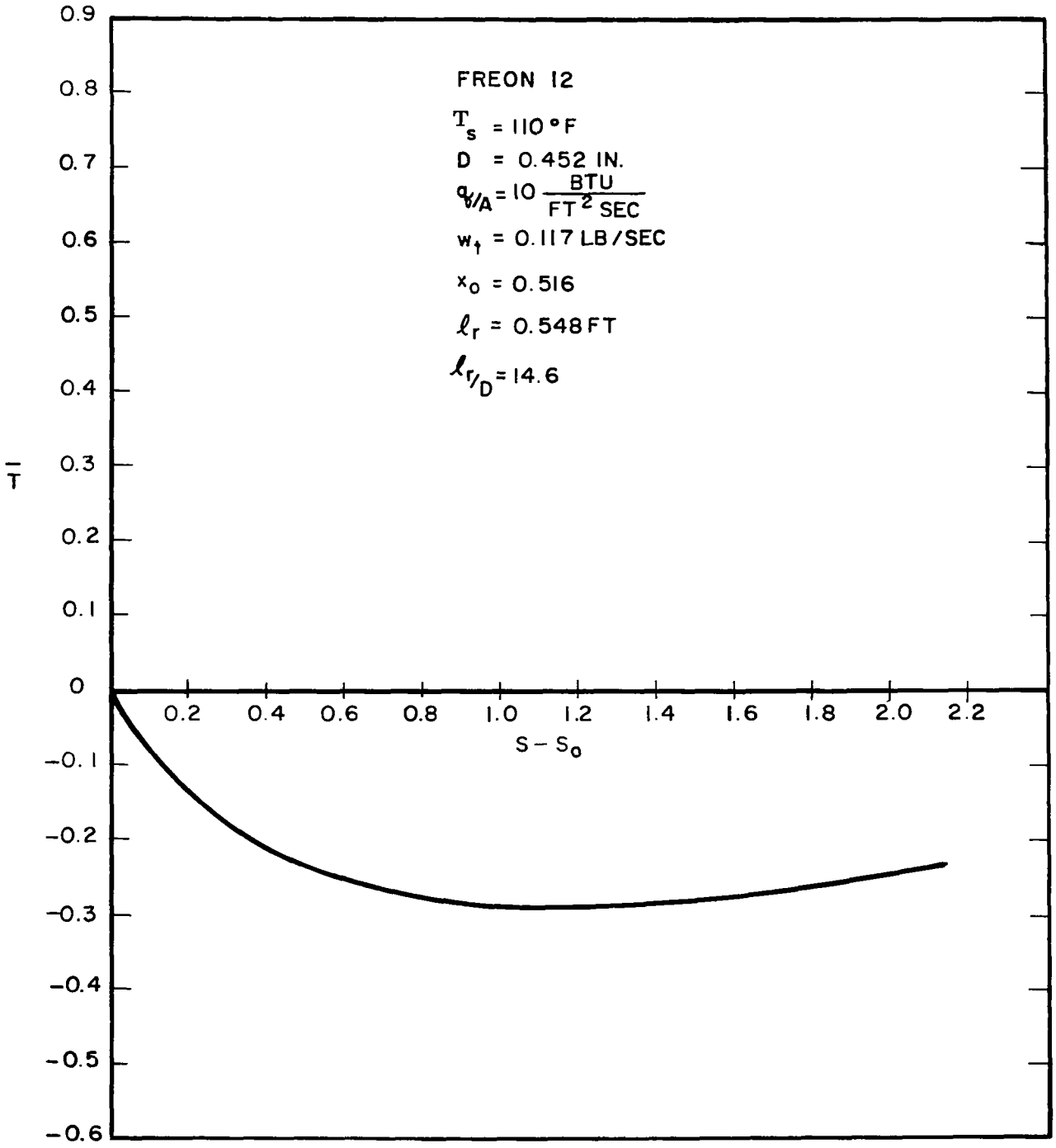

Figure 109. Vapor temperature rise downstream of end of annular flow.

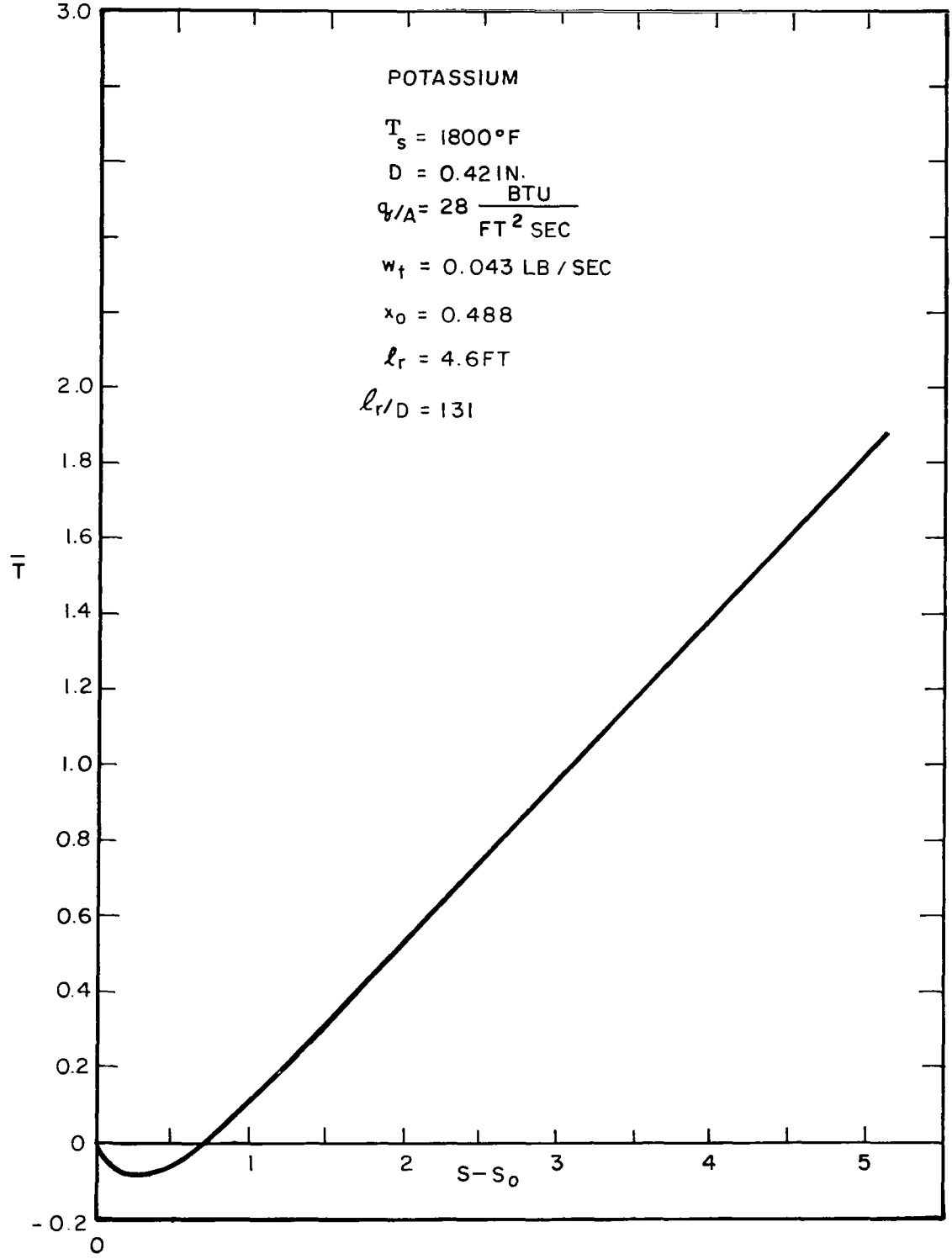

Figure 110. Vapor temperature rise downstream of end of annular flow.

for the overestimation of deposition rate is that the diffusion conductance given by Equation (80) of this report is too large for the present case. Equation (80) is appropriate for very small particles, which follow the turbulent eddies of the flow in the tube. The droplets known to exist in a boiling Freon flow are too large to follow the local eddy motion and do not, therefore, diffuse as rapidly. In addition, the flow in an actual boiler is accelerating, and has mass addition next to the wall, so that the actual turbulence level is not that of the fully established pipe flow which Equation (80) represents. It may be concluded that although a large effect of spray cooling on transition boiling heat transfer may possbily be expected in a Freon boiler, it is overestimated by the present analysis.

Figure 110, presenting the calculation results for potassium, shows a negative normalized temperature also, indicating that a liquid film is forming faster than it is being evaporated away. It may be seen in the figure that the mixed-mean vapor temperature begins to rise at $s - s_o = 0.7$, which is approximately 92 diameters downstream of the point s_o. At the point where the mixed-mean vapor temperature begins to rise the vapor quality is about 81%.

Although the analysis probably overestimates the droplet deposition rates for both Freon and potassium, it appears likely that, in some circumstances, deposition rates could be high enough to significantly affect the conductance downstream from the end of the annular film. Droplet deposition probably plays a role in some cases of transition boiling.

The postulate was made in the analysis that the liquid wets the boiler wall. It is well known that wetting will occur only if the wall temperatures are not too high above the saturation temperature. Under most conditions of uniform wall heat flux, the wall temperature will rise rather rapidly after the end of the annular film and somewhere downstream the droplets will no longer wet the wall, but will instead film boil.

At this point the present analysis will no longer apply. The calculation of boiler wall temperature rise downstream of the end of the annular film may also be performed by use of the approximation that the vapor forced convection and

Reference 14, the rivulet flow analyses of section F.2, the criterion for onset of nucleate boiling (section E.2), suitably modified for appropriate nucleating conditions, and the varying wall temperature information of section D.

The use of simple models and their combinations to make performance predictions appears to be the most promising method of avoiding a cut-and-try experimental program for each new requirement. Test programs are essential, but with an initial performance prediction, and careful analysis of the test results, using analysis as a guide, the test program may hopefully be short, and rational.

IV. NOMENCLATURE

A heat transfer area

A_d liquid droplet cross-sectional area

A_c tube wall inside area

A_ℓ tube wall inside area wetted by rivulet

A_o tube wall outside area

A_r rivulet cross-sectional area

A_T tube cross-sectional area

a 1) a constant; 2) rivulet half width

a_r radial acceleration

B 1) a constant; 2) a parameter

b a constant

b_1 a constant

C, C_1, C_2, C_3, C_4 constants

C_D drag coefficients

C_{D_m} wire drag coefficient modified for boundary layer effects

C_{D_w} drag coefficient for a circular cylinder adjacent to a solid wall

c_p vapor specific heat (constant pressure)

C_s vapor stream droplet concentration

C_w droplet concentration near tube wall

D tube inside diameter

D_e tube equivalent diameter for linear flow

D_h tube equivalent diameter for helical flow

D_m wire coil inside diameter

D_p droplet (or particle) diameter

D_t tube equivalent diameter for tangential flow (normal to tube axis)

$\mathscr{D}$ molecular diffusion coefficient

d_w helical wire diameter

$E(K)$, $E(k, \phi)$ elliptic integrals

F 1) force; 2) fraction of boiler tube inside area covered by rivulets

$F(k, \phi)$ elliptic integral

F_D drag force

F_{ft} wall friction force measured normal to tube axis

F_g gravitational force

F_H centrifugal force due to rotation of droplet around tube axis

F_n force exerted on fluid by helical wire measured normal to helical wire

F_r 1) forces restraining secondary flows; 2) radial shear forces on film due to secondary flows

F_s force driving secondary flows

F_{wt} wire drag force measured normal to tube axis

F_x vapor drag force in x direction (droplets in helical flow)

F_y vapor drag force in y direction (droplets in helical flow)

G mass velocity (of both phases) in boiler tube

g local acceleration field

g (y) variable local acceleration field

g_c proportionality constant in Newton's second law

g_e Earth's gravitational field

H normalized conductance, defined by $H = h/h_{x = 100\%}$

h heat transfer conductance

h_a apparent conductance on inside tube wall, observed from outside

$h_{an.\ film}$ heat transfer conductance with a complete annular film

h_b boiling heat transfer conductance

h_{conv} convective conductance

h_d a mass diffusion conductance

h_{forced} single phase forced convection conductance

h_{free} convective conductance due to buoyancy (natural convection)

h_h convective conductance on hot fluid side of heat exchanger surface

h_ℓ wetted wall conductance

h_v dry wall vapor conductance

h_{vap} conductance due to droplet vaporization

I 1) rotational moment of inertia; 2) an integral function

$K(k)$ an elliptic integral

k, k_1, k_2 parameters, constants

k_ℓ liquid thermal conductivity

k_v vapor thermal conductivity

k_w wall thermal conductivity

L latent heat of vaporization

$\mathcal{L}$ a characteristic length

ℓ length

ℓ_a axial tube length

ℓ_h helical path length of vapor flow

ℓ_{max} maximum altitude of droplet ejected from a horizontal liquid surface

ℓ_D axial station at which droplet motion begins

ℓ_r characteristic lengths

ℓ_t transverse distance of droplet travel

ℓ_w length of helical wire

M applied torque

m droplet mass

N_1, N_2, N_3, N_4 parameters

N_u Nusselt modulus

$N_{u_{lin.turb.vap}}$ Nusselt modulus for a linear turbulent single phase vapor flow

$N_{u_{forced}}$ Nusselt modulus of forced convection

$N_{u_{free}}$ Nusselt modulus of free convection

n number of droplets per unit length of boiler tube, number of vanes on helical divider

n_d number of droplets in an axial length equal to one tube diameter

n_o number of droplets per unit length at quality X_o

n_1, n_2 parameters

P_r Prandtl modulus

p 1) helical wire or vane pitch; 2) a point in space; 3) $\frac{dy}{dx}$; 4) $\frac{dy}{dt}$; pressure

p_c pressure at centerbody surface

p_f pressure drop due to skin friction

p_s saturation pressure

p_w pressure at tube inside wall

p_{wm} maximum pressure at tube inside surface

q/A heat flux

$(q/A)_B$ "critical" or "burnout" heat flux

$(q/A)_o$ uniform outside heat flux

Re_ℓ linear flow Reynolds modulus

R_i inside tube wall radius

R_D outside tube wall radius

r radius measured from tube centerline

r_o, r_1 radius of inner channel wall or centerbody

r_2 radius of inside surface of outer channel wall

r_c radius of centerbody

r_i radial location of liquid-vapor interface

r_s radius of curvature of rivulet surface

r_t radius of boiler tube (inside)

Sc Schmidt modulus

s normalized axial length

s_1 normalized axial length of which annular film ends

T_a absolute temperature

T_h mixed mean temperature of hot fluid

T_o outside wall temperature

T_s saturation temperature

T_v mixed mean vapor temperature

T_w wall temperature

$\overline{T}$ normalized mixed mean vapor temperature

t time

$t_{\ell \max}$ time at which droplet reaches maximum altitude

$\bar{t}_a$ normalized time for axial motion

$\bar{t}_r$ normalized time for radial motion

$\bar{t}_{r180°}$ normalized time at which droplet has traveled half way around tube

V_D droplet volume

V_p normalized particle velocity

V_s normalized slip velocity

V_v normalized vapor velocity

v velocity

v_o initial velocity of droplet ejected from liquid layer

v_a mean axial velocity

v_e critical velocity for shear entrainment

v_h helical velocity at tube surface

v_{max} maximum axial flow velocity in a tube with a velocity profile

v_n velocity component normal to helical wire

v_p droplet (or particle) velocity

v_r 1) a characteristic velocity; 2) velocity of liquid film on vane, measured in radial direction

v_s 1) slip velocity; 2) secondary flow velocity

v_t velocity component normal to tube axis

v_{to} initial transverse droplet velocity

v_{tf} velocity component normal to tube axis in fully established flow

v_{tr} transverse droplet velocity

v_v vapor velocity

v_{vx} x component of vapor velocity

v_{vy} y component of vapor velocity

v_x velocity of liquid film on vane, measured in direction of constant radius

W weight of droplet

W_t total mass flow rate

w angular velocity

w_d mass flow deposited onto tube wall

w_e entrained liquid mass flow rate

w_{eo} initial entrained liquid mass flow rate

w_ℓ weight density of liquid

w_r net flow of liquid film in radial direction

w_v 1) vapor phase flow rate; 2) weight density of vapor

X vapor quality

X_B quality at "burnout"

X_o quality at which number of droplets is known

x a space coordinate

x_o coordinate of droplet motion initiation

x_r half width of rivulet

x_e distance from rivulet center to wall station where temperature gradient is zero

Y_ℓ void fraction

y a space coordinate

$\dot{y}$ first derivative of y with respect to time

$\ddot{y}$ second derivative of y with respect to time

$\dot{y}_o$ initial velocity of bouncing droplet at $y = o$

y_1 highest point in the trajectory of a bouncing droplet

z a space coordinate lying along the boiler tube axis

$\bar{z}$ a normalized axial coordinate

z_o axial position of initial droplet motion

α 1) a parameter; 2) contact angle

α_1, α_2 parameters

α_c critical contact angle at film rupture

β volumetric thermal expansion coefficient

α a normalized gravitational force parameter

Δ a difference quantity

Δp_{hw} pressure drop in a tube containing a helical wire

ΔT wall-to-saturation temperature difference

ΔT_w temperature drop across boiler tube wall

δ 1) boiler tube wall thickness; 2) liquid film thickness

$\bar{\delta}_{riv}$ mean thickness of liquid rivulet

ϵ eddy diffusivity

ζ friction factor

ζ_D friction factor based on tube diameter

ζ_{D_m} friction factor based on wire coil inside diameter

θ angle measured about the tube axis

κ a parameter

λ a reciprocal characteristic time

μ a parameter

μ_g gas phase viscosity

μ_ℓ liquid viscosity

μ_v vapor viscosity

ρ fluid density

ρ_g gas phase density

ρ_ℓ liquid density

ρ_v vapor density

σ surface tension

τ a characteristic time

τ_a a characteristic time for axial droplet motion

τ_r a characteristic time for radial droplet motion

τ_s shear stress

ϕ a function

θ angular position in the curved channel

V. REFERENCES

1. Peterson, J. R., High Performance 'Once Through' Boiling of Potassium in Single Tubes at Saturation Temperatures of 1500° to 1750°F, NASA CR-842; August 1967.

2. Bond, J. A., and G. L. Converse, Vaporization of High Temperature Potassium in Forced Convection at Saturation Temperatures of 1800°F to 2100°F, NASA CR-843; July 1967.

3. Converse, G. L., et al., Air Water Experiments Transparent Plastic Tube, G. E., Cincinnati, Memorandum HTC-10; March 1968.

4. Converse, G. L., Air Heating Experiments, G. E., Missile and Space Division, Cincinnati, Memorandum HTC-12; April 1969.

5. Abbott, D., and S. J. Kline, Theoretical and Experimental Investigation of Flow Over Single and Double Backward Facing Steps, Dept. of Mech. Eng., Stanford University, AFOSR-TN-890; June 1961.

6. Allen, J., Inst. Civ. Engrs, U. K. Proc., Vol. 28, p. 31-8; May 1964.

7. Sams, Eldon W., Heat Transfer and Pressure Drop Characteristics of Wire-Coil Type Turbulence Promoters, Reactor Heat Transfer Conference, USAEC, New York, N. Y.; November 1956.

8. Converse, G. L., G. E. Cincinatti, private communication; April 20, 1967.

9. Gibson, A., Phil. Mag., Vol. 50, Ser. 6, pp. 199-204; 1925.

10. Neill, C. R., Proc. Amer. Soc. Civ. Engrs., Vol. 88, No. HY3, pp. 23-44; May 1962.

11. Schlichting, Boundary Layer Theory, Fourth Edition, McGraw-Hill, p. 502; 1960.

12. Kirby, G. J., Burnout in Climbing Film Two Phase Flow, a Review of Theories of the Mechanism, AEEW-R470, U. K. Atomic Energy Authority Reactor Group, Winfrith; 1966.

13. Eckert, E., Introduction to the Transfer of Heat and Mass, McGraw-Hill, p. 251; 1950.

14. Poppendiek, H. F., N. D. Greene, C. M. Sabin, L. V. Feigenbutz, G. Mouritzen, F. R. MacDonald, R. K. Livett, J. E. Chambers, P. E. Schwartz, D. J. Connelly, W. A. Morton; Summary Report on High Acceleration Field Heat Transfer for Auxiliary Nuclear Power Systems, GLR-42-SAN-409-29; AEC Contract No. AT(04-3)-409.

15. Wallis, G., J. Turner, I. Benberis, D. Kaufman; Two-Phase Flow and Boiling Heat Transfer, NYO 3114-4.

16. Seymour, E. V.; Fluid Flow Through Tubes Containing Twisted Tapes, (The Engineer: October 28, 1966).

17. Levich, V. G., Physicochemical Hydrodynamics (Prentice-Hall: 1962).

18. Bijwaard, G., F. Staub, N. Zuber, A Program of Two-Phase Flow Investigation, Tenth Quarterly Report, General Electric, San Jose, GEAD-4959; July - September 1965.

19. Holtz, R., The Prediction of Liquid Superheats Required for Initiation of Nucleate Boiling in the Liquid Metals, ASME Paper 64-WA/HT-31.

20. Staub, F. W., N. Zuber, A Program of Two Phase Flow Investigation, Second Quarterly Report, GEAP-4367; October 1963.

21. Altman, M., R. Norris, F. Staub, Local and Average Heat Transfer and Pressure Drop for Refrigerants Evaporating in Horizontal Tubes, J. of Heat Transfer, pp. 189, 198; August 1960.

22. Poppendiek, H. F., et al., Annual Technical Report on High Acceleration Field Heat Transfer for Auxiliary Space Nuclear Power Systems, AEC Contract No. AT(04-3)-409, GLR-27-SAN-409-12; September 1, 1963 to August 31, 1964.

23. Poppendiek, H. F., C. M. Sabin, L. V. Feigenbutz, N. D. Greene, Investigation of Fundamental Mechanisms and Parameters that Influence Steady State and Transient Performance of Rankine Cycle Liquid Metal Systems, GLR-55-SAN-677-15, Quarterly Report April 1 to June 30, 1967.

24. Poppendiek, H. F., N. D. Greene, W. B. Goddard, C. M. Sabin, Investigation of Fundamental Mechanisms and Parameters that Influence Steady State and Transient Performance of Rankine Cycle Liquid Metal Systems, GLR-64-SAN-677-29, Annual Report AEC Contract No. AT(04-3)-677, July 1, 1967 through June 30, 1968.

25. Poppendiek, H. F., L. V. Feigenbutz, N. D. Greene, C. M. Sabin, Investigation of Fundamental Mechanisms and Parameters that Influence Steady State and Transient Performance of Rankine Cycle Liquid Metal Systems, GLR-53-SAN-677-11, Quarterly Report, AEC Contract No. AT (04-3)-677; January 1 to March 31, 1967.

26. Poppendiek, H. F., et al., Quarterly Report on Investigation of Fundamental Mechanisms and Parameters that Influence Steady State and Transient Performance of Rankine Cycle Liquid Metal Systems, GLR-53-SAN-677-11, AEC Contract No. AT(04-3)-677; January 1 to March 31, 1967.

NASA-Langley, 1971 —— 33